UniversidadeVigo

Escola Internacional de Doutoramento

Diego Fernández Nóvoa

TESE DE DOUTORAMENTO

Characterization of the main Iberian Peninsula and French Atlantic turbid plumes using MODIS satellite data

Dirixida pola doutora: María Teresa de Castro Rodríguez

2017

"Mención internacional"

Universidade de Vigo, Campus de Ourense, Departamento de Física Aplicada, Environmental Physics Laboratory (Ephyslab).

Diego Fernández Nóvoa (diefernandez@uvigo.es).

Characterization of the main Iberian Peninsula and French Atlantic turbid plumes using MODIS satellite data.

UniversidadeVigo

Escola Internacional de Doutoramento

Dra. María Teresa de Castro Rodríguez, profesora titular do Departamento de Física Aplicada da Universidade de Vigo:

FAI CONSTAR que o presente traballo, titulado "*Characterization of the main Iberian Peninsula and French Atlantic turbid plumes using MODIS satellite data*", que presenta **DIEGO FERNÁNDEZ NÓVOA** para a obtención do título de DOUTOR POLA UNIVERSIDADE DE VIGO CON MENCIÓN INTERNACIONAL, foi elaborado baixo a súa dirección no programa de doutoramento **Marine Sciences, Technology and Management (Campus do Mar)**.

Ourense, 26 de setembro de 2017.

A directora da tese de doutoramento.

Dra. María Teresa de Castro Rodríguez

Agradecementos/Acknowledgments

En primeiro lugar teño que expresar todo o meu agradecemento a Maite e Moncho, que me deron a oportunidade de iniciar esta Tese Doutoral, e sen os cales todo este camiño non sería posible. Agradecer a súa constante axuda, dedicación, orientación e ensinanzas que fixeron posible o desenrolo desta tese e me fixeron medrar tanto persoal como profesionalmente.

Dar as gracias tamén a todas as persoas que compartiron comigo esta etapa. De xeito especial a Rubén, David e Laura, que comezaron comigo a carreira, logo o máster e posteriormente o doutoramento. Gracias polas horas xuntos, tanto de traballo como de ocio, e o apoio continuo en todo este camiño. Tamén dar gracias ao resto de persoas coas que compartín bos momentos tanto dentro como fora do laboratorio ó longo desta tese doutoral: Xurxo, Ángel, Lucía, Manolo, Marisela, Santi, Miki, Susana, Álex, así como a Renato, polo continuo intercambio de ideas, solucións e colaboracións ó longo do traballo desenrolado, e ó resto de persoas integrantes do grupo Ephyslab cos que dun xeito ou outro compartín momentos durante esta etapa.

Quero de xeito especial agradecer a meus pais, Juán José e María Elena, todo o que fixeron, fan e seguirán facendo por min. Neles teño sempre un apoio incondicional nos bos, e de xeito especial, nos non tan bos momentos. Sempre fan todo o posible para facilitarme as cousas e que non me falte de nada.
Gracias a meu irmán Adrián, que dende fai xa algo mais de 19 anos se convertiu nunha parte imprescindible da miña vida, pola complicidade mutua que temos e porque sei que sempre está ahí para apoiarnos en todos os momentos e circunstancias.
De xeito especial recordo aos meus avós, Manolo, Josefa, María, Pepe e Adelina, que sempre me coidaron, me ensinaron e me apoiaron en todos os camiños que emprendín, e que seguro estarán orgullosos de todos os meus logros.
Tamén ó resto da familia, tí@s e prim@s, polo apoio e motivación que sempre recibín deles.

Dar gracias a Cristina, que sempre confiou en min e nas miñas capacidades incluso mais que eu mesmo, polo seu ánimo, apoio e cariño incondicionais en todos os momentos, e por darme o regalo mais grande que unha persoa pode ter, Sabela, que pasou a ocupar o centro da miña vida, e cuxa sola existencia é sinónimo de felicidade, ánimo, motivación e positivismo.

Tamén agradecer @s amig@s do Coto e arredores, os cales fomos medrando, aprendendo, progresando e madurando xuntos, e que pasados os anos e aínda que cada quen seguiu camiños diferentes, seguimos unidos e apoiándonos coma o primeiro día.

Resumen

Se denomina pluma fluvial a aquella región oceánica afectada por la descarga de un río debido a lo cual adquiere diferentes propiedades que el agua oceánica que la rodea: salinidad, temperatura, composición y color. Estas diferencias son debidas a que los ríos transportan al océano agua dulce, nutrientes, sedimentos, materia orgánica e inorgánica y contaminantes, entre otros.

Por lo tanto, las plumas fluviales suponen la mayor fuente de transferencia de materiales terrestres al océano, desenvolviendo un papel fundamental en la ecología y morfo-dinámica de las zonas costeras afectadas, ya que son capaces de modular e influenciar sus características geológicas y biogeoquímicas (Körtzinger et al., 2003). Por ejemplo, las plumas fluviales afectan a la estratificación y a los patrones de circulación, debido a las diferencias de densidad causadas por la interacción entre agua dulce y salada (Uncles, 2002). Además, los ríos proporcionan nutrientes a la pluma que pueden sostener altos niveles de fitoplancton aumentando la productividad primaria, lo cual es fundamental para la subsistencia de otros ecosistemas asociados (Ribeiro et al., 2005). Por otro lado, las plumas también pueden transportar contaminantes, disminuyendo la calidad de las aguas costeras (Reifel et al., 2009). Además, las plumas fluviales transportan los sedimentos descargados por los ríos en los océanos, lo cual puede tener implicaciones negativas ya que atenúan la luz solar incidente, lo que supone una cuestión crítica para el crecimiento del fitoplancton y la productividad primaria (Huret et al., 2007). Por lo tanto, las plumas afectan el ciclo de varias especies de peces y mariscos, ya que según las características del material descargado por los ríos, pueden actuar como zonas de dispersión o retención afectando a su abundancia (Grimes and Kingsford, 1996; Wilber and Clarke, 2001). Además los sedimentos transportados desempeñan un papel clave en los procesos de erosión y sedimentación en las zonas costeras (Warrick and Milliman, 2003). También es importante destacar que algunos fenómenos costeros, entre los que se incluyen la presencia de los ríos, pueden condicionar la evolución de la temperatura debido a las diferencias que promueven con el agua oceánica que los rodea. La zona oceánica afectada por el agua de los ríos puede calentarse más intensamente que el agua adyacente o incluso tener una tendencia al enfriamiento, representando un papel fundamental como moduladores del cambio climático (Howden and Murtugudde, 2001; Park et al., 2011; Materia et al., 2012). Este hecho es especialmente relevante teniendo en cuenta el actual contexto de calentamiento global, ya que la temperatura de los océanos se está incrementando a escala global desde mediados del siglo XX (Belkin, 2009; Levitus et al., 2012).

Por todas las razones comentadas, las plumas fluviales desempeñan un papel clave en la economía de las comunidades locales a las que afectan, lo cual unido a los efectos inducidos por el cambio climático y al incremento de la población en las regiones costeras, hace que la comprensión y predicción de la dinámica de las plumas, así como el

conocimiento de su respuesta bajo ciertas condiciones, sea fundamental en términos científicos y socio-económicos.

Estas características generales de las plumas fluviales son aplicables a las formadas en la Península Ibérica, en cuyo estudio está enfocado el desarrollo de esta Tesis Doctoral. Este estudio está centrado en las plumas formadas por los principales ríos de la Península Ibérica, en términos de descarga fluvial, debido a diversas motivaciones. Primeramente, cabe destacar que muchos de los ríos más importantes de la vertiente Atlántica de Europa desembocan en la Península Ibérica (Miño, Duero, Tajo, Guadiana y Guadalquivir). Además de los ríos que desembocan en la vertiente Atlántica, cabe destacar otro río importante que vierte en el Mediterráneo, el Ebro, que forma un importante Delta en su desembocadura. Por otro lado cabe también resaltar que la zona costera de la Península Ibérica es una importante fuente de riqueza socio-económica, ya que es una zona de alta producción primaria donde se desarrollan actividades socio-económicas muy importantes entre las que se incluyen el turismo, la pesca o la acuicultura. Muchas de estas actividades se realizan en las zonas de desarrollo de las plumas fluviales, de ahí la importancia y necesidad de conocer en profundidad la variabilidad de las mismas. De hecho, varios estudios a lo largo de los años han analizado las plumas Ibéricas bajo diferentes situaciones, mostrando la importancia de estas plumas para la comunidad científica. Como ejemplos Sousa et al. (2014a) analizaron la pluma del Miño, Otero et al. (2008) la del Duero, Vaz et al. (2011) la del Tajo, Cravo et al. (2006) la del Guadiana, Caballero et al. (2014) la del Guadalquivir y Mestres et al. (2003) la del Ebro. Sin embargo, pocos estudios se desarrollaron aprovechando la potencialidad ofrecida por la teledetección remota de las plumas a través de satélites, que será la fuente de datos principal utilizada en el desarrollo de esta tesis, ya que permite analizar las plumas con una gran resolución y durante periodos de tiempo largos, tal y como se describe a continuación. Muchos de los estudios previos solamente se centraron en el análisis de ciertas situaciones particulares de plumas concretas durante periodos de tiempo limitados. Por lo tanto, el desarrollo de esta tesis supone un avance en la comprensión del comportamiento y dinámica de las principales plumas Ibéricas bajo los principales forzamientos que las afectan.

La salinidad es uno de los mejores trazadores naturales para estudiar las plumas fluviales, ya que la zona ocupada por la pluma tiene menor salinidad que la del océano adyacente debido a la influencia del agua dulce del río. Sin embargo, hasta el momento la salinidad no se puede medir a escalas temporales y/o espaciales suficientemente pequeñas como para evaluar adecuadamente el comportamiento de las plumas, ya que están caracterizadas por tener una estructura espacial fina capaz de cambiar rápidamente. Como alternativa, muchos estudios demostraron una buena correlación entre la superficie de baja salinidad causada por la descarga del río (pluma salina) y la coloración característica del océano originada por el material en suspensión transportado por el río (pluma turbia) (Dzwonkowski and Yan, 2005; Palacios et al., 2009; Saldias et al., 2012). Los sensores satelitales son capaces de detectar una señal fuerte en la zona ocupada por el material descargado por el río (pluma turbia), mientras que en las aguas oceánicas no afectadas la

señal es nula, pudiendo por lo tanto delimitar la zona ocupada por la pluma fluvial. Por lo tanto, los datos de color del océano obtenidos mediante teledetección, mostraron ser adecuados para analizar las plumas fluviales en numerosos estudios a nivel global debido a su gran resolución espacial y temporal (Miller and McKee, 2004; Nezlin et al., 2005, Wang et al., 2007; Kilham and Roverts, 2011), convirtiéndose en una herramienta muy útil para realizar estudios sobre las plumas.

Para el estudio de las plumas fluviales en esta Tesis Doctoral se utilizaron datos de radiancia proporcionados por el sensor satelital *Moderate Resolution Imaging Spectroradiometer* (MODIS), a bordo de los satélites Aqua y Terra y cuyos datos están disponibles en la página web de *Ocean Color* de la NASA (https://oceancolor.gsfc.nasa.gov/). MODIS fue seleccionado debido a que ofrece una alta resolución espacial (hasta 250 metros) y temporal (datos diarios), lo que permite identificar con precisión la variabilidad de las plumas.

La metodología desarrollada para trabajar con los datos de MODIS consistió en lo siguiente: Primeramente, se descargaron los datos brutos del nivel L1A de la página web de *Ocean Color* para cada zona de estudio. Estos datos se procesaron posteriormente al nivel L1B a través del software *SeaWIFS Data Analysis System*, versión 7.1 (SeaDAS, Baith et al., 2001), proceso durante el cual se aplicaron las calibraciones instrumentales y radiométricas. Finalmente se generaron los archivos definitivos a nivel L2 obteniendo los datos de las variables geofísicas bajo interés a la mejor resolución posible para cada caso, siguiendo un procedimiento similar al detallado por Aurin et al. (2013). En este proceso se aplicaron una serie de máscaras para reducir los datos erróneos, incluyendo las estándares recomendadas, un límite para el albedo de 0.018 a través de las bandas *Short Wave Infrared* (SWIR) para descartar la cubierta nubosa, una máscara de 3x3 píxeles alrededor de la tierra y de las nubes para evitar la luz dispersada en los bordes, así como la supresión de valores de radiancia no realistas. También se optó por usar las bandas *Near-Infrared* (NIR) para la corrección atmosférica, ya que se comprobó que son las que mejor se adaptan para el caso particular de las plumas Ibéricas. Además, se fusionaron los datos diarios proporcionados por ambos satélites para aumentar el número de píxeles disponibles incrementando así la robustez y precisión del estudio.

Una vez procesadas y obtenidas las imágenes diarias para cada pluma bajo interés, el objetivo se centró en encontrar el límite turbio característico que mejor define cada pluma, permitiendo diferenciarla del agua oceánica adyacente. Este límite puede ser diferente para cada pluma ya que es dependiente de las características terrestres y la carga sedimentaria de cada río. El límite se obtuvo a través del análisis de la relación existente entre la extensión de la pluma y la descarga fluvial.

Una vez obtenidas las imágenes diarias de cada pluma y los límites turbios, se crearon composiciones de estas imágenes que caracterizaran las principales situaciones sinópticas de las plumas, es decir, imágenes promedio que mostraran el estado de las plumas bajo la influencia de los principales forzamientos que las afectan (descarga fluvial, vientos y marea). Primeramente, se definieron las condiciones que caracterizan cada forzamiento a

analizar. Por ejemplo, para analizar el estado de la pluma cuando la descarga del río es alta, se estableció como límite el percentil 75, es decir, se promediaron todos los días con descarga mayor que ese percentil para obtener una imagen final que permita conocer el patrón general de la pluma ante ese forzamiento. En este proceso lo que se hizo fue promediar para cada píxel, los valores válidos disponibles para los días que cumplieran las condiciones preestablecidas, obteniendo una imagen final del estado medio de la pluma. Esta metodología permite caracterizar las plumas Ibéricas, así como analizar y comparar sus respuestas ante los forzamientos, ya que se establecieron las mismas condiciones para cada una de ellas. Esto permite establecer comportamientos similares entre plumas y analizar las causas que conducen a las diferencias entre ellas. Es especialmente destacable que, a pesar de la relativa proximidad geográfica entre los principales ríos Ibéricos, los forzamientos pueden afectar a las plumas de forma diferente debido al régimen mareal, a la morfología de la costa y a diferencias regionales en las corrientes costeras, entre otros factores.

Los resultados obtenidos se compararon con trabajos previos que analizaron algunos comportamientos particulares de alguna de las plumas bajo estudio, con el objetivo de corroborar la precisión de MODIS para analizar las plumas. Además, la capacidad de MODIS para detectar las plumas también se evaluó a través de la comparación con la pluma salina obtenida de la base *Atlantic-Iberian Biscay Irish-Ocean Physics Reanalysis* (IBI), mejorando así la robustez de la metodología aplicada.

Una vez analizadas y comparadas entre sí las principales plumas de la Península Ibérica, el estudio se amplió para analizar también las plumas más importantes formadas en la vertiente Atlántica de la costa Francesa, incluida en golfo de Vizcaya, ya que están sometidas a condiciones similares que las plumas Ibéricas del Océano Atlántico. En esta zona destacan las plumas formadas por los ríos Loira y Gironda, que en su conjunto proporcionan más del 75% de la descarga total en el golfo de Vizcaya (Lazure et al., 2009). El uso de MODIS para analizar la variabilidad de estas plumas constituye un paso importante debido a las dificultades encontradas en estudios previos para analizar un área tan grande durante largos periodos de tiempo mediante otras metodologías como la simulación numérica o datos *in situ*. Además, la metodología desarrollada se amplió para conocer la influencia que ejercen los principales patrones de teleconexión del Océano Atlántico, *Oscilación del Atlántico Norte* (NAO) y el *Patrón del Atlántico Este* (EA) sobre la dinámica de estas plumas.

Finalmente se analizó la influencia de las plumas formadas por los ríos Loira y Gironda sobre la temperatura del mar. La mayor extensión de estas plumas, en comparación con las plumas Ibéricas, sustenta el uso de bases de datos con menor resolución espacial, la cuales permiten analizar las propiedades termohalinas del agua oceánica. Para ello se complementó MODIS con datos de temperatura superficial del agua de la base *NOAA $1/4$ daily Optimum Interpolation Sea Surface Temperature* (OISST $1/4$), y datos de temperatura y salinidad en profundidad obtenidos de la base IBI. Como se ha comentado anteriormente, la influencia de los ríos en las propiedades del agua costera puede hacer

que la evolución de los patrones de temperatura sean diferentes respecto al agua oceánica adyacente. En el actual contexto de calentamiento global el análisis y comprensión de estos sistemas capaces de incrementar o incluso revertir esta tendencia es de vital importancia.

El trabajo de investigación desarrollado durante la realización de la Tesis Doctoral se estructuró en este manuscrito de la siguiente manera:

El capítulo 1 recoge la introducción general acerca de las plumas fluviales, su definición, sus características principales y los principales métodos disponibles para su estudio. También detalla la importancia socio-económica de las principales plumas de la Península Ibérica y de la costa Atlántica Francesa que las hacen susceptibles de estudio y recopila toda la información disponible sobre estudios previos. Finalmente, se describen las características de los principales ríos analizados y sus áreas de influencia

El capítulo 2 describe todas las bases de datos utilizadas, así como la metodología general desarrollada para lograr los objetivos planteados.

El capítulo 3 analiza en profundidad la pluma formada por el río Ebro en la vertiente Mediterránea de la Península Ibérica. Se optó por comenzar analizando la pluma formada por este río ya que el mar Mediterráneo tiene un régimen micro-mareal, y por lo tanto la marea no afecta prácticamente al desarrollo de la pluma. De esta forma la pluma del Ebro representa una buena opción para analizar el efecto de la descarga fluvial y el viento aislados de la influencia mareal. Para ello se evaluó como las variaciones de la descarga fluvial condicionan el desarrollo de la pluma, así como el impacto del viento a través de sus direcciones principales (viento soplando a lo largo de la costa o perpendicular a ella). Además, esta pluma está sometida a la influencia de una fuerte corriente que fluye hacia el suroeste en su área de desarrollo, la corriente Liguro-Provençal (LPC), por lo que también se analizó su impacto sobre la dinámica de la pluma. Como principales conclusiones se obtuvo que la descarga fluvial es el forzamiento principal, con la extensión de la pluma variando casi monótonamente con el caudal del río. El viento es un forzamiento secundario el cual ejerce una influencia especialmente destacable cuando la pluma se encuentra suficientemente desarrollada (condiciones de descarga elevada). La extensión máxima de la pluma se produce con caudales elevados y vientos del noroeste (viento Mistral), que soplan hacia el océano. Sin embargo, la influencia de la LPC es muy destacable ya que independientemente de las demás condiciones, más del 70% de la pluma se encuentra hacia el sur de la desembocadura.

El capítulo 4 analiza en profundidad la pluma turbia formada por el río Duero, el más importante de la Península Ibérica en términos de caudal. En este caso, se incorpora un forzamiento a mayores respecto al Ebro, la marea, ya que el régimen meso-mareal del Atlántico hace que la pluma esté afectada por el ciclo semi-diurno de mareas. Por lo tanto en este capítulo se da un paso más en el análisis y conocimiento de la respuesta de las plumas Ibéricas ante los forzamientos que las afectan. Además de estudiar la influencia

de la descarga del río y los vientos en la pluma de forma similar al capítulo anterior, se analizó el estado de la pluma ante situaciones de marea alta y baja. En líneas generales se observó que el río Duero solo es capaz de desarrollar la pluma cuando tiene caudales elevados, lo que hace que la descarga fluvial sea el factor principal. El viento juega un papel clave cuando la descarga es elevada, favoreciendo el transporte del material hacia el océano en caso de vientos favorables al afloramiento o vientos que soplan hacia el mar, lo cual es especialmente significativo en la zona que está alrededor de la desembocadura, donde una protuberancia en forma semicircular se observa claramente bajo ambas condiciones. Por el contrario, los vientos desfavorables al afloramiento y los vientos que soplan hacia costa tienden a dificultar el transporte del material hacia el océano, acumulándolo cerca de costa. En cuanto al efecto del ciclo semi-diurno de la marea, que también fue evaluado bajo descargas elevadas para asegurar pluma suficiente para analizar su efecto, se observó que la pluma alcanza una mayor extensión con unos valores turbios más intensos en condiciones de marea baja. Esto es debido a que la marea alta restringe la salida de material hacia el océano. Sin embargo, las diferencias en el estado de la pluma provocadas por el ciclo semi-diurno de mareas son pequeñas en comparación con los cambios promovidos por los otros factores de forzamiento (descarga fluvial y viento).

El capítulo 5 analiza en profundidad la pluma turbia formada por el río Tajo, el más largo de la Península Ibérica. Este río presenta peculiaridades importantes respecto a los ríos analizados anteriormente. Por un lado, vierte al océano dentro de una bahía semi-encerrada que puede limitar el efecto del viento en la pluma. Además, presenta uno de los estuarios más grandes de Europa antes de llegar al océano Atlántico, lo cual va a tener implicaciones importantes en el desarrollo de la pluma debido al gran tiempo de residencia del agua dentro del estuario. Una de ellas será que el ciclo quincenal de mareas (ciclo vivas-muertas) también va a influir en el desarrollo de la pluma, cuyo efecto es despreciable en ríos que vierten directamente al océano, como es el caso del Duero. Como principales conclusiones se obtuvo que la descarga del río es el forzamiento principal, aunque existe pluma incluso con caudales bajos debido a las características del Estuario. Además, la pluma del Tajo tarda 2 días en responder a cambios en el caudal debido al tiempo de residencia del Estuario, a diferencia del Ebro y el Duero, en los que el desarrollo de la pluma está en fase con las variaciones de caudal debido a que vierten directamente al océano. La respuesta de la pluma ante el viento es similar al caso del Duero, aunque con ciertas limitaciones debido al efecto de desembocar en el océano dentro de una bahía semi-encerrada. Esta configuración costera limita el impacto de los vientos del norte (favorables al afloramiento) e impide que la pluma forme una banda costera hacia el norte cuando el viento sopla del sur (vientos desfavorables al afloramiento), ya que presenta una barrera geológica que impide el movimiento de la pluma en esa dirección, constatando como las características geomorfológicas de cada área también ejercen un impacto importante en el desarrollo de la pluma. En cuanto al ciclo semi-diurno de mareas, la pluma es más extensa cuando la marea es baja, con diferencias respecto al estado en marea alta mayores que en el caso del Duero. Además, se observa una mayor

extensión de la pluma con condiciones de mareas vivas debido a la mayor cantidad de material exportado desde el estuario con respecto a condiciones de mareas muertas.

El capítulo 6 compara el comportamiento de las plumas entre sí, con el objetivo de encontrar patrones comunes y diferentes provocados por los forzamientos principales, analizando las causas que conducen a ellos. Además, analiza el nivel de impacto de cada forzamiento en cada pluma. Para cubrir las plumas más importantes de la Península Ibérica, en este capítulo se añadieron las formadas por los ríos Miño, Guadiana y Guadalquivir. Como conclusiones generales se obtuvo que las plumas formadas por los ríos que presentan un gran estuario antes de desembocar en el océano (Tajo y Guadalquivir) tienen un cierto desfase respecto la descarga del río. Sin embargo, la descarga fluvial es el factor dominante para todas las plumas, siendo la dependencia de la extensión de la pluma moderada o alta para todos los ríos analizados excepto para el Ebro. La dependencia de la pluma respecto al viento es moderada o alta para todos los ríos excepto Guadalquivir y Ebro. Además, todos los ríos de la vertiente Atlántica alcanzan su mayor extensión cuando el viento sopla hacia costa y la mínima con vientos soplando hacia el mar. El Ebro alcanza su extensión máxima y mínima en las situaciones contrarias, lo cual es en parte debido a la influencia de la corriente Liguro-Provençal. Por último, el ciclo semi-diurno de mareas afecta a todas las plumas Atlánticas, que alcanzan una mayor extensión en condiciones de marea baja, aunque la dependencia de la pluma respecto al ciclo semi-diurno de mareas es solamente alta para el Guadiana. En cuanto al ciclo quincenal, se observó que solo afecta significativamente al Tajo, siendo despreciable su efecto en los otros ríos. La pluma del Tajo es mayor en situaciones de marea viva. La pluma del Ebro no se ve afectada por ninguno de los ciclos de marea debido al régimen micro-mareal del Mediterráneo.

El capítulo 7 analiza el comportamiento de las plumas más importantes formadas en la costa Atlántica de Francia (Loira y Gironda) ante los forzamientos principales, prestando atención también al efecto de los principales patrones de teleconexión del Atlántico Norte (NAO y EA) sobre su desarrollo. En líneas generales se observó un comportamiento similar a las plumas Ibéricas formadas en el Océano Atlántico, ante la influencia de los forzamientos principales (descarga fluvial y viento). Respecto a los índices de teleconexión, se observó y cuantificó que las plumas son más grandes cuando los patrones EA y NAO están en su fase positiva. Además, en este caso, también se evaluó el impacto de estas plumas sobre las propiedades termohalinas del agua. Se observó como las propiedades termohalinas siguen dinámicas diferentes en la zona costera ocupada por la pluma y en el océano adyacente. En particular, estos ríos mantienen la estratificación invernal en el área ocupada por la pluma, lo que provoca además que la evolución de la temperatura siga patrones diferentes en ambas zonas. En concreto, se observó como en la zona ocupada por la pluma formada por ambos ríos hubo una tendencia al enfriamiento en los meses de invierno (Diciembre-Febrero) durante las últimas tres décadas, que fue especialmente intensa en la última década, lo que contrasta con la tendencia al calentamiento observada en el resto del Golfo de Vizcaya.

Abstract

A river plume can be defined as a water mass with different properties than surrounding ocean water, in terms of salinity, temperature, composition and color, due to the influence of a river discharge. This is because river inputs provide fresh water, nutrients, sediments, organic and inorganic material and/or contaminants, among others, into the ocean, modifying the physical, chemical and biological conditions of the coastal areas under influence. Therefore, plumes play a key role in the affected areas, and hence, the importance to characterize and improve the knowledge on plume dynamics.

Plume spreading into the ocean is affected by several forcing, including outflow inertia, rotation force (Coriolis), buoyancy, wind, tides, coastal currents, and in addition, the coastal configuration of each area. Therefore, although some patterns of behavior are common to most plumes, each system can behave different being necessary to analyze each river plume.

Salinity is one of the best natural tracers, however it is difficult to sense at useful spatial and temporal scales taking into account that river plumes are characterized by a fine spatial structure able to change rapidly. As alternative, ocean color imagery, as MODIS data, supposes a very useful tool to river plumes studies due to the high spatial and temporal resolution provided. Ocean color imagery detects a strong signal in the area occupied by the material discharged by the river (turbid plume) whereas the ocean waters not affected by the river discharge have negligible contributions, which allows delimiting the river plume.

Turbid plumes formed by the main Iberian Rivers were analyzed and compared, in order to determine similarities and differences among them. Five Atlantic Rivers (Minho, Douro, Tagus, Guadiana and Guadalquivir) and one Mediterranean River (Ebro) were considered. Plumes dynamic was evaluated through synoptic patterns obtained by means of MODIS imagery. Composite images were constructed averaging those days characterizing each driving force in order to obtain the mean plume state under each forcing. Then, the study was expanded to analyze the most important plumes formed in the Atlantic coast of France (Loire and Gironde plumes), which are subjected to similar conditions to those plumes formed in the Atlantic coast of Iberian Peninsula. The influence of the most important teleconnection indices on these plumes was also evaluated. In addition, the greater extension occupied by these plumes in comparison with Iberian ones supports the use of other databases with coarse spatial resolution which allow analyzing the impact of these plumes on the thermohaline properties of seawater (IBI and $OISST_{1/4}$ databases).

River discharge showed to be the main forcing affecting Iberian plumes. In fact, the dependence of plume extension on runoff is moderate or high for all rivers, except for Ebro. In addition, most of river plumes adapt immediately to river discharge variations.

Only the extension of Tagus and Guadalquivir plumes is lagged respect to river runoff, due to the high residence time promoted by their large estuaries.

Wind is a secondary forcing on Iberian plumes, being noticeable under high river discharges. The dependence of plume extension on wind is moderate or high for all rivers, except Guadalquivir and Ebro. All the Atlantic Rivers show the maximum (minimum) plume extension under landward (seaward) cross-shore winds. The opposite situation was observed for the Ebro River.

Tide is also a secondary forcing on Iberian plumes although less important than wind. All Atlantic River plumes still have some dependence on semidiurnal tidal cycle, increasing their extension under low tides and decreasing under high tides. However, the dependence of plume extension on tide is only high for Guadiana River. In addition, Tagus River plume is also dependent on the fortnightly tidal cycle being larger during spring tides than during neap tides. This is due to the particular shape of the estuary, where the river debouches into a semi-enclosed embayment connected to the Atlantic Ocean through a strait.

Ebro River constitutes a particular case since it has a low dependence on runoff and wind and a negligible dependence on tide. In fact, its plume is mainly driven by the Liguro-Provençal coastal current flowing to the southwest. Guadalquivir River also shows some unique features due to its high sediment load. It generates the largest Iberian plume in terms of turbid signal and extension even being the second smallest river in terms of discharge.

French Atlantic turbid plumes show a similar behavior than Iberian plumes formed in the Atlantic Ocean. River discharge is the main forcing with wind having a noticeable effect when plumes are well developed. Plumes also reach the maximum extension under landward winds. In addition, a larger extension was reached under positives indices of EA and NAO patterns. Thermohaline properties differed inside and outside the area affected by both rivers. In particular, these rivers maintain winter stratification inside the turbid plume, which results in a different warming rate when compared with the adjacent ocean. In fact, cooling was detected in the area occupied by the plume whereas the adjacent oceanic area warms.

Table of Contents

Chapter 1:

Introduction

1.1. River plumes

1.1.1. Definition and implications on ecosystems

River plumes are formed in the oceanic areas near river mouths due to freshwater and suspended material discharged by rivers, which can include nutrients, sediments, organic and inorganic compounds and contaminants, among others. These inputs provoke a different behavior and characteristics between water affected by river discharge (plume area) and oceanic surrounding water. Therefore, a river plume can be defined as the water mass around a river mouth with different properties (salinity, temperature, composition, and/or color) than the surrounding oceanic water due to river discharge influence.

River plumes suppose the major source of transference from land materials to coastal ocean, playing a key role in the ecology and morphodynamics of the affected areas, modulating their geological and biogeochemical characteristics (Turner and Millward, 2002; Körtzinger, 2003; Dagg et al., 2004). As main important features, river plumes affect the stratification (Zavialov et al., 2003; Santos et al., 2004) and flow circulation patterns, since in these areas the circulation is primary governed by differences of density due to the interaction between fresh and salt water (Uncles, 2002). These density differences promote the formation of plume jets of rapid transport, convergences and trapping at frontal boundaries on the edges (deCastro et al., 2006). In addition, the large amount of terrestrial nutrients provided by river discharge sustains high levels of phytoplankton biomass enhancing the primary coastal productivity, which promotes a

cascading effect over other ecosystems (Le Fèvre and Frontier, 1988; Ribeiro et al., 2005). River plume constituents also affect the life cycle of fish and shellfish species, acting as dispersion or retention zones affecting their abundance (Grimes and Kingsford, 1996; Wilber and Clarke, 2001; Le Pape et al., 2003; Schiller et al., 2011). Sediments carried by plumes have important implications affecting light attenuation, a critical issue of phytoplankton grow and primary productivity (May et al., 2003; Huret et al., 2007; Xu et al., 2011) as well as erosion-sedimentation processes in coastal areas since transport most of the particulate materials entering the ocean (Warrick and Milliman, 2003; Dagg et al., 2004). River discharge into the ocean can also imply the transport of pollutants affecting the quality of coastal waters (Uncles et al., 1988; Reifel et al., 2009). In addition, anthropogenic perturbations occurred in river basins lead to a considerable eutrophication of coastal areas under plume influence (Turner and Rabalais, 1994; Wang, 2006). By last, it is an undeniable fact that ocean temperature has increased worldwide since mid-20th century (Belkin, 2009; Levitus et al., 2012). Nevertheless, some coastal phenomena, as the presence of rivers inputs, can promote different warming trends or even induce cooling patterns in seawater, playing a key role as modulator of global change (Howden and Murtugudde, 2001; Vizy and Cook, 2010; Park et al., 2011; Materia et al., 2012).

1.1.2. General description

The plume development into the ocean can occur in different ways. In general, plume influence into the ocean is decomposed in three interacting components: the estuary, the near-field region and the far-field region (Garvine, 1982; Hetland, 2005). The estuary and the near field region are characterized by an intense mixing of fresh water and salt water, and it is the area where the river-runoff control is more effective and the contrast with ambient ocean water is larger. The far-field region is where the final merge of source water with the ambient water occurs, both presenting similar conditions.

Each river plume presents unique features influenced by several factors as outflow inertia, buoyancy forcing, rotation (Coriolis) effects, wind stress, tide, oceanic currents or coastline morphology (Fong and Geyer, 2001; Walker et al., 2005; Lentz and Largier, 2006; Valente and da Silva, 2009; Sousa et al., 2014a). However, although there are several factors able to affect plume development, typical features characterize most of river plume systems. First, plumes tend to spread radially from river mouth forming an anticyclonic bulge with a plume deflection to the right in the Northern Hemisphere due to Coriolis force, and then feed a buoyant coastal-attached current flowing in the direction of the Kelvin wave propagation (Yankovsky and Chapman, 1997; Fennel and Mutzke, 1997). This is the classical view in the absence of other forcing.

If wind is considered, it also affects plume structure (Fennel and Mutzke, 1997; Chao, 1998; Choi and Wilkin, 2007). Alongshore winds produce plume displacement due to Ekman transport, which in combination with Earth's rotation, induces movement of plumes offshore (upwelling) or onshore (downwelling) (Fong and Geyer, 2001; Alvarez

et al., 2008; Jurisa and Chant, 2012). Cross-shore winds affect the cross-shelf circulation and, therefore, plume movement, favoring (or limiting) its dilution in seawater (Chao, 1998; Choi and Wilkin, 2007; Lentz and Fewings, 2012). Tide is also an important constraint factor on plume dynamics when its range is noticeable (Vaz et al., 2009). In general terms, the high phase of the semidiurnal cycle limits plume formation (Vaz et al., 2009). Moreover, the spring-neap tidal cycle can generate changes in the concentration of suspended material within the plume, with maximum turbidity values usually occurring during spring tides (Valente and da Silva, 2009; Vaz et al., 2011).

Horner-Devine et al. (2015) summarized the six plume morphologies most observed around the world attending to different factors and forcing conditions: the prototypical, nonrotational, wide estuary, angled inflow, delta and friction plumes.

Prototypical plumes are characterized by a relatively high discharge and a narrow mouth, with the dynamics strongly affected by Earth's rotation. Examples of this type of plumes are the Columbia plume (Hickey et al., 2010) or the Hudson plume (Chant et al., 2008).

The nonrotational plumes are characterized by the slightly impact of Earth's rotation due to rivers mouths are located close to the equator, as for example the Amazon plume, (Molleri et al., 2010) or the discharge is very small, as for example the Teign plume (England) (Pritchard and Huntley, 2006).

Wide estuary plumes not form a bulge in front of river mouth because have a wide mouth enough to separate freshwater to one side of the estuary induced by Earth's rotation. These plumes are showed as a geostrophic coastal current. Chesapeake plume is an example of this configuration (Dzwonkowski and Yan, 2005; Whitney and Garvine, 2005).

Angled inflow plumes not shown a bulge in their spreading because the inflow is at a small angle to the coast, which drives the direction of plume propagation. As example, the Eel plume (United States) (Geyer et al., 2000).

Delta plumes consist in the exit of river water along several channels, having multiple interacting regions since plume formed by each channel can influence other channel. Mississippi is an example of this type of plumes (Walker, 1996).

In the friction plumes the interaction with the bottom is important and controls the plume development. This type of plumes is usually formed in shallow marginal seas. An example, the Rhine plume (Simpson et al., 1993).

Therefore, in spite that some characteristics can be common, each plume system presents unique features and, hence, must be individually studied.

1.2. River plumes tracking

Salinity is one of the best natural tracers for river plumes, but to date it cannot be sensed at useful spatial and/or temporal scales. For example, buoys and ships measurements are

limited in terms of spatial and temporal resolution, respectively. Surface salinity can be also sensed by means of remote sensing (such as the Soil Moisture and Ocean Salinity (SMOS) mission from European Space Agency (ESA) or the Aquarius mission from National Aeronautics and Space Administration (NASA)), however the spatial and temporal resolution are not enough for mapping the main features of river plumes, which are characterized by a fine-spatial structure able to change rapidly. Models simulating ocean water salinity near the river mouths represent another option to study river plumes. However, in spite of the models validation, it should be taking into account that modelling supposes an approximation to the real ocean behavior. As alternative, several authors have demonstrated a good relation between surface salinity and the characteristic ocean color matter originated from fresh water runoff, which can be remotely measured at useful spatial and temporal scales (Binding and Bowers, 2003; Dzwonkowski and Yan, 2005; Thomas and Weatherbee, 2006; Palacios et al., 2009; Saldias et al., 2012). The suspended material carried by river discharge results in a strong signal detected by satellite sensors whereas ocean clear waters have negligible contributions (Otero and Siegel, 2004; Nezlin et al., 2005, Wang et al., 2007; Petus et al., 2014). Therefore, most of rivers worldwide shown a good correlation between the area influenced by freshwater (salinity plume) and the area occupied by the suspension and dissolved material (turbid plume) both induced by river discharge (Saldias et al., 2012; 2016a). Although the area occupied by the plume is very coincidental using both definitions, could exist some differences in the frontal region that should be put into context (Hu et al., 2003; Saldias et al., 2012; 2016b). However, the turbid plume is the definition which presents a major impact and importance in ocean water because represents the area more affected by river discharge. Turbid plume is the region with greater salinity differences respect to open oceanic areas and where the suspended and diluted material plays a key role, provoking most of the implications commented above (Walker, 1996; Turner and Millward, 2002; Zheng et al., 2015). Beyond the turbid plume, the ocean water can still be characterized by lower salinities but there is not suspension material, therefore river impact is much smaller.

Thus, ocean color remote sensing data, such as data from the Moderate Resolution Imaging Spectroradiometer (MODIS), have been successfully tested in numerous studies worldwide for the analysis of turbid plumes, becoming a very useful tool to perform synoptic plume studies due to the high spatial (1 km or less) and time (daily) resolution provided. As examples: Danube plume (Güttler et al., 2013), plumes in the Bay of Biscay (Petus et al., 2010; 2014), the Chesapeake plume (Dzwonkowski and Yan, 2005), Mississippi plume (Miller and McKee, 2004; Walker et al., 2005; Shi and Wang, 2009), Southern California plumes (Nezlin et al., 2005; Lahet and Stramski, 2010), Columbia plume (Thomas and Weatherbee, 2006; Palacios et al., 2009), Amazon plume (Kilham and Roverts, 2011), plumes off central Chile (Saldías et al., 2012), plumes in the eastern coastal region of China (Wang et al., 2007), Congo plume (Hopkins et al., 2013), among others.

1.3. State of the art

Few researches were developed using MODIS data to study river plumes in the Iberian Peninsula (Figure 1.1). The majority of these studies were performed under limited time periods and individual plumes in order to assess very particular situations. Arnau et al. (2004) used MODIS imagery to evaluate Ebro plume state under specific conditions lasting just a few days (as flooding events) and Valente and da Silva (2009) analyzed fortnightly cycle influence on Tagus River plume using three years of MODIS imagery (2003-2005). MODIS ocean color data were also used to analyze punctual days to act as complement of numerical models in order to test their accuracy for the study of river plumes in the oceanic region of Basque Country (Ferrer et al., 2009) and in the NW coast of Iberian Peninsula (Mendes et al., 2016). Caballero et al. (2014) also used MODIS data for punctual days in order to test similar parameters provided by other satellite sensors in Guadalquivir plume.

Figure 1.1. Example of true-color MODIS-Aqua imagery of the Iberian Peninsula. Credit: Jeff Schmaltz, MODIS Rapid Response Team, NASA/GSFC. Plumes can be identified by the high sediment load.

However, several researches were developed using alternative methodologies to analyze Iberian plumes dynamics, showing the great importance of these plumes for the scientific community:

Most of studies related to Minho plume were centered in the analysis of its capacity to reach the Rias Baixas (located north of Minho River mouth). For that, Minho plume was evaluated under river discharge and wind conditions promoting its dispersion to the north using *in situ* data during 1998 (Alvarez et al., 2006), and the MOHID numerical model simulating typical forcing situations lasting some days (Sousa et al., 2014a; b). These

studies revealed that the greater impact of Minho plume on Rias Baixas occurs under high discharges and southerly winds.

Douro plume size was delimited by Teodoro et al. (2009) and Gonçalves et al. (2012) using 20 images during 2005 and 71 during 2009 from the Medium Resolution Imaging Spectrometer (MERIS), showing that plume is only noticeable under river discharges exceeding 400 m^3s^{-1}. However, most of the studies related to Douro plume were centered in the impact of alongshore winds, which can lead in a net exportation (under upwelling conditions) or confinement (under downwelling conditions) of the plume. These studies were performed by means of: in *situ data* from 5-7 September 1998 complemented with data from the Advanced Very High Resolution Radiometer (AVHRR) for the period August-September 1998 (Peliz et al., 2002); the Regional Ocean Modelling System (ROMS) with real forcing and climatologic data during 3 months (Otero et al., 2008); or complementing ROMS with *in situ* data from December 2009 to January 2010 (Otero et al., 2013). They found that under high discharges and downwelling wind conditions, Douro plume can reach the Minho plume forming the Western Iberian Buoyant Plume (WIBP) in concordance with Mendes et al. (2016), who analyzed the WIBP formation under representative winter conditions during January and February 2010.

Main studies about Tagus plume analyzed its response under wind and tide forcing using the MOHID model. Vaz et al. (2009) reveal the offshore expansion of the plume under north (upwelling) winds considering the river discharge and wind forcing occurring in January 2007. Vaz et al. (2011) concluded that suspended sediments and salinity gradients vary according to the semidiurnal tidal cycle, evaluating the conditions occurred from 2008-2009. In addition, they also found that spring tides induce most amount of sediment than neaps, resulting in a greater plume. This pattern was also observed by Valente and da Silva (2009) through MODIS imagery over the period 2003-2005.

Cravo et al. (2006) collected water samples from the spreading area of the Guadiana plume for three consecutive winters (1999-2001). They found maximum concentrations of suspended particulate and minimum salinity values near the river mouth, decreasing both gradually toward the ocean. They also observed a river regulated plume, presenting a considerable impact in the adjacent ocean when river discharge is high and with a scarcely development under low discharges. Once plume is developed its movement follows the prevailing wind direction.

Guadalquivir plume was analyzed using eight daily scenes obtained from DEIMOS-1 sensor, which measures the Total Suspended concentrations (TSS) (Caballero et al., 2014). The images selected represent the autumn-winter and spring-summer conditions between 2010 and 2011. They observed a plume forming a semicircular pattern when spreads over the ocean, showing a most consistent pattern when river discharge is high.

Sierra et al. (2002) through *in situ* data obtained from two field campaigns during spring and summer 1997 and Mestres et al. (2003) by means of the TRIM3D hydrodynamic model combined with field data campaigns in July 1999 and February 2000, showed that

the spreading of the Ebro plume near mouth is dependent on the river discharge and the wind forcing. Tide scarcely affects Ebro plume due to the micro-tidal environment of the region. Xing and Davies (1999) analyzed Ebro plume displacement through a 3D numerical model for typical forcing situations lasting few days. They observed that Ebro plume shows a characteristic bulge near mouth being displaced to the south due to an anticyclonic gyre together with a southward alongshore flow. The predominant southward movement of Ebro plume was corroborated by Arnau et al. (2004) through satellite imagery. Xing and Davies (1999) also analyzed wind influence on Ebro plume. Southerly (upwelling) winds promote the offshore spreading of the plume whereas northerly (downwelling) winds retain the plume to the coast due to the onshore associated currents. Xing and Davies (2002) analyzed the influence of the main wind regime, the Mistral (northwesterly) wind, on plume displacement by means of a 3D numerical model. They found that Mistral wind favors the offshore displacement of the Ebro plume but maintaining its predominant southward spreading.

Plumes formed in the north coast of Iberian Peninsula are smaller in comparison with the plumes commented above, but some researches analyzed some features of them. González-Nuevo and Nogueira (2014) studied the variability of plumes formed in the North Iberian shelf using data acquired in 20 cruises between 1987 and 2007. They found that the annual variability of these plumes is associated to the precipitation and the river runoff of each area. Ferrer et al. (2009) found that plumes formed in this area are also conditioned by the wind-induced currents, combining field data of buoys, model results and satellite imagery for March 2007.

Several authors were also interested in analyzing the plumes formed in the French Atlantic coast, very close to the Iberian Peninsula and subjected to similar conditions and characteristics to those of the Atlantic Iberian coast. In spite of some rivers flow into the French Atlantic coast, most important plumes are formed by Loire and Gironde discharges, since provide more than 75 % of total runoff into the Bay of Biscay (Lazure et al., 2009). Historically, the study of these plumes has been an arduous task due to the inherent difficulties to sampling a wide area over long time periods. Thus, most of the studies were mainly based on punctual sampling and cruises during short periods or using coarse spatial resolution models. Koutsikopoulos and LeCann (1996) by means of punctual samplings, and Lazure and Jegou (1998) using a 3D numerical model over 7 years (1990-1996) combined with *in situ* data, analyzed Loire and Gironde plumes dynamic. They found that under high discharge conditions, both plumes can merge forming a great plume occupying most of the French Atlantic shelf, due to the synchronisms of both rivers. In addition, they shown that although Loire and Gironde plumes are usually oriented to the NW due to Coriolis effect, their development is mainly driven by the variability of river discharge and wind stress. In fact, the NW predominant orientation of plumes can change after large periods of winds with north component (Koutsikopoulos and LeCann, 1996; Lazure and Jegou, 1998). In general terms, greater plumes are formed during winter months due to maximum river discharges with smaller plumes during summer. The seasonality of wind pattern also influence Loire and Gironde

plumes movement. A northward movement of plumes with a development near coast is induced during autumn and winter by the predominant southwesterly winds whereas during spring and summer the prevailing northwesterly winds spread the plume material seaward since promote conditions favorable to upwelling (Lazure et al., 2009). Puillat et al. (2004; 2006) studied the inter-annual thermohaline variability along the French continental shelf by means of 25 cruises carried out over the period 1992-2000 and 8 cruises during 1997-2000. They found that salinity patterns present a marked seasonal variability provoked by Loire and Gironde discharges, diminishing the salinity values in seasons when discharges are high. In addition, wind stress is able to influence the location of the lenses of low salinity provoked by rivers discharge, which follow the predominant wind direction, according to previous studies commented above. Kelly-Gerreyn et al. (2006) analyzed the northward movement of low salinity intrusions over the period 2002-2004 by means of ships of opportunity, observing as freshwater from Loire and Gironde plumes can reach latitudes of 50.7º under the favorable conditions of high discharge and winds with a south component.

Although most of the studies related to plumes dynamic along the French Atlantic continental shelf are about Loire and Gironde plumes, some authors also analyze other smaller plumes formed in this area. Petus et al. (2010; 2014) analyzed the Adour River plume, formed south of Gironde mouth, by means of MODIS-Aqua images obtained from 2006 to 2010. They found a plume dynamic mainly controlled by the variability of river discharge and the orientation and strength of wind, following a similar pattern to the Loire and Gironde plumes.

The majority of studies related to plumes in this area were interested on Loire and Gironde plumes dynamic, as commented above, however some researches were developed in order to analyze the influence of these plumes on oceanic parameters, as temperature. Related studies showed that these plumes can impact the temperature dynamic of the affected area, causing a different behavior than in the rest of the Bay of Biscay. For example, Koutsikopoulos and Le Cann (1996) observed thermal inversions due to freshwater inputs during winter by means of punctual samplings, showing the Loire and Gironde plumes influence on temperature. Puillat et al. (2004; 2006) also observed the influence of these plumes on thermal stratification of the water column, which can imply a different behavior of temperature patterns respect to the rest of the Bay of Biscay. The plume influence on temperature patterns is especially important taking into account that previous studies showed a clear warming trend along the rest of the Bay (Planque et al., 2003; Llope et al., 2006; Fontán et al., 2008; Gómez-Gesteira et al., 2008; deCastro et al., 2009; Goikoetxea et al., 2009; García-Soto and Pingree, 2012; Costoya et al., 2015), whose intensity is dependent on temporal and spatial scales. The possibility of these plumes to modulate the warming observed in the rest of the Bay of Biscay has a key importance in the actual context of global warming.

1.4. Study areas

1.4.1. Iberian Peninsula Rivers

The Iberian Peninsula is located in the North Atlantic Ocean, Southwestern Europe, under the national jurisdiction of Portugal and Spain. It is delimited north by Cantabrian Sea and France, west-southwest by the Atlantic Ocean and southeast-east by the Mediterranean Sea. Iberian Peninsula (including the continental shelf) is enclosed in the area to the south of 44ºN and to the north of 36ºN. The western limit is defined by 11º W and the eastern limit by 4º E (Figure 1.2). The Iberian continental shelf is characterized by an extension between 15 and 70 km in the Mediterranean Sea and NE-SW orientation. In Bay of Cadiz, in Atlantic Ocean, continental shelf has an extension of about 50 km forming an arc with a SE-NW orientation. The west continental shelf of Iberian Peninsula, in the Atlantic Ocean, is slightly broader than 50 km widening northward, with a marked S-N orientation. The continental shelf suffers a narrowing at Cantabrian Sea decreasing to 15 km with a marked W-E orientation (Figure 1.2). The Iberian Peninsula coast is a rich environment with high primary production that supports important socio-economic activities as tourism, fishing and aquaculture, among others, resulting fundamental for the economy of these areas. Usually, these activities are developed near the mouth of the most important rivers, namely, in the development area of their plumes. The main Iberian Rivers are: Minho, Douro, Tagus, Guadiana, Guadalquivir and Ebro. The most important implications of plumes formed by these rivers are described below.
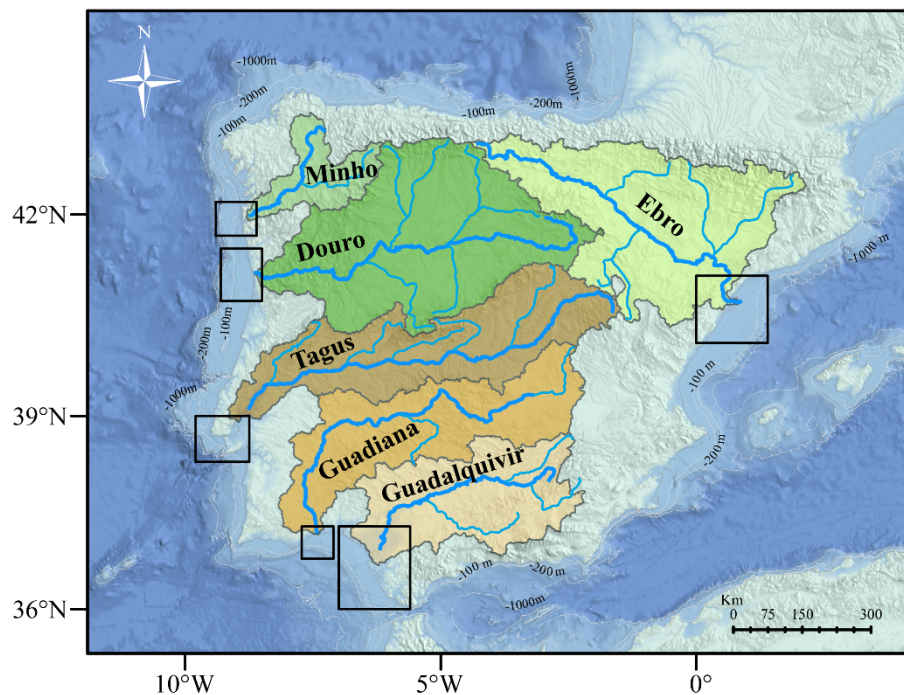
Figure 1.2. Location of main rivers and their catchment areas in the Iberian Peninsula. Empty squares indicate the area defined to evaluate each turbid plume.

Minho River:

The Minho River flows in the northwest corner into the Atlantic Ocean, acting as natural border between Spain and Portugal (Figure 1.2). It has a length of about 350 km from Serra de Meira (Lugo, Spain) to La Guardia (Spain) - Caminha (Portugal), with a catchment area of approximately 17,000 km^2 and an average flow of about 350 m^{3}s^{-1} (OSPAR Commission, 2000). Minho Estuary extends 40 km inland (Dias et al., 2002). Minho River mouth is located 30 km south of the Rias Baixas, which are characterized by a high primary production associated to upwelling events (Tenore et al., 1995). As example, the production of mussels per year in this area can reach 250,000 t, which suppose around 15% of world production. Therefore, its economy is mainly supported by fisheries, aquaculture, fishing industry and tourism. Under some conditions Minho plume can reach and even moves into the Rias Baixas, reversing the normal circulation and the biochemical patterns, influencing the production of this area. On the one hand, if the plume just reach the Rias, can revert the circulation pattern and increases the residence time, by the other hand, if plume moves into the Rias, can contribute to fertilize the area (Alvarez et al., 2006; deCastro et al., 2006; Sousa et al., 2014a). Minho River is the secondly main contributor to the Western Iberian Buoyant Plume (WIBP).

Douro River:

The Douro River flows in the northwest into the Atlantic Ocean (Figure 1.2). It has a length of about 930 km from Picos de Urbión (Soria, Spain) to Porto (Portugal), with a catchment area of approximately 98,800 km^2 and an average flow of about 700 m^{3}s^{-1} (OSPAR Commission, 2000). Douro Estuary is limited inland by Crestuma dam, decreasing its length from 35 to 21 km. According to Dias (1987) Douro River is the major contributor to fluvial sediments in the NW Iberian coast (90%), so the variability of its plume is very important in associated processes as erosion (Dias, 1990). Moreover, Douro plume has a great relevance as modulator of the biogeochemical patterns of the NW Iberian coast due to the large amount of terrestrial nutrients transported by the plume into the ocean (Ribeiro et al., 2005), which contribute to increase the primary production (Santos et al., 2004; Prego et al., 2007). Douro River is the main contributor to the WIBP.

Tagus River:

The Tagus River flows in the west into the Atlantic Ocean (Figure 1.2). It has a length of about 1000 km from Albarracín (Teruel, Spain) to Lisbon (Portugal), with a catchment area of approximately 80,000 km^2 and an average flow of about 450 m^{3}s^{-1} (OSPAR Commission, 2000). Tagus River is the main contributor to Tagus Estuary, which is the most important of the Iberian Peninsula and one of the greatest in Western European. It reaches 80 km inland from Lisbon, covering an area of 300 km^2 at low tide and 340 km^2 at high tide (Vale and Sundby, 1987), with a mean volume of 1900×10^6 m^3. These characteristics promote a particular pattern associated with plume development due to the large water residence time in the estuary. In addition, Tagus plume is associated with the retention and dispersion of larvae in the area under influence (Vaz et al., 2015).

Guadiana River:

The Guadiana River flows in the southwest corner into the Atlantic Ocean, acting as natural border between Spain and Portugal (Figure 1.2). It has a length of about 750 km from Villarrubia de los Ojos (Ciudad Real, Spain) to Vila Real (Portugal) - Ayamonte (Spain), with a catchment area of approximately 65,000 km^2 and an average flow of about 180 m^{3}s^{-1} (OSPAR Commission, 2000). Guadiana Estuary extends about 70 km inland. Its mouth is in a prograding phase due to the interaction of coastal processes, sufficient sediment supply and a relatively stable sea level (Morales et al., 2006). Guadiana plume plays a key role controlling the primary production and composition in the Western Gulf of Cadiz, with an important implication in the biogeochemical cycling of nutrients and the structure of the trophic chain in the area, also affecting its ecological balance (Cravo et al., 2006).

Guadalquivir River:

The Guadalquivir River flows in the southwest into the Atlantic Ocean (Figure 1.2). It has a length of about 650 km from Sierra de Cazorla (Jaén, Spain) to Sanlúcar de Barrameda (Cádiz, Spain), with a catchment area of approximately 55,000 km^2 and an average flow of about 230 m^{3}s^{-1} (OSPAR Commission, 2000). Guadalquivir Estuary extends to Alcalá del Río dam 110 km inland and it is an important environmental and socio-economical area. Situated at the estuary mouth are Doñana Natural and National Parks, which are UNESCO-MAB Biosphere Reserve. During the last decades the extension occupied by farmlands and urban settlements has increased in the area (Díez-Minguito et al., 2012), providing more material to carry by river discharge. Guadalquivir plume is a crucial factor for the pelagic ecosystem of the Eastern Gulf of Cadiz since governs the phytoplankton and biological productivity of this area (Navarro and Ruiz, 2006; Caballero et al., 2014).

Ebro River:

The Ebro River flows in the northeast into the Mediterranean Sea (Figure 1.2). It has a length of about 950 km from Fontibre (Cantabria, Spain) to Deltebre (Tarragona, Spain), with a catchment area of approximately 85,000 km^2 and an average flow of about 425 m^{3}s^{-1} (Mestres et al., 2003; Arnau et al., 2004). Ebro River forms a Delta in its mouth, which occupies an area of 320 km^2, with an offshore extension of 27 km, supporting important economic activities. Approximately 77% of the area is dedicated to agriculture and the remainder to natural spaces as beaches, marshes or lagoons dedicated to tourism, hunting and fishing (Sierra et al., 2002). Unlike Atlantic Ocean, tidal regime in the Mediterranean Sea is micro-tidal, scarcely affecting plume development (Mestres et al., 2003). In addition, the regional oceanic circulation is very important in the development area of the Ebro plume. Circulation is dominated by the Liguro-Provençal Current (LPC) (Font et al., 1990), which flows to the southwest at that location. The Ebro plume modulates the sediments, nutrients and contaminants of the Ebro Delta, playing a key role on its development.

The main characteristics of the most important Iberian Rivers: river mouth location, basin extension, river and estuary length, mean river discharge and plume implications on coastal area are summarized in Table 1.1.

River	Mouth Location direction/ocean	Basin (km^2)	River length (km)	Estuary length (km)	Mean discharge (m^{3}s^{-1})	River plume influences
Minho	NW / AO	17,000	350	40	350	- Normal circulation, primary production and biochemical patterns of Rias Baixas.
Douro	NW / AO	98,800	930	21	700	- Coastal erosion processes and biogeochemical patterns.
Tagus	W / AO	80,000	1,000	80	450	- Retention and dispersion of larvae.
Guadiana	SW / AO	65,000	750	70	180	- Primary production and composition in the Western Gulf of Cadiz.
Guadalquivir	SW / AO	55,000	650	110	230	- Pelagic ecosystem and biological and phytoplankton productivity, in the Eastern Gulf of Cadiz
Ebro	NE / MS	85,000	950	27 (Delta)	425	- Sediments, nutrients and contaminants of the Delta.

Table 1.1. Main characteristics of the most important Iberian Rivers. Cardinal points representing mouth location are referred to the Iberian Peninsula. Atlantic Ocean is defined as AO and Mediterranean Sea as MS. Data of rivers were obtained from the OSPAR Commission, (2000) except Ebro River data which were obtained from Mestres et al. (2003) and Arnau et al. (2004).

1.4.2. French Atlantic Rivers

The west coast of France is located in the North Atlantic Ocean, Western Europe, in the eastern limit of the Bay of Biscay. The French Atlantic continental shelf is characterized by a width that varies between 60 km to 160 km widening northward (Figure 1.3), with a N-S orientation to Gironde Estuary and a SE-NW orientation northward. Gironde and Loire Rivers are the most important freshwater inputs into this area, with important implications as will be described below.

Loire and Gironde Rivers:

The Gironde River (Estuary) flows in the southwest of France into the Atlantic Ocean (Figure 1.3) with an average flow of about 1000 m^{3}s^{-1}. Gironde Estuary is the largest in Europe occupying a surface area of 625 km^2 and reaching 80 km inland (OSPAR Commission, 2000). Gironde River is formed by the contributions of Garonne and Dordogne Rivers. Garonne River has a length of about 600 km from Aran Valley, in the Pyrenees (Spain) to the Gironde Estuary, in Bec d´Ambés (Bordeaux, France), with a catchment area of approximately 56,000 km^2 and an average flow of about 650 m^{3}s^{-1}. Dordogne River has a length of about 485 km from the Puy of Sancy, in the mountains of Auvergne (France), to the Gironde Estuary, with a catchment area of approximately 24,000 km^2 and an average flow of about 350 m^{3}s^{-1} (OSPAR Commission, 2000).

The Loire River flows in the west of France into the Atlantic Ocean (Figure 1.3). It has a length of about 1020 km from Mont Gerbier de Jonc, in the Massif Central (France) to Nantes at St Nazaire (France), with a catchment area of approximately 118,420 km^2 and an average flow of about 825 m^{3}s^{-1} (OSPAR Commission, 2000).

The area affected by these plumes has a high socio-economical importance due to supports important economic activities as tourism, shellfish farming, or intensive fisheries (Lazure et al., 2009). In this sense, several studies have shown Loire and Gironde plumes as the preferred spawning area of anchovy and sardine along the French continental shelf (Bellier et al., 2007; Planque et al., 2007).
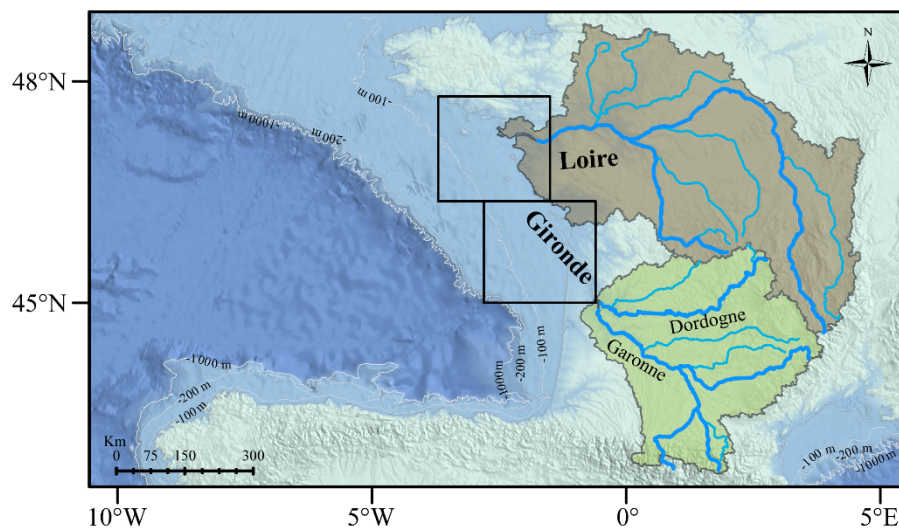
Figure 1.3. Location of the main rivers and their catchment areas in the Atlantic coast of France. Empty squares indicate the area defined to evaluate each turbid plume.

The main characteristics of the most important French Atlantic Rivers: river mouth location, basin extension, river and estuary length, mean river discharge and plume implications on coastal area are summarized in Table 1.2.

River	Mouth Location direction/Ocean	Basin (km^2)	River length (km)	Estuary length (km)	Mean discharge (m^{3}s^{-1})	River plume influences
Garonne	SW / AO	56,000	600	80	650	Support important socio-economic activities.
Dordogne	SW / AO	24,000	485	80	350	
Loire	W / AO	118,420	1,020	60	825	Spawning area of anchovy and sardine.

Table 1.2. Main characteristics of the most important French Atlantic Rivers. Cardinal points representing mouth location are referred to France. Atlantic Ocean is defined as AO. Data of rivers were obtained from the OSPAR Commission, (2000).

1.5. The aim

River plumes are able to modify the physical, chemical and biological characteristics of the coastal areas under influence, playing a key role in the socio-economic conditions of the local communities affected. Therefore, taking also into account the expected effects of climate change and the population increase in these regions, the understanding of plumes dynamic and the prediction of their response under certain conditions, are essential in terms of scientific and socio-economic purposes.

In spite that several studies were performed in order to analyze some characteristics of the Iberian plumes, they only focused on specific features of individual river plumes during particular and usually short time periods. In addition, some of these studies are constrained due to limitations of *in situ* data or the coarse resolution of the numerical models or satellite data employed. Therefore, most of these studies shown some particular behaviors of plumes but without delimit and quantify the plume characteristics (area, turbidity (salinity) ranges, impact degree of each forcing), making an analysis based on qualitative issues. In general terms, the lack of a large spatial and temporal scale analysis, as well as a quantitative evaluation and a comparison between Iberian plumes behaviors under the main forcing, have precluded an in-depth analysis of the dynamics of Iberian plumes.

MODIS data allow analyzing the plumes in a fine scale due to the high spatial and time resolution provided. This allows characterizing the mean state of the plumes under the main forcing, averaged over large time periods (synoptic patterns), which shows the general plume response, not only its situation under specific and time-limited events. Therefore, this methodology allows the analysis and comparison between Iberian plumes, finding common features and highlighting differences among them, evaluating the causes which induce the observed patterns. This is especially important taking into account that despite the relative geographic proximity of Iberian Rivers, plumes can be affected in a different manner by forcing due to regional differences in coastal currents, wave regime or coastal morphology, among others. The obtained results will improve the knowledge and understanding of Iberian turbid plumes because aims to deeply characterize and analyze their spatial and time variability in relation to the principal driving mechanisms, which was not previously addressed. In turn, this will allow predicting their behavior to future situations. Moreover, obtained results will be compared with other works developed by means of other methodologies for some similar situations, in order to test the accuracy of MODIS data to analyze these plumes. MODIS capability to determine each plume will be also tested by means of salinity data derived from the Atlantic-Iberian Biscay Irish-Ocean Physics Reanalysis (IBI) database, enhancing the robustness of the methodology applied.

The developed methodology will be applied to other important plumes in the proximities of Iberian Peninsula as those formed along the Atlantic part of the French continental coast for several reasons. Firstly, these plumes are subjected to similar conditions than

Atlantic Iberian plumes. Secondly, the application of the high spatial and temporal resolution provided by MODIS for the analysis of Loire and Gironde plumes variability constitutes an important step forward because allows analyzing this wide area over large periods. The behavior of these plumes to the main forcing was not previously addressed. In addition, the methodology will be expanded in order to also analyze the relation between the main teleconnection patterns and Loire and Gironde plumes development. By last, the combination of MODIS with other databases as the $NOAA_{1/4}$ daily Optimum Interpolation Sea Surface Temperature ($OISST_{1/4}$), which provides sea surface temperature data, and reanalysis data of salinity and temperature in subsurface derived from IBI database, also allows the evaluation of plume impact on the thermohaline properties of seawater. The evolution of temperature patterns in the areas affected by rivers has specially importance in the actual context of global warming since can follow a different behavior than the surrounding ocean water, as commented above. Although these databases present a coarser spatial resolution, it is enough to analyze the thermohaline properties of the plumes formed by these rivers due the greater extension in comparison with Iberian plumes.

Chapter 2:

Data and Methodology

The aim of this chapter is to describe the methodology developed to adequately characterize turbid plumes formed by the most important rivers of the Iberian Peninsula, as well as to analyze their response to the main forcing affecting them (river discharge, wind and tide). For that, the normalized water-leaving radiance (nLw) provided by MODIS, which acts as a good proxy to determine plumes, will be processed and assessed in order to obtain images of the plumes as well as the turbid limit which best delimit each turbid plume. After that, the methodology will be applied in river plumes located in the adjacent coast of France. Finally, the influence of the most important climate patterns in the North Atlantic region on plumes dynamic, as well as, the impact of most important French Atlantic plumes on seawater thermohaline properties will be analyzed by means of the databases described below.

2.1. Turbid plumes characterization

As ocean color measurements suppose a good proxy to represent turbid plumes, as commented in *Chapter 1 "Introduction"*, the methodology developed to analyze Iberian turbid plumes will be based on data obtained from MODIS, which offers a good enough spatial and temporal resolution to these purposes.

2.1.1. MODIS

MODIS is a sensor (Figure 2.1) located onboard the Aqua and Terra satellites (Figure 2.2), providing information on several parameters. Both satellites are set at a sun-synchronous orbit at 705 km of altitude, acquiring data in 36 spectral bands ranging in wavelength from 0.4 μm to 14.4 μm. Terra's orbit around the Earth is timed so that it passes from north to south across the equator in the morning (at 10:30 a.m. descending node) while Aqua passes south to north over the equator in the afternoon (at 1.30 p.m. ascending node). MODIS achieves a 2330 km swath viewing the entire Earth's surface every 1 to 2 days.
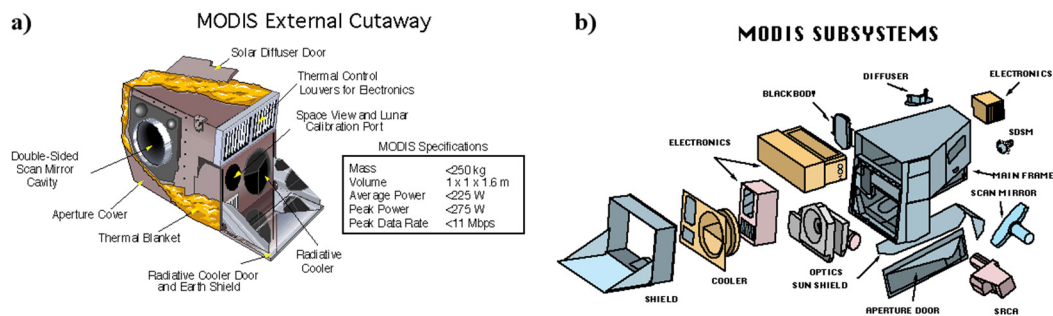
Figure 2.1. MODIS instrument. (a) MODIS external components and (b) MODIS subsystems (http://mcst.gsfc.nasa.gov/).
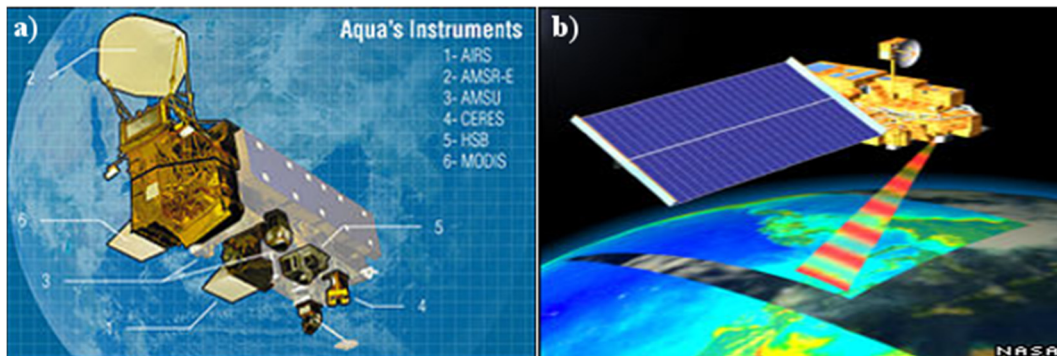
Figure 2.2. (a) Aqua satellite components (http://aqua.nasa.gov) and (b) Terra satellite functioning (http://terra.nasa.gov).

MODIS Aqua and Terra sensors were designed to provide measurements in large-scale global dynamics, including changes in Earth's cloud cover, radiation budgets, ocean processes and global change, having a key role in the environmental studies. Nowadays the MODIS-Terra and MODIS-Aqua are fully operational since February 2000 and June 2002, respectively. All the information about this sensor and the produced data are available in the NASA Ocean Color web site (http://oceancolor.gsfc.nasa.gov).

2.1.2. Normalized water-leaving radiance (nLw) data

The ocean-color data is a passive remote sensing method which consists in the measurement of spectral distribution of radiance (or reflectance) upwelling from the ocean in the visible part of the electromagnetic spectrum. The sensor measures the light emitted (or reflected) by the water mass. These variables are associated with the water *cloudiness* (or turbidity), which is linked to the presence of suspended and dissolved mater (Davies-Colley and Smith, 2001; Güttler et al., 2013). Therefore, these measurements result in a good tracer of river plumes since they are promoted by suspended material carried by the rivers, as commented in *Chapter 1 "Introduction"*, which allow their distinction in relation to the surrounding ocean clear water, especially in the red and green light wavebands (Loisel et al., 2013). The Remote sensing reflectance (Rrs) and the normalized water-leaving radiance (nLw) are the MODIS parameters usually used to determine these properties.

The primary radiometric product from ocean-color measurements is the radiance emerging from the sea surface, knowing as water-leaving radiance (L_w). In general terms, the radiance L at a point in space (underwater at depth z) is the radiant flux, Φ, at that point in a given direction per unit of solid angle per unit of projected area, A (IOCCG, 2011):

$$L(\theta, \varphi, z, \lambda) = \frac{d^2\Phi}{dw dA} \qquad (2.1)$$

where λ is the respective wavelength, and $dA = ds\,cos\theta$ the projected area of the surface element ds, seen from the direction of propagation, which is determined by the zenith (θ) and the azimuth (φ) angles, onto the plane perpendicular to this direction.

Water-leaving radiance, $L_w(\pi, 0, 0^+, \lambda)$, can be defined as the radiance leaving the sea at nadir and quantified just above surface ($z=0^+$), taking into account refraction and reflection at the interface. To derive this product is necessary to remove atmospheric path radiances and sea surface reflectances, in a process denominated as atmospheric correction. After that, the water-leaving radiance estimated by the ocean-color measurements is coming from an angle and azimuth defined by the viewing angle and position of the satellite sensor and not nadir (IOCCG, 2011).

The normalization of L_w allows to reduce the dependence on the Sun´s elevation and the viewing incidence angle (Robinson, 2010; IOCCG, 2011). However, the knowing of the downward irradiance is necessary to realize this step.

The irradiance E at a given depth, z, can be defined as the radiant flux per unit area of surface (Kirk, 1994):

$$E(z, \lambda) = \frac{d\Phi}{ds} \qquad (2.2)$$

where downward irradiance, E_d, and upward irradiance, E_u, represent the irradiance for the downwelling and upwelling light, respectively, at water surface.

Therefore, the normalized water-leaving radiance (nLw) is represented as:

$$nLw(0^+, \lambda) = \frac{L_w(0^+, \lambda)}{E_d(0^+, \lambda)} F_0(\lambda) \qquad (2.3)$$

where F_0 is the extraterrestrial solar flux.

Then, the normalized water-leaving radiance can be defined as the radiance that would exit the ocean in the absence of the atmosphere, with the sun at the zenith, at the mean earth-sun distance (http://modis.gsfc.nasa.gov).

Rrs represents the proportion of light incident onto the water surface that is eventually scattered back to the sensor through the surface, being also defined by the viewing angle and position of the satellite sensor (IOCCG, 2011). Rrs is determined by the ratio between the water-leaving radiance, *Lw*, and the downward irradiance *Ed*:

$$R_{rs}(\pi, 0, \lambda) = \frac{L_w(\pi, 0, 0^+, \lambda)}{E_d(0^+, \lambda)} \qquad (2.4)$$

Therefore, taking into account that F_0 is constant, the *nLw* is function of *Rrs*.

For more detailed information about these products the lector is referred to IOCCG, 2011.

Taking into account the features commented above the normalized water-leaving radiance was selected as the most adequately MODIS product to analyze turbid plumes throughout this thesis.

2.1.3. Data processing

Level 1A files were obtained from the NASA Ocean Color web site (http://oceancolor.gsfc.nasa.gov). These files are unprocessed instrument data at full resolution, time-referenced and annotated with ancillary information, including radiometric and geometric calibration coefficients and georeferenced parameters computed and appended but not applied to the Level 0 data. L1A files were processed to L1B files using the SeaDAS software (SeaWIFS Data Analysis System, version 7.1, Baith et al., 2001), following standard procedures recommended for raw data files processing. Level 1B data can be defined as L1A data with instrument/radiometric calibrations applied. L1B files were then converted to L2 files by applying a methodology similar to that provided by Aurin et al. (2013). Level 2 files are data of derived geophysical variables at the same resolution as the source L1 data. As main processing features, clouds with a threshold albedo of 0.018 were masked using the 2130 nm SWIR (Short Wave Infrared) bands and the high light masks were disabled. Moreover, stray light masks with a 3x3 array were applied around land and clouds and the unrealistic values of remote sensing reflectance were discarded. The produced L2 data were processed at resolutions of 0.5

km in the case of Iberian plumes and 1 km for French Atlantic plumes, obtaining daily images of normalized water-leaving radiance (associated to turbidity) interpolated into a regular mesh. This resolution allows resolving most of the optical variability of these plumes. In addition, the creation of these images is based on other assumptions in order to improve their quality. These assumptions were evaluated for the Tagus plume case, since it is an intermediate Iberian plume in terms of extension and turbidity.

2.1.4. Most suitable bands to determine turbid plumes

MODIS allows working with several nLws. Some elements need consideration when selecting the most suitable band to study the Iberian turbid plumes. First, a high spatial resolution is needed, thus only the nLw469, 555 and 645 bands are acceptable for a 500 m spatial resolution (Table 2.1). The best coverage (in number of days) is provided by bands 488, 531, 547 and 555 and the best correlation with the river discharge is obtained through bands 645, 667 and 678 (Table 2.1). Overall, nLw555 and 645 seem to be the appropriate bands to use. However, although the band centered at 555 nm provides a strong turbid signal (Nezlin et al., 2005; Saldias et al., 2012), the nLw645 band was chosen because it has a lower water penetration depth (Chen et al., 2007), avoiding the interference of bottom in shallow areas and reducing the influence of radiance caused by upwelling or re-suspension processes.

Band (nm)	MODIS_Aqua (Terra) satellite sensor				
	Spatial resolution (m)	**p (%)**	r		
			lag 0	lag 1	lag 2
412	1000	20 (24)	0.01 (0.01)	0.01 (-0.01)	0.03 (0.02)
443	1000	28 (29)	0.14 (0.13)	0.13 (0.12)	0.11(0.10)
469	500	30 (30)	0.23 (0.20)	0.23 (0.19)	0.21 (0.17)
488	1000	31 (31)	0.29 (0.28)	0.28 (0.28)	0.27 (0.27)
531	1000	31 (31)	0.38 (0.38)	0.38 (0.38)	0.37 (0.37)
547	1000	31 (31)	0.40 (0.40)	0.40 (0.40)	0.40 (0.40)
555	500	31 (31)	0.41 (0.41)	0.41 (0.41)	0.42 (0.41)
645	250	20 (22)	0.56 (0.52)	0.56 (0.53)	0.57 (0.54)
667	1000	17 (19)	0.59 (0.54)	0.59 (0.55)	0.59 (0.55)
678	1000	21 (25)	0.57 (0.50)	0.58 (0.50)	0.57 (0.51)

Table 2.1. Comparison of the different available bands for nLw from the Aqua and Terra satellites for the period 2003-2015. The parameters considered were: the spatial resolution, percentage of available days (p) (daily images were considered valid if more than 70 % of the pixels were available), and the correlation between nLw and river discharge (r) under different lags. For all parameters, the first number corresponds to the Aqua satellite and the number in brackets relates to the Terra satellite.

2.1.5. NIR *vs* SWIR_NIR bands for atmospheric correction

In standard MODIS ocean color data processing for atmospheric correction, the ocean is viewed black by the 748 and 869 nm Near-Infrared (NIR) bands. However, some studies

indicated the processed NIR ocean color images are not valid for assessing very turbid waters because of the contribution of ocean water-leaving radiance (invalid NIR black ocean assumption) (Wang et al., 2007; Wang and Shi, 2009). A combined SWIR_NIR algorithm was developed for very turbid waters since the *black assumption* is generally valid for Short Wave Infrared (SWIR) bands (1240 and 2130 nm wavelenghts). However, the use of SWIR bands introduces greater noise in the processed images (Wang and Shi, 2009). Both atmospheric corrections NIR and SWIR_NIR were evaluated to apply the most suitable one for the moderate turbid areas of the Tagus plume.

Tagus plume image composites were constructed from the Aqua satellite data for river discharges > 66th percentile occurring in 2003 (Figure 2.3), in order to have enough plume to evaluate both processes. Figure 2.3a shows the atmospheric corrected composite image assembled from NIR bands, whereas Figure 2.3b displays the composite image created with an alternative SWIR_NIR algorithm described by Wang and Shi (2009) and used by Saldias et al. (2012). Both corrections have been preferably used in turbid plume studies.
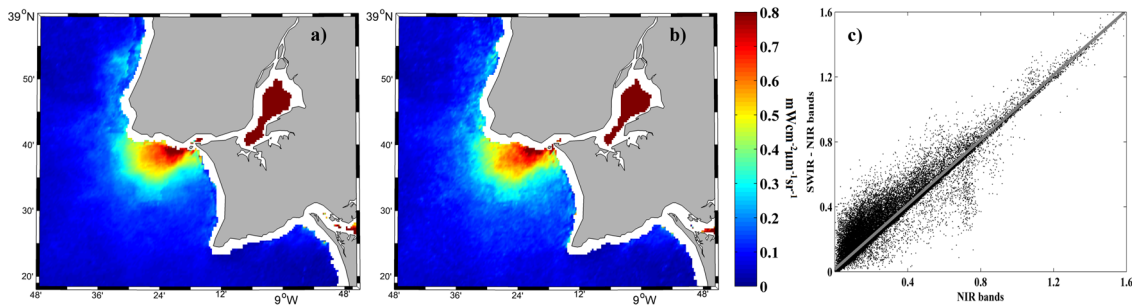
Figure 2.3. Mean normalized water-leaving radiance (mWcm^{-2}µm^{-1}sr^{-1}) composite at 645 nm for all MODIS images under high river discharge (> 66th percentile) occurring in 2003 for Tagus plume. Results compare the effect of atmospheric corrections using NIR (a) and SWIR_NIR (b) channels. Scatterplot (c) of corresponding available pixels in each image.

Similar composites were obtained by the application of both atmospheric corrections probably due to the moderate local turbid values (Figures 2.3a and b). When valid pixels provided by both corrections were compared, a linear regression (SWIR_NIR = 0.997 NIR + 0.015), with r^2 equal to 0.96, was obtained (Figure 2.3c). The linear regression was calculated for the area of plume development. Similar or better linear regressions were achieved (in terms of equivalence between both atmospheric corrections) when all river discharges or/and the entire area covered by the images were incorporated. The comparison allows the application of both correction methods and, although NIR bands can produce significant errors for extremely turbid waters, the moderate turbidity of the Tagus plume mitigates their production.

The normalized standard deviation is an indication of the dispersion (the ratio between the standard deviation and the mean value) associated with both atmospheric correction procedures. It reaches 10.77 % for SWIR_NIR and 8.97 % for NIR, thus the NIR

atmospheric correction is slightly better. SWIR derived products are noisier because SWIR bands were originally designed for atmospheric and land applications and have lower signal-noise ratio (SNR) values (Wang and Shi, 2009).

Therefore, attending to the obtained results, NIR atmospheric correction was selected and used to process MODIS radiance data for Tagus plume. This atmospheric correction was also applied to the other plumes under study because are subjected to similar turbid values.

2.1.6. Merging data from Aqua and Terra satellites

Merging daily images of plumes acquired from both satellites enhances the robustness and precision of the study by increasing the number of available pixels. If a pixel only has a valid value from one satellite, this value is assumed and if it has valid values from both satellites, both values are averaged. This process is made for each pixel in order to obtain a daily image using data from both satellites. Therefore, the differences between both satellites imagery must be addressed for their suitability in the case of the Tagus plume.

Composites created with images from the Aqua and Terra satellites show a similar plume development pattern (Figures 2.4a and b). Composites were generated from 2003 to 2015 during periods of river discharges > 66th percentile. Differences between the composite images are mainly due to the availability of days without cloud coverage for each satellite.
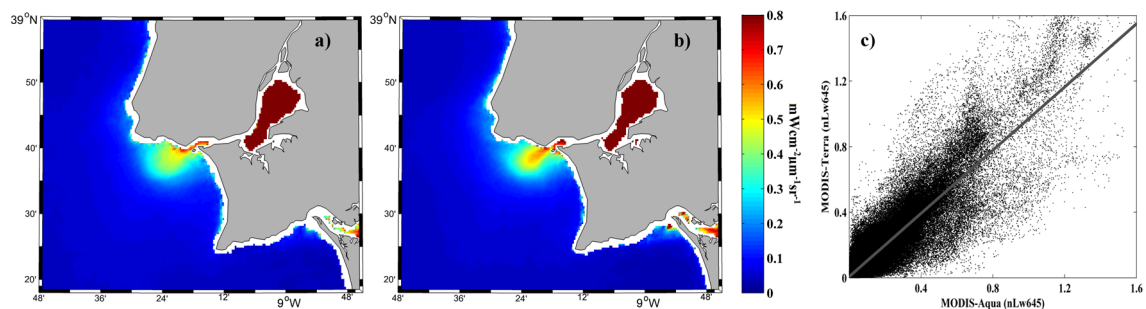
Figure 2.4. Mean normalized water-leaving radiance (mWcm^{-2}μm^{-1}sr^{-1}) composite at 645 nm for all MODIS images under high river discharge (> 66th percentile) over the period 2003-2015 for Tagus plume. Results compare data obtained from Aqua (a) and Terra (b) satellites. Scatterplot (c) of corresponding pixels in each image.

A good linear regression was obtained when the values of daily available pixels acquired from both satellites were compared (MODIS_Terra = 0.964 MODIS_Aqua + 0.007) with a correlation coefficient (r^2) equal to 0.89 (Figure 2.4c). The linear regressions had similar or better correlation coefficients when all discharges and/or the entire area depicted in the images were considered.

The results indicate that the differences between the data obtained from both satellites are negligible for the purpose of this research. In summary, merging daily data from both satellites is justified when analyzing the role of river discharge and wind on plumes development. A difference of a few hours in the overpass of both satellites is negligible to study the mean state of the plume under these drivers. Increasing the percentage of available pixels is especially important for the less frequent events.

However, data merging is not justified when the influence of tides is analyzed, because the tide status is acquired at the instant of the satellite overpass. If data obtained from both satellites were merged, different tidal states (out of phase by 2-3 hours) would be recorded. Thus, the tide influence on plume development will be analyzed using imagery only from the Aqua satellite to avoid ambiguities in tidal state and because of a greater number of available pixels provided by this satellite.

Once this analysis was made, it is interesting to know the typical valid data into each pixel of composites, as well as its variance. The percentage of valid values to create a composite when both satellites are merged, was analyzed under high river discharges (above the 66th percentile), when Tagus plume is well developed. Figure 2.5a shows 40% of valid data in the plume development area, therefore, taking into account the period of study, these pixels include around 650 valid data, which remarks the robustly of the methodology developed. In addition, if mean value of each pixel (Figure 2.5b) and its deviation (Figure 2.5c) are compared, a great dispersion in the plume development area is observed, with values around 0.3 $mWcm^{-2}\mu m^{-1}sr^{-1}$, a deviation near to mean values (0.5 $mWcm^{-2}\mu m^{-1}sr^{-1}$). This behavior is due to the selected percentile, which includes days with discharges ranging between 196 and 997 m^3s^{-1} and different wind and tidal conditions that influence the turbidity of the area. This implies that pixels in plume development area can reach values between 0.2 and above 1.2 $mWcm^{-2}\mu m^{-1}sr^{-1}$, showing their high variance.
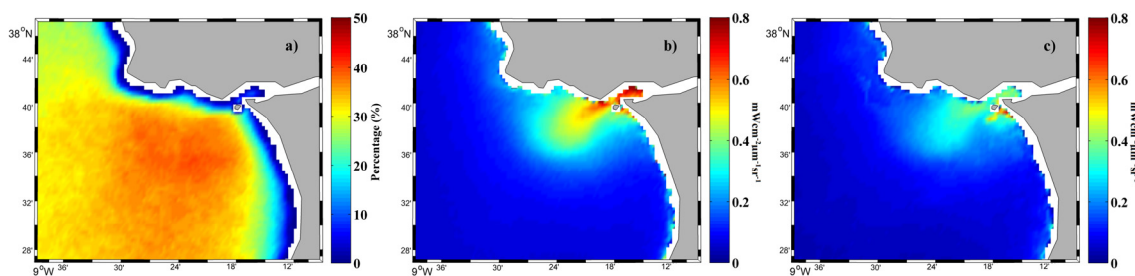
Figure 2.5. (a) Percentage of valid values, (b) mean value, and (c) standard deviation for each pixel of the composite considering all MODIS images under high river discharge (> 66th percentile) over the period 2003-2015 for Tagus plume.

2.1.7. Turbidity threshold to delimit turbid plume area

A proper definition of the turbid limit is crucial since it allows the adequately distinction of water areas affected by the turbid plume from the adjacent "clear" seawater. Its

definition is dependent on the terrestrial characteristics and sediment load from the river, therefore, each plume has a particular turbid limit. The general method developed to obtain the limit consists in the evaluation of the maximum correlation between river discharge and turbid plume extension under different delays for distinct threshold values in an area nearby to river mouth, a similar procedure to that used by Lahet and Stramski (2010). Only daily images containing > 70% of the available data covering the areas under analysis were gathered to remove disturbances caused by the lack of valid pixels, resulting in series containing around of 700 valid values from 2003 to 2014 for Iberian Rivers. The turbid value which offers the maximum correlation between plume development and river discharge was selected as the most precise to represent turbid plume area (Figure 2.6).
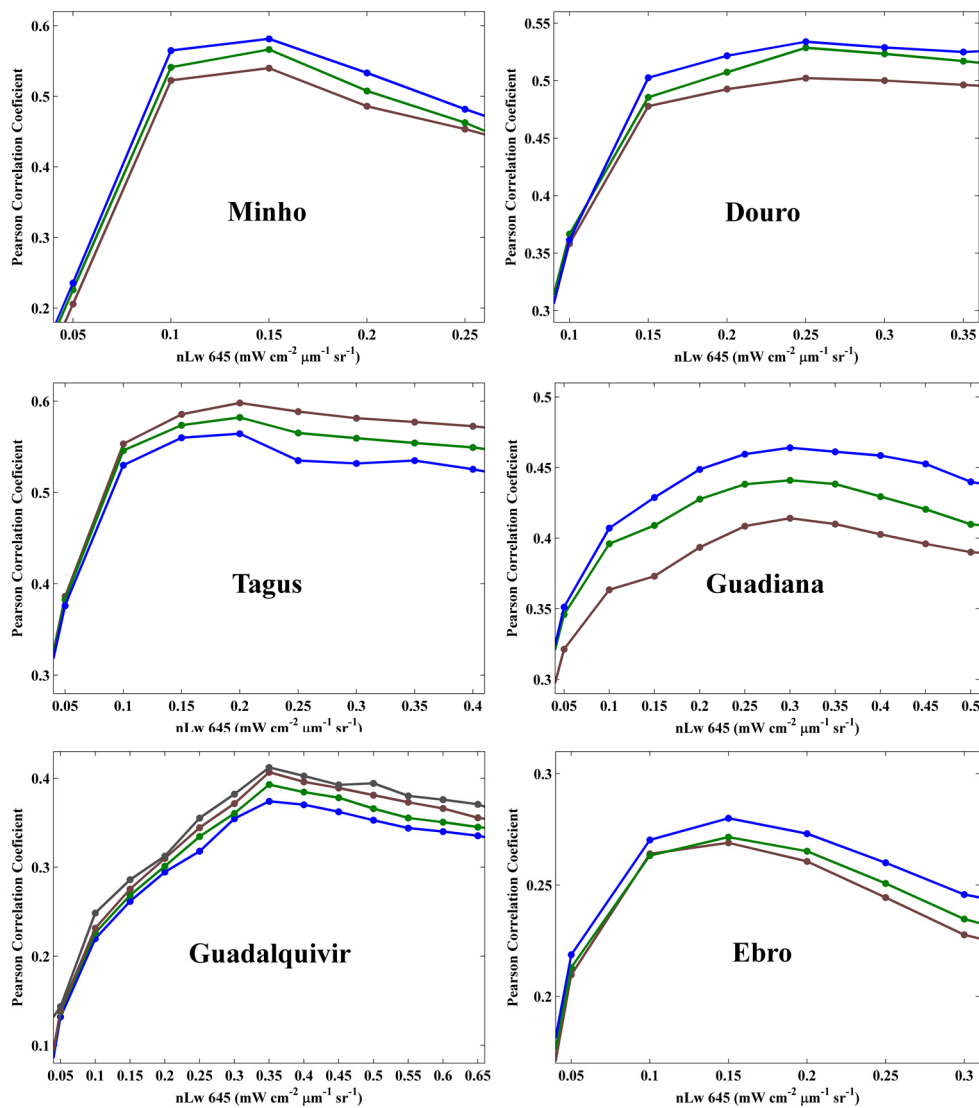
Figure 2.6. Correlation coefficient between plume area and daily river discharge (with different delays), as function of different threshold values. The threshold value obtaining the best correlation to each river plume was selected as the most adequately turbid limit. Blue line represents 0 delay, green line 1 day delay, brown line 2 days delay, and grey line 3 days delay (grey line only was showed in Guadalquivir case because in the other cases the correlation decreases drastically).

Although we refer to the turbid plume as an entity, we can consider that the threshold really define the near-field of the turbid plume based on its definition, since is defined as the oceanic area where the river influence is more intense and the contrast with ocean waters is larger (Garvine, 1982; Hetland, 2005). Thus, pixels above this limit define the plume area where the water differs more from ocean water due to the major influence of material and freshwater discharged by the river, and therefore, where the main processes occur, modifying and differentiating water properties from the adjacent seawater. Although some turbidity can be detected below this value (far-field plume), the material and freshwater are diluted enough to follow a similar dynamic than the ocean water since represents the final merge in ocean waters. For sake of clarity and simplicity, throughout the thesis the area enclosed for this limit will be referred as turbid plume.

The turbid limit was evaluated for the most important Iberian plumes using the nLw645 band, obtaining different values for each river plume due to their different features (Figure 2.6).

This methodology was compared with other methods used in previous researches in order to test its accuracy. A histogram of the distribution of radiance (nLw645) for days characterized by a negligible plume (Figure 2.7a) and days showing a well-developed plume (Figure 2.7b) was analyzed for Tagus, similarly to the methodology previously used by Saldias et al. (2012). More than 97% of the pixels were below the 0.2 mWcm^{-2}μm^{-1}sr^{-1} threshold in situations without plume. Therefore, values ranging from 0 to 0.2 mWcm^{-2}μm^{-1}sr^{-1} can be considered as residual turbidity in ambient seawater. In contrast, Figure 2.7b displays a large percentage of pixels with a value > 0.2 mWcm^{-2}μm^{-1}sr^{-1} for a well-developed plume.

This method also confirms the 0.2 mWcm^{-2}μm^{-1}sr^{-1} threshold as the most appropriate to delimit the Tagus turbid plume for a wavelength centered on 645 nm, which increases the confidence and robustly of the turbid limits obtained for the Iberian plumes.
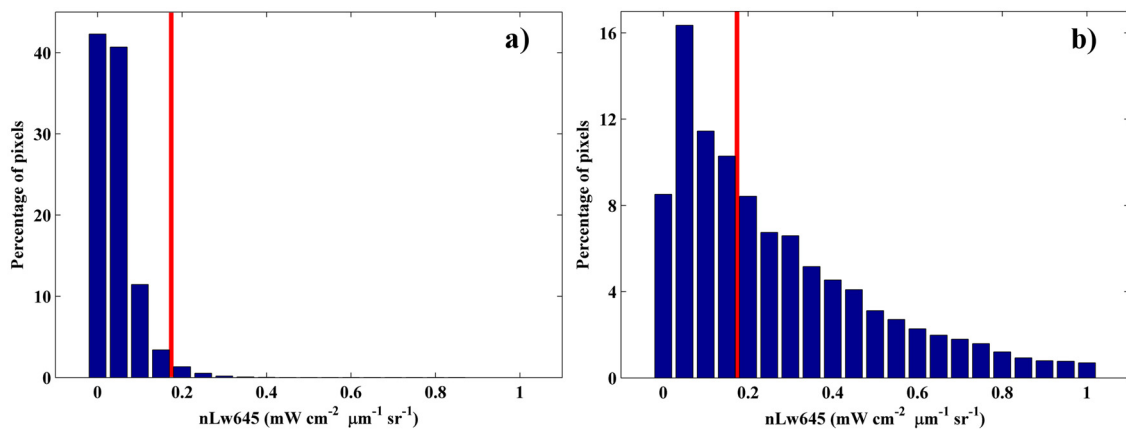
Figure 2.7. Distribution of pixels for different threshold intervals are shown for images with (a) a negligible plume and (b) a well-developed plume, for the Tagus case.

2.1.8. MODIS imagery composites

The daily images of radiance were obtained for each area under interest with the processing described above. These images were used to create turbidity composites of each river plume characterizing its mean state under the influence of each forcing. For that, the valid pixels available for each day fulfilling the conditions characterizing each driving force were averaged. For example, the images of all days when river discharge was high would be averaged in order to obtain an image representing the general state of the plume affected by high discharges. This processing will be realized to each forcing affecting plumes. The comparison between these composites allows the evaluation of plume behavior under the influence of the different forcing factors, as well as the comparison between different plumes.

2.2. Turbid plume forcing databases

In spite that several forcing can impact plumes development, as commented in *Chapter 1 "Introduction"*, plumes under analysis are mainly affected by river discharge, wind and tide. In turn, teleconnection patterns influence these forcing, therefore also impact plumes dynamic. In addition, plume development also affects thermohaline properties of the adjacent seawater. The data period selected for the analysis of these parameters was dependent on each specific study, so it will be defined for each corresponding case.

2.2.1. River discharge data

Ebro River discharge, measured at Tortosa station, was obtained from "Confederación Hidrográfica del Ebro" (www.chebro.es).

Guadalquivir River discharge, measured at Alcalá del Río station, was obtained from "Confederación Hidrográfica del Guadalquivir" (www.chguadalquivir.es). Guadalete River discharge at Arcos de la Frontera station (including the discharge of Majaceite River, its main tributary, at Guadalcín station) was added because it debouches into ocean close to Guadalquivir mouth and their effects on plume development are linked.

Guadiana (Monte da Vinha station), Tagus (Almourol and Ómnias stations) and Douro (Crestuma-Lever station) River discharges were obtained from "Sistema Nacional de Informação de Recursos Hídricos" (SNIRH) (www.snirh.pt).

Minho River discharge was obtained from "Confederación Hidrográfica del Miño-Sil" (www.chminosil.es). Minho River discharge was considered as the outflow at Frieira dam plus Tea River discharge since it is an important tributary that flows into the Minho after its last measuring station.

Gironde and Loire River discharges were obtained from the Banque Hydro French Database (http://www.hydro.eaufrance.fr/). Gironde discharge was obtained as the sum

of Dordogne (Pessac-sur-Dordogne station) and Garonne (Tonneins station) River discharges. Loire discharge was sampled at Nantes station.

Daily discharges of the rivers under analysis were sampled at the measuring station as close as possible to the river mouth when the whole period under study was available (Figure 2.8).

The evaluation of river discharge influence on turbid plumes was carried out considering the plume state under the extreme situations of this forcing (low and high river discharges). Low discharge conditions will be considered when river discharge is below the 25th percentile taking into account the daily discharge series for the respective river, and high discharge conditions when river discharge is above the 75th percentile.
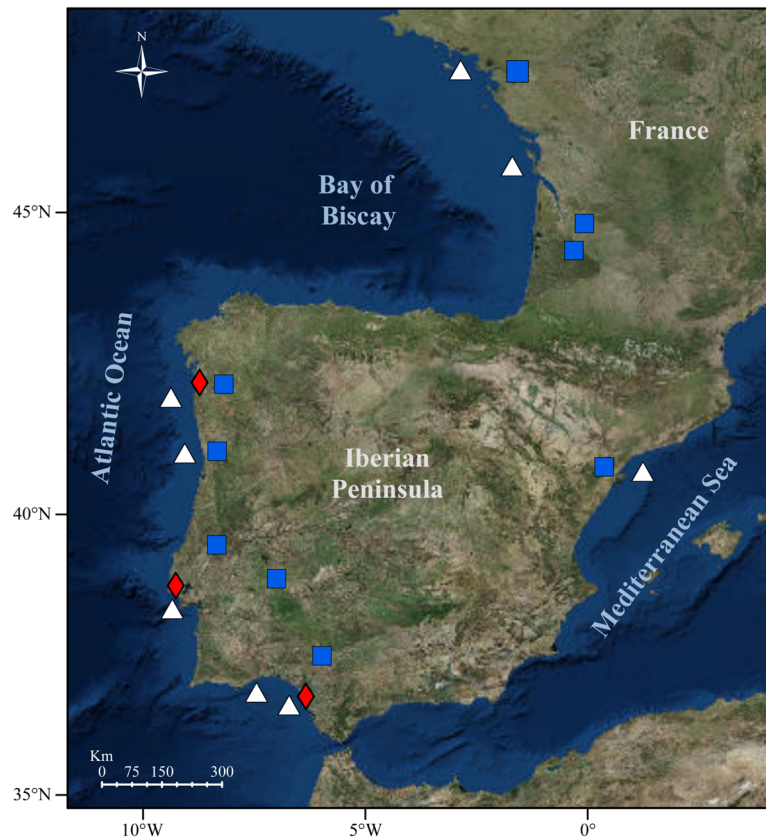
Figure 2.8. Location where forcing data were acquired. Blue filled squares indicate the location where river discharge was sampled. White triangles mark the location where wind data were obtained. Red diamonds indicate the location where tidal data were sampled.

2.2.2. Wind data

Wind data were retrieved from Climate Forecast System Reanalysis (CFSR) database, which was developed by NOAA's National Centers for Environmental Prediction (NCEP) (http://rda.ucar.edu/pub/cfsr.html). CFSR data are available at NOAA's National Operational Model Archive and Distribution System (NOMADS), which is maintained

at NOAA's National Climatic Data Center (NCDC) (Saha et al., 2010). This wind product provides a global coverage with spatial resolution of 0.3º x 0.3º and 6 hour time resolution, covering the atmosphere, ocean, sea ice and land. CFSR wind database is an accurate tool to studies related with wind because of its high spatial and temporal resolution and the great correlation with *in situ* wind measurements along the Atlantic Iberian coast (Alvarez et al., 2014). Wind data were daily averaged at a reference height of 10 m for an ocean location close to each river mouth (Figure 2.8).

Four main directions were considered to evaluate the influence of winds on plumes dynamic. Alongshore winds were split into alongshore winds which cause an Ekman transport offshore (AS$^+$) and which cause an Ekman transport onshore (AS$^-$). Cross-shore winds were split into seaward (CS$^+$) and landward (CS$^-$) winds. These wind directions were defined following the particular coast orientation at each river mouth allowing a deviation of ± 45º. Moreover, only mean winds higher than 2 ms^{-1} over the 2 days previous to plume sampling were considered in order to avoid calm intervals. This period of 2 days was imposed to allow plumes response to wind influence since oceanic inertia is considerably higher than the atmospheric one.

2.2.3. Tidal data

Tidal effect on river plumes has only been analyzed for rivers flowing into the Atlantic Ocean since tidal influence is negligible on Ebro River plume due to the micro-tidal Mediterranean regime (Mestres et al., 2003).

Hourly tidal data were obtained from "Puertos del Estado" (www.puertos.es) at Vigo (used for Minho and Douro) and Bonanza (used for Guadiana and Guadalquivir) stations and through an estuarine model system validated in the Tagus Estuary for a point located near the mouth of the estuary (Vaz et al., 2011) (Figure 2.8).

The evaluation of the semidiurnal tidal influence on river plumes was carried out considering tidal states at the hour when the satellite overpasses the study area (~ 13:30 UTC for Aqua satellite). High tides were considered when tidal state was higher than 0.5 m and low tides when it was lower than -0.5 m, using tidal series centered in 0 m. Fortnightly cycle influence was evaluated considering the daily tidal amplitude. Spring tides were considered when daily amplitude was over the 75th percentile and neap tides when below the 25th percentile.

2.2.4. Atmospheric and oceanographic climate indices

Monthly indices of the most important atmospheric modes in the area under study, the North Atlantic Oscillation (NAO) and the East Atlantic pattern (EA), were obtained from the Climate Prediction Center at the National Center of Environmental Prediction (http://www.cpc.noaa.gov).

NAO is the most prominent teleconnection pattern influencing the North Atlantic (Barnston and Livezey, 1987). NAO consists of a north-south dipole with one center located over Greenland and the other over a region spanning between 35-40ºN in the central North Atlantic. The index is calculated as the geopotential anomalies between both centers (Thompson and Wallace, 1998).

EA is the second most important teleconnection pattern over the North Atlantic. It consists of a north-south dipole that spans the entire North Atlantic, being structurally similar to NAO, but with the centers displaced southeastward respect to the NAO (55ºN, 20-35ºW and 25-35ºN, 0-10ºW).

Changes in NAO and EA indices are able to influence temperature, precipitation and wind patterns over western and central Europe (Hurrell, 1995; Lorenzo and Taboada, 2005; deCastro et al., 2006; 2008).

Monthly index of the most representative oceanographic mode, the Atlantic Multidecadal Oscillation (AMO), was obtained from the NOAA website (http://www.esrl.noaa.gov/psd/data/timeseries/AMO/).

AMO is a mode of natural variability representing the sea surface temperature (SST) in the North Atlantic Ocean. It is calculated from averaging SST anomalies in the Atlantic north of the equator (Enfield et al., 2001).

2.3. Oceanographic databases

2.3.1. Sea Surface Temperature (SST) data

Daily values of SST were obtained from the NOAA$_{1/4}$ daily Optimum Interpolation Sea Surface Temperature (OISST) database (Reynolds et al., 2007). Data from the Advanced Very High Resolution Radiometer (AVHRR) sensor were used since it is located on board NOAA polar-orbiting satellites and provides an uninterrupted SST data series since March 1981 from the same class of instrument (Casey et al., 2010). This database also adds *in situ* data from ships and buoys to construct a regular global grid by means of a special form of kriging called Optimal Interpolation. This procedure retains large-scale correlation structures and allows assimilating very sparse data coverage (Reynolds, 2009; Reynolds and Chelton, 2010). Version 2 of this SST product was selected in this thesis. It includes bias adjustments of satellite and ship data using buoys data. Daily files with a spatial resolution of 0.25ºx0.25º were retrieved from the NOAA website (http://www.ndc.noaa.gov/sst/). Daily SST values were averaged at monthly scale in order to calculate SST trends assuming linear regression.

Daily SST data were also downloaded from the NASA Ocean Color Web Site (http://oceancolor.gsfc.nasa.gov) with the full resolution of 1 km (Level 2 files). SST data were obtained using 11-12 µm channels since these bands are located close to the maximum of the Earth´s emission and have larger bandwidth than other available

channels (Reinart and Reinhold, 2008). In addition only nighttime SST data were considered because have fewer fluctuations than daytime ones due to their independence of the solar radiation. These MODIS SST data present a closely relation to *in situ* data in coastal areas, representing a useful choice to evaluate the temperature of these areas due to the time and spatial resolution provided (Chavula et al., 2009).

2.3.2. Ocean salinity and temperature data

Ocean salinity and temperature data were obtained from the Atlantic-Iberian Biscay Irish-Ocean Physics Reanalysis (IBI) database, which is included in the Copernicus Marine Service (http://marine.copernicus.eu/). This product was developed by Mercator Ocean in collaboration with Puertos del Estado by means of NEMO model (see detailed information in Levier et al., 2016; Aznar et al., 2016). The dataset provides a daily temporal resolution with a horizontal resolution of 1/12º and a vertical resolution of 50 levels reaching a maximum depth of 5698 meters. Daily temperature and salinity values were monthly averaged in order to calculate trends assuming linear regressions. Unlike the other used databases which have a global coverage, this database is delimited for the area enclosed from 26 ºN to 56 ºN in latitude and from 19 ºW to 5 ºE in longitude.

2.3.3. Heat flux data

Heat fluxes (shortwave, longwave, latent heat and sensible heat) data were obtained from the CFSR database at monthly scale. The net heat flux (Q_T) through the ocean surface was evaluated following Eq. (2.5):

$$Q_T = Q_{SW} + Q_{LW} + Q_S + Q_L \qquad (2.5)$$

where Q_{SW} is the shortwave flux, Q_{LW} is the longwave flux, Q_S is the sensible heat flux and Q_L is the latent heat flux. According to the selected sign criterion, negative (positive) heat fluxes imply that ocean is losing (gaining) heat.

2.4. Accuracy of MODIS radiance to represent river plumes

The capability of MODIS radiance data to detect turbid plumes along the Iberian Peninsula coast was evaluated by means of salinity data from IBI database, taking into account the relation between both variables previously commented. The comparison was made for the available period of IBI, that is from 2003 to 2014. Turbidity and salinity data were monthly averaged in a window near each river mouth to carry out this process. Monthly average guarantees filling gaps in MODIS data, providing a good determination of the dominant monthly variability of the plume. In addition, only months presenting enough available data from MODIS (more than 20 % of available data for each pixel) were considered in order to add a more robust quality control. After that, both time series

were compared for each river (Table 2.2), following a similar methodology used by other authors in previous studies (Palacios et al., 2009; Molleri et al., 2010; Saldías et al., 2016 a; b). Significant and negative correlations were obtained in the rivers flowing into the Atlantic Ocean (Table 2.2).

River	Correlation *Radiance vs Salinity*	Series length
Minho	-0.62*	121
Douro	-0.65*	128
Tagus	-0.45*	129
Guadiana	-0.50*	140
Guadalquivir	-0.73*	139
Ebro	0.11	136

Table 2.2. Correlation coefficients between radiance data (from MODIS) and salinity data (from IBI) for the plumes of the main Iberian Rivers from 2003 to 2014. The asterisk means a significance level higher than 99%. Series length is the number of months with more than 20% of available data from MODIS.

This fact remarks the relation of turbid values with low salinities, both associated to river discharges. However, no correlation was found for Ebro River. This is mainly due to the high amount of low salinity water in the Ebro area during summer months, in spite that the river discharge is very low. The discrepancy could be related to the presence of fresh and less saline water from Rhone River (in the northern Gulf of Lion) which spreads southward, especially from early spring to August, and reaches the northernmost part of the Iberian Mediterranean coast (Masó and Tintoré, 1991; Ulses et al., 2008). However, this influence is very weak in the Ebro area and not explain the observed behavior. So, the discrepancy seems to be related to the different stratification patterns occurring in the area. Salat et al. (2002) analyzed the salinity plume of the Ebro River by means of *in situ* data obtained from three cruises characterizing autumn, winter and summer situations. They observed a much larger salinity plume in July than in November, in spite of the lower discharge. This was attributed to the high stratification occurred during summer months, which prevents or delays the vertical mixing, increasing the residence time of low salinity water in surface layers. Therefore, in spite that Ebro discharge is very low in summer, the freshwater water exported can easily spread across the area maintaining its character farther thanks to the limited mixing (Salat et al., 2002). The high stratification is supported by the micro-tidal regime of the Mediterranean Sea (Mestres et al., 2003) and the weak winds during this season (Durand et al., 2002). In autumn and winter the water column is more homogeneous (Salat et al., 2002). Therefore, during summer, the turbidity plume obtained from MODIS is more related to the daily Ebro discharge than salinity plume. In addition, Salat et al. (2002) found a good agreement between turbidity and salinity plumes during February, which represents months with high river discharges, the situation mostly analyzed during this work.

For visual analysis purposes, salinity and turbidity fields were represented for each river from December to February over the period 2003-2014 (Figure 2.9) since, on average, river plumes achieve their maximum extension during these months.
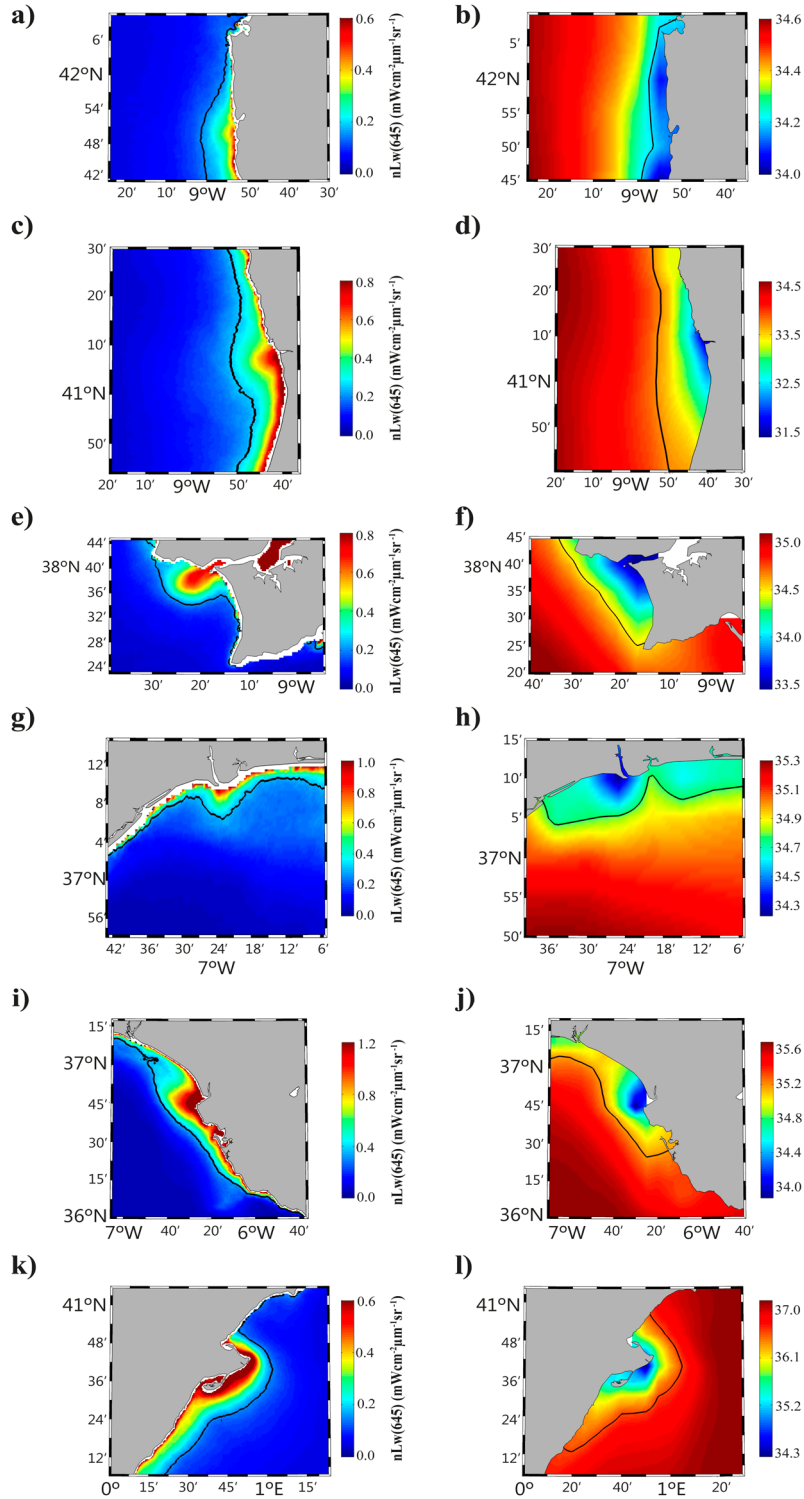
Figure 2.9. Comparison between the mean turbid plume obtained from MODIS (left panels) and the mean salinity plume obtained from COPERNICUS database (right panels) for Minho (a, b), Douro (c, d), Tagus (e, f), Guadiana (g, h), Guadalquivir (i, j) and Ebro (k, l) Rivers from December to February over the period 2003-2014. The black contour line represents the respective plume limit.

In general terms, these images corroborate the coherence between the development area of turbid and salinity plumes in the Atlantic Iberian coast. In the Ebro case, despite the difference between turbidity and salinity commented above, the predominant southward displacement of Ebro plume is observed in both figures.

The obtained results remark the accuracy of MODIS database to properly characterize Iberian turbid plumes.

Chapter 3:

Influence of main forcing on the Ebro turbid plume

3.1. Motivation

Ebro is the only main Iberian plume not affected by tidal effects due to the micro-tidal regime of the Mediterranean Sea (Mestres et al., 2003). Therefore, Ebro plume represents a good choice to analyze river discharge and wind effects on plume dynamic isolated from tidal forcing. For this reason, the Ebro plume was the first plume analyzed applying the methodology previously described.

In addition, in this case exists another important external forcing since the regional oceanic circulation plays a key role on plume displacement. The general circulation in the area is dominated by the east to west and then north to south, Liguro-Provençal or Northern current (Font et al., 1990) (Figure 3.1, right panel). This anticlockwise circulation feature, with intensities from 0.1 to 0.5 ms^{-1}, follows the shelf along the Mediterranean coasts of Italy, then France, and finally Spain, where a bifurcation occurs south of Valencia; part of the flux continues southwards (i.e., along the Spanish coast) while the other branch is deflected by the Balearic Islands and travels eastwards towards Corsica (Figure 3.1, right panel). It also generates and advects a number of mesoscale eddies that result in a pulsating feature. This current and the Coriolis effect tend to displace river plumes to the south in the Ebro area; they only veer northwards when directly affected by one of the mesoscale eddies just mentioned. The more frequent

pattern is a southward advection, which may generate a clockwise eddy in the lee side of deltaic forms or coastal protuberances. This allows analyzing the behavior of a plume also affected by an important and permanent current.
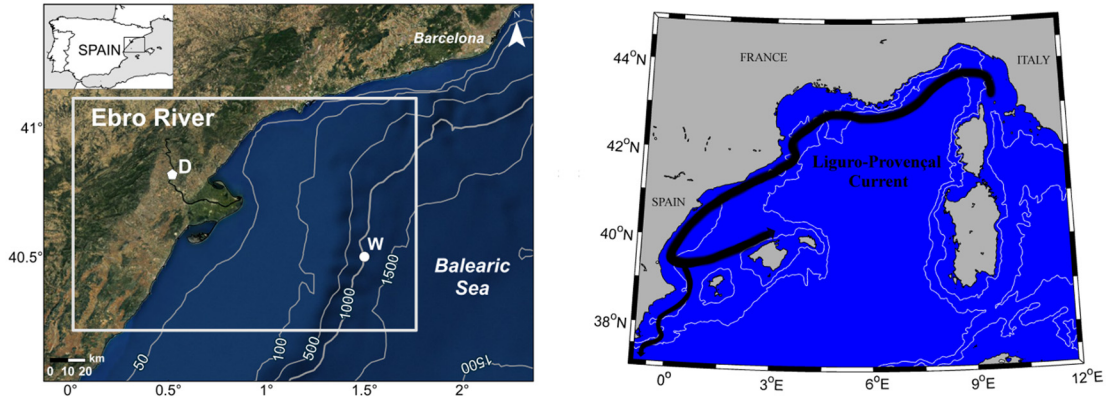
Figure 3.1. Left panel: Location of the study area. D indicates the location where river discharge was sampled. W marks the location where wind data were obtained. Right panel: Sketch of the main circulation in the area. White lines represent the bathymetry: 500 and 2000 m depth, respectively. Black line represents the Liguro Provençal current.

The goal of this chapter is to evaluate the role of the main forcing (river discharge, wind and regional circulation) on Ebro plume from 2003 to 2011, using the developed methodology described in *Chapter 2 "Data and Methodology"*. The study of the Ebro plume variability will be conducted using normalized water leaving radiance centered at 645 nm (nLw645) obtained from MODIS Aqua and Terra satellite sensors.

3.2. Main forcing affecting Ebro plume

Daily river runoff data were provided by Confederación Hidrográfica del Ebro at Tortosa Station, which is located 42 km upstream from the river mouth (Figure 3.1, left panel). Ebro River discharge presented daily values falling down to 80 m^3s^{-1} under severe drought conditions and exceeding 2000 m^3s^{-1} during periods of heavy rainfall, with a mean annual flow of 278 m^3s^{-1} over the study period (2003-2011). Ebro River discharge shows a clear seasonal pattern with higher discharges in winter and spring (December to May) and a significant reduction during the dry season (July to October) (Figure 3.2a). The maximum monthly discharge (~500 m^3s^{-1}) was observed in March, and the minimum occurred in August (scarcely exceeding 100 m^3s^{-1}). Months with high mean river discharge showed stronger deviations because they coincided with localized periods of abundant rainfall that cause large variations in river flow.

Daily wind data were obtained from CFSR database at an ocean location close to river mouth (Figure 3.1, left panel). The main winds that characterized the Ebro plume area

during the period under study were strong northwesterly winds (Mistral) followed by northeasterly and southwesterly winds (Figure 3.2b). Winds from the southeast were negligible. Winds were normally weak (2-8 ms^{-1}), except for the Mistral winds that reached the highest speeds (12-14 ms^{-1}), according to Durand et al. (2002).
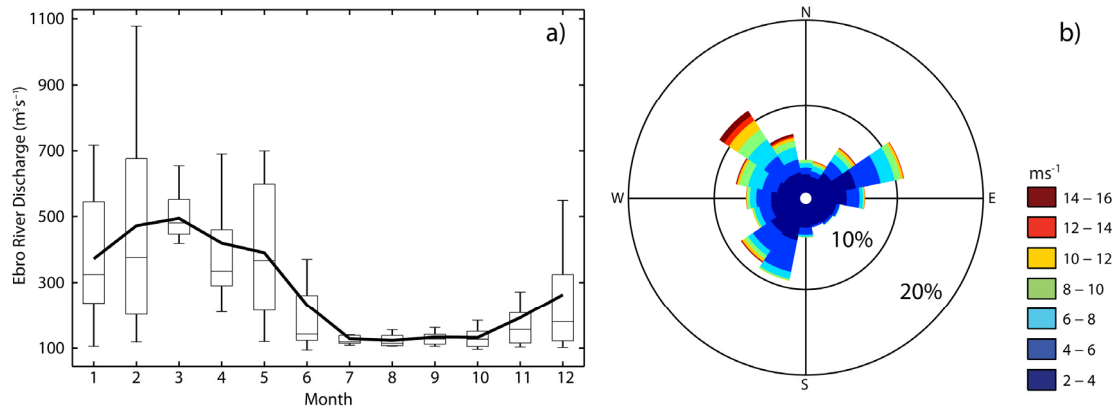
Figure 3.2. (a) Annual hydrologic cycle variability (m^{3}s^{-1}) for the Ebro River flow from 2003 to 2011. Solid black line: monthly average; line inside each box: median for each month; lower and upper whiskers: minimum and maximum river flow, respectively; lower and upper box limits: first and third quartiles, respectively. (b) Wind rose (ms^{-1}) of the Ebro basin over the period 2003-2011.

3.3. Results and discussion

3.3.1. River discharge influence on Ebro plume

The correlation coefficient between plume area and daily river discharge (Figure 3.3) shows that plume development responds immediately (at daily scale) to river discharge fluctuations, since maximum correlation was obtained when not delay is applied. In addition, the maximum correlation occurs for a turbidity threshold of 0.15 mWcm^{-2}µm^{-1}sr^{-1}, which is the same obtained in *Section 2.1.7. "Turbidity threshold"*, for a different time period. This remarks the robustness of the method used to obtain the turbid limit which best define the area occupied by the turbid plume, since is independent of the time period selected.

The intra-annual variability of the Ebro turbid plume extension (Figure 3.4) is calculated for comparison purposes with the annual flow cycle. The area of the turbid plume shows a clear seasonal variation that is similar to the one shown for river discharge in Figure 3.2a. In spite of the similarity between both patterns, some differences can be observed, which can be due to the influence of the other important forcing on plume development, the wind. In general terms, the maximum extension ($\sim$2000 km^2) occurs in February and the minimum one ($\sim$200 km^2) in June. In addition, February is the month with the highest deviation, probably due to episodes of strong rainfall, which support a larger extension of the plume.
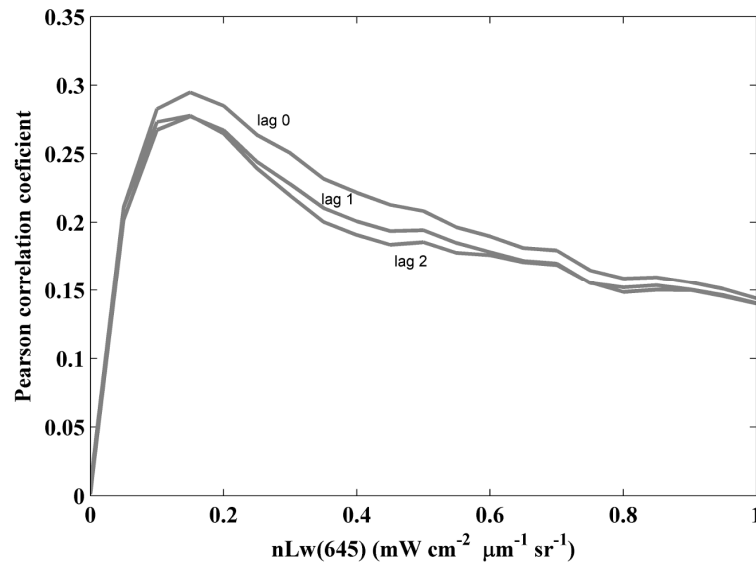
Figure 3.3. Pearson correlation coefficient between the plume area and daily river discharge (with different delays), as a function of different threshold values from 2003 to 2011.
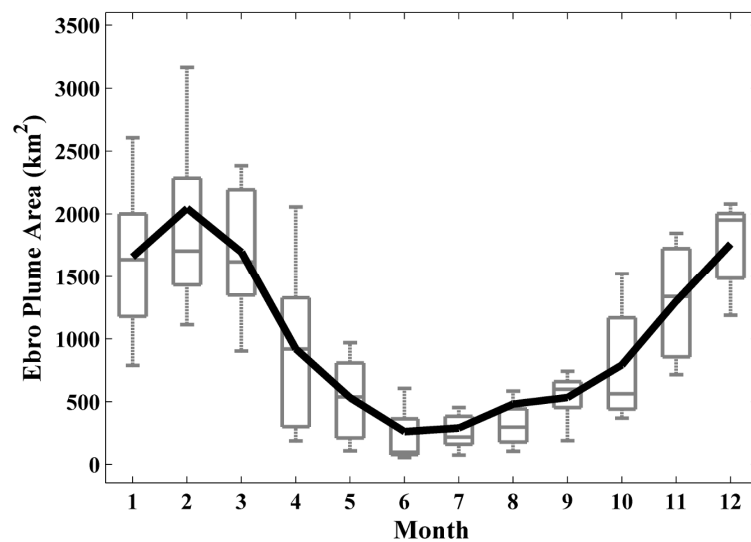
Figure 3.4. Annual cycle of Ebro plume extension (km^2) calculated over the period 2003-2011. Solid black line: monthly average; line inside each box: median for each month; lower and upper whiskers: minimum and maximum, respectively; lower and upper box limits: first and third quartiles, respectively.

The influence of the Ebro discharge on the coastal plume can also be observed when the turbid area is calculated under different river flow percentiles (Figure 3.5). The area of the turbid plume clearly increases with increased river flow, which generates more suspended matter drag to the mouth.
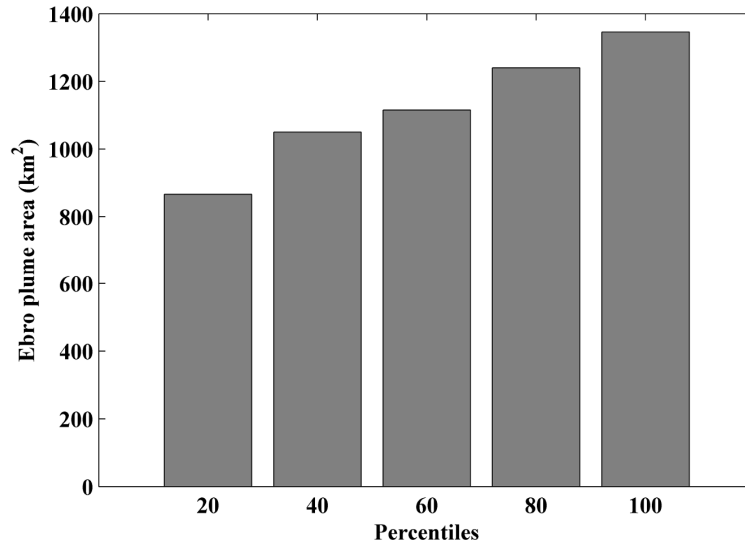
Figure 3.5. Ebro plume area (km^2) defined by river discharge percentiles.

In addition, Figure 3.6 shows the turbid area composite calculated under low river discharge (< 25th percentile (117 m^{3}s^{-1}) in Figure 3.6a) and high river discharge (>75th percentile (355 m^{3}s^{-1}) in Figure 3.6b). The observed pattern in both situations consists of a bulge near river mouth with a southern displacement of the turbid plume along the coast that can also be influenced by coastal Kelvin waves (Fennel and Mutzke, 1997). This pattern can be reinforced by the regional oceanic circulation of the area. The mean plume extends offshore to a maximum distance of 13 km (21 km) under low (high) river flow. In the latter situation, the most intense turbid values can surpass 0.6 mWcm^{-2}μm^{-1}sr^{-1}.
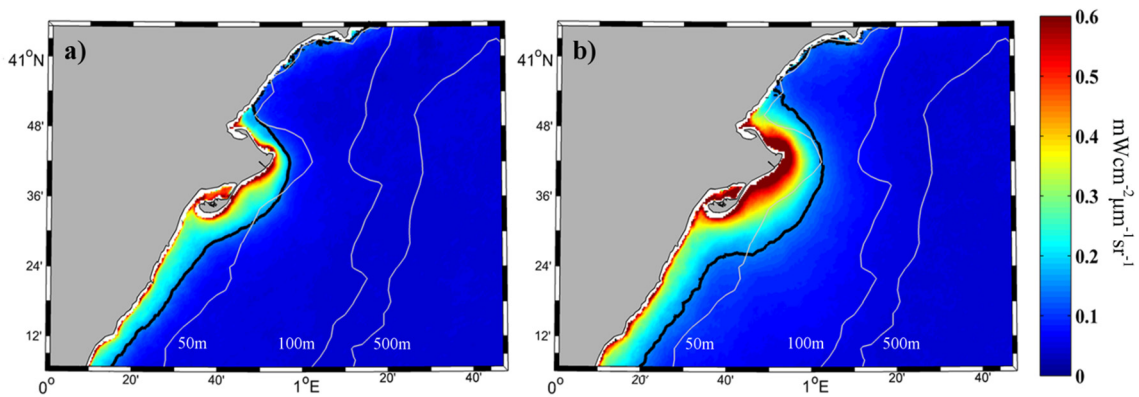
Figure 3.6. (a) Average turbid plume field (mWcm^{-2}μm^{-1}sr^{-1}) when river discharge is less than the 25th percentile. (b) Average turbid plume field (mWcm^{-2}μm^{-1}sr^{-1}) when river discharge exceeds the 75th percentile. The contour line corresponds to the turbid threshold (0.15 mWcm^{-2}μm^{-1}sr^{-1}).

3.3.2. Wind influence on Ebro plume

Wind influence on Ebro plume was only analyzed when coinciding with high daily river discharges (>355 m^3s^{-1}, which corresponds to the 75th percentile) because is the main driver and guarantees plume enough to be significantly affected by wind stress. The wind influence was analyzed taking into account alongshore (Figure 3.7) and cross-shore (Figure 3.8) winds, defined in *Section 2.2.2. "Wind data"*.

Alongshore winds with a northern component (AS$^-$) (Figure 3.7a) mostly range from 4 to 10 ms^{-1}. This type of wind occurs mainly in winter and spring (Durand et al., 2002), as it prevails in seasons when the river discharge is high. These downwelling favorable winds compress the plume against the coast because Ekman transport is onshore, which, along with the regional oceanic circulation, causes the formation of a turbid band along the coast with high turbid values (Figure 3.7b). The plume extends around 19 km offshore. The maximum turbid values (> 0.5 $mWcm^{-2}\mu m^{-1}sr^{-1}$) are achieved especially around the whole delta, with a seaward extension close to 11 km. These values can also be found along the southern coast, although to a lesser extent. According to Table 3.1, Ebro plume covers an area of 1758 km^2 under these conditions (244 km^2 north of the mouth and 1514 km^2 to the south), with a mean value of 0.48 $mWcm^{-2}\mu m^{-1}sr^{-1}$.
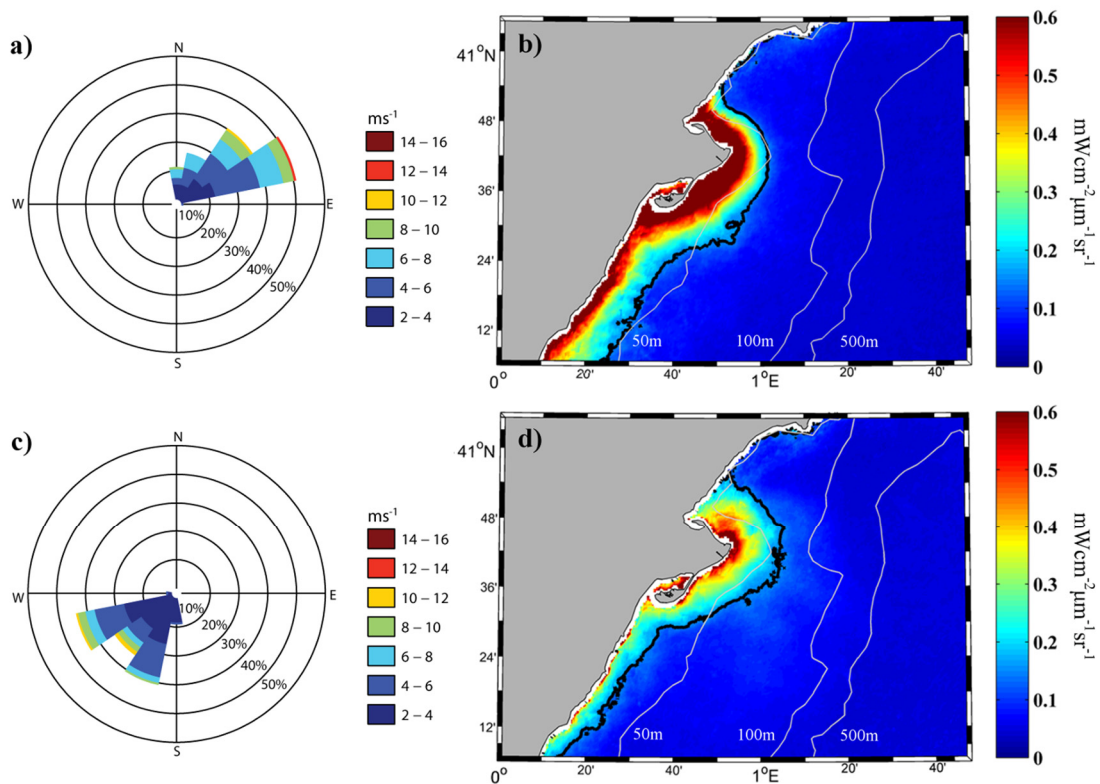
Figure 3.7. (a, c) Northern and southern alongshore wind roses (ms^{-1}) and (b, d) the associated turbid plume composite ($mWcm^{-2}\mu m^{-1}sr^{-1}$). The contour line corresponds to the turbid threshold (0.15 $mWcm^{-2}\mu m^{-1}sr^{-1}$).

Alongshore winds with a southern component (AS$^+$) (Figure 3.7c) mostly range from 2 to 10 ms^{-1}. This type of wind is present throughout the year and is generally weak (Durand et al., 2002). These upwelling favorable winds induce seaward movement of the Ebro plume due to the offshore Ekman transport, especially near the river mouth where the formation of a large bulge is observed. Under these conditions the plume can reach a maximum distance of 18 km offshore (Figure 3.7d). In this case, however, the plume did not reach a seaward extension as expected when compared with the previous situation, probably due to dilution with the surrounding seawater under these conditions (Fennel and Mutzke, 1997), which causes that many pixels reach lower values than the turbid threshold established. For this reason, the Ebro plume occupies an area with low mean turbid values. The maximum values (> 0.5 mWcm^{-2}µm^{-1}sr^{-1}) are observed around the delta and extend less than 4 km offshore. The total area occupied by the plume is 1325 km^2 (378 km^2 north of the mouth and 947 km^2 to the south) with a mean value of 0.30 mWcm^{-2}µm^{-1}sr^{-1} (Table 3.1).

Meteorological Synoptic Conditions		Plume Characteristics				Implications
River (m^{3}s^{-1})	Wind (calm discarded)	Extent (km^2)			Mean turbid value (mWcm^{-2} µm^{-1} sr^{-1})	
		North	South	Total		
629	Northern alongshore (AS$^-$)	244	1514	1758	0.48	Transport mainly along the south coast
645	Southern alongshore (AS$^+$)	378	947	1325	0.30	Offshore dispersion
711	Landward (CS$^-$)	320	1203	1523	0.37	Compression mainly around the whole delta
644	Seaward (CS$^+$) (Mistral)	279	1614	1893	0.33	Southwesterly movement in a large area

Table 3.1. Characteristics and implications of the Ebro turbid plume under different meteorological synoptic conditions. Extent: area referred to the fate of fluvial material that reaches the river mouth; North: north of the river mouth; South: south of the river mouth; Total: the total turbid plume area.

The influence of cross-shore winds on the distribution of the plume is shown in Figure 3.8. Landward winds (CS$^-$) mostly range from 2 to 8 ms^{-1} (Figure 3.8a). These winds are typical during the dry season (Durand et al., 2002). The landward winds compress the plume against the coast, especially near the river mouth, with an offshore extension not exceeding 17 km (Figure 3.8b). The maximum turbid values (> 0.5 mWcm^{-2}µm^{-1}sr^{-1}) are observed around the whole delta, with a seaward extension close to 8 km. The plume occupies a total area of 1523 km^2 (320 km^2 north of the mouth and 1203 km^2 to the south) with a mean value of 0.37 mWcm^{-2}µm^{-1}sr^{-1} (Table 3.1). The pixelation observed in this image is due to the low number of available days because this wind situation (winds from southeast) is the less frequent as commented above (Figure 3.2b).
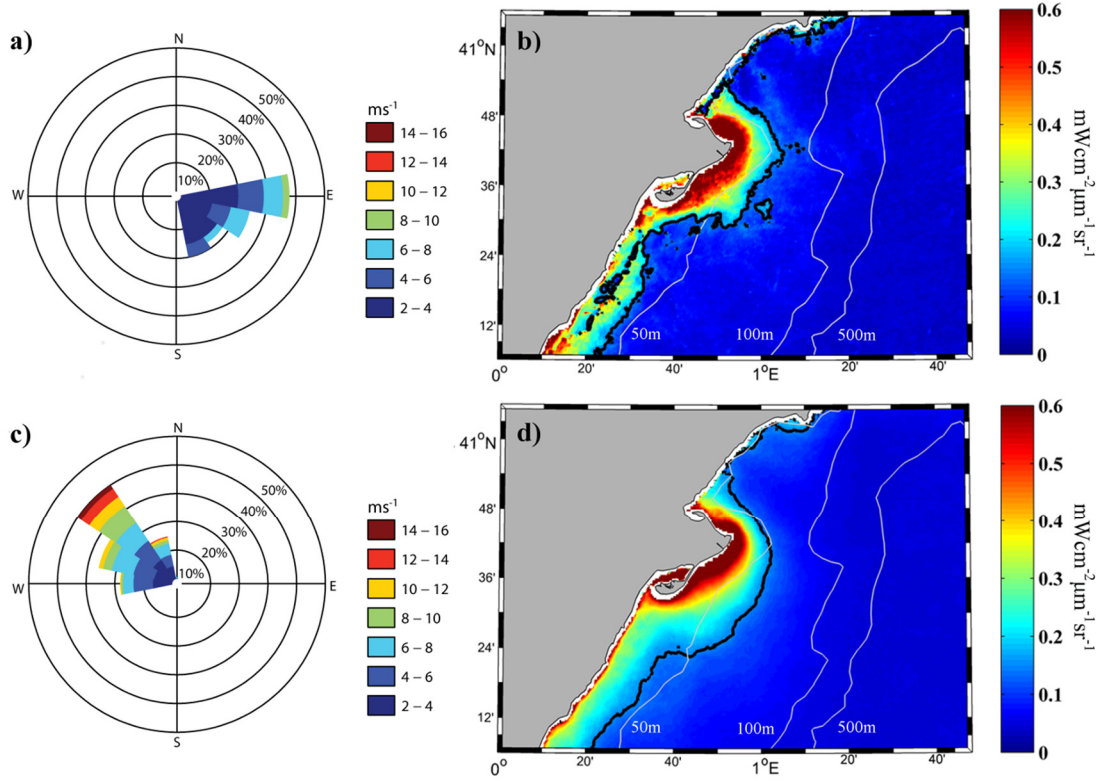
Figure 3.8. (a, c) Landward and seaward wind roses (ms⁻¹) and (b, d) the associated turbid plume composite (mWcm⁻²µm⁻¹sr⁻¹). The contour line corresponds to the turbid threshold (0.15 mWcm⁻²µm⁻¹sr⁻¹).

Seaward (mistral) winds (CS$^+$) mostly range from 4 to 14 ms⁻¹ (Figure 3.8c). This type of winds mainly occurs during autumn and winter (Durand et al., 2002), coinciding with high river discharges. Mistral winds tend to extend the plume offshore, which, along with the regional oceanic circulation, produces the largest spread of the plume to the south of the mouth (Figure 3.8d). Thus, the plume reaches a maximum offshore extension of around 28 km. High turbid values (> 0.5 mWcm⁻²µm⁻¹sr⁻¹) are found near the river mouth and farther south surrounding the delta area and extend 7 km offshore. The total area occupied by the plume is 1893 km² (279 km² north of the mouth and 1614 km² to the south) with a mean value of 0.33 mWcm⁻²µm⁻¹sr⁻¹ (Table 3.1).

Maps of differences on the turbid plume under different wind regimes are shown in Figure 3.9. Figure 3.9a shows the difference of composites for alongshore winds ($\Delta Turb_{AS} = Turb_{AS}^+ - Turb_{AS}^-$, where $Turb$ refers to turbid values, the subscript AS to alongshore winds and the superscript plus (minus) to the southern (northern) component of the wind as described above). The turbid pattern shows a strong negative difference along the coast and a fringe of positive difference offshore. This positive fringe is more intense north of the river mouth. This result is consistent with the prevailing wind induced currents.
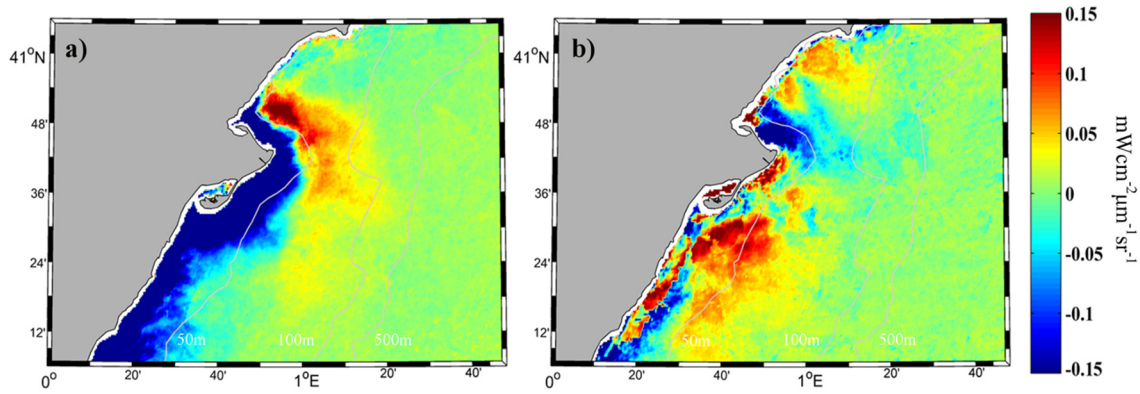
Figure 3.9. (a) Map of differences on the turbid plume field (mWcm⁻²μm⁻¹sr⁻¹) between alongshore winds (southern component minus northern component). (b) Map of differences on the turbid plume field (mWcm⁻²μm⁻¹sr⁻¹) between cross-shore winds (seaward minus landward).

The map of differences under cross-shore winds ($\Delta Turb_{CS} = Turb_{SW}^{+} - Turb_{LW}^{-}$, the subscripts *CS*, *SW* and *LW* refer to cross-shore, seaward and landward, respectively) is shown in Figure 3.9b. A positive difference is present, especially south of the river mouth, whereas a negative difference is present in the area of the mouth; this result is consistent with the prevailing winds.

In general terms, the highest (lowest) mean turbid value is observed for alongshore winds with a northern (southern) component and the largest (smallest) extension of the plume occurs under Mistral (southern alongshore) winds. The ratio between the area occupied by the plume to the north and to the south of the mouth is similar for the four situations under analysis. In average, 80% of the plume is found in the south, which can be explained by the influence of the regional oceanic circulation that exists in the area. The differences observed both in the extension of the plume and in the mean turbid values are not related to river discharge, which was similar for the different wind situations (differences are less than 15%; Table 3.1 first column).

3.4. Conclusions

The characteristics of the Ebro River plume under different meteorological and oceanographic conditions using MODIS-Aqua and MODIS-Terra remote sensing imagery were evaluated for the first time.

- Results show that the plume extension responses immediately to flow variations, increasing monotonically with the increase of river discharge, which illustrates that discharge is the main driving force.

- Wind is a secondary driver that has an important impact under high river discharge. A southward displacement of the plume occurs even in the absence of wind. More than 70% of the plume is located south of the river mouth under any

wind condition. This pattern is supported by the regional oceanic circulation of the area. Alongshore and cross-shore winds can enhance or inhibit this general pattern.

- Mistral winds produced the largest turbid plume extending offshore which, along with the regional oceanic circulation, generated the maximum plume extension with 1893 km^2. The plume extension was the smallest under southern alongshore winds (1325 km^2), as upwelling favorable winds tend to spread the plume offshore and favor its dilution with sea water due to the offshore Ekman transport. This difference in the plume extension can be also affected by the fact that the Mistral wind is the strongest and most persistent wind in the area. Alongshore winds with a northern component caused the highest mean turbid value (0.48 mWcm^{-2}μm^{-1}sr^{-1}), as downwelling favorable winds tend to confine the plume near shore as a consequence of the onshore Ekman transport. In contrast, alongshore winds with a southern component scatter the plume offshore, resulting in the lowest mean turbid value (0.30 mWcm^{-2}μm^{-1}sr^{-1}).

Chapter 4:

Influence of main forcing on the Douro turbid plume

4.1. Motivation

Douro River represents the most important freshwater input into the Iberian Peninsula coast (Figure 4.1). Plume formed by Douro River is significantly modulated by discharge and wind, as Ebro plume, but it is also affected by tidal forcing due to the meso-tidal regime of the Atlantic Ocean, which introduces a new forcing to be analyzed. This allows taking a step forward in the analysis and knowledge of plumes behavior under different forcing drivers.

The goal of this chapter is to evaluate the role of the river discharge, wind, and tide on Douro plume from 2003 to 2013, by means of the methodology described in *Chapter 2 "Data and Methodology"*. Douro plume variability will be analyzed using normalized water leaving radiance centered at 645 nm (nLw645) obtained from MODIS Aqua and Terra satellite sensors.
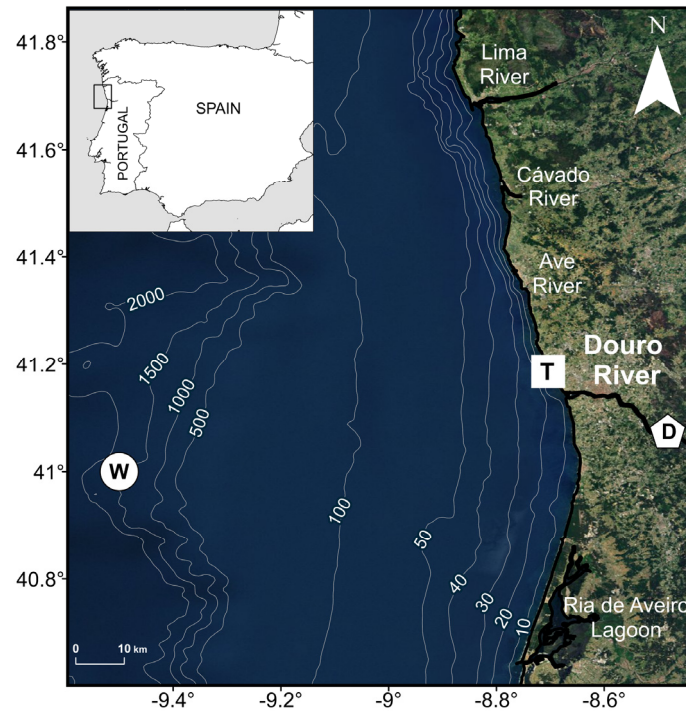
Figure 4.1. Location of the study area. D indicates the location where river discharge was sampled. W marks the location where wind data were obtained. T indicates the location where tidal data were sampled.

4.2. Main forcing affecting Douro plume

Daily mean Douro River discharge was obtained from the SNIRH database (www.snirh.pt) at the Crestuma-Lever dam from 2003 to 2013 (Figure 4.1). Douro River flow presents a seasonal variation, with high discharges during winter months and low ones during summer (Figure 4.2a). In addition, winter months present a stronger deviation because the discharge can range from values near to 0 m^{3}s^{-1} to values over 2500 m^{3}s^{-1} associated to periods of abundant rainfall. In general terms, the maximum mean monthly discharge occurred in January, 863 m^{3}s^{-1}, and the minimum in August with 113 m^{3}s^{-1}.

Daily wind data were obtained from CFSR database at an ocean location close to the river mouth (Figure 4.1). In the Western Iberian ocean region wind tends to be aligned with the coastal orientation (Figure 4.2b) (Gomez-Gesteira et al., 2006; Alvarez et al., 2008; Alvarez et al., 2011; Sousa et al., 2013). The wind pattern is characterized by strong north-northwesterly winds (upwelling favorable conditions), especially during summer, that can also occur during winter but with lower intensity and predominance. Additionally, strong southwesterly winds occur during winter linked to cyclogenetic processes, which generate frequent rainfall episodes (Trigo and DaCamara, 2000; Lorenzo et al., 2008).

Synthetic tidal data were calculated for a location near the mouth of the estuary for the period 2003-2013, using the T_Tide package (Pawlowicz et al., 2002), based on the major local tidal constituents. These were determined from hourly sea surfaced elevation measured at a tidal gauge located at Leixões harbor (Figure 4.1), during 2003 (Figure 4.2

c and d). A strong semidiurnal signature is observed. The average tidal range was 2.8 m with a maximum of about 3.8 m during equinoctial spring tides. The results agree with information described in the literature (Vieira and Bordalo, 2000; Marta-Almeida and Dubert, 2006).
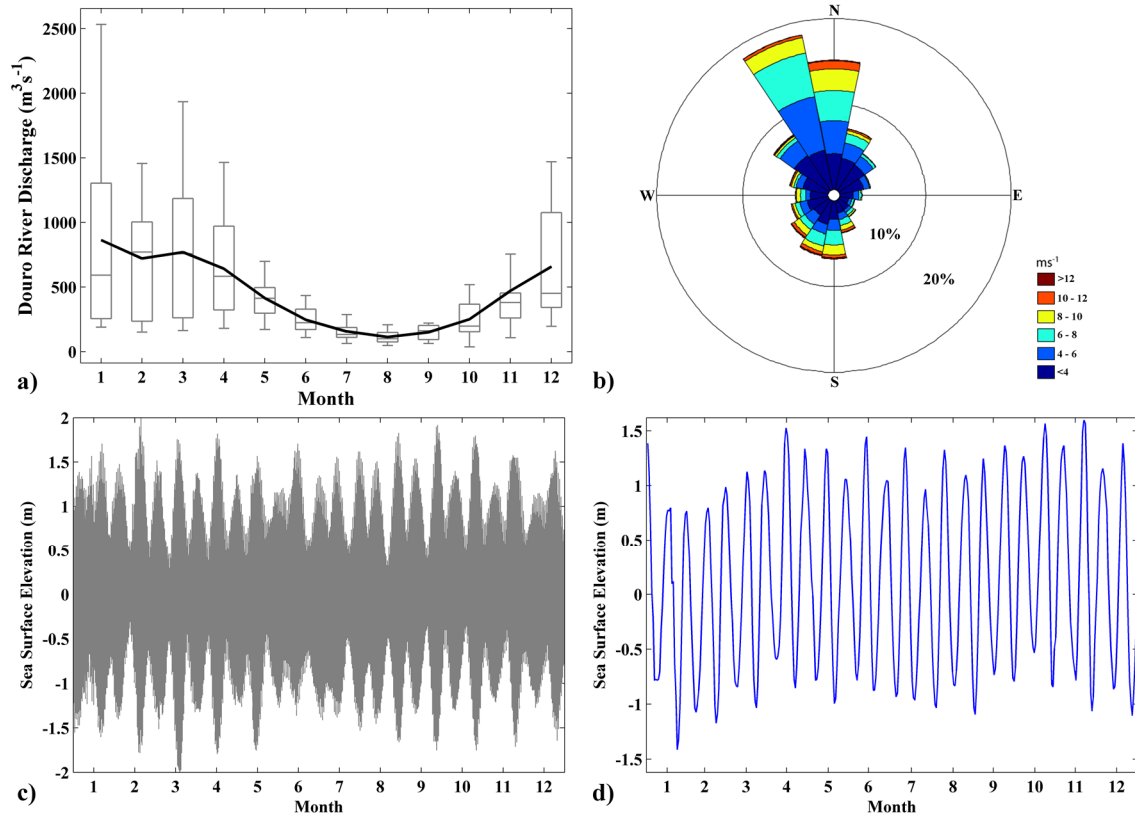
Figure 4.2. (a) Annual hydrologic cycle for Douro River discharge (m^3s^{-1}) from 2003 to 2013. Solid black line: monthly average; the line inside each box indicates the median; lower and upper whiskers: minimum and maximum, respectively; lower and upper box limits: first and third quartiles, respectively. (b) Wind rose diagram (ms^{-1}) for a location in front of Douro River mouth from 2003 to 2013. (c) Hourly sea surface elevation at Leixões harbor for 2003. (d) Sea surface elevation at Leixões harbor at the hour when Aqua satellite overpasses the Douro area for 2003.

The general conditions of the synoptic situations characterizing the main forcing under analysis are depicted in Table 4.1.

	Discharge		Wind				Tide	
	<25th	>75th	North	South	East	West	Low	High
Number of days	923	949	264	286	116	181	311	329
Mean river discharge (m^3s^{-1})	79	1146	890	1338	1066	1385	1235	1116

Table 4.1. General conditions of the main forcing affecting the Douro turbid plume. Number of days is referred to those days, which met the conditions imposed for each forcing and used to create the composites. Mean river discharge is referred to the average of daily discharges of those days representing each condition under analysis.

4.3. Results

4.3.1. River discharge influence on Douro plume

First of all, the correlation coefficient between plume area and daily river discharge (Figure 2.6) reaches the maximum when not lag is applied (above 0.5). This shows as Douro plume development responds immediately (at daily scale) to river discharge variations. The maximum correlation was reached for the threshold of 0.25 mWcm^{-2}µm^{-1}sr^{-1}, which represents the turbid limit for delimiting the Douro turbid plume.

The nLw645 mean turbid fields under low river discharge conditions (lower than 145 m^{3}s^{-1}, 25th percentile) and under high river discharges (higher than 542 m^{3}s^{-1}, 75th percentile) are depicted in Figure 4.3.
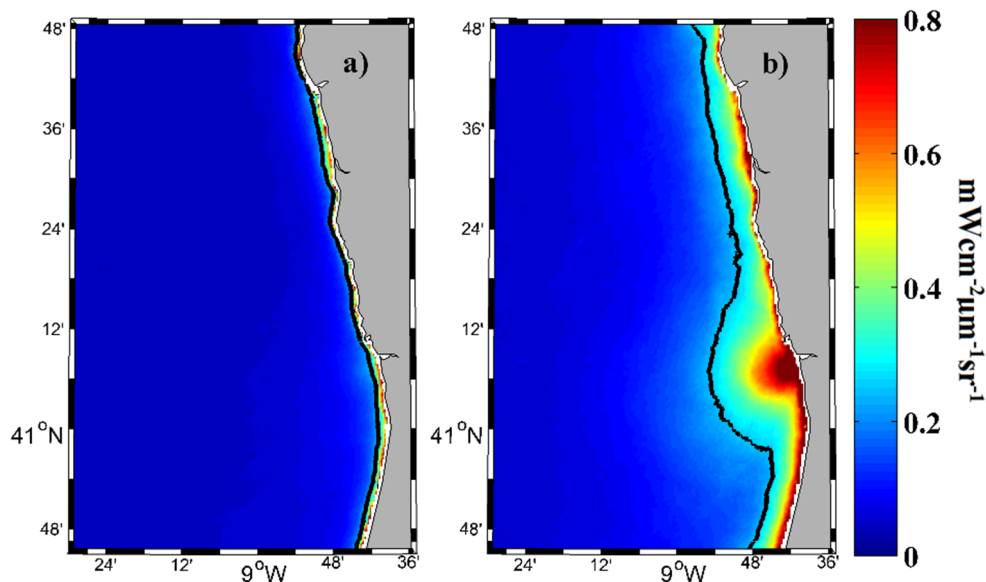
Figure 4.3. Douro turbid plume composite under (a) low river discharges (< 25th percentile) and (b) high river discharges (> 75th percentile). The black contour line corresponds to the turbid threshold (0.25 mWcm^{-2}µm^{-1}sr^{-1}).

Under low discharge conditions, a negligible turbid signal is detected, that is, Douro River is not able to form plume (Figure 4.3a). The pixel distribution is almost unimodal with most of the values below the turbid limit (0.25 mWcm^{-2}µm^{-1}sr^{-1}). Under high river discharges, the distribution of nLw645 values is markedly bimodal with a clear difference between ocean and coastal turbid waters (Figure 4.3b). A bulge is visible near the Douro Estuary mouth which reaches a maximum offshore extension of approximately 20 km forming a well defined plume under these conditions. A bulge is considered when a radially turbid coherent structure is detectable extending offshore from the estuary mouth. The bulge is wider than the alongshore coastal turbid band and has high turbid values. This shows the strong relationship between Douro River discharge and the turbid signal

detected by nLw645 band, which increases with the Douro discharge. This also implies that the other drivers should be evaluated under high discharge conditions (above 75th percentile) in order to have a plume sufficiently developed to be significantly affected by them.

4.3.2. Wind influence on Douro plume

First of all, it is necessary to take into account that there are important differences concerning the robustness of the results for the wind mean states. Northerly, southerly, and westerly winds have a larger number of possible scenes than easterly winds (Table 4.1). In addition, since southerly and westerly winds are linked to cyclogenetic processes in the Douro plume area, their scenes are more contaminated by clouds. This fact also explains that under these wind regimes the mean Douro River discharge for the possible scenes is higher.

The nLw645 mean turbid fields under different wind regimes (North, South, East, and West) are depicted in Figures 4.4 and 4.5. Upwelling favorable (northerly) winds (AS$^+$) induce an offshore expansion of the Douro estuarine outflow plume. This pattern is especially visible near the mouth, where the bulge can reach an extension close to 30 km with a slight inclination southwestward (Figure 4.4a). In addition, two turbid coastal bands are detectable in opposite directions from the Douro Estuary mouth. Although the southward turbid band has stronger intensity, the Cávado River appears to have a non-negligible contribution for the coastal turbid band northward, since a local increase in the turbid values is detected nearby the river mouth.

Despite the plume cannot be so clearly identified as in the counter case, under downwelling favorable (southerly) winds (AS$^-$) an alongshore plume confinement to the coast along the north direction can be detected (Figure 4.4b). This coastal plume band scarcely surpasses 10 km width and the bulge formation is not perceptible. An irregular and weak turbid signal is again detected southward.

Concerning wind direction, Figures 4.4c and d show a predominance of strong winds blowing from north-northeast and south-southwest in upwelling and downwelling favorable conditions, respectively. In terms of wind intensity and percentage of occurrence, the results present a similar pattern for both cases, mostly ranging from 4 to 10 ms^{-1}. In addition, composite under southerly winds is under a mean river discharge higher than composite under northerly winds, due to they are linked to cyclogenetic processes as commented above (Table 4.1).
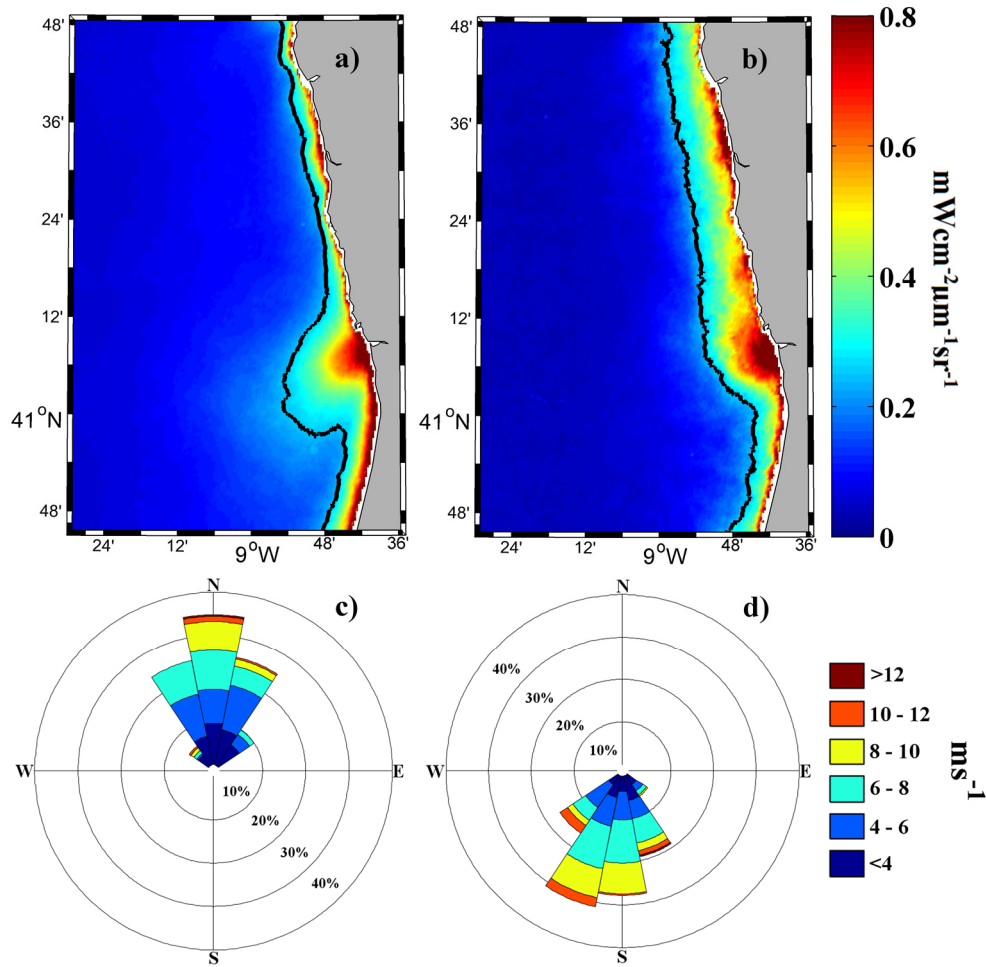
Figure 4.4. Douro turbid plume composite under (a) upwelling favorable (northerly) winds and (b) downwelling favorable (southerly) winds. The black contour line corresponds to the turbid threshold (0.25 mWcm^{-2}μm^{-1}sr^{-1}). (c, d) Respective wind roses.

The impact of cross-shore winds on Douro plume is shown in Figure 4.5. Under seaward (easterly) winds (CS$^+$), a bulge is identified with a clear detachment from the coast and a northward orientation. A thin turbid coastal band is only detected south of the bulge (Figure 4.5a). The nLw645 mean turbid field under landward (westerly) winds (CS$^-$) shows a plume confinement to the coast in both alongshore directions, with a continuous coastal turbid band of about 25 km width (Figure 4.5b). Although the bulge delimitation is unclear, higher turbid values (> 0.6 mWcm^{-2}μm^{-1}sr^{-1}) form a semi-circular pattern at the Douro Estuary mouth.

Concerning wind magnitude and direction, some differences must be taken into account in the analysis of cross-shore wind influence. The predominant directions of westerly winds are from west-southwest (Figure 4.5d), mostly ranging from 4 to 10 ms^{-1}. Otherwise, all easterly winds are weaker (mostly ranging from 2 to 6 ms^{-1}) with a major predominance of east-northeast direction (Figure 4.5c). In addition, composite under

westerly winds presents a mean river discharge higher than the one under easterly winds because are linked to cyclogenetic processes (Table 4.1).
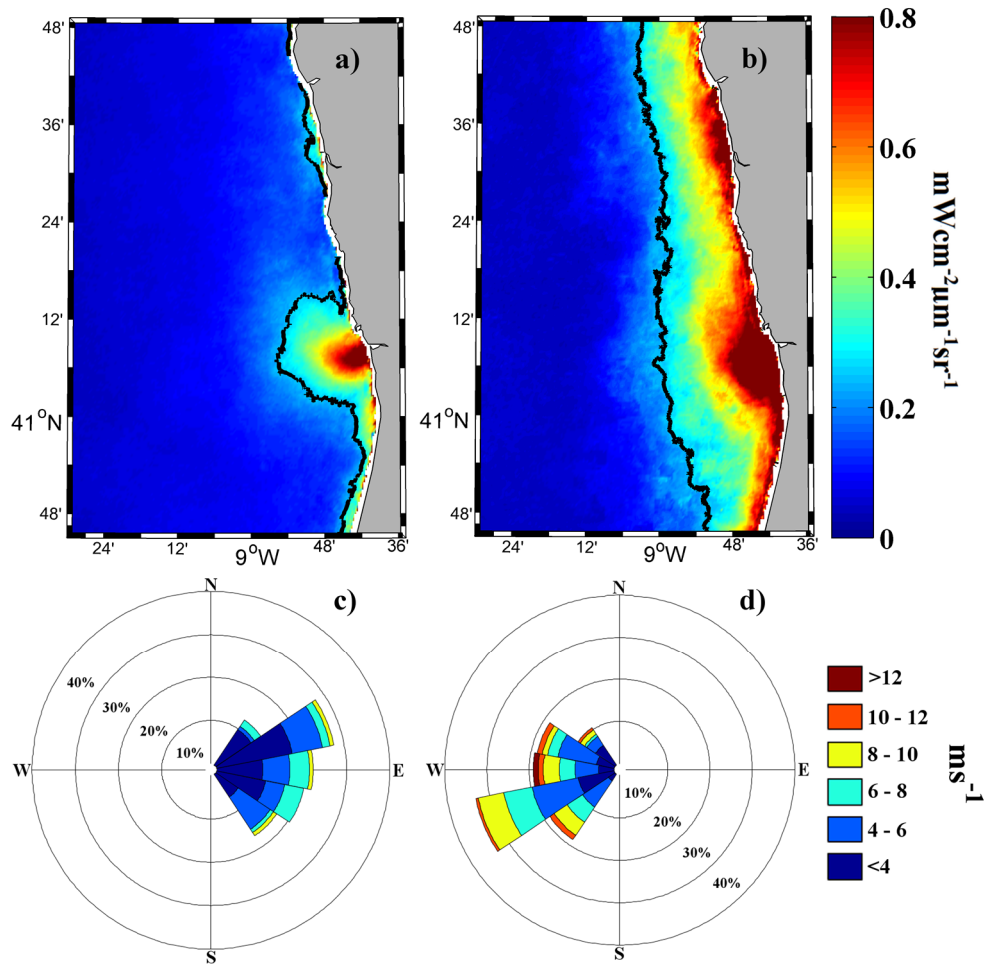
Figure 4.5. Douro turbid plume composite under (a) seaward (easterly) winds and (b) landward (westerly) winds. The black contour line corresponds to the turbid threshold (0.25 mWcm^{-2}μm^{-1}sr^{-1}). (c, d) Respective wind roses.

Maps of differences between alongshore (downwelling minus upwelling) and cross-shore (landward minus seaward) winds are depicted in Figures 4.6a and b, respectively. In the first scenario, the southerly winds cause a large coastal region of positive differences (> 0.15 mWcm^{-2}μm^{-1}sr^{-1}), which is visible northward from the estuary mouth (Figure 4.6a). This region of influence is a very regular structure about 15 km wide. On the other hand, the bulge region and the thin coastal band southward present the major negative differences (< -0.15 mWcm^{-2}μm^{-1}sr^{-1}). In fact, the bulge region under high negative differences reaches an extension surpassing 50 km. In addition, it is important to note that even in the northern part of the area represented there is a remarkable influence of the northerly winds above 15 km offshore.

Map of differences between cross-shore winds shows as westerly winds provoke a band of strong positive differences all along the coast (Figure 4.6b). These high positive values, above 0.15 mWcm^{-2}μm^{-1}sr^{-1}, are maintained until 25-30 km from the coast, when negative values, promoted by the major influence of easterly winds, became dominant, although with low intensity (~-0.05 mWcm^{-2}μm^{-1}sr^{-1}), probably affected by the weakness of these winds.
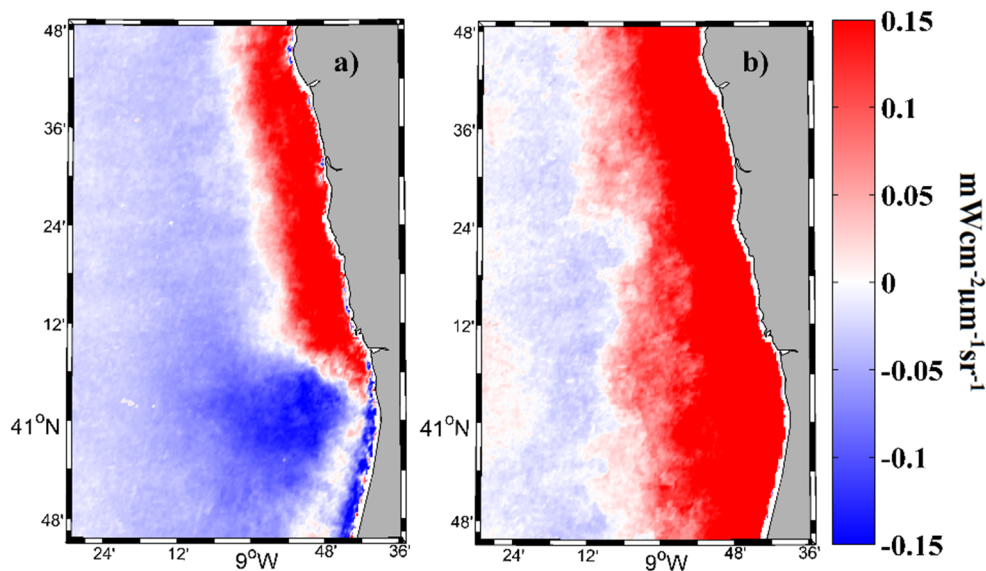
Figure 4.6. Map of differences on the Douro turbid field between (a) alongshore winds (downwelling minus upwelling) and (b) cross-shore winds (landward minus seaward).

The wind impact on Douro plume was also analyzed by means of turbidity transects both in the alongshore and across-shore directions. The turbidity transect in the alongshore direction (parallel to the coast) starts at the Douro mouth and extends northward (negative values) and southward (positive values) at a coastal distance of approximately 8 km (Figures 4.7a and b). Turbidity along this transect shows that upwelling winds (Figure 4.7a, red line) produce a rapidly decrease of turbidity from the mouth toward both sides, although more moderate to the south, which corroborate the bulge form with a southwestward inclination detected in Figure 4.4a. Downwelling winds (Figure 4.7a, blue line) promote higher turbid values due to the plume accumulation from the mouth toward the north, where high turbid values are maintained larger distances. This behavior is in accordance with the coastal turbid band observed northward in Figure 4.4b. On the other hand, an abrupt decrease in turbid values is observed to the south, showing the predominant plume movement toward the north under downwelling favorable winds.

Both cross-shore winds present a similar pattern along the alongshore transect, with maximum values near the mouth, descending away from it. In the case of seaward winds (Figure 4.7b, red line), the turbid values are rapidly below the limit, which indicate the formation of a well defined plume bulge around river mouth corroborating the visual

information obtained in Figure 4.5a. On the other hand, western cross-shore winds (Figure 4.7b, blue line) are able to maintain high turbid values, above the turbid limit, in both alongshore directions over large distances, which indicate the formation of a large coastal plume band as shown in Figure 4.5b.
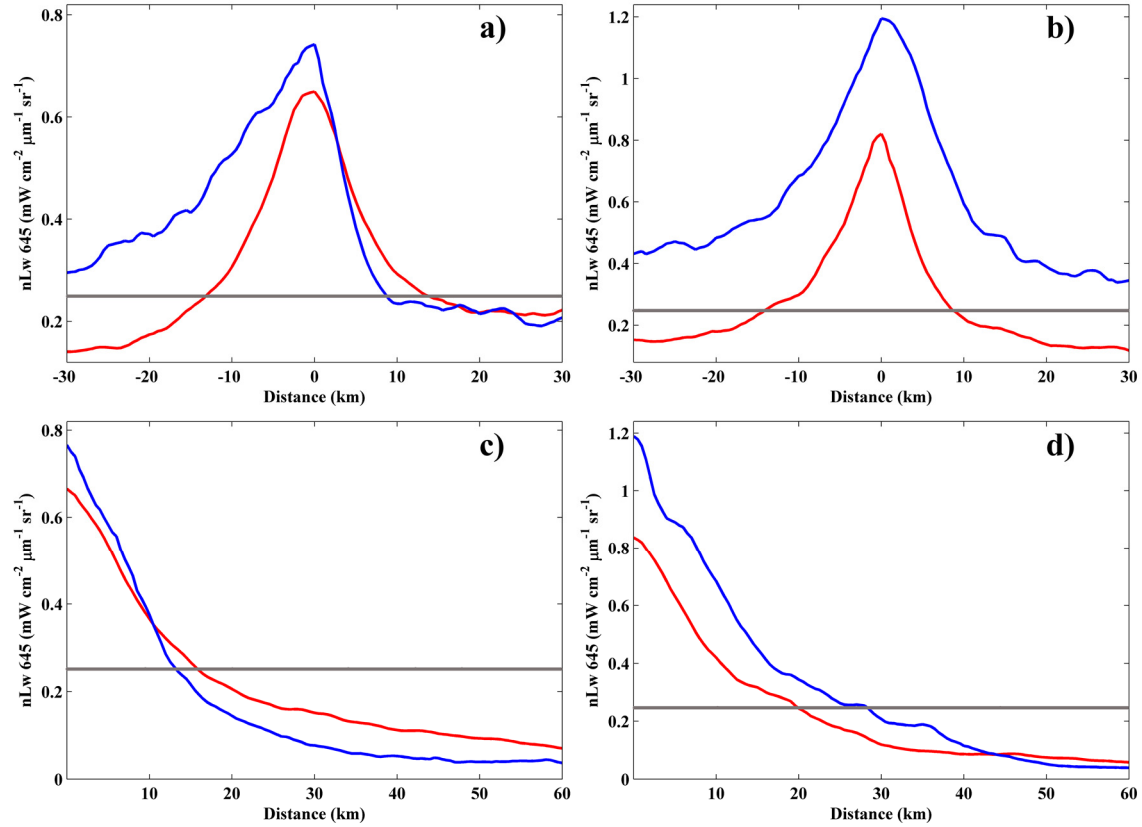
Figure 4.7. Turbidity along a transect parallel to the coast at a distance of about 8 km for (a) alongshore and (b) cross-shore winds. Turbidity along a transect perpendicular to the coast for (c) alongshore and (d) cross-shore winds. Blue line represents downwelling (landward) winds and red line upwelling (seaward) winds for alongshore (cross-shore) winds. Grey line represents the turbid threshold. The zero marks the river mouth and negative distances refer to the region located north to the river mouth.

The turbidity transect in the cross-shore direction, starts at the river mouth and moves offshore in the perpendicular direction to the coast. In the case of alongshore winds, turbidity along this transect shows that higher maximum turbid values are reached near the mouth (about 0.8 mWcm^{-2}μm^{-1}sr^{-1}) under southerly winds, due to the confinement of plume material near coast (Figure 4.7c, blue line). This confinement also provokes an abrupt decrease of turbid values with the distance until reach negligible values from 30 km. Maximum turbid values are lower under upwelling winds (scarcely surpass 0.6 mWcm^{-2}μm^{-1}sr^{-1}), descending moderately with the distance due to the offshore dispersion and dilution promoted (Figure 4.7c, red line). Therefore, upwelling winds show their capability to transport plume material large distances over the ocean since values above the residual ocean turbidity can be detected several kilometers offshore, corroborating the

visual information obtained in Figures 4.4a and 4.6a. On the other hand, turbid values descend drastically away from the coast under downwelling winds (Figure 4.7c, blue line), which indicates that most of the material is retained near coast, as can be observed in Figures 4.4b and 4.6a.

Similar patterns can be detected under cross-shore winds (Figure 4.7d), with maximum values of turbidity reached under landward winds (Figure 4.7d, blue line) near the Douro mouth (about 1.2 mWcm^{-2}μm^{-1}sr^{-1}). Landward winds dominate the whole near shore area maintaining higher turbid values over a large distance in the ocean. Under seaward winds (Figure 4.7d, red line) maximum turbid values scarcely surpass 0.8 mWcm^{-2}μm^{-1}sr^{-1}.

4.3.3. Tide influence on Douro plume

The nLw645 mean turbid fields during high and low tides are shown in Figures 4.8a and b, respectively. Although no significant differences can be found between composite images during high and low tide periods, a slight greater expansion of the plume with higher turbid values can be detected during low tides. The strongest changes are observed close to the Douro Estuary mouth where a retraction of the bulge is detected during high tides (Figure 4.8a).
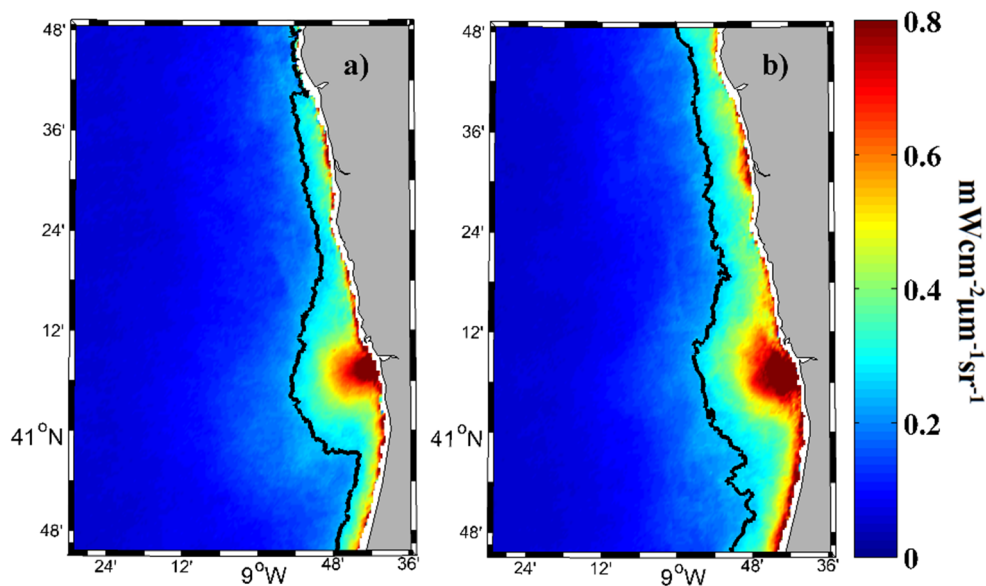
Figure 4.8. Douro turbid plume composite under (a) high tides and (b) low tides. The black contour line corresponds to the turbid threshold (0.25 mWcm^{-2}μm^{-1}sr^{-1}).

The robustness and composite balance between the two tidal phases are very satisfactory, since both cases have high representativeness (Table 4.1). In addition, the mean river discharge is similar in the two tidal phases, which further increases the significance of the obtained results.

4.4. Discussion

The present study showed a marked influence of river discharge on turbid patterns in the Douro River coastal zone. There is a consistent relation between the spatial distribution of nLw645 and the daily river discharge. Plume area increases with the increasing in river inflow (Figure 4.3). During low river discharges it is very unlikely to find turbid values above 0.25 mWcm^{-2}μm^{-1}sr^{-1}. However, a circular turbid pattern is well distinct under high river discharges. This result is consistent with the values discussed in previous works by Mourato (2008) and Teodoro et al. (2009).

The role of alongshore winds on the Douro plume displacement is crucial during high river discharge conditions, when there is enough plume material to be modulated by wind forcing. Under upwelling favorable winds, an offshore expansion of the bulge with a southwestward orientation is observed (Figure 4.4a). This is attributed to the offshore Ekman current generated by these winds. This bulge feature is corroborated when transects of turbidity are analyzed showing as most of plume material is centered at the river mouth with a significant expansion to the ocean oriented to the south (Figures 4.7a and c). The plume extension and its southwestward advection by surface currents agree with modeling results presented in previous works (Otero et al., 2008; 2013), representing a common feature along the Portuguese coast as studied by Vaz et al. (2009) for the Tagus estuarine plume. However, the southward turbid band attached to the coast detected was not described in those studies. In fact, a plume movement to right of the estuary mouth is expected in the Northern Hemisphere due to the Coriolis deflection. The southward turbid band observed under upwelling winds could be explained as the result of southward wind-driven surface currents. In regions shallower than the surface boundary-layer the surface cross-shore transport decreases being more important in the direction of the wind-driven circulation (Lentz and Fewings, 2012). This could explain the southward turbid band appearance under upwelling winds. However this band not only occur with northerly winds since it is also observed under south, east (weak but visible) and west wind regimes. These features were also observed in numerical models, when an ambient flow (10 cms^{-1}) is imposed in the opposite direction of the Kelvin wave propagation (García Berdeal et al., 2002). The area under scope has a northwest dominant wave direction, which represents about 72% of the occurrences (Rusu and Guedes Soares, 2013). The predominant wave direction induces a surface current in the north-south direction that could represent this ambient flow (Veloso-Gomes et al., 2004). This littoral drift could play an important role in southward sediment transport near the coast (Dias et al., 2002; Coelho and Veloso-Gomes, 2004). The spatial orientation of the estuary axis (direction of the discharge relative to the coast) can also play an important role in this near coastal flux (Yankovsky, 2000; Garvine, 2001). The angle between coastline and Douro Estuary inlet orientation is approximately 45°, in the opposite direction of Coriolis deflection, which can promote a southward flux near the estuary mouth.

Under downwelling favorable winds a northward confinement of the estuarine plume along the coast is observed (Figure 4.4b). This plume feature is also corroborated

analyzing the turbidity transects, where high turbid values are only detected to the north (Figures 4.7a and c). This is due to the combined effect of wind and Coriolis force on the Northern Hemisphere, forcing an onshore current which tends to push the plume towards the coast. This coastal turbid band scarcely surpass 10 km wide, which agree with the numerical modeling results of Otero et al. (2008) for the Western Iberian Buoyant Plume. The formation of the bulge is not so clear and increases the chance of the freshwater from the Douro Estuary to merge with water from smaller rivers located further north (i.e. from Ave, Cávado and Lima Rivers). Thus, a continuous coastal-attached turbid band is generated to the north. Important biogeochemical consequences would take place, since water from these smaller rivers spreads their constituents over a much larger area, amplified by the Douro Estuary input from the south (Warrick and Fong, 2004; Saldías et al., 2012).

The cross-shore winds also present an important impact on Douro plume displacement since in shallow waters the cross-shelf wind stress is a non-negligible term in the cross shelf momentum balance (Lentz and Fewings, 2012). Seaward winds tend to move the material discharged into the ocean generating a bulge in front of the estuary mouth (Figure 4.5a), which is also corroborated by means of the turbidity transects analyzed (Figures 4.7b and d). The bulge presents a clear detachment from the coast with a deflection to the right. Although these winds also promote the seaward expansion of the plume, the offshore advection is significantly higher under upwelling favorable winds. This can be explained in terms of wind magnitude, which is more intense for the upwelling winds. In addition, offshore surface transport seems to reach a stationary location (25 km) under seaward winds, then turning to an alongshore direction, while during northerly winds offshore spreading occurs until the plume waters are no longer distinguishable from the ocean waters. These results are consistent with those presented by Chao (1988), Choi and Wilkin (2007), and Jurisa and Chant (2012). Landward winds tend to accumulate freshwater along the coastline and to decrease the cross-shore transport (Figure 4.5b). The bulge is squeezed towards the coast generating an alongshore turbid band both in northward and southward directions, which is also detected when the turbidity transects are analyzed (Figures 4.7b and d). A similar pattern can be found in numerical simulations carried out by Chao (1988).

Tides influence the Douro turbid plume especially close to the coast and at the estuary mouth. In general, the offshore advection is slightly greater under low tides, however, opposite that the other forcing analyzed, small differences were found (Figure 4.8). The major discrepancies were observed in the near-field bulge, where tidal currents are more important. The area occupied by the highest turbid values (> 0.6 mWcm^{-2}μm^{-1}sr^{-1}) is greater under low tides, forming a well-defined semicircular pattern from the river mouth. This shows as high tides act as constraint factor on plume formation. This area of influence seems to be representative of a pulsed tidal plume zone under sharp fronts with semi-circular form (Horner-Devine et al., 2009). The region of tidal influence for the Douro estuarine plume only extends 20 km offshore, radially from the estuary mouth. The analysis of high and low tidal impact on Douro plume must be cautious because of

tidal aliasing, which can mask the "real" differences between low and high tides, as pointed out by Valente and da Silva (2009) for the Tagus turbid plume. However, the fortnightly tidal cycle seems to have negligible impact on the Douro plume, probably because the water residence time inside the Douro Estuary is too short to enhance turbidity during spring tides. Tagus River presents a large estuary before reaching the ocean, which generates a longer water residence time (Braunschweig et al., 2003).

4.5. Conclusions

Daily nLw645 images from MODIS sensor onboard of Aqua and Terra satellites allow a robust analysis of the Douro plume behavior under the influence of its main forcing drivers. Mean turbid fields of the synoptic situations characterizing the main driving mechanics (river discharge, wind and tide) were constructed in order to describe the mean state feature of this turbid plume under each forcing. Accordingly the main conclusions of this study are the following:

- A strong relationship was found between Douro River flow and nLw645 data, whose signal increases according to river discharge. A circular turbid pattern is well distinct when the flow exceeds 500 m^3s^{-1}. However, there is no plume evidence under low discharge regime.

- An offshore plume expansion is observed under upwelling favorable winds forming a well-defined bulge in front of river mouth with a clear southwestward inclination. On the other hand, a plume confinement along the north coast is detected under downwelling favorable winds. In this case the bulge formation is not clear and the possibility of the plume to merge with water from smaller rivers located northward increases.

- Under seaward winds a bulge generation with an offshore detachment from the coast and an inclination to the north is detected. A smaller offshore spreading is observed in comparison with upwelling favorable wind situation, probable due to the weakness of easterly winds. Landward winds tend to accumulate the material discharged by the river near shore in both alongshore directions, and consequently a decreasing in the cross-shore advection. The bulge is confined to the coast producing a continuous and large turbid band toward both sides of the mouth.

- Lower differences are found in the turbid plume patterns between high and low tide periods. However, a slightly greater offshore expansion of the turbid plume is detected under low tidal periods.

Chapter 5:

Influence of main forcing on the Tagus turbid plume

5.1. Motivation

Tagus is the largest river of the Iberian Peninsula representing one of the most important inputs on the Iberian coast. Plume formed by Tagus River is affected by discharge patterns, wind stress and semidiurnal tidal cycle, as same than Douro plume. However, Tagus plume is also significantly modulated by the fortnightly tidal cycle due to the longer water residence time promoted by the large estuary formed before empty into the Atlantic Ocean, which is large enough to enhance turbidity (Braunschweig et al., 2003; Valente and da Silva, 2009). The effect of overlapping semidiurnal and fortnightly tidal cycles on plumes formed by rivers discharging in large estuaries has not been previously investigated. The water residence time provoked by the Tagus Estuary is an important component on plume behavior and dispersion when compared to rivers directly flowing into the ocean, as Ebro or Douro. In addition, the coast configuration also makes differences respect to the other rivers analyzed, because Tagus Estuary empty in the ocean into a semi-enclosed embayment (Figure 5.1). In spite that West Iberian coast has a predominant S-N orientation, the coast is oriented SE to NW near the Tagus River mouth, playing a key role on plume dynamics. In fact, Tagus plume development is protected from the waves, which have a dominant NW direction, by the configuration and orientation of the coastline with only the southern part of the estuarine channel exposed

to the swells (Figure 5.1) (Rusu et al., 2011). In addition, Sintra mountains, located north of Lisbon, can affect wind patterns.
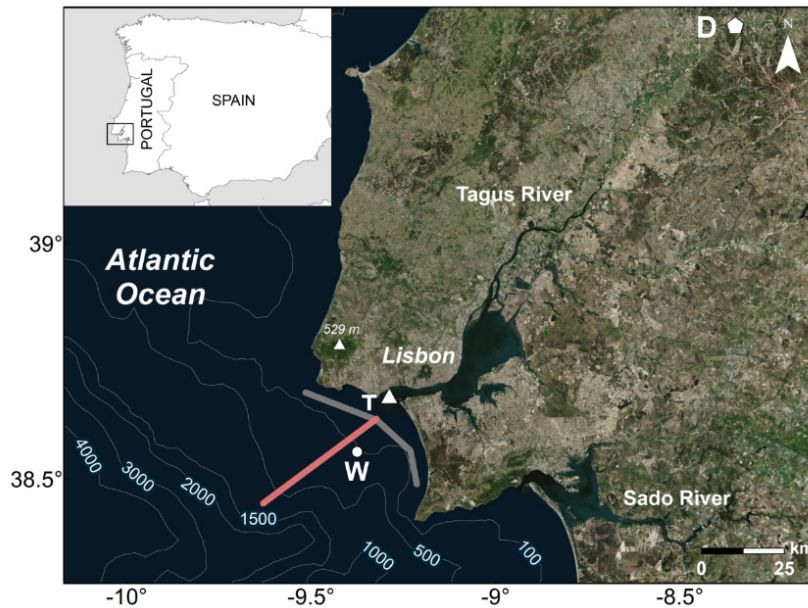
Figure 5.1. Localization of the study area. Tagus River mouth is located between capes Espichel and Raso (Tagus ROFI area). D marks the position of the Almourol station where river discharge data were obtained. W indicates the point where wind data were acquired. T represents the area of Cascais where tidal data were predicted. Grey and pink lines mark the alongshore and cross-shore transects used to analyze turbidity. Service Layer Credits Source: Esri, DigitalGlobe, GeoEye, icubed, Earthstar, Geographics, CENS/Airbus DS, USDA, USGS, AEX, Getmapping, Aerogrid, IGN, IGP, swisstopo, and the GIS User Community.

The goal of this chapter is to evaluate the role of the main forcing, river discharge, wind, and the semidiurnal and fortnightly tidal cycles, on Tagus plume from 2003 to 2015 using the developed methodology described in *Chapter 2 "Data and Methodology"*. Impact of the topography and morphology of the coast on Tagus plume patterns will be also analyzed. Spatial and temporal variability analysis of the Tagus turbid plume will be conducted using normalized water leaving radiance centered at 645 nm (nLw645) obtained from MODIS Aqua and Terra satellite sensors.

5.2. Study area

The study area covers a region comprised between 38.3ºN-39ºN latitude and 8.75ºW-9.8ºW longitude. However, special attention will be paid to the shelf area enclosed by the bay comprised between 38.41ºN-38.78ºN latitude and 9.22ºW-9.51ºW longitude, which will be thereby labeled the Tagus ROFI (Region Of Freshwater Influence). This region only takes into account the effect of the Tagus plume minimizing the influence of other small river plumes (principally the Sado River plume) and/or overestimations of turbidity caused by other processes as upwelling blooms or resuspension (Oliveira et al., 2009).

5.3. Methods

The methodology followed to analyze Tagus plume response to the main forcing was the same explained in the *Chapter 2 "Data and Methodology"*, but introducing some modifications in order to better analyze Tagus plume. Tagus River discharge was evaluated only taking into account days under calm intervals, that is, days with wind velocities < 2 ms^{-1} lasting for a 2 day period before the date of recording, in order to avoid the wind influence which could mask river discharge impact on river plume. This is a critical issue for Tagus plume since the particular coast configuration together with the predominant north component of winds most of the year, promote conditions favorable to produce superficial upwelling blooms, which can generate radiances not associated with river discharges west of Tagus ROFI (Moita et al., 2003; Valente and da Silva, 2009). In addition, high discharges will be considered above the 66th percentile and avoiding extreme flows above the 95th percentile because under extreme high discharges Tagus plume can be large enough to reach the upwelling blooms making both patterns undistinguishable (Valente and da Silva, 2009). Wind influence on Tagus plume will be analyzed allowing only a deviation of $\pm 30°$ due to the configuration of the Tagus ROFI. In addition, the impact of the semidiurnal tidal cycle on Tagus plume was evaluated in the middle of the fortnightly cycle, out of spring or neap tides, in order to isolate the semidiurnal effect. The same for the evaluation of the fortnightly cycle on Tagus plume. It was evaluated in the middle of the semidiurnal cycle, out of high or low tides. In spite of these adjustments all the situations under scope present an enough number of images to adequately evaluate plume patterns (Table 5.1).

Synoptic Situation	Number of days	River Discharge (m³s⁻¹)			
		Mean	Min	Max	Std
River Discharge					
Low	**148**	**45.06**	4.53	76.52	14.38
High	**161**	**374.80**	208.70	942.43	123.98
Wind condition					
Northern alongshore	**361**	**374.59**	208.66	991.23	144.08
Southern alongshore	**102**	**439.42**	211.46	995.96	198.63
Eastern cross-shore	**146**	**402.94**	208.10	995.63	173.98
Western cross-shore	**151**	**449.34**	211.41	990.34	181.16
Fortnightly tidal state					
Before Spring	**125**	**409.78**	211.99	931.42	169.41
Spring	**178**	**405.53**	208.10	999.01	192.02
Before Neap	**130**	**388.54**	214.29	926.41	162.63
Neap	**212**	**387.27**	208.66	953.30	157.17
Semidiurnal tidal state					
High Tide	**237**	**406.23**	197.82	974.16	169.48
Low Tide	**181**	**402.61**	198.29	940.07	171.78

Table 5.1. Main synoptic conditions analyzed in this study. Number of days is referred to the available days representing each condition and used to create the respective composites. The main conditions of Tagus River discharge associated to each situation (mean, minimum, maximum and deviation values) are also shown.

5.4. Main forcing affecting Tagus plume

Daily runoff data were obtained from the SNIRH ("Sistema Nacional de Informação de Recursos Hídricos") database (www.snirh.pt) at Almourol hydrometric Station (Figure 5.1) from 2003 to 2015. The river flow presents seasonal variation, with high discharges in winter reaching a maximum in February with a mean monthly value of ~ 450 m^3s^{-1} and low discharges in summer showing a minimum in September with a mean monthly value of ~ 100 m^3s^{-1} (Figure 5.2a). The mean daily river discharge over the period under study was 249 m^3s^{-1}, with a minimum daily value of 1 m^3s^{-1} and a maximum of 5010 m^3s^{-1}.
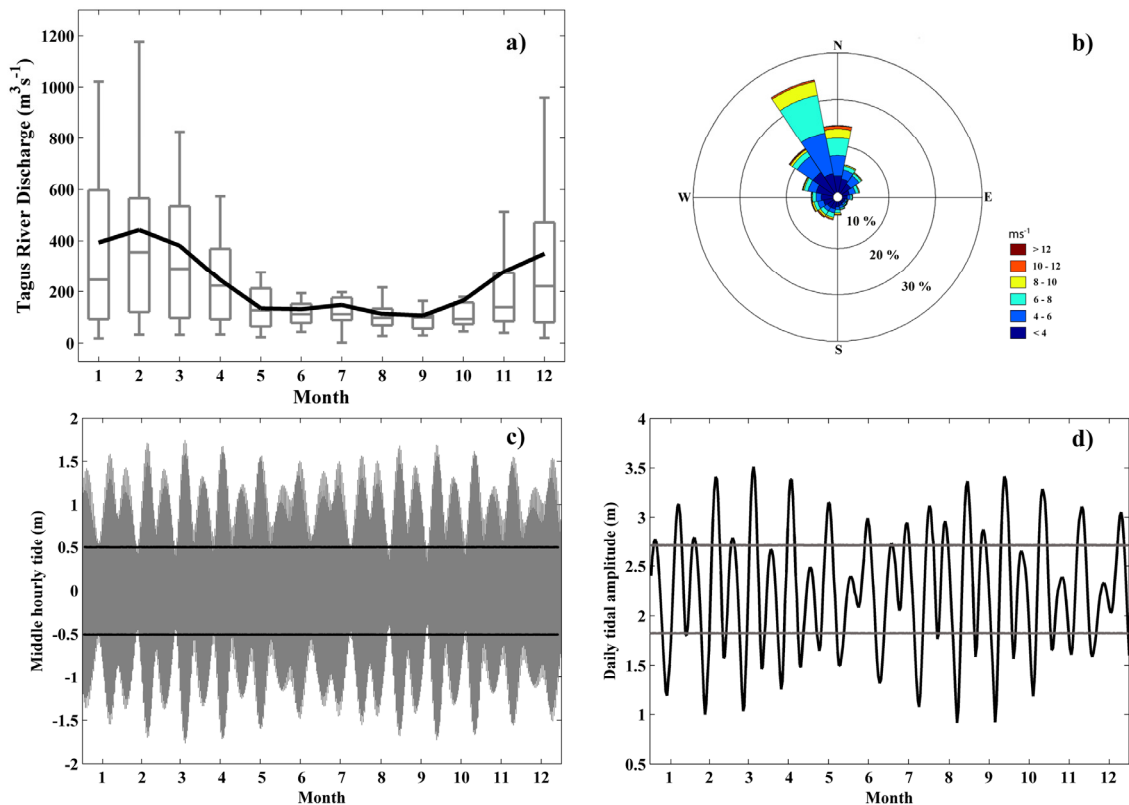
Figure 5.2. (a) Annual hydrologic cycle for Tagus River discharge (m^3s^{-1}) obtained from 2003 to 2015. Solid black line: monthly average; the line inside each box indicates the median; lower and upper whiskers: minimum and maximum, respectively; lower and upper box limits: first and third quartiles, respectively. (b) Wind rose (ms^{-1}) of the Tagus ROFI during the period of 2003 to 2015. (c) Surface elevation of seawater at Cascais for 2007. Solid lines represent the limits of high and low tide. (d) Daily tidal amplitude at Cascais for 2007. The solid lines indicate the limits of spring and neap tides.

Daily wind data were obtained from CFSR database at an ocean location close to the river mouth (Figure 5.1). Tagus ROFI area was principally subjected to predominant northerly and northwesterly winds, followed by northeasterly and southwesterly winds, with velocities mostly ranging from 4 to 10 ms^{-1} (Figure 5.2b).

Tidal data were predicted for a specific point located near Cascais (outside the estuary) and situated within the Tagus plume propagation region. The maximum sea surface

elevation was 1.81 m, whereas the minimum was -1.77 m, taking into account series centered in 0 m (Figure 5.2c). The maximum daily tidal amplitude attained 3.59 m and the minimum 0.83 m, with a mean range of 2.26 m (Figure 5.2d).

5.5. Dynamical plume parameters

Dynamical classification of Tagus plume by evaluating non-dimensional numbers allows knowing the influence of factors such as outflow inertia, buoyancy forcing and Coriolis effect on plume behavior.

The importance of inertial and rotation processes on plume formation can be evaluated through the Kelvin number at the estuary mouth (K_m) (Garvine, 1995), such as:

$$K_m = \frac{W_m}{R_D} \qquad (5.1)$$

where, W_m is the mouth width and R_D the internal Rossby radius, expressed by

$$R_D = \frac{\sqrt{g' h_p}}{f} \qquad (5.2)$$

where, f is the Coriolis parameter, g' represents the reduced gravity ($g' = g(\rho_{amb} - \rho_0)/\rho_0$) with g as the gravitational acceleration, ρ_{amb} is the ambient ocean density and ρ_0 the estuarine input density.

In addition, h_p represents the plume thickness calculated by the formula used by (Yankovsky and Chapman, 1997):

$$h_p = \left(2\, L\, v\, h_0 \frac{f}{g'} \right)^{\frac{1}{2}} \qquad (5.3)$$

where, L is the inflow width, v the inflow velocity and h_0 the inflow depth.

The Kelvin number can also be calculated using different length scales. The bulk Kelvin number (K_b) uses the extension of the plume across-shelf. W_b was obtained from MODIS image composites.

The inflow Rossby number is evaluated to estimate the relative strength of inertial and rotational processes in terms of flow velocity (Horner-Devine et al., 2015), using the equation

$$R_m = \frac{u}{fL} \qquad (5.4)$$

where, u is the velocity of the flow current at the estuary mouth.

The densimetric Froude Number (F_m) is also determined at the estuary mouth and calculated in the upper water layer to evaluate whether the plume flow is governed by baroclinic or inertial processes (Garvine, 1995), thus:

$$F_m = \frac{u}{\sqrt{g'h_p}} \qquad (5.5)$$

5.6. Results

5.6.1. River discharge influence on Tagus plume

The correlation coefficients between plume development and river discharge were assessed for different lags in Figure 2.6. Tagus plume does not immediately react to river discharge variations despite presenting a high correlation coefficient (above 0.6). The maximum correlation between both variables was obtained with a 2 day delay showing as Tagus plume takes two days, in average, to react to variations in river flow. Therefore, the plume extension is strongly controlled by the discharge occurring for the last three days, including the present day. Attending to this, the plume extension for d (a day), will be compared with average river discharges calculated at d, $d-1$ and $d-2$. In addition, the maximum correlation for the lags applied was obtained under a threshold value of 0.20 mWcm^{-2}μm^{-1}sr^{-1}, which is defined as the turbid limit most adequately to represent the Tagus turbid plume.

The annual cycle of the Tagus plume is presented in Figure 5.3a. The observed pattern is consistent to that observed for the river discharge (Figure 5.2a), with high values of both variables during winter months and low values during summer, which demonstrates the key role of Tagus River discharge on plume development. In quantitative terms, January corresponds to the maximum plume extension (~400 km^2) and July the minimum one (~60 km^2). Although both present a similar pattern some differences occur that can be attributed to the interaction of winds and tides, which also affect plume development.

The role of low and high river discharges is also exhibited in Figures 5.3b and c, respectively, for image composites of the turbid plume. When the river discharge is < 33th percentile (< 74 m^{3}s^{-1}) the turbid plume is located very close to the river mouth occupying a small area with low turbidity values (Figure 5.3b). Under high river discharges (> 66th percentile, 198 m^{3}s^{-1}) the plume extension is much larger, increasing more than double respect to low discharges (Figure 5.3c).
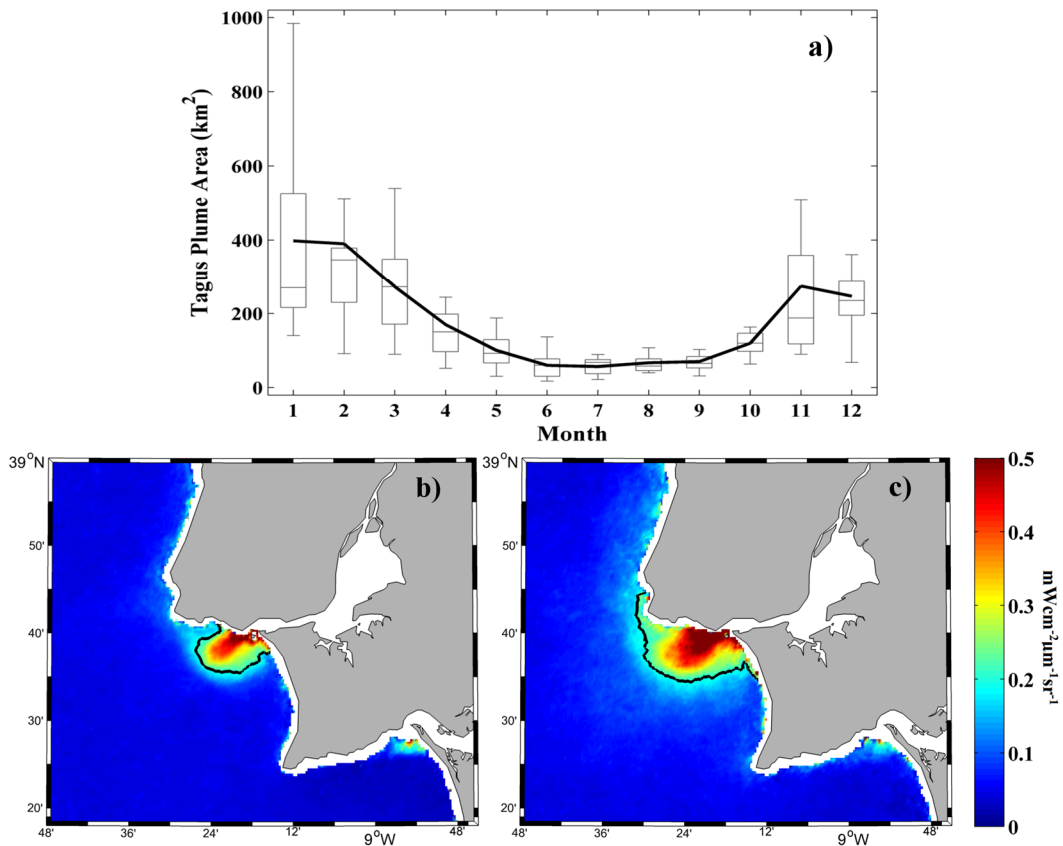
Figure 5.3. (a) Annual cycle variability of the Tagus River plume extension (km^2) over the period of 2003 to 2015. Solid black line: monthly average; line inside each box: median; lower and upper whiskers: minimum and maximum, respectively; lower and upper box limits: first and third quartiles, respectively. Mean water-leaving radiance (mWcm^{-2}μm^{-1}sr^{-1}) composite at 645 nm for all MODIS images under (b) low river discharge (< 33th percentile) and (c) high river discharge (> 66th percentile) over the period 2003-2015. The black line represents the turbid threshold (0.2 mWcm^{-2}μm^{-1}sr^{-1}).

5.6.2. Wind influence on Tagus plume

The role of the wind was evaluated when the turbid plume area is large enough to be significantly modified by the wind stress. Therefore, only the data for the average river discharge > 66th percentile were taken. In addition, days under extreme flows, over the 95th percentile, were avoided in order to remove outliers and maintain similar river discharges (differences lower than 15 %) for the different conditions analyzed. In the Tagus area southerly and westerly winds are linked to cyclogenetic processes related to episodes of extreme rainfall associated with high river discharges (Lorenzo et al., 2008). The wind directions were rotated counter-clockwise to follow the shoreline. However, for sake of clarity we still refer to the wind directions by their cardinal points. For example, a northern alongshore wind corresponds to a NNW direction (on average).

Alongshore wind composites are shown in Figure 5.4. Northern alongshore (upwelling) winds (AS$^+$) tend to displace the plume material toward the sea due to the offshore Ekman transport. Under these conditions, the velocity of the offshore Ekman current ranges from

0.06 to 0.11 ms^{-1} (at depths of 0 to 5 m) according to Pond and Pickard (1998). This behavior can be identified in Figure 5.4a where a rapidly decrease in turbidity values, following a semicircular pattern from the mouth to the ocean, is observed. The dispersion promoted by northern alongshore winds not allow the accumulation of material, which is characterized by the highest turbid values (above 0.5 mWcm^{-2}μm^{-1}sr^{-1}). In addition, a band of high turbidity is observed along the coast north of Cape Roca. This high turbidity band is associated to other processes not related to Tagus discharge since it presents a spatial discontinuity with the Tagus plume. The area characterized by values exceeding the turbid threshold reaches 172 km^2, with a mean turbid value of 0.36 mWcm^{-2}μm^{-1}sr^{-1}. These winds blow with velocities mostly varying from 4 to 8 ms^{-1}, with peaks at 12 ms^{-1}.
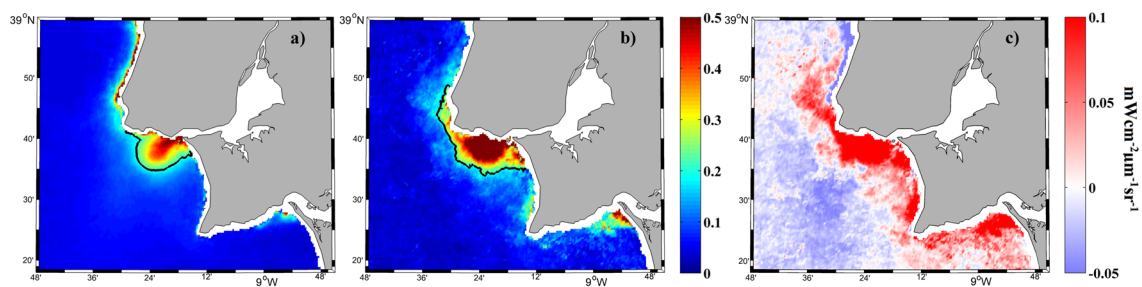
Figure 5.4. Mean water-leaving radiance (mWcm^{-2}μm^{-1}sr^{-1}) composite at 645 nm for all MODIS images under (a) northern and (b) southern alongshore winds over the period 2003-2015. Black line represents the turbid threshold (0.2 mWcm^{-2}μm^{-1}sr^{-1}). (c) Map of differences on the Tagus turbid plume field under alongshore winds (southern minus northern winds).

Southern alongshore (downwelling) winds (AS$^-$) drive the plume against the north coast of the Tagus ROFI, with current velocities ranging from 0.04 to 0.07 ms^{-1} (at depths of 0 to 5 m), due to the onshore Ekman transport. The plume occupies the northern part of the ROFI exceeding it toward the north (Figure 5.4b). In this case, a semicircular pattern of high turbid values (> 0.5 mWcm^{-2}μm^{-1}sr^{-1}) can be detected around the river mouth. The dispersion and dilution of the material into the ocean is more difficult under these conditions. The turbid plume occupies an area of 306 km^2 with a mean turbidity value of 0.43 mWcm^{-2}μm^{-1}sr^{-1}. The southern alongshore wind velocities mostly vary from 4 to 8 ms^{-1}, with peaks of 12 ms^{-1}.

Turbidity along a transect perpendicular to ROFI coast allows to better know the effects provoked by both types of alongshore winds in terms of plume dispersion (Figure 5.5a). Under upwelling winds maximum turbidity values are around 0.4 mWcm^{-2}μm^{-1}sr^{-1} near the mouth (grey line, Figure 5.5a), descending moderately and maintaining detectable values large distances over the ocean (~ 50 km), showing the dispersion and dilution of material seaward. On the other hand, turbidity values surpass 0.6 mWcm^{-2}μm^{-1}sr^{-1} near coast under downwelling winds (black line, Figure 5.5a), diminishing drastically until reach negligible values from 30 km. This shows as the majority of the material exported by the river is retained near coast, probably due to the reduction of the cross-shore

transport. In addition another transect starting at the Tagus mouth and extending along the north ROFI coast (negative values) and along the south ROFI coast (positive values) was evaluated to know the extension of the turbid plume under alongshore winds (Figure 5.5b). Downwelling winds promote higher turbid values than upwelling winds, maintaining values above 0.2 mWcm^{-2}µm^{-1}sr^{-1} over a larger extension on both sides of the mouth, and especially to the north ROFI coast (black line, Figure 5.5b). Upwelling winds show a similar pattern on both sides of the mouth with values descending rapidly below the turbid limit (grey line, Figure 5.5b), which can be attributed to the dispersion promoted. Therefore, although material exported by the river can reach greater distances over the ocean under upwelling winds, this also causes a strong dispersion into ocean water. The plume material dispersion and dilution into ocean water makes turbidity values rapidly reach values lower than the turbid limit, reducing the area occupied by the plume. On the other hand, downwelling winds maintain higher values of turbidity near coast since limit its dispersion on seawater, provoking a bigger plume.
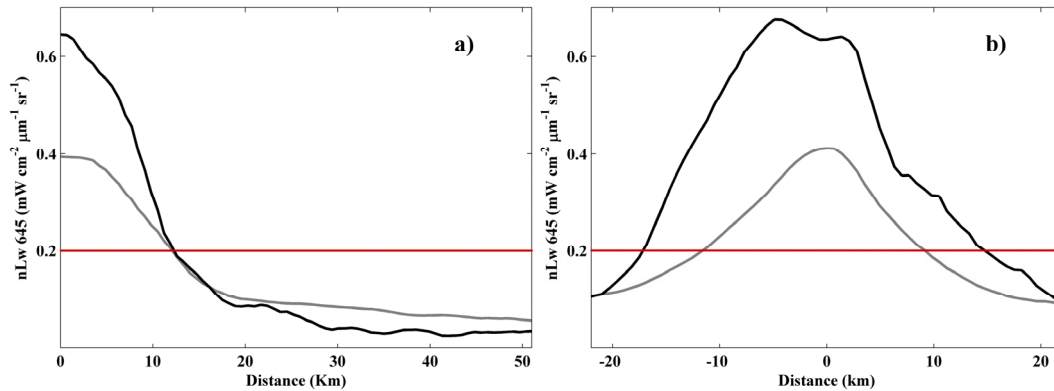
Figure 5.5. Transect of turbidity for alongshore winds for the (a) perpendicular and (b) parallel directions refer to ROFI coast (see Figure 5.1). Black line represents southern alongshore winds and grey line northern alongshore winds. Red line represents the turbid threshold. The zero marks the river mouth and negative distances refer to the region located northern to the river mouth.

The effect of cross-shore winds on the Tagus plume is shown in Figure 5.6. Eastern cross-shore (seaward) winds (CS^{+}) will stretch the plume offshore, promoting the dispersion of the material on the adjacent seawater. Therefore, the highest turbid values, exceeding 0.5 mWcm^{-2}µm^{-1}sr^{-1}, are only detected in the area nearest to river mouth (Figure 5.6a). The turbid plume is located in the northern part of the ROFI occupying an area of 187 km^2 with an average turbid value of 0.39 mWcm^{-2}µm^{-1}sr^{-1}. Eastern cross-shore winds blow with velocities mostly ranging from 2 to 6 ms^{-1}, with peaks of 12 ms^{-1}.

Western cross-shore (landward) winds (CS^{-}) retain Tagus plume material inside the ROFI in both alongshore directions, reducing its spreading in ocean waters. Therefore, these winds are capable to maintain high turbid values along a larger area, as shows Figure 5.6b, occupying much of the Tagus ROFI filling a total extent of 389 km^2 with a mean

value of 0.41 mWcm⁻²µm⁻¹sr⁻¹. The retention of plume material toward the coast produces a visible pattern around the river mouth, characterized by high turbid values (> 0.5 mWcm⁻²µm⁻¹sr⁻¹), although less extent than under southern alongshore winds. Western cross-shore wind velocities mostly range from 4 to 8 ms⁻¹, with peaks of 14 ms⁻¹.
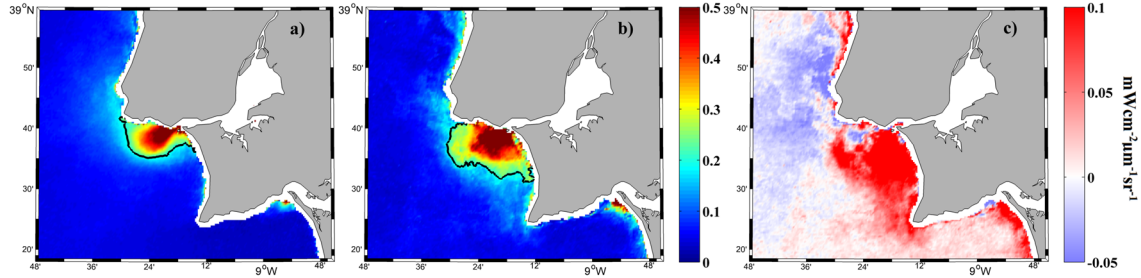
Figure 5.6. Mean water-leaving radiance (mWcm⁻²µm⁻¹sr⁻¹) composite at 645 nm for all MODIS images under (a) eastern and (b) western cross-shore winds over the period 2003-2015. The black line represents the turbid threshold (0.2 mWcm⁻²µm⁻¹sr⁻¹). (c) Map of differences on the Tagus turbid plume field under cross-shore winds (western minus eastern winds).

A transect was also considered to analyze the plume movement under each type of cross-shore winds (Figure 5.7). In this case, as these winds tend to move the plume along the north coast of the ROFI (seaward winds) or to both sides of the mouth (landward winds), the transect runs from the mouth to both alongshore directions being positive in the southward direction.
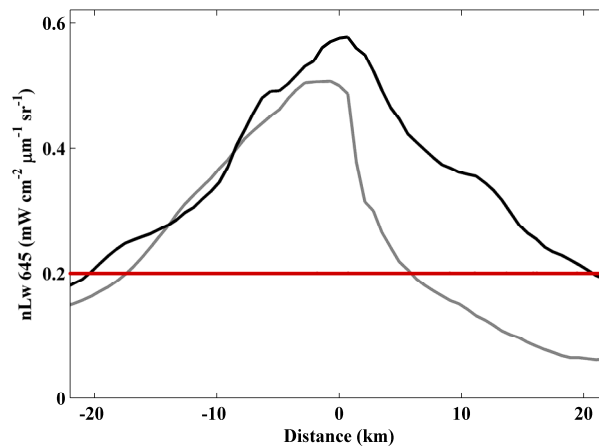
Figure 5.7. Transect of turbidity for cross-shore winds for the parallel direction refer to ROFI coast (see Figure 5.1). Black line represents western cross-shore winds and grey line eastern cross-shore winds. Red line represents the turbid threshold. The zero marks the river mouth and negative distances refer to the region located northern to the river mouth.

Under landward winds a maximum turbidity near to 0.6 mWcm^{-2}μm^{-1}sr^{-1} is detected near the mouth decreasing in a similar way to both sides of the mouth (black line, Figure 5.7). On the other hand, this pattern is only observed to the north side of the river mouth under seaward winds (grey line, Figure 5.7). In this case, turbidity reaches a maximum value of 0.5 mWcm^{-2}μm^{-1}sr^{-1} at the river mouth diminishing abruptly southward. Results show as landward winds retain plume material in both alongshore directions with a plume reaching larger distances whereas seaward winds move the material only along the north coast of the ROFI avoiding the formation of high values of turbidity due to the offshore movement promoted.

The main characteristics of the Tagus plume are summarized in Table 5.2 under different meteorological synoptic conditions. Overall, the turbid plume reaches its highest extension when western cross-shore winds prevail.

Meteorological synoptic conditions		Plume characteristics		Implications
River (m^{3}s^{-1})	Wind (calm discarded)	Extent (km^2)	Mean turbid value (mWcm^{-2} μm^{-1} sr^{-1})	
375	*Northern alongshore (AS$^+$)*	172	0.36	Intense offshore transport
439	*Southern alongshore (AS$^-$)*	306	0.43	Retention north of ROFI
403	*Eastern cross-shore (CS$^+$)*	187	0.39	Offshore and northward dispersion
449	*Western cross-shore (CS$^-$)*	389	0.41	Retention occupying the whole ROFI area

Table 5.2. Characteristics and implications of the Tagus turbid plume under wind forcing

5.6.3. Tidal influence on Tagus plume

Fortnightly (spring and neap) and semidiurnal (high and low) tidal periodicities were analyzed using imaging composites of turbidity obtained during days showing a river discharge > 66th percentile and avoiding extreme flows above 95th percentile for the reasons commented above. In addition, the tidal composites can be affected by the upwelling blooms out of ROFI limits, causing radiance not associated to river discharge, as it was commented in *Section 5.3*. Therefore, as Tagus plume under the conditions described not surpass the Tagus ROFI, images were reduced to this area. To evaluate the influence of the fortnightly tidal periodicity, average nLw645 fields before spring and neap tides (Figures 5.8a and c) and during-after spring and neap tides (Figures 5.8b and d) were composed. During-after spring tides maximum turbid values and plume extension were obtained (0.43 mWcm^{-2}μm^{-1}sr^{-1} and 302 km^2, respectively). In fact, it is the only case where a distinguishable circular pattern of high turbid values (> 0.5 mWcm^{-2}μm^{-1}sr^{-1}) is detected around the river mouth. The minimum values were obtained during-after

neap tides (0.31 mWcm^{-2}μm^{-1}sr^{-1} and 141 km^2, respectively), where turbid values do not surpass 0.4 mWcm^{-2}μm^{-1}sr^{-1}. The mean turbid value and extension of the Tagus plume indicate an intermediate status before spring and neap tides, although values are larger before neap tides.
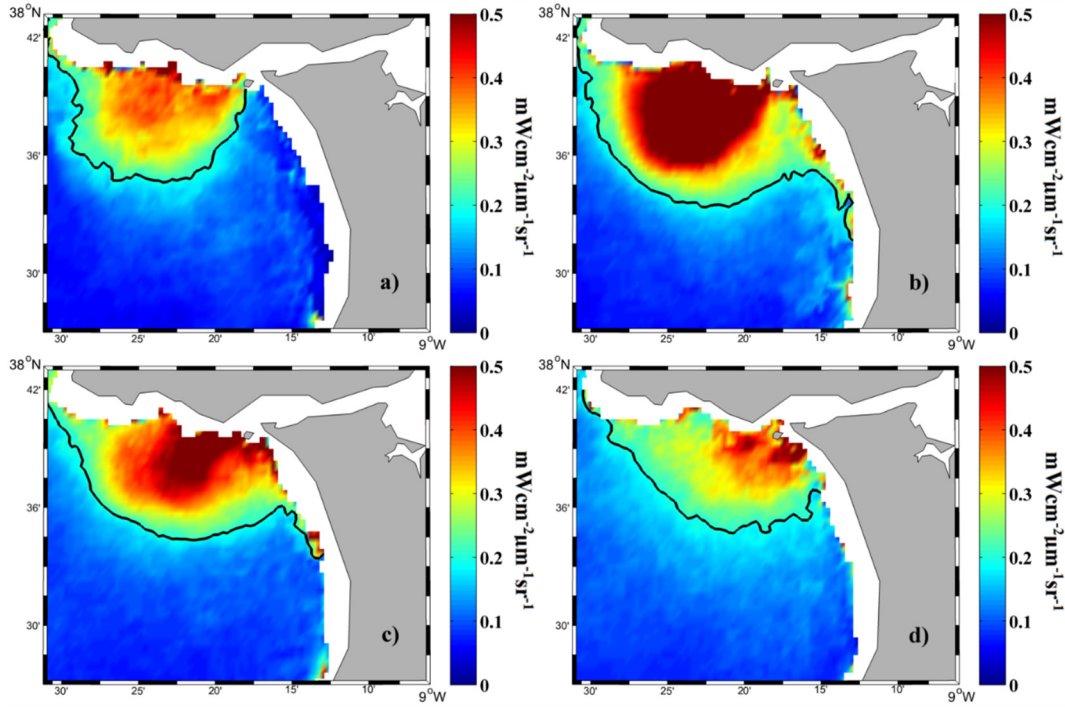
Figure 5.8. Mean water-leaving radiance (mWcm^{-2}μm^{-1}sr^{-1}) composite at 645 nm for all MODIS images (a) before spring tides, (b) during and after spring tides, (c) before neap tides and (d) during and after neap tides, over the period 2003-2015. The black line represents the turbid threshold (0.2 mWcm^{-2}μm^{-1}sr^{-1}).

High and low phases of tide were evaluated by means of the composites showed in Figure 5.9.
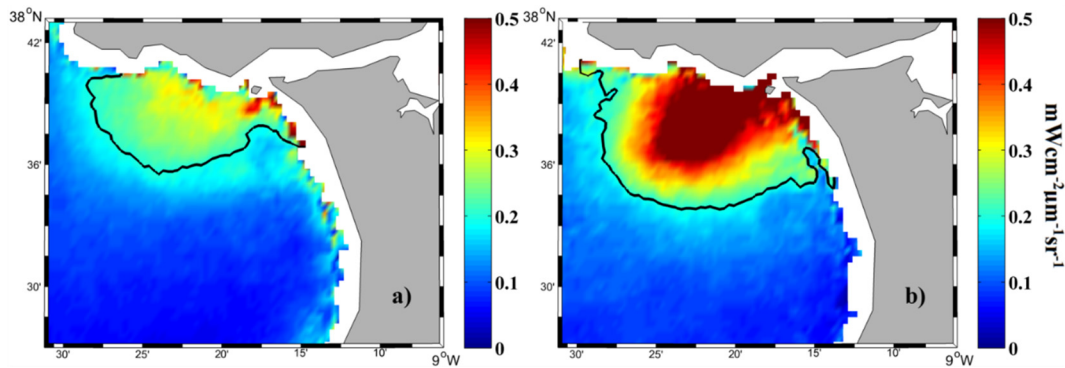
Figure 5.9. Mean water-leaving radiance (mWcm^{-2}μm^{-1}sr^{-1}) composite at 645 nm for all MODIS images for (a) high and (b) low tides over the period 2003-2015. The black line represents the turbid threshold (0.2 mWcm^{-2}μm^{-1}sr^{-1}).

The results reveal the plume extension to be larger and the mean turbid value higher under low tides. In addition, pixels above 0.5 mWcm^{-2}μm^{-1}sr^{-1} are only detected under low tides whereas values are below 0.4 mWcm^{-2}μm^{-1}sr^{-1} under high tides. In quantitative terms, Tagus plume reaches an extension and mean turbidity of 188 km^2 and 0.29 mWcm^{-2}μm^{-1}sr^{-1}, respectively for high tides, and 294 km^2 and 0.39 mWcm^{-2}μm^{-1}sr^{-1} under low tides.

The characteristics of the Tagus plume under tidal synoptic conditions are summarized in Table 5.3. Both semidiurnal and fortnightly periodicities have an important impact on the size and turbidity of the Tagus River plume. Here, the highest differences in river discharge are around 10%, smaller than previously mentioned when analyzing the effect of wind. Thus, tidal analysis is not conditioned by variations in the average river discharge.

Tidal synoptic conditions		Plume characteristics		Implications
River (m^{3}s^{-1})	Tidal state	Extent (km^2)	Mean turbid value (mWcm^{-2} μm^{-1} sr^{-1})	Fortnightly periodicity
410	*Before spring*	198	0.33	Intermediate situation
406	*During/after spring*	302	0.43	Largest plume extension with intense turbidity
389	*Before neap*	242	0.38	Intermediate situation
387	*During/after neap*	141	0.31	Smallest plume extension with low turbidity
				Semidiurnal periodicity
406	*High*	188	0.29	Smaller plume extension with less intense turbidity
403	*Low*	294	0.39	Larger plume extension with more intense turbidity

Table 5.3. Characteristics and implications of the Tagus turbid plume under tidal forcing.

5.6.4. Plume parameters

The Tagus plume dynamic was evaluated under river discharges > 66th percentile, which define the scope of this study. The flow velocity at the estuary mouth usually varies between 0.4 ms^{-1} at neap tides and 1.4 ms^{-1} at spring tides (Neves, 2010).

The Kelvin number at the Tagus estuary mouth (K_m) is < 1 under all flow conditions (Table 5.4). This suggests that the Tagus plume is mainly controlled by inertial processes at the estuary mouth, with the river discharge likely forming a re-circulating bulge at the front (Garvine, 1995). This hypothesis is corroborated by a Rossby number (R_m) > 1 under all typical flow conditions. The Rossby number indicates the great influence of inertial processes and a negligible impact of rotational ones at the estuary mouth. The Froude number (F_m), which is < 1 under low flows, reveals a subcritical flow and the importance of the stratification process, with the plume tending to form a far-field region upon river

discharge from the estuary. At medium-to-high flow, the Froude number is > 1. This implies a supercritical flow dominated by inertial processes. The supercritical values also demonstrate the plume ability to generate a near-field region which is a mixing area characteristic of prototypal plumes (Horner-Devine et al., 2015).

At low flow, the bulk Kelvin number (K_b) is slightly smaller than 1, therefore the Tagus plume is controlled by inertial processes although rotational ones are also important. When the flow is medium-to-high, K_b is > 1. This defines the plume as "Large-scale", indicating the important role of the Coriolis effect when the Tagus plume is developed (Garvine, 1995) (Table 5.4).

	Low current *(0.4 ms⁻¹)*	*Intermediate current* *(0.9 ms⁻¹)*	*High current* *(1.4 ms⁻¹)*
h_p (plume thickness)	2.49 m	4.18 m	6.16 m
R_D (Radius Deformation)	6531 m	8462 m	10273 m
W_b (Plume extent)	6195 m	17699 m	23008 m
Bulk Kelvin number (K_b)	**0.93**	**2.06**	**2.21**
Mouth Kelvin number (K_m)	**0.31**	**0.24**	**0.19**
Mouth Rossby number (R_m)	**2.21**	**4.98**	**7.74**
Mouth Froude number (F_m)	**0.68**	**1.18**	**1.51**

Table 5.4. Dynamical parameters of the Tagus turbid plume.

5.7. Discussion

The analysis of the Tagus turbid plume under its main forcing shows a marked control of river discharge on plume development. This is clearly observed when both annual patterns are compared (Figures 5.2a and 5.3a), showing a similar behavior with high values in winter months and low ones during summer. Therefore, Tagus plume extension increases with river discharge, as can be observed in Figure 5.3b and c where Tagus plume occupies more than double area under high discharges than under low ones. In addition, a semicircular pattern formed by the highest turbid values (> 0.5 mWcm⁻²μm⁻¹sr⁻¹) is clearly observed when Tagus discharge is high while it is very unlike to find under low discharge. The observed findings are attributed to the greater amount of material exported from the estuary as the flow increases (Vaz et al., 2009), since the flow increasing enhances the capability of the river to drag suspended matter to the mouth. This behavior was also observed for Ebro and Douro Rivers in the previous chapters, for which the river discharge is the main support to plume development. However, although Tagus turbid plume is highly dominated by the discharge pattern, it is not able to adapt immediately to its variations, taking 2 days to cope with flow fluctuations, in contrast with Ebro and Douro Rivers, which respond immediately to discharge variations. This delay is probably due to the long residence time of water caused by the shape and size of the estuary. The Tagus River debouches into a great estuary before reaching the ocean while the Ebro and Douro Rivers flow directly into the sea. The observed delay could be in part attributed to

the distance of the discharge gauge to the estuary mouth. To check this, the river discharge data from the Almourol station located ˜90 km from the estuary entrance and from the Ómnias station situated only 45 km from the estuary entrance were compared for a period lasting from 1990 to 2002; the Ómnias station stopped providing data in 2002. Results show the Almourol and Ómnias stations river discharges are in phase. This confirms that the observed delay between plume development and river discharge is related to the shape and characteristics of the Tagus Estuary, which is constituted of a large region of mixing water, approximately 25 km long×10 km wide, extending from the mouth to the upper reaches of the estuary.

Once Tagus plume is well developed (under high discharges) the wind impact on its dispersion is of great importance. Upwelling favorable winds transport plume material large distances over the ocean due to the offshore Ekman transport, promoting its dispersion and dilution in ocean water (Figure 5.5a). This movement can be detected in Figure 5.4a as a rapidly decrease in the turbidity, which provokes that very high turbid values (> 0.5 mWcm^{-2}μm^{-1}sr^{-1}) were not detected near coast. This behavior is in agreement with the reduction of salinity differences between coastal waters affected by river discharge and ocean waters due to the mixing promoted by upwelling winds shown in previous works (Fong and Geyer, 2001). The difference in the turbid plume field between alongshore winds (downwelling minus upwelling winds) represented in Figure 5.4c shows a dominance of negative values (dominance of upwelling winds) in the far field in front of the river mouth. This fact shows the capability of upwelling winds to transport plume material affecting large distances over the ocean, which was previously found for Tagus plume through numerical models (Vaz et al., 2009) and agrees with previous works that detected the offshore advection of plumes caused by upwelling winds (Fong and Geyer, 2001; Choi and Wilkin, 2007). This dispersion of plume material provokes that although some turbidity can be detected to great distances over the ocean, its value is rapidly below the turbid limit, and therefore, the area occupied by turbidity values surpassing the limit (near-field plume) is smaller. This can contrast with the studies mentioned above which described a larger plume promoted by upwelling winds due to the greater expansion over the ocean. These studies account the entire area where salinity is lower than oceanic one due to discharge influence, whereas in our case we are centered in the near-field turbid plume, the area where the contrast is greater. From this point of view the smaller area is obtained under winds that tend to extend the plume material over the ocean because promote a lower contrast with ocean water, and therefore, the area characterized by a strong contrast with ocean water is reduced. In addition, a great bulge was not clearly observed in front of Tagus River mouth under upwelling winds as it was observed for the Douro. This is probably due to the shape of Tagus coast and/or the attenuation of northerly winds caused by the Sintra mountains. Both can limit the effect of northerly winds and the bulge formation.

A coastal turbid fringe is also detected north of cape Roca (Figures 5.4a and c) under upwelling winds. This fringe of turbidity is not caused by the material exported by Tagus River neither by the material discharged by rivers located northward, because there are

not main rivers in that area. The cause supporting the appearance of this fringe of turbidity north of Tagus ROFI under upwelling winds was explained by Moita et al. (2003) and Valente and da Silva (2009). They found that this type of winds are able to promote upwelling blooms causing radiance not associated with the river discharge. In fact, Valente and da Silva (2009) found that under extreme high discharges, Tagus plume can be large enough to reach these upwelling blooms making both patterns undistinguishable. However, with our methodology, this fringe of turbidity is not spatially continuous to the Tagus plume, and therefore, we can delimit the Tagus plume and differentiate it from the turbid fringe caused by upwelling blooms.

Downwelling winds dominate the area near coast in the north of Tagus ROFI due to the onshore Ekman transport promoted, retaining the material exported by the river in that area and limiting its dilution in the ocean water (Figure 5.4b and 5.5a). This explains the high turbid values detected in Figure 5.4b and promotes that values surpassing the turbid limit occupy a larger area (Figure 5.5b). This behavior is corroborated by Figure 5.4c where a fringe of positive values (dominance of downwelling winds) dominate the near shore area, extending northward to Tagus ROFI. This behavior is in a good agreement with previous works that show as downwelling winds dominate the coastal area on the side of the mouth toward wind blows (Fong and Geyer, 2002; Choi and Wilkin, 2007; Otero et al., 2008). However, these studies detected a fringe of plume material along the coast following wind direction which was not observed northward of cape Roca. This is probably caused by the retention of Tagus plume against north of ROFI due to the shape of the bay, limiting that plume surpasses this area, which prevents its propagation northward. In the case of studies mentioned above, as well as for Douro plume, there are no geological barriers avoiding the formation of this coastal band following wind direction. This fact and the time delay between river discharge and river plume variations caused by the size and the shape of the Tagus Estuary highlight the importance of coastal geomorphology in the Tagus case.

Eastern cross-shore winds tend to push the plume material offshore, which causes that the highest values of turbidity (> 0.5 mWcm^{-2}μm^{-1}sr^{-1}) were scarcely detected not allowing the material accumulation near coast (Figure 5.6a and 5.7). The turbid plume occupies a small area located north of ROFI. Unlike the upwelling winds that move the material in the perpendicular direction to the ROFI coast, seaward winds move the material predominantly offshore following the north coast of the ROFI and toward the north when the ROFI is surpassed, following the coastline geometry and probably affected by Coriolis deflection to the right in the Northern Hemisphere. This behavior is clearly observed when the map of differences between cross-shore winds (landward minus seaward winds) is assessed (Figure 5.6c). The negative values (dominance of seaward winds) are observed to the north of river mouth showing as eastern winds tend to displace the plume offshore and to the north when the ROFI is surpassed. The offshore movement of the plume under eastern winds and the deflection to the right was also observed in Douro plume. On the other hand, landward winds retain most of plume material against the coast in both alongshore directions (Figure 5.7), limiting its spreading in ocean water

and therefore, maintaining values above the limit in a larger area inside the ROFI (Figure 5.6b). In fact, the highest turbid values form a defined semicircular pattern around the mouth. This behavior is corroborated by Figure 5.6c where positive values (dominance of landward winds) dominate the area enclosed by the bay excepting the north part, which is also affected by seaward winds.

Then, plume material is affected in a different manner depending on the predominant wind direction. Upwelling winds tend to disperse plume material over the ocean following a perpendicular direction to the ROFI coast, provoking a plume which occupies the smallest area located in the north of ROFI and defined by the lowest mean turbid value (Figure 5.4a, c and Figure 5.5, Table 5.2). Downwelling winds provoke that Tagus plume occupies all the north of ROFI since maintain the material discharged by the river in that area due to the onshore Ekman transport generated, which limits the transport of material to other areas. This promotes a plume defined by the highest mean turbid value and with an inclination to the north (Figure 5.4b, c and Figure 5.5, Table 5.2). Seaward winds displace plume material toward the ocean and following the north coast when the ROFI is surpassed, causing a small plume characterized by low turbidity values preserved in the north of ROFI (Figure 5.6a, c and Figure 5.7, Table 5.2). Finally, landward winds retain plume material in both alongshore directions, which provoke the largest plume characterized by high turbid values, which occupies a large part of the area enclosed by the bay due to the inhibition of cross-shore transport (Figure 5.6b, c and Figure 5.7, Table 5.2).

Tagus dynamic is also affected by fortnightly and semidiurnal tidal cycles. The effect of overlapping both cycles is not observed in other main rivers analyzed in the Iberian Peninsula. Ebro plume is not affected by tides due to the micro-tidal regime of Mediterranean Sea, and Douro plume is only affected by the semidiurnal cycle, although it has the same mesotidal Atlantic regime than Tagus. This fact is due to Douro River directly flows into the sea, whereas Tagus presents a large estuary before debouching into the ocean. Large estuaries, as Tagus, generate a longer water residence, which can modify turbidity patterns according to fortnightly tidal cycle (Braunschweig et al., 2003) whereas the residence time in the Douro Estuary is too short to observe this effect.

A clear pattern of variability according to the fortnightly period is observed in the Tagus plume (Figure 5.8). It reaches the maximum extension and turbidity during spring tides descending to its minimum values during neap tides, with an intermediate plume observed before neap tides (Table 5.3). The same behavior occurs between neap and spring tides. The extension of the plume as well as the turbidity increase to reach maximum values during spring tides, and therefore, an intermediate plume is observed before spring tides (Table 5.3). The observed patterns can be attributed to a larger turbid plume ejected from the estuary during and after spring tides, enhanced by the ebb-dominated Tagus Estuary (Vaz and Dias, 2014). This is due to the differences in tidal amplitude and the current velocity between spring and neaps, which are more intense during spring tides. During neaps, low velocities are found and residence time within the estuary is changed. In fact,

in neaps estuarine outflow is reduced due to low ebb velocities and the water properties are "trapped" inside the estuary, due to low exchange in its mouth. This affects the plume propagation to the coastal ocean as studied by Valente and da Silva (2009). In a coastal plain estuary like the Tagus, which presents a large width in its mixing region, the estuary remains well mixed due to a large lateral spreading of freshwater through a low depth region. Also, the tide always acts to produce well mixed estuarine conditions. However, different tidal conditions induce changes in current velocities and also in estuarine outflow, and the estuary exports more particulate and solute material during spring than during neaps. In addition, plume behavior can be different before and after neap or spring tides, as was observed in this chapter. These results are in good agreement with those of Valente and da Silva (2009) and Vaz et al. (2011).

The semidiurnal tidal cycle also presents an important impact on Tagus plume development. In fact, a larger and more turbid plume is observed under low tides in comparison with the situation under high tides (Figure 5.9 and Table 5.3). This behavior is attributed to the plume retraction provoked by the high tide, which limits its development, as was previously observed in the Douro turbid plume.

5.8. Conclusions

The spatial and temporal variability of the Tagus plume was evaluated considering the effects of river discharge, wind and tide from 2003-2015. The study was carried out using composites constructed of daily images taken from the MODIS Aqua and Terra satellites. The study allowed to reach the following conclusions:

- The maximum correlation between river discharge and the Tagus plume extension was obtained with a lag of 2 days, i.e., plume at day d is compared with the runoff at day $d-2$. The plume does not react immediately to changes in river discharge due to the geomorphology and dimension of the estuary.

- The Tagus plume occupied a small area located near the estuary mouth under low river discharges. The plume showed an increase in extension and turbidity at higher river discharges, showing plume dependence on river flow.

- The influence of wind was investigated under high river discharges. Maximum plume extension (389 km^2) was observed under western cross-shore winds whereas the maximum mean turbidity (0.43 mWcm^{-2}μm^{-1}sr^{-1}) was induced by southern alongshore winds. Both wind conditions limit the dispersion of material exported by the river in ocean waters, which maintains values above the turbid limit over a large area. On the other hand, northern alongshore winds produced the minimum plume extension and turbidity (172 km^2 and 0.36 mWcm^{-2}μm^{-1}sr^{-1}, respectively). Eastern cross-shore winds also caused low plume extension and turbidity since both wind conditions favor the material dispersion in ocean waters

provoking a rapidly decrease in turbidity values and therefore, in the area occupied by the values surpassing the turbid limit.

- The role of tides was analyzed under high river discharges. Low tides caused a larger Tagus turbid plume with higher turbidity values than at high tides. In addition, Tagus turbid plume reached its maximum extension (302 km^2) and mean turbidity (0.43 mWcm^{-2}μm^{-1}sr^{-1}) during and after spring tides, when the fortnightly tidal cycle was considered. The minimum plume extension and mean turbid value were obtained during and after neap tides (141 km^2 and 0.31 mWcm^{-2}μm^{-1}sr^{-1}, respectively). Therefore, semidiurnal and fortnightly tide periods, are important for the plume size and turbidity. When the two periods overlap, the maximum plume extension and mean turbidity were acquired at during-after spring tides under low tides, whereas the minimum plume and mean turbidity were observed during-after neap tides under high tides.

Chapter 6:

Main Iberian turbid plumes: characterization and comparison

6.1. Motivation

In previous chapters the three most important Iberian plumes (Ebro, Douro and Tagus) were individually analyzed in depth. Their responses under the main forcing were evaluated since these plumes cover the main important driving factors affecting Iberian plumes. River discharge and wind in all of them, a strong and permanent regional oceanic circulation on the Ebro plume, the semidiurnal tidal cycle on the Douro and Tagus plumes, and the fortnightly tidal cycle on the Tagus plume. The behavior of each plume to the forcing was described, analyzed and explained, but plumes were not compared between them in depth.

The goal of this chapter is to compare the behavior of the most important Iberian plumes under the main forcing factors. The purpose is twofold, finding common features among plumes and highlighting differences among them due to coastal and river mouth morphology, coastal wave regime or regional differences in coastal currents among others. For that, Minho, Guadiana and Guadalquivir plumes were added to the study in order to cover all the most important Iberian plumes in terms of river discharge. The images of the Ebro, Douro and Tagus plumes under the main forcing will no longer be included in this chapter because were showed in previous chapters. In spite of some slightly differences, as the number of years averaged or the percentiles selected in the

case of the Tagus, the general behavior under the different forcing is the same and, therefore, the images are very similar to those showed in previous chapters. Only Tagus plume state under low and high tides (semidiurnal tidal cycle) will be showed because it will be considered for the same fortnightly period, during spring tides and during neap tides, in order to isolate the semidiurnal effect. In *Chapter 5* semidiurnal impact on Tagus plume was only evaluated during an intermediate state of the fortnightly cycle. In this way can be checked if the effect of the semidiurnal cycle is totally independent of the fortnightly state. The extension and turbidity of the main Iberian plumes under each situation considered from 2003 to 2014 will be included for comparison purposes.

6.2. Study areas

Areas selected to study the most important Iberian plumes are defined in Figure 1.2 (empty black squares). Each area was chosen taking into account the region where the influence of each turbid plume is greater and avoiding, as far as possible, the influence of other minor river plumes in its proximity, which could partly mask the observed behaviors. An example was explained in *Chapter 5* for Tagus River. In spite that the initial area selected to analyze the plume was larger, it was reduced to avoid the influence of other sources of turbidity which can overestimate the plume. A turbid plume usually forms a pattern with the turbidity descending with the distance to the river mouth. When there is a discontinuity in turbidity pattern or an increase with the distance is usually associated to other sources of turbidity, which present most importance at that location. The areas defined to analyze the plumes were defined from this point of view, selecting the region dominated by each turbid plume.

6.3. Methods

The same forcing conditions will be imposed to analyze the main Iberian plumes for comparison purposes. Following the findings obtained in previous chapters, river discharge impact on Iberian plumes will be analyzed taking into account days with low river discharge (below the 25th percentile) and days with high river discharge (over the 75th percentile). Wind directions considered will be alongshore (upwelling and downwelling) and cross-shore (seaward and landward) with a deviation of $\pm 45°$ following coast orientation in each case. High tides will be considered under tidal states higher than 0.5 m and low tides lower than -0.5 m at the hour when Aqua satellite overpasses the plume areas. Spring and neap tides will be considered under daily amplitudes over than 75th percentile and below the 25th percentile, respectively. Wind and tidal forcing will be evaluated under river discharges higher than the 75th percentile in order to ensure plumes developed enough to be modulated by these forcing. For detailed information see *Chapter 2, Section 2.2. "Turbid plume forcing databases"*.

A criterion was established to quantify the influence of each forcing on river plume based on the evaluation of the plume extension. The capability of each forcing to modulate that extension was obtained in terms of:

$$R_{<E>} = \left(\frac{<E>^{max} - <E>^{min}}{(<E>^{max} + <E>^{min})/2} \right) \qquad (6.1)$$

where $<E>^{max}$ is the largest plume extension and $<E>^{min}$ the smallest one promoted by each forcing. This dimensionless parameter allows comparing different drivers (discharge, wind, tide…) and locations (Minho, Douro, …) since it is the ratio between the extent of change in plume extension and the mean plume extension promoted by each forcing. Thus, when the effect of a given driver is high (low), the value of the parameter increases (decreases). Three ranges of forcing influence on plume development can be defined: high influence (H), when amplitude of plume extension is higher than the mean value, moderate influence (M), when the amplitude is between one half and the mean extension and low influence (L) when the amplitude is lower than one half of the mean plume extension. Values are shown in Table 6.3.

6.4. Main forcing affecting the most important Iberian plumes

The general characteristics of the main forcing affecting Iberian plumes for the period 2003-2014 are showed in Figure 6.1.

The annual hydrologic cycle of the rivers under analysis can be divided in two main regimes. A pluvial regime, characterized by a river discharge reaching the maximum in winter months (January or February) and descending then to reach the minimum during summer, is typical for Minho, Douro and Tagus Rivers. On the other hand, a pluvio-nival regime characterized by a river discharge increase in winter months, with a peak also recorded in spring months (March-April) and minimum values during summer, is typical for Guadiana, Guadalquivir and Ebro Rivers (Figure 6.1a). In general terms, during the period under study, maximum monthly discharge, 922 m^3s^{-1}, was reached by Douro River in January and the minimum one, 13 m^3s^{-1}, by Guadiana River in July. In addition, Douro (Guadiana) River presented the maximum (minimum) mean annual flow, about 477 (73) m^3s^{-1}, for the period under study.

The wind rose depicted in Figure 6.1b (left panel) corresponds to a location in front of Douro mouth. The pattern is characterized by prevailing north-northwesterly winds followed by south-southwesterly winds. Velocities range from 4 to 12 ms^{-1}. This pattern is in good agreement with previous research (Gomez-Gesteira et al., 2006; Alvarez et al., 2011) and it is similar in front of Minho and Tagus mouths.

The pattern shown in Figure 6.1b (middle panel) characterizes the wind regime in front of Guadiana River mouth. There is not a clear prevalent direction, although most of winds come from the west. Wind velocity usually ranges from 4 to 8 ms^{-1}. This regime is characteristic of the Bay of Cadiz and it is similar in front of Guadalquivir River mouth.

This rose is similar to the one shown in Carvalho et al. (2014) using data provided by a meteorological buoy located at the Gulf of Cadiz.

The area near Ebro mouth shows prevailing northwesterly winds followed by northeasterly winds, with velocities usually ranging between 4 and 14 ms^{-1} in the first case and between 2 and 8 ms^{-1} in the second one (Figure 6.1b, right panel). This pattern is in good agreement with Durand et al. (2002) who showed the prevalence of Mistral (northwesterly) wind, which is more persistent during autumn and winter although it blows throughout the year.
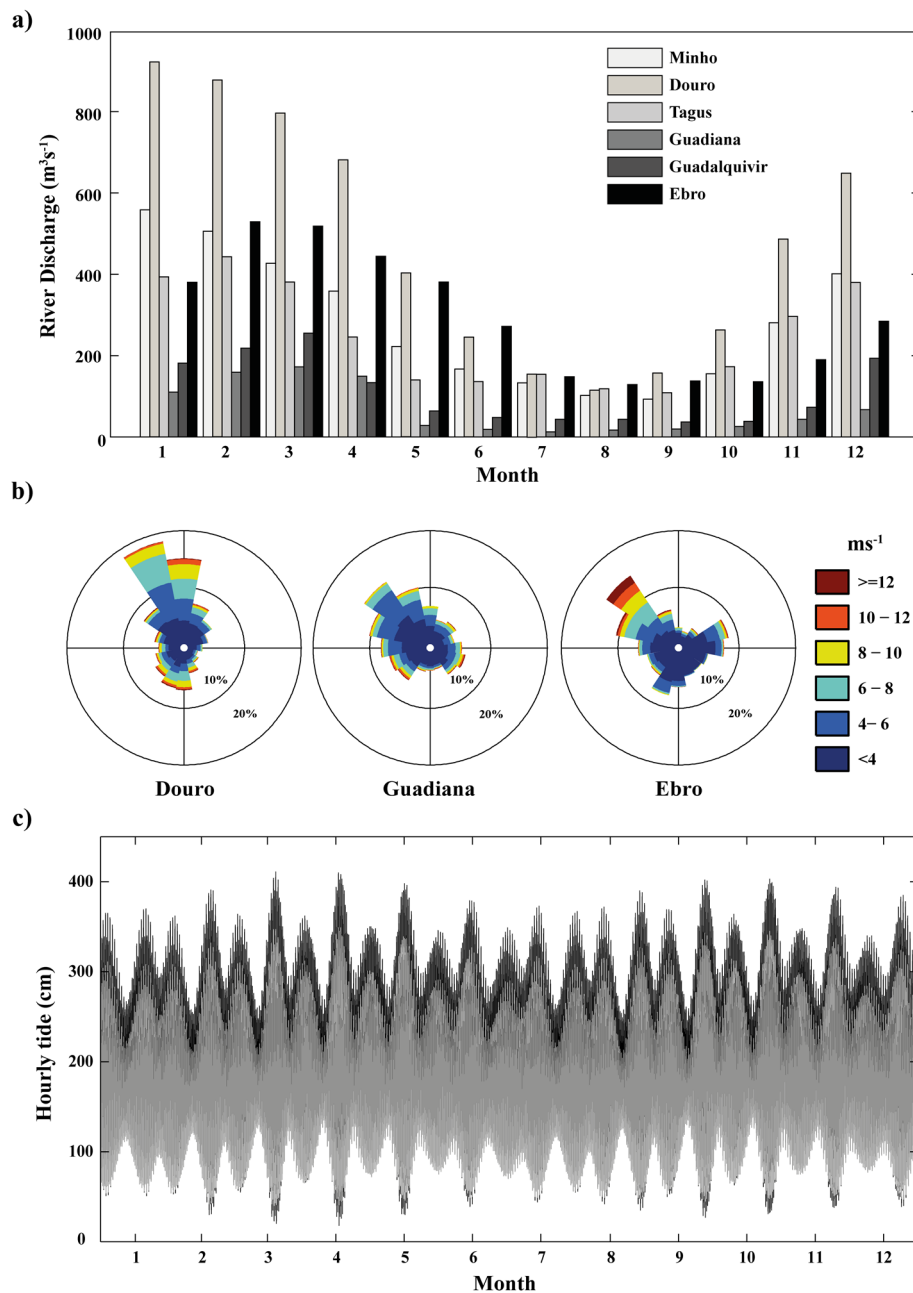
Figure 6.1. (a) Annual hydrologic cycle for the main Iberian Rivers from 2003 to 2014 (monthly average, in m^{3}s^{-1}). (b) Wind rose (ms^{-1}) of Douro, Guadiana and Ebro plume areas from left to right, for the period 2003-2014. (c) Hourly sea surface elevation (cm) at Vigo (black) and Bonanza (grey) stations during 2007.

Sea surface elevation for Vigo and Bonanza stations during 2007 is showed in Figure 6.1c. The daily mean amplitude of sea surface elevation for the period under study was 240 cm at Vigo station, 225 cm at Tagus Estuary (Cascais station) and 197 cm at Bonanza station.

6.5. Results and discussion

6.5.1. Characterization of the main Iberian plumes

The basic features of each river plume were characterized before analyzing their behavior under different synoptic conditions. The turbid threshold (T_t) distinguishes water influenced by plume from clear ocean water. This turbid limit is different for each river plume due to their different features (Figure 2.6 and Table 6.1). Only Minho and Ebro plumes present the same T_t value, 0.15 mWcm^{-2}μm^{-1}sr^{-1}. The other plumes have higher threshold values, in particular Guadalquivir plume reached the maximum value (0.35 mWcm^{-2}μm^{-1}sr^{-1}). As for the time response (Lag), Minho, Douro, Guadiana and Ebro Rivers have not delay between river discharge and plume development, whereas Tagus and Guadalquivir Rivers present a delay of 2 and 3 days, respectively (Figure 2.6 and Table 6.1). These results corroborate that plumes of rivers flowing directly into the ocean immediately adapt to river discharge fluctuations. Nevertheless, the plume needs some time to adapt to discharge variations in rivers with a large estuary.

Plume Characterization					
River	**Mean discharge**	**T_t**	**Lag**	**<E>**	**<T>**
Minho	282	0.15	0	179	0.30±0.20
Douro	477	0.25	0	369	0.47±0.30
Tagus	260	0.20	2	208	0.39±0.27
Guadiana	73	0.30	0	89	0.51±0.21
Guadalquivir	110	0.35	3	940	0.72±0.42
Ebro	296	0.15	0	1277	0.36±0.26

Table 6.1. General characterization of the most important Iberian turbid plumes from 2003 to 2014. Mean discharge is measured in m^{3}s^{-1}, lag in days, mean extension (<E>) in km^2 and turbid threshold (T_t) and mean turbid value (<T>) in mWcm^{-2}μm^{-1}sr^{-1}. Dispersion was calculated by means of the standard deviation. Mean extension has not error because it was calculated counting the number of pixels that surpass the turbid threshold.

Therefore, discharge conditions imposed to observe plumes states will be referred to the same day of plume sampling, *d*, for rivers without delay between river discharge and plume development and to the average discharge at days *d, d – 1 … d – delay* for rivers with some delay in order to take into account river runoff influence on plume formation during these days.

The mean extension <E> and turbid value <T> of plumes averaged for the whole period under study are also shown in Table 6.1. Ebro River presents the maximum mean plume area, 1277 km^2, while Guadiana River has the minimum one, 89 km^2. Minho, Douro, Tagus and Guadalquivir Rivers have intermediate plume extensions, ranging from 179 km^2 for Minho to 940 km^2 for Guadalquivir. Regarding turbid values, which are related to the suspended material carried by plumes, Guadalquivir plume has the maximum mean turbid value, 0.72 ± 0.42 mWcm^{-2}μm^{-1}sr^{-1}, while Minho has the minimum one, 0.30 ± 0.20 mWcm^{-2}μm^{-1}sr^{-1}. The other rivers under analysis have intermediate turbid values ranging from 0.36 ± 0.26 mWcm^{-2}μm^{-1}sr^{-1} for Ebro to 0.51 ± 0.21 mWcm^{-2}μm^{-1}sr^{-1} for Guadiana.

Table 6.1 also highlights that a high river discharge does not necessarily involve larger and more turbid plumes. For example, Guadalquivir River, which is the fifth in annual mean discharge, presents the most turbid plume and it is the second in plume extension. Thus, although river discharge is important to transport material to the ocean, other factors like sediment load can also be crucial to determine the properties of the turbid plume. For example, the extension occupied by farmlands and urban settlements has increased in the Guadalquivir basin in the last decades, providing more material that can be carried by the river to the ocean (Díez-Minguito et al., 2012). On the contrary, other rivers have reduced their material load during the last decades (Douro, Oliveira et al., 1982, or Ebro, Ibáñez et al., 1996). Another example is the Ebro River, which presents the maximum mean extension despite having medium discharges and having reduced the available material load during the last decades. This is probably caused by a still high amount of available material due to the agricultural activities of the Delta (Ibáñez et al., 1996) and by the plume displacement provoked by the Liguro-Provençal current, as was explained in *Chapter 3*.

6.5.2. River discharge influence on the main Iberian plumes

The annual cycle of the main Iberian plumes is represented in Figure 6.2. It shows the monthly variability of the mean extension occupied by each turbid plume. All of them present a general annual pattern characterized by high values during winter and minimum ones during summer. Minho, Douro and Tagus showed a similar annual pattern between plume extension and river discharge. However, Guadiana, Guadalquivir, and Ebro although present a seasonal cycle in both cases, some discrepancies can be assessed. They have similar plume extensions during autumn-winter and early spring months, in spite of the higher discharge in the last case. This could be explained by differences in the other seasonal forcing, the wind. A clear example occurs in Ebro plume, where Mistral wind promotes a larger plume extension during autumn-winter months, as was observed in *Chapter 3*. This provokes a plume area as large during autumn-winter than during early spring months, in spite the higher river discharges in the last case. In absolute terms, the maximum monthly average extension (~2000 km^2) is reached by Guadalquivir plume in January whereas the minimum one (<25 km^2) is reached by Guadiana plume in August.
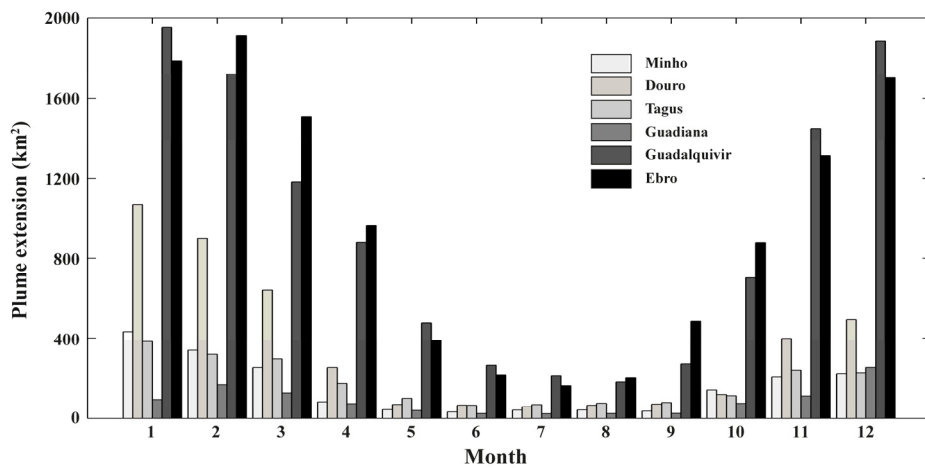
Figure 6.2. Annual cycle of mean plume extension for the most important Iberian Rivers from 2003 to 2014 (monthly average, in km^2).

In spite of the similarities between river discharge and plume extension patterns, the calculation of the plume extension in terms of river discharges is not straightforward due to the effect of other drivers as wind or tides. Nevertheless, the linear correlation between river discharge and plume extension provides useful information about the plume in terms of runoff (Table 6.2). Higher correlations (~0.60) were obtained for northern Atlantic Iberian Rivers (Minho, Douro and Tagus). The smaller correlations (0.28 and 0.40) were obtained for Ebro and Guadalquivir Rivers. The lower correlation obtained for these rivers can be supported by the seasonal wind pattern together with the pluvio-nival regime as commented above. All correlations are significant (> 99 %).

River	Correlation (discharge *vs* \<E\>)	Series length	River Discharge Condition	
			< 25 % **Plume State**	>75 % **\<E\>**
Minho	0.60	1,022	N	451
Douro	0.61	1,269	N	998
Tagus	0.59	1,402	MD	362
Guadiana	0.47	1,686	MD	333
Guadalquivir	0.40	1,756	WD	1973
Ebro	0.28	1,261	WD	1675

Table 6.2. Correlation coefficients between river discharge and mean plume extension (\<E\>) and main characteristics of turbid plumes under extreme river discharge situations. All correlations are significant (> 99%). Plume states: Negligible (N), moderately developed (MD) and well developed (WD). \<E\> is measured in km^2. Series length is the number of days taking into account the number of available pixels from MODIS, greater than 70 %, and the existence of river discharge data.

Plume behavior was also evaluated under extreme river discharge conditions (low and high discharges) (Figure 6.3).
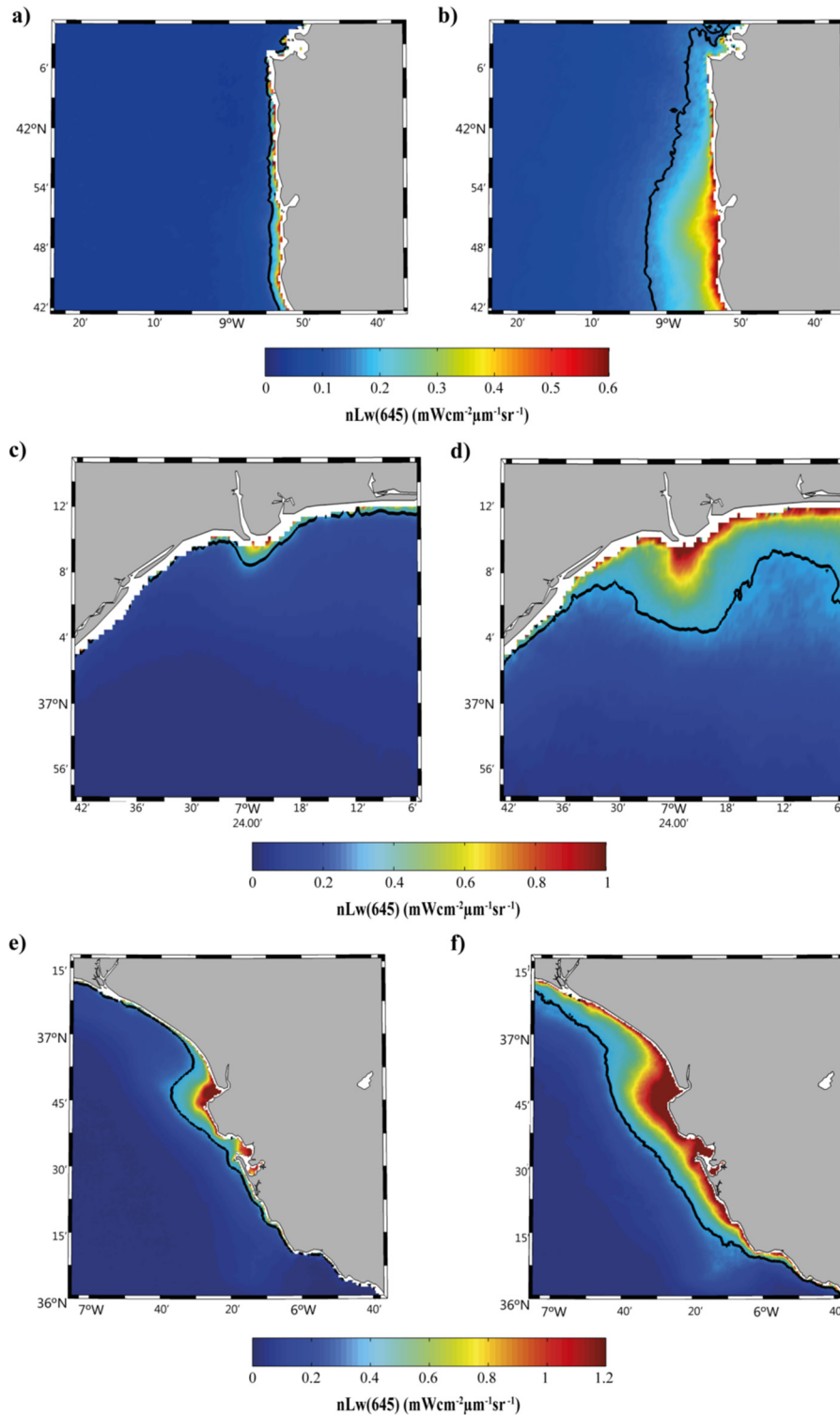
Figure 6.3. Turbid plume composites under low (< 25th percentile, left panels) and high (>75th percentile, right panels) river discharges, for (a, b) Minho, (c, d) Guadiana, and (e, f) Guadalquivir plumes. Black line represents the respective turbid threshold.

Three possible plume states have been identified under low discharge conditions: negligible plume (N), moderately developed plume (MD) and well developed plume (WD). A plume is considered completely developed when the turbid value of pixels decreases radially from the river mouth, forming a well-defined pattern in front of it.

Only Guadalquivir and Ebro Rivers present a plume completely developed under low river discharges due to the high sediment load. Minho and Douro show the opposite behavior with a negligible plume. Tagus and Guadiana Rivers present an intermediate situation with visible plume pattern but not completely developed. Under high discharge conditions all rivers form completely developed plumes, reaching Guadalquivir plume the maximum mean extension, 1,973 km^2, and Guadiana the minimum one, 333 km^2.

Figure 6.3 represents the three possible situations for a turbid plume. Minho plume represents an example of negligible plume under low river discharges (Figure 6.3a), showing a well-developed pattern, especially in front of river mouth, under high discharges (Figure 6.3b). A radially turbid pattern is visible under low river discharge conditions around Guadiana mouth (Figure 6.3c) being well developed under high discharge conditions (Figure 6.3d). Guadalquivir plume presents a well-developed plume under low (Figure 6.3e) and high (Figure 6.3f) discharges, with extension increasing with discharge. Ebro, Douro and Tagus plumes under low and high river discharges were showed in Figures 3.6, 4.3 and 5.3, respectively.

The importance of river discharge forcing on each plume development was analyzed by means of the $R_{<E>}$ parameter defined in eq. 6.1 (Table 6.3). $<E>^{max}$ is the plume area under high river discharges and $<E>^{min}$ under low discharges. In general terms, Minho, Douro and Guadiana Rivers present a plume extension highly influenced by river discharge while this influence is small for the Ebro River (Table 6.3).

River	$R_{<E>}$		
	Discharge	Wind	Tide
Minho	1.5	1.1	0.5
Douro	1.6	1.1	0.3
Tagus	0.9	0.8	0.7 (0.3)
Guadiana	1.6	1.6	1.1
Guadalquivir	1.0	0.4	0.2
Ebro	0.3	0.4	-

Table 6.3. River discharge, wind and tide influence on the development of Iberian turbid plumes by means of $R_{<E>}$ parameter (eq. 6.1).

6.5.3. Wind influence on the main Iberian plumes

The main characteristics of the most important Iberian plumes under wind forcing are shown in Table 6.4. The impact of cross-shore winds is shown in Figure 6.4 for Minho,

Guadiana and Guadalquivir, and in Figures 3.8, 4.5 and 5.6 for Ebro, Douro, and Tagus, respectively.
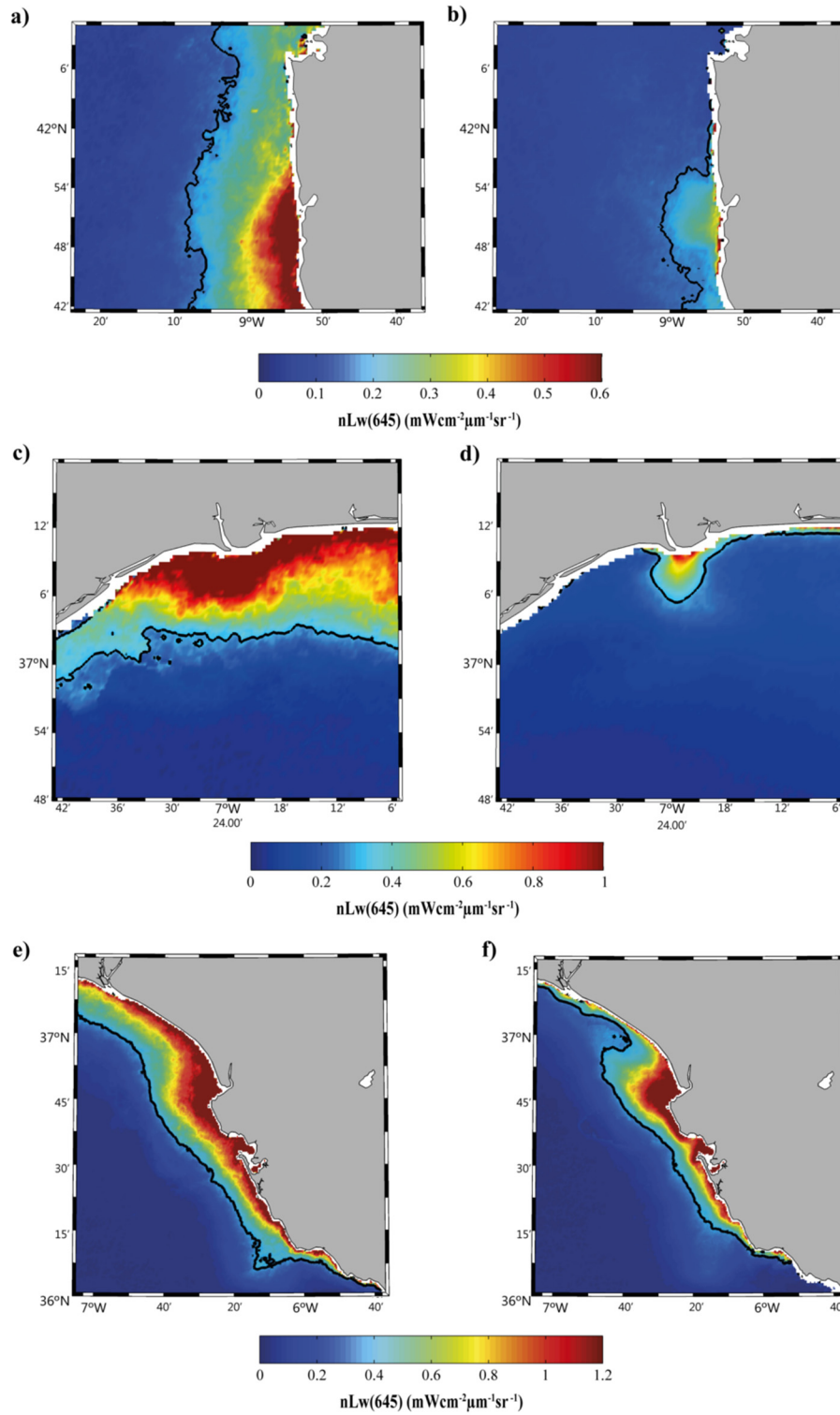
Figure 6.4. Turbid plume composites under landward (left panels) and seaward (right panels) cross-shore winds, for (a, b) Minho, (c, d) Guadiana, and (e, f) Guadalquivir plumes. Black line represents the respective turbid threshold.

All Atlantic Rivers reach maximum <E> and <T> values under CS$^-$ winds for the period under study (see Figure 6.4 and Table 6.4). This fact is due to landward winds accumulate the material exported by the rivers near coast, on both sides of the river mouth, decreasing seaward transport. This type of winds limits the loss of material by dilution in ocean waters provoking that values surpassing the turbid limit occupy a large area characterized by high turbid values (Figure 6.4, left panels). Most of Atlantic Rivers reach minimum <E> and <T> values under CS$^+$ winds. Seaward winds produce the fast dilution of plume material with the adjacent seawater causing turbidity to be quickly below the turbid limit due to the intense mixing promoted. Therefore, the plume area characterized by the values above the turbid limit, reaches its smallest extension and low mean turbid value under these conditions (Figure 6.4 right panels).

Most of rivers draining in the Atlantic margin of the Iberian Peninsula show intermediate <E> and <T> values under AS$^+$ and AS$^-$ winds (Table 6.4). The impact of alongshore winds on Iberian plumes is shown in Figure 6.5 for Minho, Guadiana and Guadalquivir, and in Figures 3.7, 4.4 and 5.4 for Ebro, Douro, and Tagus, respectively. AS$^+$ (upwelling) winds tend to displace the plumes offshore favoring the mix between plume and ocean water due to offshore Ekman transport, especially in front of river mouths (Figure 6.5, left panels). Under these upwelling winds, the mean turbidity decreases by an intense dilution in ocean water. AS$^-$ (downwelling) winds show the opposite effect compressing the plume against the coast especially to the side toward where wind blow, as a consequence of onshore Ekman transport (Figure 6.5, right panels). This provokes the retention of the plume in that area increasing the turbidity respect to the situation described above. Only Guadalquivir River reaches lower mean turbidity under downwelling than under upwelling winds. This is probably affected by the configuration of the coast around the Guadalquivir mouth, where exists a coastal protuberance south of river mouth. Taking into account that downwelling favorable winds are from southeast in the Guadalquivir area, this coastal feature can limit their effect, and therefore, the onshore currents generated.

The Ebro plume, which drains into Mediterranean Sea, reaches maximum and minimum values of <E> under wind conditions completely different to those for rivers draining in the Atlantic Ocean (see Figures 3.7 and 3.8). Ebro plume reaches its largest mean extension under CS$^+$ winds, whereas that remaining plumes present their smallest mean extension under these conditions (Table 6.4). This exceptional feature is due to the effect of the Liguro-Provençal current (LPC), which flows southwestward in that area. Seaward winds extend the plume offshore however, LPC displaces it southwestward along the coast decreasing cross-shore transport and dilution with seawater, distributing the plume in a large area (see detailed information in *Chapter 3*). In addition, Ebro plume reaches its minimum extension under CS$^-$ winds. This behavior, which is influenced by the LPC, is opposite to the observed for the rest of Iberian plumes. Ebro plume reaches its maximum and minimum <T> value under AS winds. The maximum <T> value (0.50±0.36 mWcm^{-2}μm^{-1}sr^{-1}) was reached under AS$^-$ winds due to the combined effect of the LPC and the landward Ekman transport.
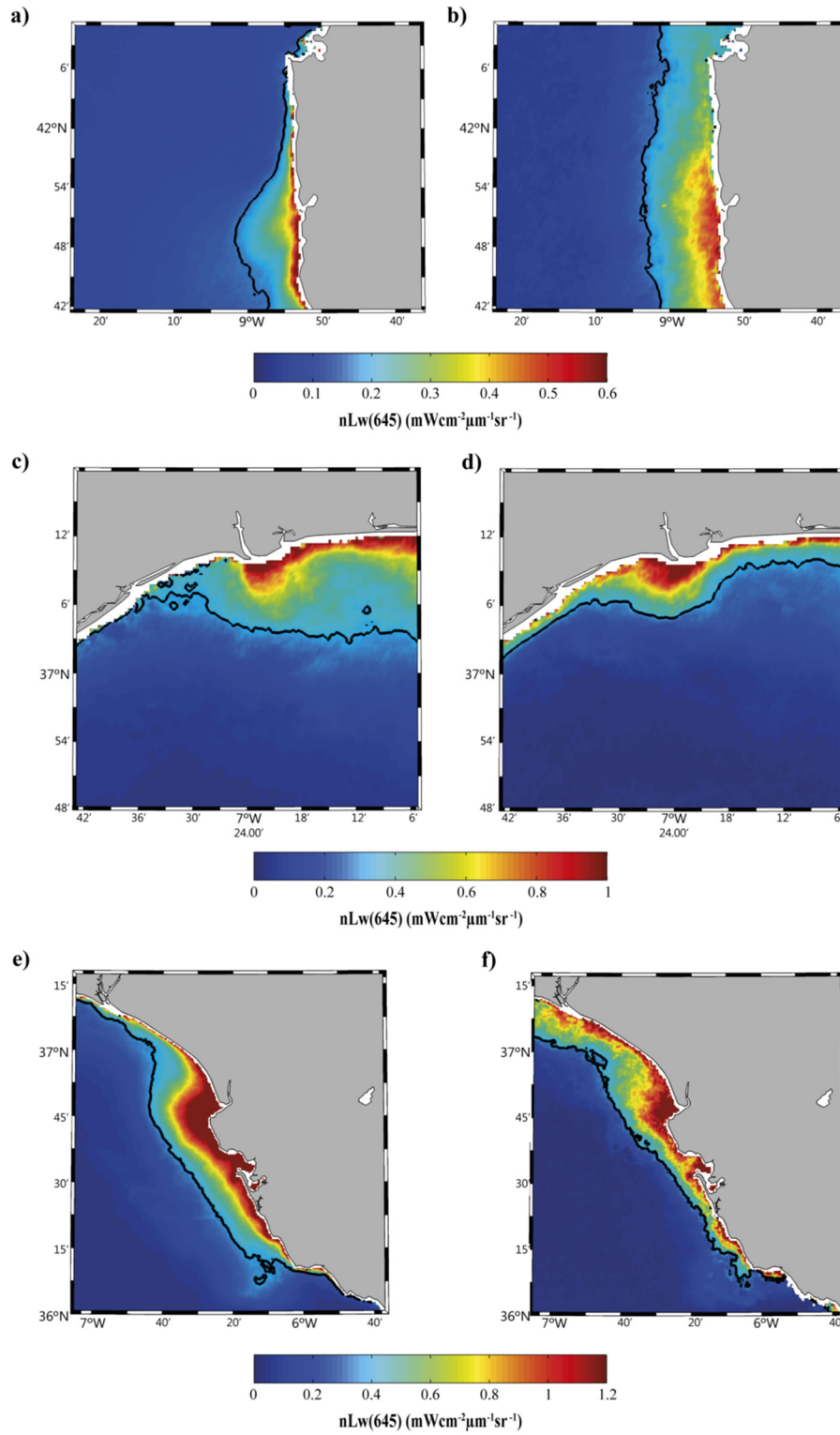
Figure 6.5. Turbid plume composites under upwelling (left panels) and downwelling (right panels) alongshore winds, for (a, b) Minho, (c, d) Guadiana, and (e, f) Guadalquivir plumes. Black line represents the respective turbid threshold.

In absolute terms, the largest <E> and the highest <T> values are reached by Guadalquivir plume under CS⁻ (landward) winds with 2309 km² and 0.88±0.47 mWcm⁻²μm⁻¹sr⁻¹, respectively. In contrast, Guadiana plume reaches the smallest extension, 89 km², and Minho plume the lowest turbidity, 0.24±0.15 mWcm⁻²μm⁻¹sr⁻¹, under CS⁺ (seaward) winds.

The importance of wind forcing on each plume development was also analyzed by means of the $R_{<E>}$ parameter defined in eq. 6.1 (Table 6.3). In this case, $<E>^{max}$ corresponds to the winds that cause the maximum mean extension of the river plume (CS⁺ for Ebro River and CS⁻ for the rest, Table 6.4) and $<E>^{min}$ to the winds that cause the minimum plume extension (CS⁻ for Ebro River and CS⁺ for the rest, Table 6.4). Guadiana plume extension shows to be highly influenced by wind while Ebro and Guadalquivir have low wind influence (Table 6.3).

River	Meteorological Conditions							
	AS⁺		AS⁻		CS⁺		CS⁻	
	<E>	<T>	<E>	<T>	<E>	<T>	<E>	<T>
Minho	269	0.30±0.22	569	0.30±0.17	*224*	*0.24±0.15*	**785**	**0.34±0.21**
Douro	806	0.47±0.27	940	0.51±0.31	*539*	*0.44±0.23*	**1788**	**0.55±0.30**
Tagus	288	*0.36±0.17*	323	0.39±0.17	*276*	0.37±0.17	**634**	**0.41±0.23**
Guadiana	512	0.52±0.26	278	0.60±0.28	*89*	*0.48±0.17*	**754**	**0.73±0.37**
Guadalquivir	2057	0.84±0.49	1680	*0.81±0.44*	*1536*	0.83±0.49	**2309**	**0.88±0.47**
Ebro	1422	*0.33±0.25*	1817	**0.50±0.36**	**1867**	0.34±0.23	*1288*	0.34±0.21

Table 6.4. Main characteristics of the most important Iberian turbid plumes under wind influence. Wind directions considered: alongshore winds which cause an Ekman transport offshore (AS⁺), alongshore winds which cause an Ekman transport onshore (AS⁻), seaward cross-shore (CS⁺) and landward cross-shore (CS⁻) winds. Mean extension (<E>) is measured in km² and mean turbid value (<T>) in mWcm⁻²μm⁻¹sr⁻¹. Bold italic numbers represent maximum values of <E> and <T> for each river and italic numbers the minimum ones. Dispersion was calculated by means of the standard deviation. Mean extension has not error because it was calculated counting the number of pixels that surpass the turbid threshold.

6.5.4. Tidal influence on the main Iberian plumes

Tidal effect on Iberian plumes is summarized in Table 6.5. Fortnightly cycle (spring and neap tides) only has an important influence on plumes formed by rivers that discharge in large estuaries with a residence time big enough to enhance turbidity (Braunschweig et al., 2003; Valente and da Silva, 2009). Although Tagus and Guadalquivir Rivers can fulfill this condition, only Tagus plume presents significant variability during the spring-neap tidal cycle (see Figure 5.8). The plume reaches its maximum mean extension and turbidity (411 km² and 0.41±0.17 mWcm⁻²μm⁻¹sr⁻¹) during and after spring tides. On the other hand, Tagus plume reaches its minimum extension and turbidity (239 km² and 0.32±0.13 mWcm⁻²μm⁻¹sr⁻¹, respectively) during and after neap tides (Table 6.5). Under this last situation Tagus plume is limited to the area near the river mouth with low turbid values (see Figure 5.8). On the contrary, during and after spring tides turbid values increase considerably and Tagus plume extends along the bay (see Figure 5.8). This

behavior is due to the larger amount of material exported from the estuary during spring tides, which is enhanced by the ebb-dominated Tagus Estuary (Vaz and Dias, 2014). These results are in good agreement with previous research carried out in the area (Valente and da Silva, 2009; Vaz et al., 2011; Vaz and Dias, 2014).

River	Tidal Conditions							
	Semidiurnal cycle				Fortnightly cycle			
	Low		*High*		*Spring*		*Neap*	
	<E>	*<T>*	*<E>*	*<T>*	*<E>*	*<T>*	*<E>*	*<T>*
Minho	519	0.25±0.12	293	0.21±0.07	-	-	-	-
Douro	1126	0.45±0.21	868	0.43±0.20	-	-	-	-
Tagus	641 [278]	0.45±0.30 [0.39±0.21]	293 [198]	0.40±0.16 [0.30±0.11]	411	0.41±0.17	239	0.32±0.13
Guadiana	259	0.44±0.16	79	0.36±0.11	-	-	-	-
Guadalquivir	2036	0.86±0.55	1644	0.78±0.48	-	-	-	-
Ebro	-	-	-	-	-	-	-	-

Table 6.5. Main characteristics of the most important Iberian turbid plumes under tidal influence. Tagus plume values of <E> and <T> for low and high tides are measured during spring tides and during neap tides (number in brackets) in order to isolate semidiurnal tidal cycle to the influence of fortnightly tidal periodicity. The symbol "-" indicates "negligible influence". Mean extension (<E>) is measured in km^2 and mean turbid value (<T>) in $mWcm^{-2}\mu m^{-1}sr^{-1}$. Dispersion was calculated by means of the standard deviation. Mean extension has not error because it was calculated counting the number of pixels that surpass the turbid threshold.

The semidiurnal tidal cycle (low and high tides) has remarkable impact on the development of the Atlantic Iberian plumes, which are under a mesotidal regime. Its effect is shown in Figure 6.6 for Minho, Guadiana and Guadalquivir, and in Figures 4.8 and 5.9 for Douro, and Tagus, respectively. All Atlantic Iberian plumes are larger and more turbid under low tides (Figure 6.6, left panels) than under high tides (Figure 6.6, right panels). This is due to high tides provoke the retraction of the plume hindering the exportation of material to the ocean and limiting the plume development. Tidal effect is negligible for the Ebro plume due to the micro-tidal regime of the Mediterranean Sea (Mestres et al., 2003).

The effect of low and high tidal states on Tagus plume was analyzed in *Chapter 5* for the same fortnightly period (intermediate state out of spring or neap tides), in order to isolate the semidiurnal effect because the different phases of the fortnightly periodicity affect Tagus plume development. Semidiurnal impact on Tagus plume was also evaluated in this chapter under periods of spring tides and neap tides, in order to proof if the semidiurnal effect is the same regardless the fortnightly state. In both cases, Tagus plume was greater and the turbidity higher under low tides (Figure 6.7), following the same behavior than the rest of Atlantic plumes and showing as semidiurnal tidal effect is independent of the fortnightly tidal state.
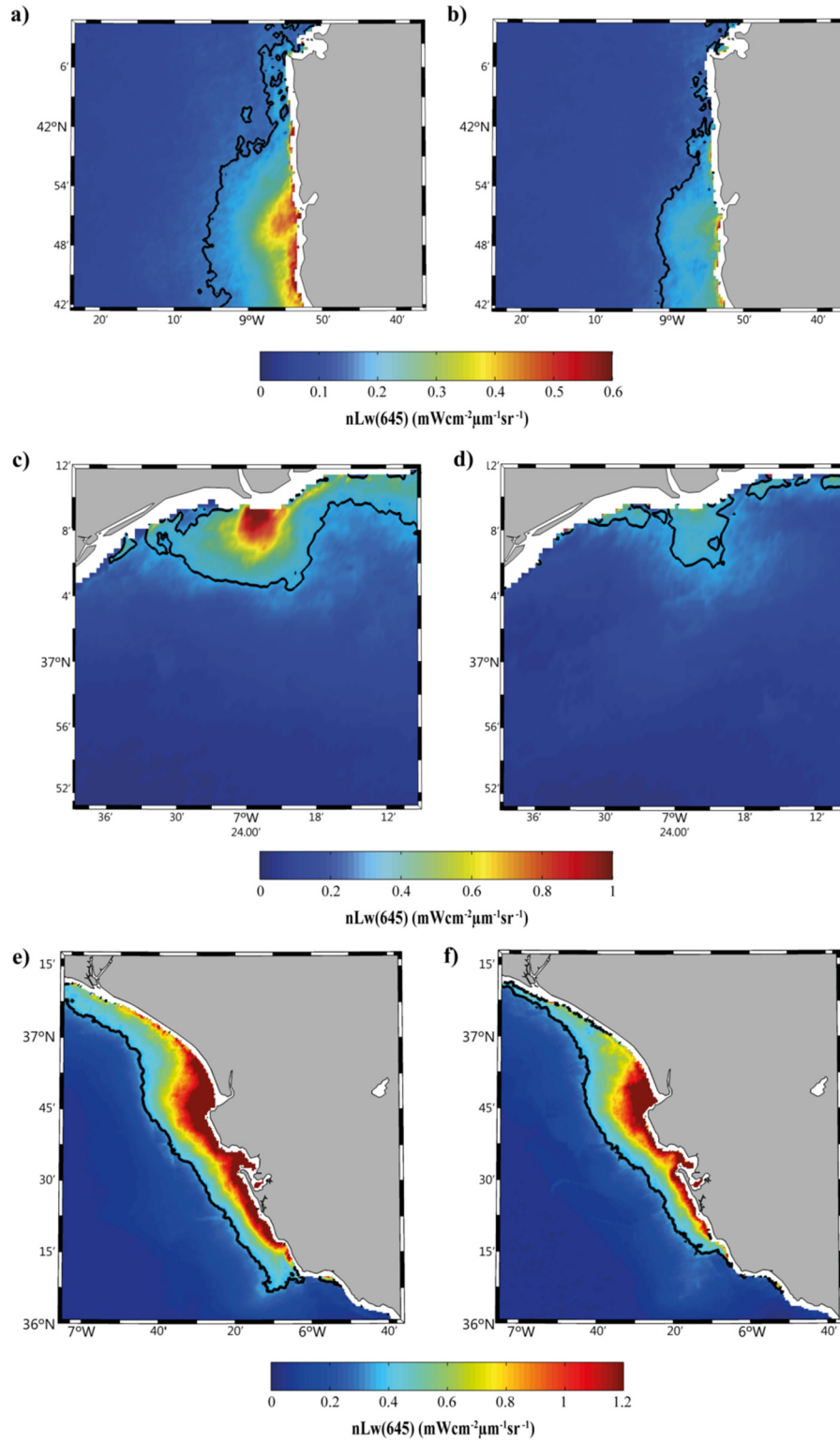
Figure 6.6. Turbid plume composites under low (left panels) and high (right panels) tides, for (a, b) Minho, (c, d) Guadiana, and (e, f) Guadalquivir plumes. Black line represents the respective turbid threshold.
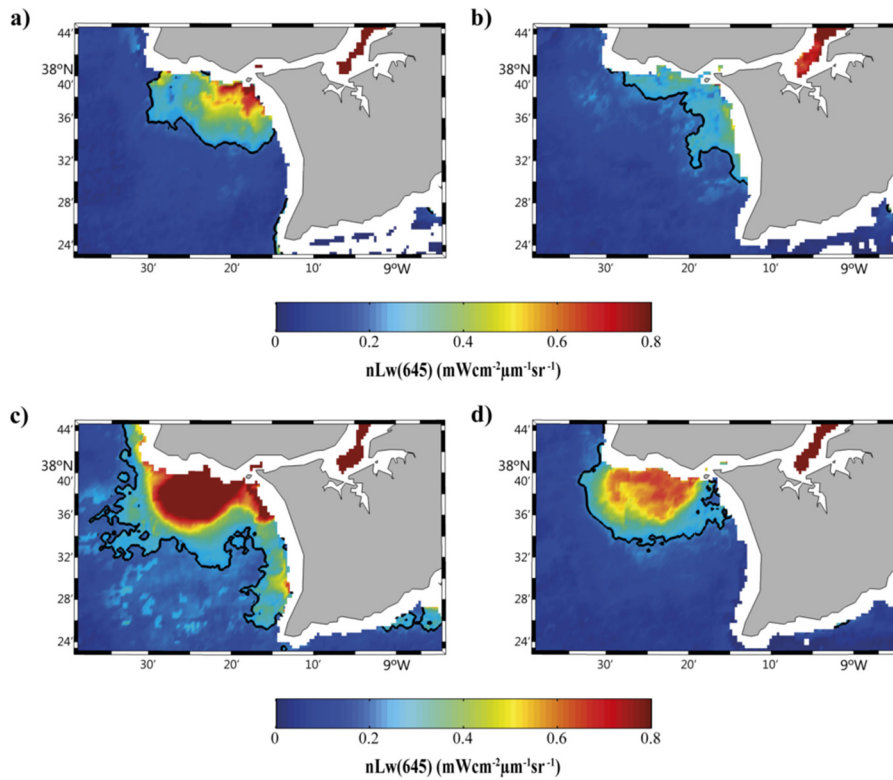
Figure 6.7. Tagus turbid plume composites under low (left panels) and high (right panels) tides, during neap (upper panels) and spring (lower panels) tides.

The impact of semidiurnal cycle on the development of each plume was analyzed by means of the $R_{<E>}$ parameter defined in eq. 6.1 (Table 6.3). In this case, $<E>^{max}$ represents situations under low tides that generate the maximum mean extension of the river plumes (Table 6.5) and $<E>^{min}$ under high tides that generate the minimum plume extension (Table 6.5). The $R_{<E>}$ parameter was calculated under spring (neap) tides for Tagus plume due to its significant variability during the spring-neap tidal cycle. Semidiurnal tidal cycle has important influence for Guadiana plume, and for Tagus plume under spring tides. On the contrary, semidiurnal tidal cycle has low influence for Guadalquivir and Douro plumes and for Tagus plume under neap tides.

The impact of the fortnightly cycle on Tagus plume development was quantified with a $R_{<E>}$ value of 0.5 indicating a moderate influence on plume extension.

6.5.5. Particular features of the main Iberian plumes

Some particular features of the main Iberian plumes linked to the regional coastal dynamic can be inferred with the methodology developed. A plume movement to the north of estuary mouths is expected due to the Coriolis deflection in the North Atlantic Iberian coast. However, a southward turbid coastal attached band is observed in the composites analyzing Minho and Douro plumes, both subjected to similar coastal

dynamics, as was detected for the Douro in *Chapter 4*. This turbid band can be expected under northerly winds as part of the water transport in the direction of the wind-driven circulation in shallow regions (Lentz and Fewings, 2012). Nevertheless, this southward turbidity fringe is also detected under other wind conditions. The littoral drift current resulting as a consequence of the northwest dominant wave direction (Veloso-Gomes et al., 2004; Rusu and Guedes Soares, 2013), which transports part of the sediments southward (Dias et al., 2002; Mendes et al., 2014), can be part of the explanation. Moreover, the southward flux could be also increased by the spatial orientation of both estuary axis (Yankovsky, 2000). The angle between coastline and Minho and Douro inlet orientations is about 45º in the opposite direction of Coriolis deflection, which can promote a southward water movement near both estuary mouths. Oppositely, there is not a southward turbid band in the Tagus plume. In this case, the topography, the morphology and the configuration of the region of influence of Tagus estuarine outflow protect the plume from northerly waves and winds (Rusu et al., 2011), as was explained in *Chapter 5*. Tagus plume material is only transported southward under landward winds due to the plume accumulation on both sides of the mouth, highlighting the importance of coastline geometry. In addition, Minho and Douro present a northward plume movement under southerly winds which is neither observed in the Tagus plume. Once more the shape of the Tagus bay is the responsible of limiting the plume displacement to the north, whereas Minho and Douro have not geological barriers blocking the generation of this plume feature.

Compared with the rest of the rivers flowing into the Atlantic Ocean, the Guadiana and Guadalquivir plumes present some particularities due to the change in the shoreline orientation of this region. The coastal wave regime in the Gulf of Cadiz is dominated by waves providing from the W-SW, in such way that the net annual littoral drift current is in the W-E direction (Gonzalez et al., 2001; Gonzalez et al., 2007; Sanchez-García et al., 2013). This can be inferred from Guadiana composites where a predominant eastward plume development is observed under all drivers. Only under easterly winds the main bulge of the plume is displaced westward. This predominant movement associated to the littoral drift current is not clearly observed in Guadalquivir plume, probably due to the NW-SE coastal orientation, which limits the effect of the littoral current. This limitation can also be reinforced by the coastal protuberance in the southern part of the mouth. However, under high discharges some material is detected southeastward, which could be related to the interaction with the southeastward flow of the North Atlantic Surface Water (NASW) (Lobo et al., 2004).

By last, Ebro plume is affected by the regional oceanic circulation along the Mediterranean Sea, which is dominated by Liguro-Provençal current, flowing southwestward in the Ebro plume development area (Font et al., 1990). Both Coriolis and the Liguro-Provençal current tend to displace river plumes to the southwest in the Mediterranean Iberian coast. The predominant southward advection may generate a clockwise eddy in the lee side of the Delta. In fact, a quasi-permanent anticyclonic gyre exists south of the Ebro River mouth (Arnau et al., 2004). This anticyclonic gyre together

with the Liguro-Provençal current explain that more than 70 % of plume material is located south of the river mouth, even under southwesterly winds, as was detailed in *Chapter 3*. This behavior is different from Atlantic plumes where most of plume movement is driven by wind. In addition, weak winds during summer months (Durand et al., 2002) and the micro-tidal regime in the Mediterranean Sea (Mestres et al., 2003), intensify the stratification inhibiting vertical mixing and making different the salinity and turbidity plumes propagation as was explained in *Chapter 2, Section 2.4. "Accuracy of MODIS radiance to represent river plumes"*.

6.6. Conclusions

River plumes of the main Iberian Rivers were characterized by means of synoptic patterns obtained through MODIS imagery over the period 2003-2014. Minho, Douro, Tagus, Guadiana, Guadalquivir and Ebro plumes extension and turbidity were characterized as well as their variability under the main forcing: river discharge, wind and tidal forcing. Common features and differences among rivers are included in Table 6.6.

Plume Characterization								
River	Plume delay (days)	Wind effect $<E>^{max}$ ($<E>^{min}$)	External currents influence	Semidiurnal tidal effect	Fortnightly tidal effect	Runoff impact	Wind impact	Tide impact
Minho	0	CS^- (CS^+)	-	+	-	H	H	M
Douro	0	CS^- (CS^+)	-	+	-	H	H	L
Tagus	2	CS^- (CS^+)	-	+	+	M	M	M
Guadiana	0	CS^- (CS^+)	-	+	-	H	H	H
Guadalquivir	3	CS^- (CS^+)	-	+	-	H	L	L
Ebro	0	CS^+ (CS^-)	+	-	-	L	L	-

Table 6.6. Common features and differences among the most representative Iberian River plumes. River plume characterization and plume behavior under main forcing: runoff, wind and tide for the period 2003-2014. + (–) means that there is (not) influence of this forcing on plume extension. Three ranges of forcing influence on plume development were defined: high influence (H), when the amplitude of plume extension is higher than the mean value, moderate influence (M), when the amplitude is between one half and the mean extension, and low influence (L) when the amplitude is lower than one half of the mean plume extension.

The main findings of the chapter can be summarized as follows:

- Extension and turbidity of plumes of the different rivers cannot be easily compared since they are strongly dependent on the sediment load, which is characteristic of every river (Table 6.1).

- Plumes of rivers with large estuaries (Tagus and Guadalquivir) are lagged compared to river discharge (Tables 6.1 and 6.6).

- River discharge showed to be the main forcing affecting plume extension (Tables 6.2, 6.3 and 6.6). Actually, the dependence of extension on runoff is moderate or high for all rivers, except Ebro. Wind and tide are secondary forcing.

- The dependence of plume extension on wind is moderate or high for all rivers, except Guadalquivir and Ebro (Tables 6.3, 6.4 and 6.6).

- Landward cross-shore winds (CS^-) produced the largest plumes for all Atlantic Rivers. The smallest plumes were obtained under seaward cross-shore winds (CS^+) (Tables 6.4 and 6.6).

- All Atlantic River plumes have a certain dependence on the semidiurnal tidal cycle. They increased during low tides and decreased during high tides (Tables 6.5 and 6.6). That dependence is only high for Guadiana River. In addition, Tagus River plume also depends on the fortnightly tidal cycle (it was higher during spring tides): This dependence is mainly due to the complexity of the estuary, since the river debouches into a semi-enclosed embayment (*Mar da Palha*, ~ 320 km^2) which connects to the Atlantic Ocean through a Strait. As was mentioned above, plume extension and runoff are lagged for this river.

- Ebro River constitutes a particular case. On the one hand, CS^+ (CS^-) winds produced the largest (smallest) plume (Tables 6.4 and 6.6). On the other hand, the plume shows a low dependence on runoff and wind, and a negligible dependence on tide (Tables 6.3 and 6.6). Basically, the plume is driven by a coastal current (the Liguro-Provençal current)

- Guadalquivir River also constitutes a particular case, since its plume is highly dependent on river discharge but with low tidal and wind influence. In spite of being the second smallest river in terms of discharge, it generated the largest plume in terms of turbidity and extension. This is due to its high sediment load generated from farmlands, urban settlements and from Doñana Natural and National Park situated at the river mouth.

Chapter 7:

Analysis of Loire and Gironde plumes dynamic and their impact on thermohaline properties

7.1. Motivation

In previous chapters the methodology to characterize, analyze and compare the most important Iberian turbid plumes was developed. Therefore, a robustly procedure to know and predict the plume behavior under the effect of the forcing drivers was designed. A step forward was given in this chapter. Besides to analyze the behavior of the most important French plumes formed in the Atlantic Ocean (Figure 7.1) under the main forcing, the impact of the most important teleconnection indices on plume development was also evaluated. In addition, the impact of these plumes on the thermohaline properties of the seawater was also assessed. The knowledge of the plume influence on the evolution of sea temperature patterns is especially important in the actual context of global warming.

The goal of this chapter is to analyze the synoptic conditions that characterize the Loire and Gironde River plumes from 2003 to 2015, as well as, the impact of teleconnection indices on plumes development. In addition, the influence of these plumes on thermohaline properties in the adjacent ocean will be also analyzed by means of salinity and temperature data derived from the Copernicus program (IBI database) from 2002 to

2014, the available period of this database. Impact of Loire and Gironde plumes on sea surface temperature was also compared with data obtained from other datasets (OISST$_{1/4}$ and MODIS), in order to test the accuracy of Copernicus data and if the observed effects on temperature evolution are regardless of the database and time period used.
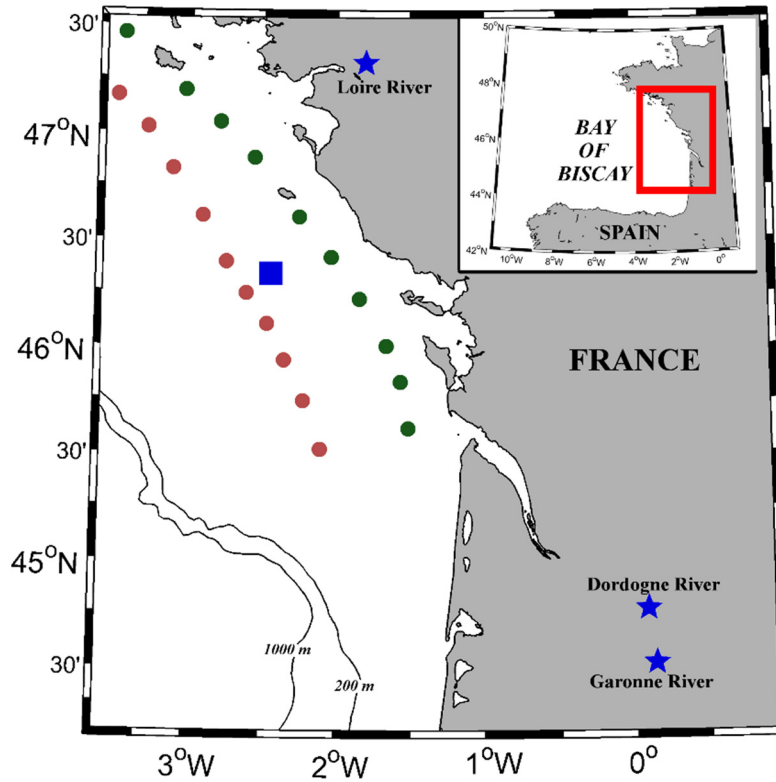
Figure 7.1. Bathymetry of the French Atlantic continental shelf. Solid black lines represent the 200 and 1000 m isobaths. Blue asterisks mark the locations where river discharge was measured. The blue square marks the location where wind data were obtained. Green (magenta) circles mark the locations where sea temperature data were obtained at coastal (oceanic) locations. All coastal points have in common a depth of about 40 m.

7.2. Methods

The methodology followed to analyze Loire and Gironde plumes response to the main forcing and teleconnection patterns was the same explained in the *Chapter 2, Section 2.2. "Turbid plume forcing databases"*. Wind data were selected in a location between both estuaries because are very similar to wind data in front of Loire and Gironde River mouths (correlations above 0.9).

The analysis of plume influence on thermohaline properties of seawater was conducted using the databases and methodology defined in *Chapter 2, Section 2.3. "Oceanographic databases"*.

Intra-annual thermohaline variability was analyzed in the first 40 m of the water column along the French continental shelf using data from the IBI database. To carry out this analysis, temperature, salinity and density data were monthly averaged at 10 coastal (green dots, Figure 7.1) and 10 oceanic (magenta dots, Figure 7.1) locations. Trends were calculated assuming linear regressions.

7.3. Main forcing affecting Loire and Gironde plumes

The general characterization of the main forcing affecting Loire and Gironde plumes (river discharge and wind) is depicted in Figure 7.2.
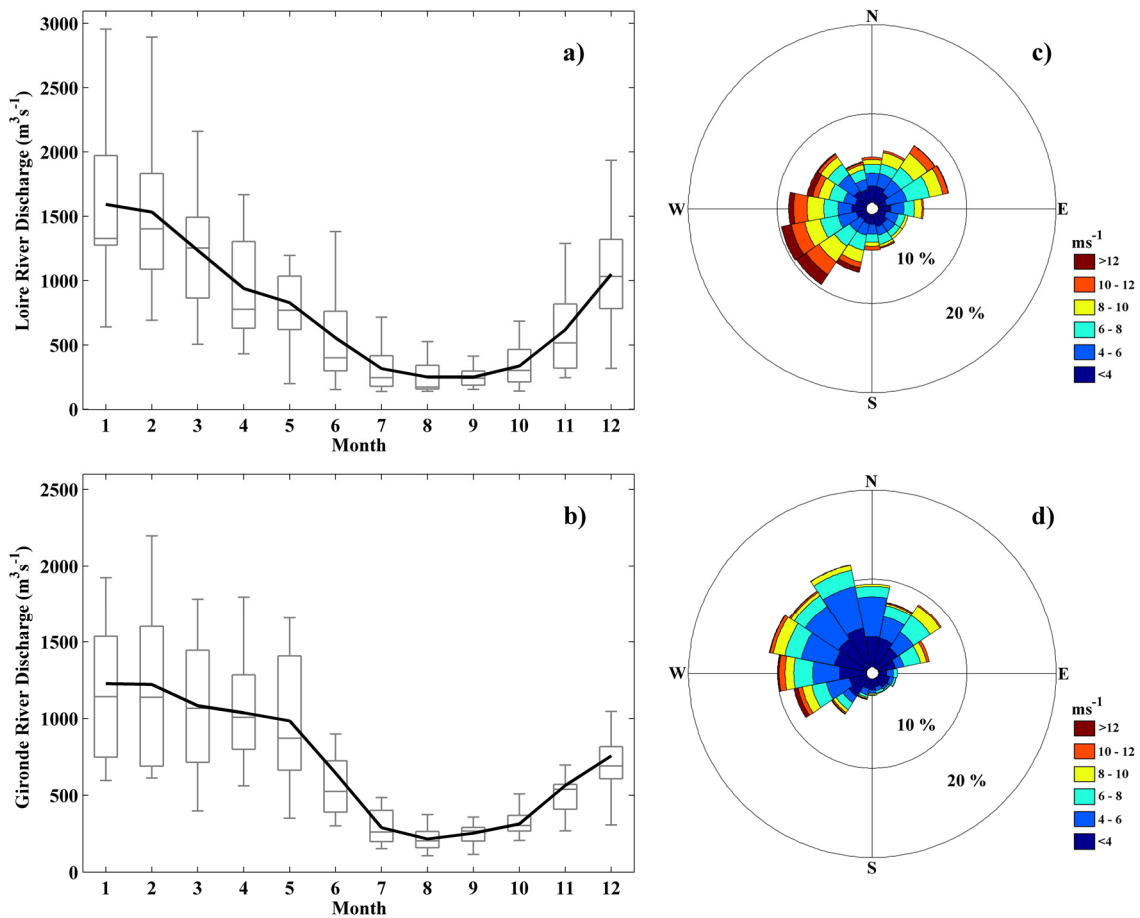
Figure 7.2. Annual hydrologic cycle for (a) Loire and (b) Gironde River discharges (m^3s^{-1}) from 2003 to 2015. Solid black line: monthly average; the line inside each box indicates the median; lower and upper whiskers: minimum and maximum, respectively; lower and upper box limits: first and third quartiles, respectively. Wind rose diagram (ms^{-1}) for a location between Loire and Gironde Estuaries from 2003 to 2015 for (c) October-March and (d) April-September periods.

Daily Loire and Gironde River discharges were obtained from the Banque Hydro French Database (http://www.hydro.eau-france.fr/). River runoff is available over the period 1997-2015 for the Gironde River and 1982-2015 for the Loire River, although special attention was paid over the period 2003-2015 coinciding with MODIS data (Figure 7.2, left panels). Both rivers present a clear seasonal pattern with the highest discharges reached in January-February and the lowest ones in August-September, showing the synchronism of both rivers (Koutsikoupoulos and Le Cann, 1996; Lazure and Jegou, 1998). In quantitative terms, the maximum mean monthly discharge was about 1600 m^3s^{-1} for Loire River and 1200 m^3s^{-1} for Gironde River in January and the minimum one was about 250 m^3s^{-1} and 200 m^3s^{-1} in August for Loire and Gironde Rivers, respectively.

Daily wind data were obtained from CFSR database at an ocean location between both estuaries from 1982 to 2015. Winds showed a marked interannual variability. Strong southwesterly winds prevail from October to March with velocities mostly ranging between 6-14 ms^{-1}, whereas northwesterly winds prevail from April to September, with velocities mostly ranging between 2-8 ms^{-1} (Figure 7.2, right panels), as was previously observed by Puillat et al. (2004, 2006).

7.4. Results and Discussion

7.4.1. River discharge influence on Loire and Gironde plumes

Development of the Loire and Gironde plumes is mainly affected by river discharge variability (Figure 7.3), as a high correlation was observed between plume development and discharge when daily data were compared for an area close to each river mouth. The Loire plume immediately responds to discharge variations, as the maximum correlation (0.7) was obtained when no lag was applied (Figure 7.3a). On the other hand, the Gironde plume reacts to river discharge variations with a delay of 2 days (Figure 7.3b), which may be due to the great estuary formed before emptying into the ocean. The maximum correlation was close to 0.6 in this case. Both rivers show the maximum correlation for a turbidity value of 0.2 $mWcm^{-2}\mu m^{-1}sr^{-1}$, representing the turbidity threshold used to delimit the plumes. Plume development is strongly influenced by the river discharge that occurred over the prior 4 days, and radiance at day d is well correlated with river discharge from day $d–3$ to day d, decreasing considerably for previous days. Hereafter, plume analysis in terms of daily river discharge considered the average discharge over those 4 days.
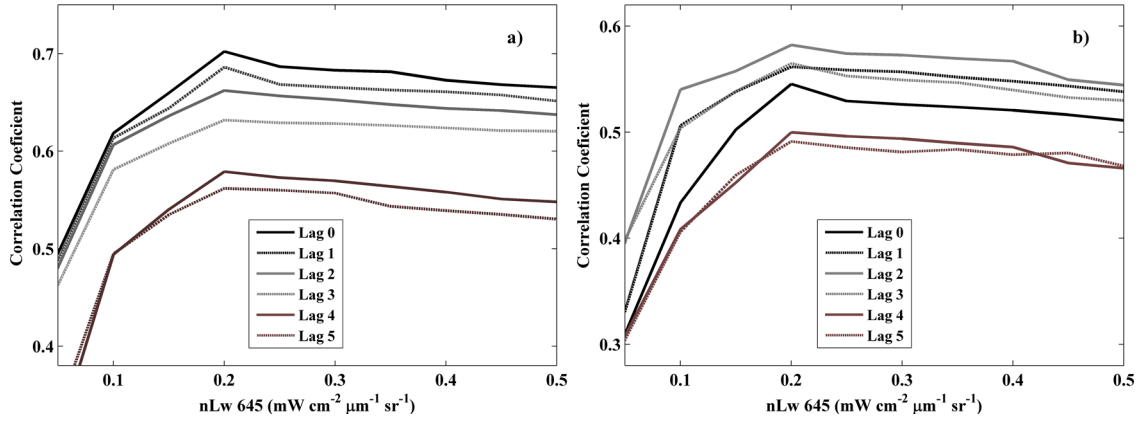
Figure 7.3. Correlation coefficient between plume extension and daily river discharge (with different delays) under different threshold values for (a) Loire and (b) Gironde Rivers. Only daily plume images with more than 70% of available pixels were used in order to avoid disturbances provoked by the lack of valid pixels.

Figure 7.4 shows the annual cycle of river discharge and plume extension. Because a continuous plume was observed between both estuaries in months of high discharge (Lazure and Jegou, 1998), the plume extension was calculated considering both estuaries and river discharge as the sum of both rivers. In general, high values of river discharge and plume extension occur during winter months, whereas low values take place during summer. The maximum extension was attained in January ($\sim 2.9 \times 10^4$ km^2) and the minimum occurred in July ($\sim 3.8 \times 10^3$ km^2). The maximum discharge was reached in January ($\sim 2.8 \times 10^3$ m^{3}s^{-1}) and the minimum one in August ($\sim 5.0 \times 10^2$ m^{3}s^{-1}). The extension of the plume not exactly follow the annual discharge pattern due to the influence of wind, which is an important forcing factor affecting plume development, as was observed for the Iberian Rivers in previous chapters.
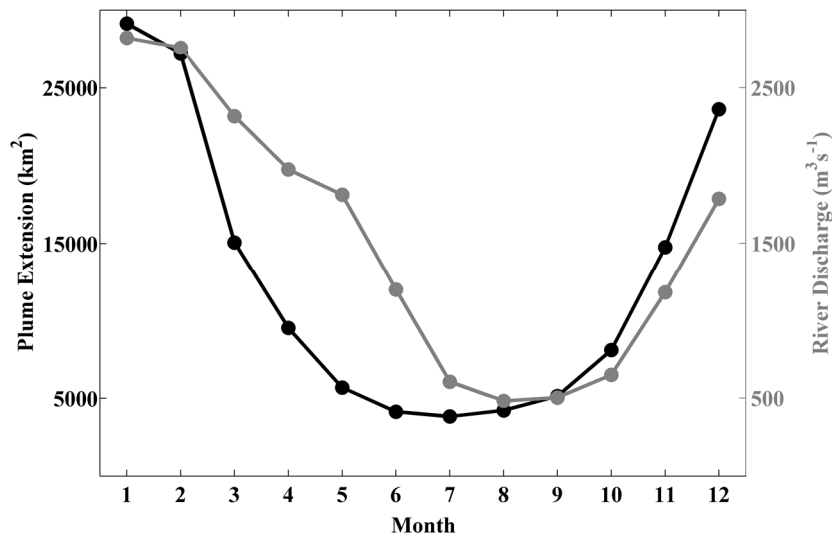
Figure 7.4. Annual cycle of Loire-Gironde plume extension (black dots) and river discharge (grey dots) from 2003 to 2015.

The influence of river discharge on the turbid plume was also evaluated under extreme flow conditions (Figure 7.5). Turbid material is located near the mouth of each river under low discharges covering a small area (Figure 7.5a). In contrast, turbid material forms a large and continuous plume between both estuaries under high discharges (Figure 7.5b). Plume extension clearly increases with the increasing of river discharge, which illustrates how river runoff controls its development. Therefore, river discharge is the most important driver modulating the Loire and Gironde plumes, which has been observed in the previous chapters for Iberian Peninsula.
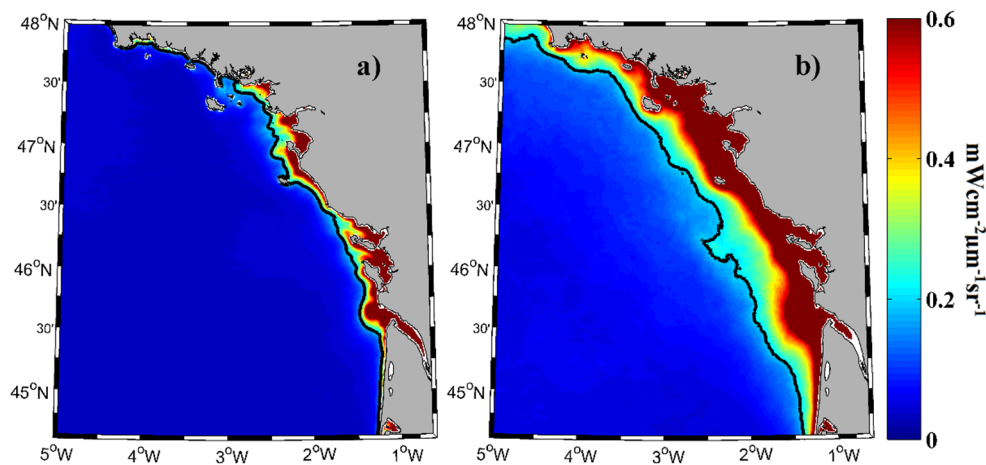
Figure 7.5. The Loire-Gironde turbid plume under (a) low ($< 25^{th}$ percentile) and (b) high ($> 75^{th}$ percentile) river discharges. Black line represents the turbid threshold (0.2 mWcm^{-2}μm^{-1}sr^{-1}).

7.4.2. Wind influence on Loire and Gironde plumes

As mentioned above, river discharge is the main forcing affecting plumes in the study area. The effect of wind is noticeable only when enough material is transported by the plume, which occurs under periods of high river discharge. Thus, the influence of wind on plume dynamics was analyzed for daily river discharges above the 70th percentile (for the average of the last 4 days) in order to have a sufficiently developed plume to evaluate the wind effect. In addition, extreme flows over the 95th percentile were discarded to remove outliers and maintain similar river discharges for the different wind conditions under analysis.

Figure 7.6 shows the influence of alongshore winds on the Loire-Gironde plume. Upwelling winds favor the spreading of the plume material seaward because offshore Ekman transport produces a more intense decrease in turbidity due to dilution of the plume with ocean water (Figure 7.6a). This behavior agrees with previous works that detected a reduction of salinity differences between coastal and ocean waters due to the mixing promoted by upwelling winds (Fong and Geyer, 2001). Thus, although some turbidity was detected at greater distances over the ocean, its value is under the turbidity threshold. On the other hand, downwelling winds promote the retention of suspended

material along the coast northward of Gironde mouth as a consequence of onshore Ekman transport (Figure 7.6b). This explains the presence of higher turbidity values along the coast and a higher turbid plume. The difference between turbid plumes under alongshore winds (downwelling minus upwelling winds) is assessed in Figure 7.6c. A fringe of positive values (dominance of downwelling winds) is visible along the coast to the north of the Gironde River mouth, which indicates that the suspended material carried by the plume is maintained mainly in this area. This pattern agrees with other works that analyzed wind impact on Atlantic Iberian plumes (Otero et al., 2008). In addition, negative values (dominance of upwelling winds) are observed offshore, showing the capability of upwelling winds to transport plume material over large distances in the ocean. This behavior is in good agreement with previous works reporting that plumes tend to be advected offshore under upwelling winds (Fong and Geyer, 2001). Finally, a negative band is observed south of the Gironde mouth due to the northward component of upwelling winds.
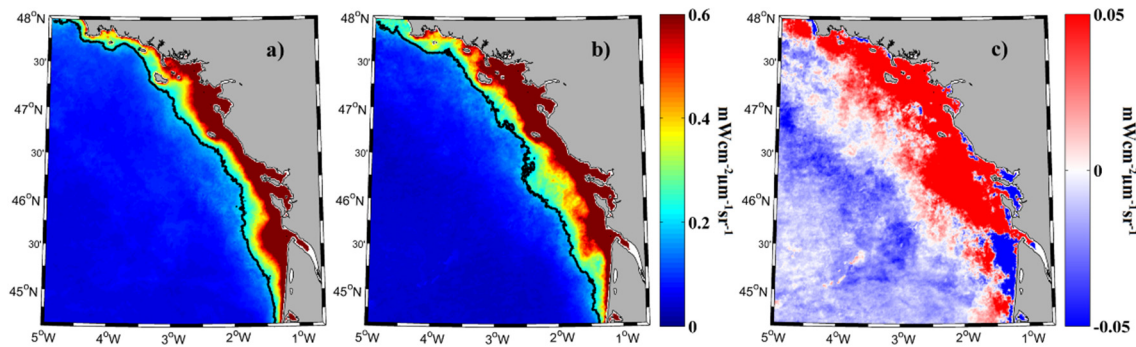
Figure 7.6. The Loire-Gironde turbid plume under (a) upwelling and (b) downwelling favorable winds. (c) Loire-Gironde plume differences for alongshore winds (downwelling minus upwelling winds). Black line represents the turbid threshold (0.2 mWcm^{-2}μm^{-1}sr^{-1}).

The influence of cross-shore winds on plume dynamics can be observed in Figure 7.7. Seaward winds tend to push river material toward the ocean (Figure 7.7a), whereas landward winds tend to accumulate the material near shore in both alongshore directions, decreasing the cross-shore transport, which is represented by a greater area occupied by the highest turbid values (> 0.6 mWcm^{-2}μm^{-1}sr^{-1}) (Figure 7.7b). The turbid plume is greater under landward winds than under seaward winds. Similar to the alongshore winds situation, seaward winds promote the dispersion of plume material toward the ocean, which produces a rapid decrease of turbid values and diminishes the turbid plume area. The difference between turbid plumes under cross-shore winds (landward minus seaward winds) is shown in Figure 7.7c. A wide fringe of positive values (dominance of landward winds) dominates the coastal area, showing the retention of the material discharged by the rivers under landward winds. Negative values (dominance of seaward winds) are detected over large distances in the ocean, showing the capability of seaward winds to move and disperse the river material offshore. This behavior was previously observed in

the Atlantic Rivers of the Iberian Peninsula. The influence of each wind pattern on plume development is shown in Table 7.1; the results indicate greater extension of the turbid plume under landward and downwelling favorable winds.
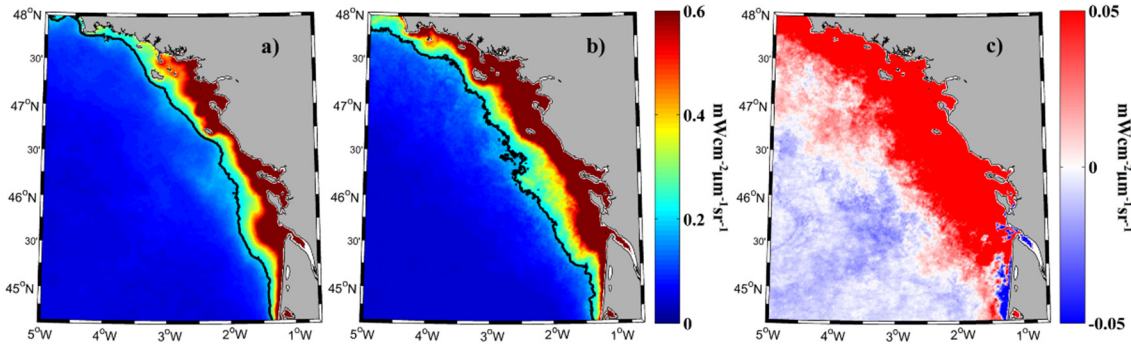
Figure 7.7. The Loire-Gironde turbid plume under (a) seaward and (b) landward winds. (c) Loire-Gironde plume differences for cross-shore winds (landward minus seaward winds). Black line represents the turbid threshold (0.2 mWcm^{-2}μm^{-1}sr^{-1}).

In summary, although the wind effect is dependent on river discharge, it has a considerable influence on plume development and spreading, either favoring or limiting the plume's mixing with adjacent ocean water. Downwelling and landward winds inhibit cross-shore transport and limit mixing between plume and ocean water, thereby isolating both water masses and enhancing the differences between their thermohaline properties.

Wind condition	Plume Extension ($\times 10^4$ km^2)	Effect
Downwelling	2.0	Retention of plume material along the coast north of the Gironde mouth.
Upwelling	1.6	Spreading and dilution of plume material into ocean water and south of the Gironde mouth.
Landward	2.2	Accumulation of plume material along the coast in both alongshore directions.
Seaward	1.5	Spreading and dilution of the plume.

Table 7.1. Characteristics of the Loire-Gironde turbid plume under wind influence.

7.4.3. Teleconnection patterns influence on Loire and Gironde plumes

EA and NAO are the most representative patterns of atmospheric variation in the Northern Hemisphere (Barnston and Livezey, 1987). These teleconnection patterns influence precipitation (and therefore river discharge) and wind dynamics, presenting higher amplitudes during winter (Lorenzo and Taboada, 2005; deCastro et al., 2006; 2008). Table 7.2 shows the influence of EA and NAO on plume development and plume forcing

during winter months (from December to February). The analysis was carried out for the correlation between EA and NAO and river discharge, intensity of landward winds, and extension of the plume. Only landward (southwesterly) winds were considered because they are prevalent during this season (Puillat et al., 2004, 2006).

	NAO	EA
Loire Discharge	-	0.32
Gironde Discharge	-	0.29
Landward Wind	0.37	0.59
Plume Extension	0.35	0.53

Table 7.2. Correlation coefficients between NAO and EA teleconnection indices and river discharge, landward winds, and plume extension for the Loire and Gironde Rivers. All values are significant at 99% from 2003 to 2015.

Significant positive correlations (Table 7.2) were found among the indices and the above mentioned factors during winter months. Thus, NAO shows a positive correlation with landward winds and the plume extension. EA is positively correlated with river discharge and landward winds, and, therefore, with the plume extension, being the correlations higher than those observed for NAO. Therefore, positive values of both indices imply larger plumes: NAO through the increase of landward winds and EA via the increase of landward winds and river discharge. In summary, EA exerts a major impact on the plumes, with correlation coefficients that were slightly higher than those for NAO. This fact is mainly due to the location of the Bay of Biscay, which is between two regions with different wind and precipitation responses to NAO (Pérez et al., 2000) and closer to one of the centers of the EA dipole (west of the British Isles; Borja et al., 2008). The EA pattern is a north-south dipole with its centers displaced southeastward with respect to the NAO.

Figure 7.8 illustrates the influence of NAO and EA indices on the merged plume. Composites were created for positive (negative) values of both teleconnection indices above (below) 0.25 (-0.25). The total extent of the plume formed by both rivers occupies a larger area under positive values of both indices (Figures 7.8b and d) than under negative ones (Figures 7.8a and c). Thus, the extent was about 3.0×10^4 km^2 (~2.8×10^4 km^2) for positive EA (NAO) and 2.1×10^4 km^2 (~2.3×10^4 km^2) for negative EA (NAO). The information provided by these composites can be summarized as follows: (i) the extent of the plume was around 30% higher under positive indices; (ii) the dependence was stronger for EA, for which the difference between the maximum and minimum extension of the plume was higher than for NAO. This corroborates the results shown in Table 7.2. Finally, the obtained results are also consistent with previous works related to the impact of teleconnection indices on plume dynamics along the French continental shelf (Borja et al., 2008; Massei et al., 2010).
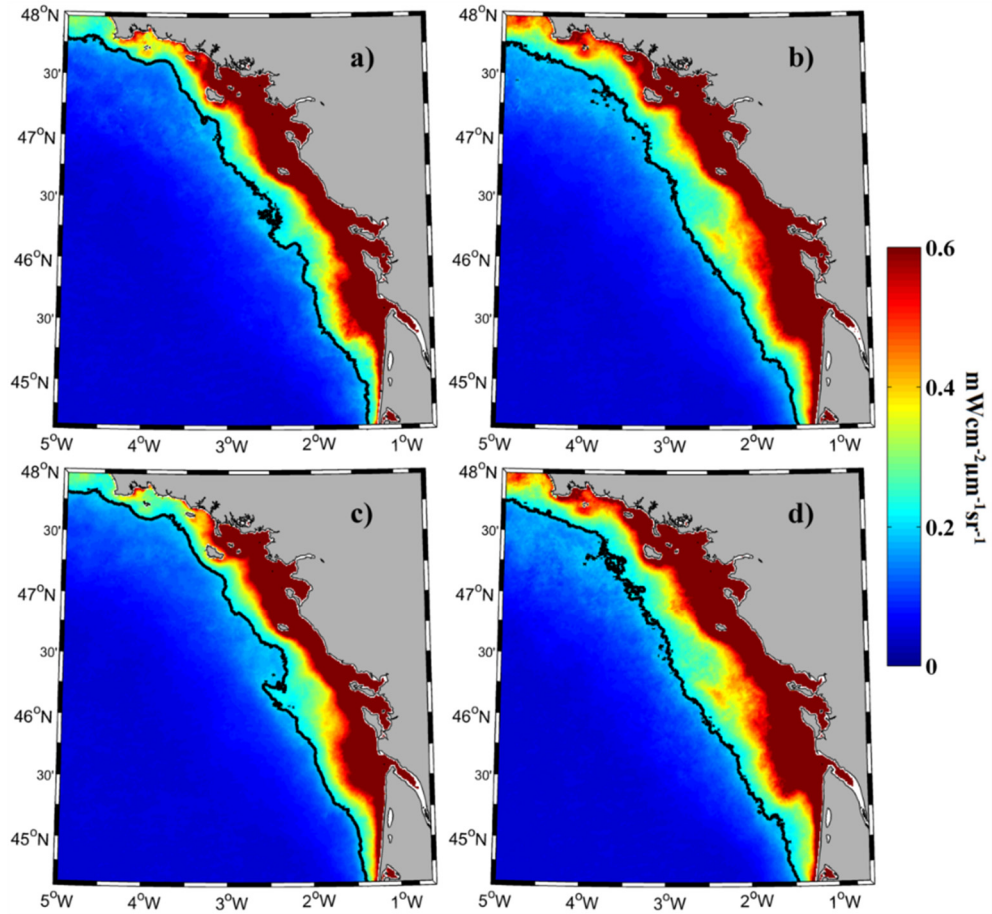
Figure 7.8. The Loire-Gironde turbid plume under (a) negative and (b) positive values of the NAO index. The Loire-Gironde turbid plume under (c) negative and (d) positive values of the EA index. Black line represents the turbid threshold (0.2 mWcm^{-2}μm^{-1}sr^{-1}).

7.4.4. Loire-Gironde plume influence on seawater thermohaline properties

The presence of river plumes has a key impact on the thermohaline properties of the surrounding water. This effect is enhanced by the great width of the French continental shelf in the area where the Loire and Gironde Rivers flow into the Bay of Biscay (Figure 1.3). This fact, in conjunction with high discharges and the prevailing southwesterly (landward) winds during winter, strongly conditions the thermohaline properties of water in a vast area along the French coast during that season (e.g., Kelly-Gerreyn et al., 2006; Costoya et al., 2015). In fact, plume achieves its greatest extension from December to February (Figure 7.4). It is important to consider that freshwater inputs in the area have important physical and biological implications (see Puillat et al. (2006) for a detailed description). For these reasons, thermohaline features were analyzed both inside and outside the area occupied by the turbid plume from December to February (DJF).

7.4.4.1. Loire-Gironde plume influence on sea surface water

Salinity and temperature values in the sea surface were averaged from December to February during 2002-2014, the period available from IBI database. The mean DJF plume was averaged over the same period in order to compare with salinity and temperature patterns (the upper limit of the colorbar was adjusted for comparison purposes) (Figure 7.9). It has an offshore extension about 100 km and maximum turbid values above 2 mWcm^{-2}μm^{-1}sr^{-1} near Loire and Gironde Estuaries.
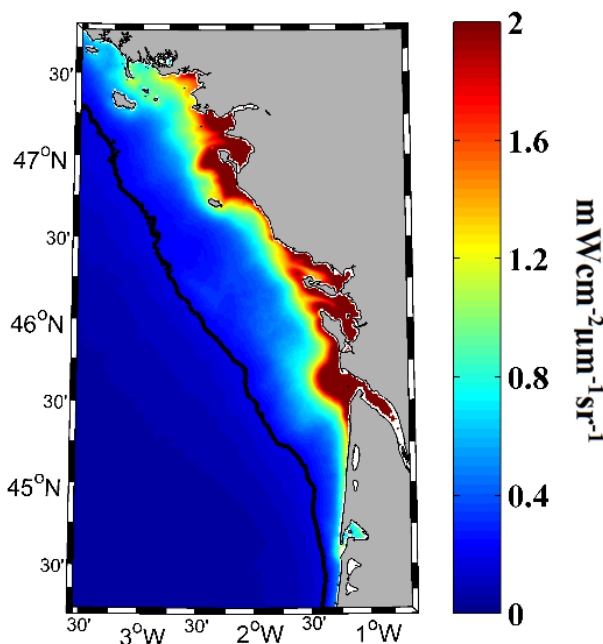
Figure 7.9. Mean turbid plume averaged from December to February for the period 2002-2014. Black line represents the turbid threshold (0.2 mWcm^{-2}μm^{-1}sr^{-1}).

The effect of freshwater inputs is also clearly reflected in surface salinity along the continental shelf, with values lower than 34 in the area occupied by the turbid plume (Figure 7.10a). The lowest salinity values were observed around the Loire and Gironde Estuaries. This shows again the great relation existent between the turbid plume measured with MODIS and the salinity obtained from IBI, as was also observed in the Iberian plumes. Regarding to temperature, a cooler band (below 11 ºC) was observed along the French coast in the area occupied by the turbid plume (Figure 7.10b), with the minimum values (close to 9 ºC) located near the mouth of both rivers, which suggests that the coldest SST values are related to the distribution of the turbid plume. In addition, a cross-shore gradient between coastal and oceanic locations with differences greater than 3 ºC was detected.
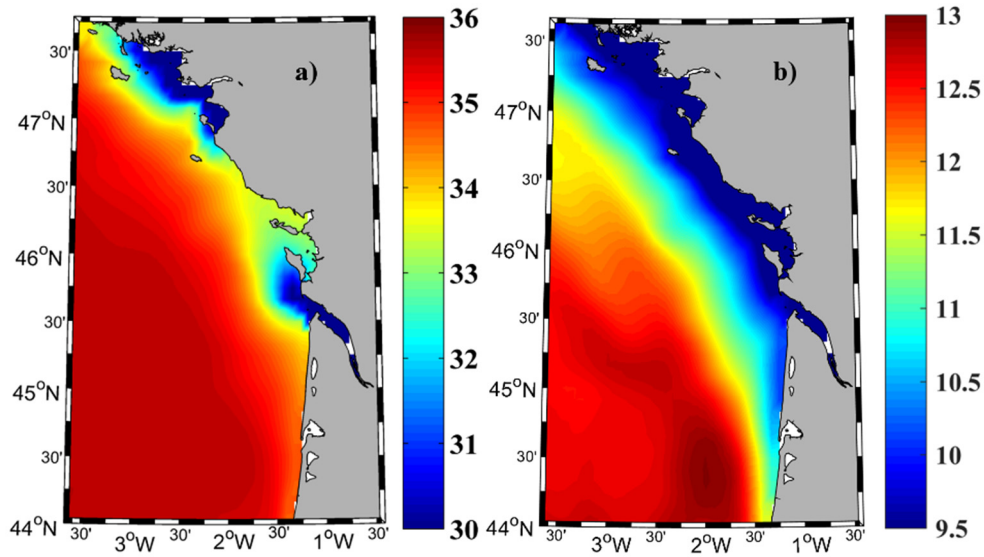
Figure 7.10. (a) Mean salinity and (b) mean SST (ºC) calculated from December to February over the period 2002-2014 from IBI database.

Sea surface temperature pattern was also evaluated using other databases in order to test the accuracy and robustness of the results. The mean DJF SST fields calculated from MODIS and OISSST$_{1/4}$ data averaged over the period 2002-2014 are shown in Figures 7.11a and b, respectively. The general pattern is very similar to the one calculated with IBI data, with the coolest values observed in the area occupied by the plume. Some differences can be observed in the OISTT$_{1/4}$ composite, where slightly higher temperature values were obtained. However, the three databases show a clear contrast between the area occupied by the plume and the oceanic area, with a gradient above 3 ºC.
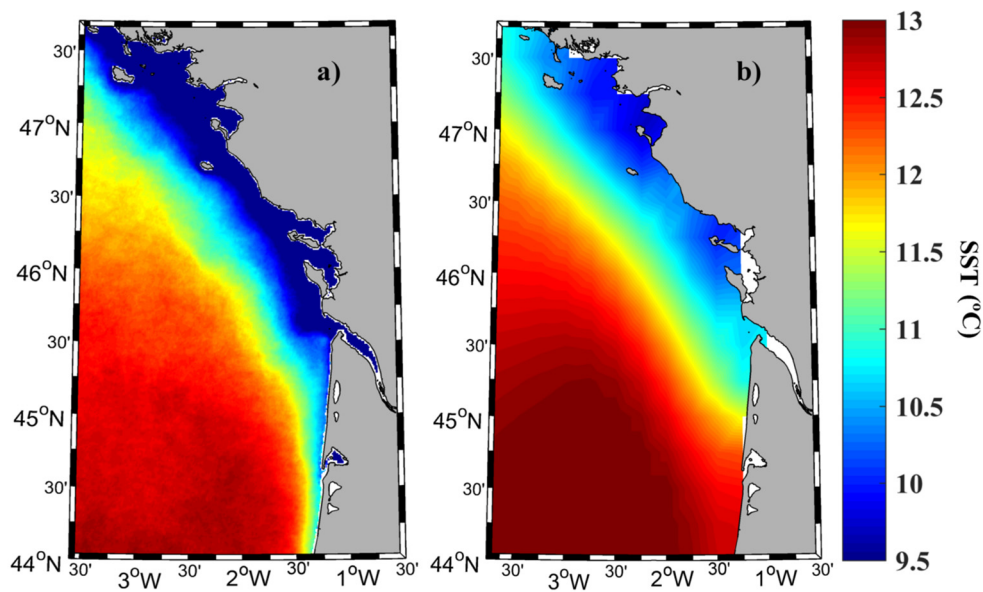
Figure 7.11. Mean SST (ºC) calculated from December to February over the period 2002-2014 from (a) MODIS and (b) OISTT$_{1/4}$ databases.

Due to the great temperature contrast between coastal and ocean locations its variability was also analyzed. Figure 7.12 shows the influence of freshwater inputs on SST variability from December to February over the period 2002-2014 using data from IBI. SST trends show a different pattern in the area occupied by the turbid plume when compared with oceanic locations. Cooling with maximum values around -0.5 ºC dec^{-1} was observed along the French continental shelf north of the Gironde Estuary. However, warming with maximum values of 0.5 ºC dec^{-1} was observed in the adjacent oceanic area.
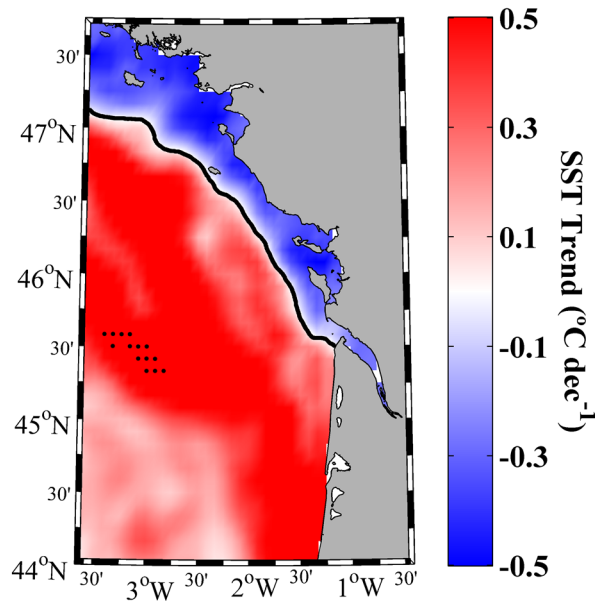
Figure 7.12. SST trend (ºC dec^{-1}) calculated from December to February over the period 2002-2014 using data from IBI. Black contour line corresponds to null trend. Black dots represent grid points with significance higher than 90 %.

A similar pattern was obtained using OISST$_{1/4}$ database (Figure 7.13a), which allows extending back the period of study to its total length (1982-2014) (Figure 7.13b). The pattern depicted in Figure 7.13b is similar to the ones described in Figures 7.12 and 7.13a but covering a longer period. Overall, warming (~0.3 ºC dec^{-1}) was observed in most of the area under scope, with the exception of near shore areas close to the mouths of Gironde and Loire, where a maximum cooling rate of approximately -0.15 ºC dec^{-1} was detected. In summary, coastal cooling is maintained even using different databases or when the period under study is extended to the last 30 years, although its intensity and extension are greater in the last decade. This shows that coastal and oceanic areas behave differently regardless of the time period or the database considered. This phenomenon is not a particular event that occurs only during the short period of time covered by IBI data.
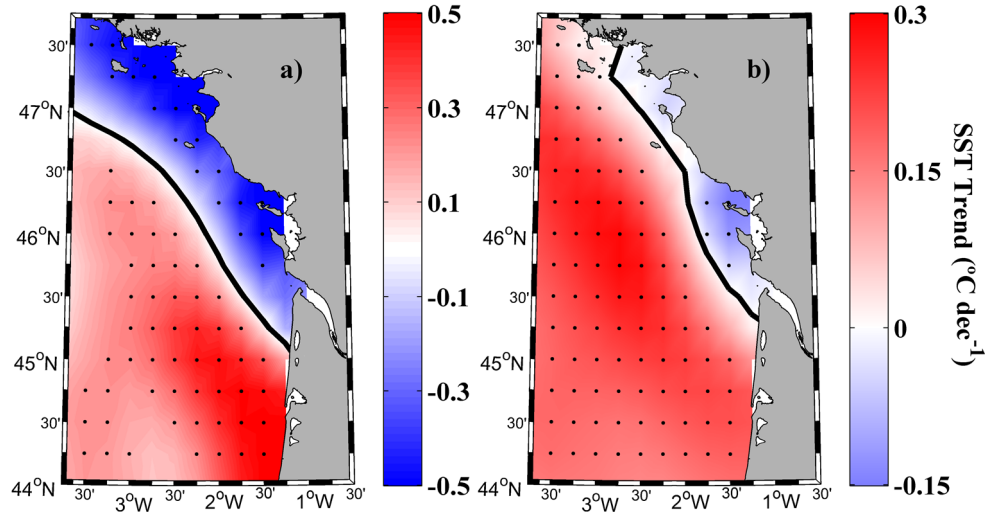
Figure 7.13. SST trend (°C dec^{-1}) calculated from December to February using data from OISST$_{1/4}$ over the period (a) 2002-2014 and (b) 1982-2014. Black contour line corresponds to null trend. Black dots represent grid points with significance higher than 90 %.

In order to analyze the factors affecting the different SST evolution between oceanic and coastal locations DJF trends in total heat flux (Figure 7.14) calculated over the period 1982-2014 show a similar pattern to the one observed for DJF SST trends (Figure 7.13b), with marked differences between coastal and oceanic areas. Ocean trends range from -7 to -11 W m^{-2} dec^{-1} whilst the trend in the nearshore strip ranges from -3 to -5 W m^{-2} dec^{-1}, showing the differences between the ocean and the area occupied by the plume. Note that ocean loses heat during DJF, so a negative trend means that the loss rate has increased. So, ocean is losing heat now at a higher rate than three decades ago.
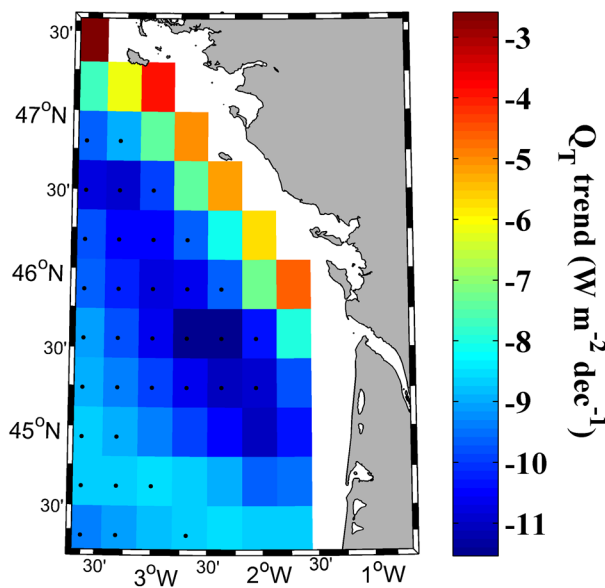
Figure 7.14. DJF trend in total heat fluxes (W m^{-2} dec^{-1}) calculated over the period 1982-2014 with CFSR data. Black dots represent grid points with significance higher than 95%.

Differences between ocean and coastal areas can be also analyzed in terms of oceanic indices (AMO). The influence of AMO on SST anomaly was studied for DJF over the period 1982-2014 (Figure 7.15). The correlation between both signals is close to zero in the area affected by the river plume whilst it is significantly positive for the rest of the region. This fact evidences that the nearshore strip influenced by Loire and Gironde discharges follows a different SST behavior when compared to the oceanic part of the bay. We should note that AMO represents the SST anomaly of the North Atlantic. The lack of correlation with the coastal zone close to Loire and Gironde Rivers demonstrates that the SST at that particular area is more dependent on coastal than on oceanic features.
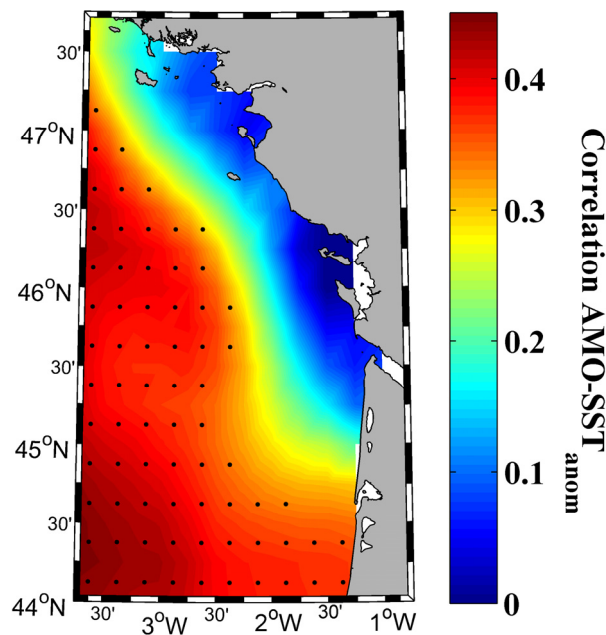
Figure 7.15. Correlation between DJF AMO index and SST anomaly from OISST$_{1/4}$ over the period 1982-2014. Black dots represent grid points with significance higher than 95%.

Previous studies that analyzed wintertime SST trends in this coastal area over a similar period are not conclusive. Gómez-Gesteira et al. (2008) mentioned that coastal warming is negligible along the French coast over the period 1985-2005 during winter and fall, whilst they observed a high increase during spring and summer. However, Planque et al. (2003) showed that warming was greater in the southeastern corner of the Bay during winter.

In a wider context, there are several drivers that can cause different coastal SST trends when compared with the ones observed at adjacent oceanic areas. Possibly, coastal upwelling is the most studied cause (Relvas et al., 2009; deCastro et al., 2009; Santos et al., 2011, 2012a, 2012b, 2012c). Nevertheless, upwelling is not a key phenomenon in the area, especially in winter. The southeastern corner of the Bay is characterized by a high continental influence during summer due to the concavity of this area (Valencia et al., 2003; 2004; Costoya et al., 2015). However, advection from land to ocean was also

discarded in the area following Cattiaux et al. (2011). Different authors have identified the presence of large rivers as the main cause of unusual cooling (Howden and Murtugudde, 2001) or warming (Belkin, 2009; Vizy and Cook, 2010; Park et al., 2011; Materia et al., 2012). The importance of the river discharge can be put into context for the particular case under study since the combined discharge of both rivers (~2500 m^{3}s^{-1}) is higher than the flow per kilometer of coast of upwelled water observed for the main upwelling systems over the world (Patti et al., 2008).

The mechanism proposed by different authors (Belkin, 2009; Vizy and Cook, 2010; Park et al., 2011; Materia et al., 2012) to explain the especially intense surface warming observed at certain areas affected by large rivers is based on the development of a buoyant surface layer that traps solar radiation and enhances vertical stratification. The mechanism is strengthened by positive feedback since the partially isolated surface layer is warmed by solar radiation that increases surface temperature which results in density decrease and hence reinforcement of stratification. These previous studies are focused on spring-summer periods when riverine water is warmer than offshore water. A similar mechanism can be invoked in the present study. The river plume is much fresher and colder (Figures 7.10b and 7.11) than the surrounding water. In addition, the stability of the water column is kept due to the continuous supply of freshwater. Overall, the surface water near coast is cooled by the atmosphere but vertical mixing is inhibited by density differences produced by near surface fresh water, reinforcing the cooling of surface waters in the area affected by plume. Thus, in a context of global warming, offshore water warms at a much higher rate than near shore water. Here, the positive feedback mechanism mentioned for other areas is no longer valid since surface water tends to cool and surface density to increase. In addition, the combined discharge of both rivers is rather moderate when compared to the rivers considered in the studies mentioned above (Congo, Amazonas or Yangtze). Thus, in spite of the shallowness of the area, the zone affected by the river plume is much smaller than observed for those large rivers.

The extension of the plume is strongly dependent on river runoff and prevailing winds, as showed in previous chapters for Iberian plumes. The important role of these forcing on the French Atlantic plumes is also corroborated by different works (Lazure and Jegou, 1998; Puillat et al., 2004; 2006). In the present case, changes in DJF river runoff over the period 1982-2014 can be considered negligible for Loire River (on the order of -40 m^{3}s^{-1}dec^{-1}). Actually, the observed trends are not statistically significant and strongly dependent on the length of the series. To remove or add a single year can drive the trend from positive to negative (or vice-versa). River runoff increases at a rate on the order of 120 m^{3}s^{-1}dec^{-1} (still not significant) when considering the last period (2002-2014) (Table 7.3), which coincides with a stronger coastal cooling as shown in Figures 7.12 and 7.13a. As we mentioned above, the area affected by the plume has little horizontal mixing with the rest of the area due to the prevailing southwesterly (landward) winds that tend to confine the plume near coast decreasing the cross-shore transport and dilution (Chao, 1988). This behavior favors the retention and maintenance of the plume on a large area, partially isolated from the rest of the bay. Changes in the duration and intensity of

prevailing DJF southwesterly winds were also analyzed (Table 7.3). Null trends were observed for duration and intensity of these winds over the period 1982 to 2014. Nevertheless, trends are positive and significant (Table 7.3) when considering the short period 2002-2014. SW winds tend to intensify and be more frequent during this period. This results in a higher retention of the plume near coast which, in turns, results in a more marked cooling in that area as depicted in Figures 7.12 and 7.13a. Although tidal forcing also affects plume development, its influence on plume spreading is balanced over time because it has a cyclic effect on plume dynamics.

Period	SW winds		River Runoff ($m^3s^{-1}dec^{-1}$)	
	Duration (days dec^{-1})	Intensity (ms^{-1}dec^{-1})	Loire	Gironde
2002-2014	12*	1.6**	126	122
1982-2014	--	--	-40	n/a

Table 7.3. Trends in wind intensity and duration and in river discharge. Values with null trends are marked with --. Statistical significance at 95% || 99% is marked with * || **.

In summary, we can conclude that the extension of the plume has experienced little changes over the period 1982-2014. Thus, at coastal areas, the mere presence of a freshwater layer is able to modulate the warming observed at the adjacent ocean locations even in absence of significant changes in the properties of the plume like its extent or freshwater content. The ocean area warms while the coastal area suffers a light cooling. The mechanism is reinforced during periods when river discharge and SW winds are over their mean values (e.g. 2002-2014). This results in a significant cooling in the area influenced by freshwater input.

7.4.4.2. Loire-Gironde plume influence on sea water column

Mean temperature, salinity, and density values in the top 40 m of the water column were monthly averaged both near the coast (Figure 7.16, left panels) and in the adjacent ocean out of plume influence (Figure 7.16, right panels) from 2002 to 2014. The influence of the turbid plume on temperature is particularly evident during winter and spring months along the coast (Figure 16a), favoring thermal inversion from December to April. This effect was not observed in the adjacent ocean, where the water column exhibited homogenous thermohaline properties due to the ocean heat loss during winter months (Figure 16b). Thermal inversions due to freshwater inputs during winter were previously detected by Koutsikopoulos and Le Cann (1996) by means of punctual samplings. These authors observed a thermal inversion near the estuaries, but it was also detected along the isobath of 40 m in the present study. Haline forcing was the main cause of the thermal inversion alongshore, which is clearly reflected in Figure 16c. The lowest salinity values were detected in the first 5 m (< 34) from January to April. However, the lowest salinity

values (< 35) in the adjacent oceanic area were found near the surface from May to August. The water column was quasi homogenous for salinity during the rest of the year (Figure 16d). Puillat et al. (2004) detected low salinity lenses along the French continental shelf during different cruises carried out in April and June. They attributed the presence of these lenses to the prevalence of the northwesterly (upwelling favorable) winds during summer months. Therefore, the lowest salinity values in the oceanic zone during summer months seem to be explained by the interannual variability of wind.
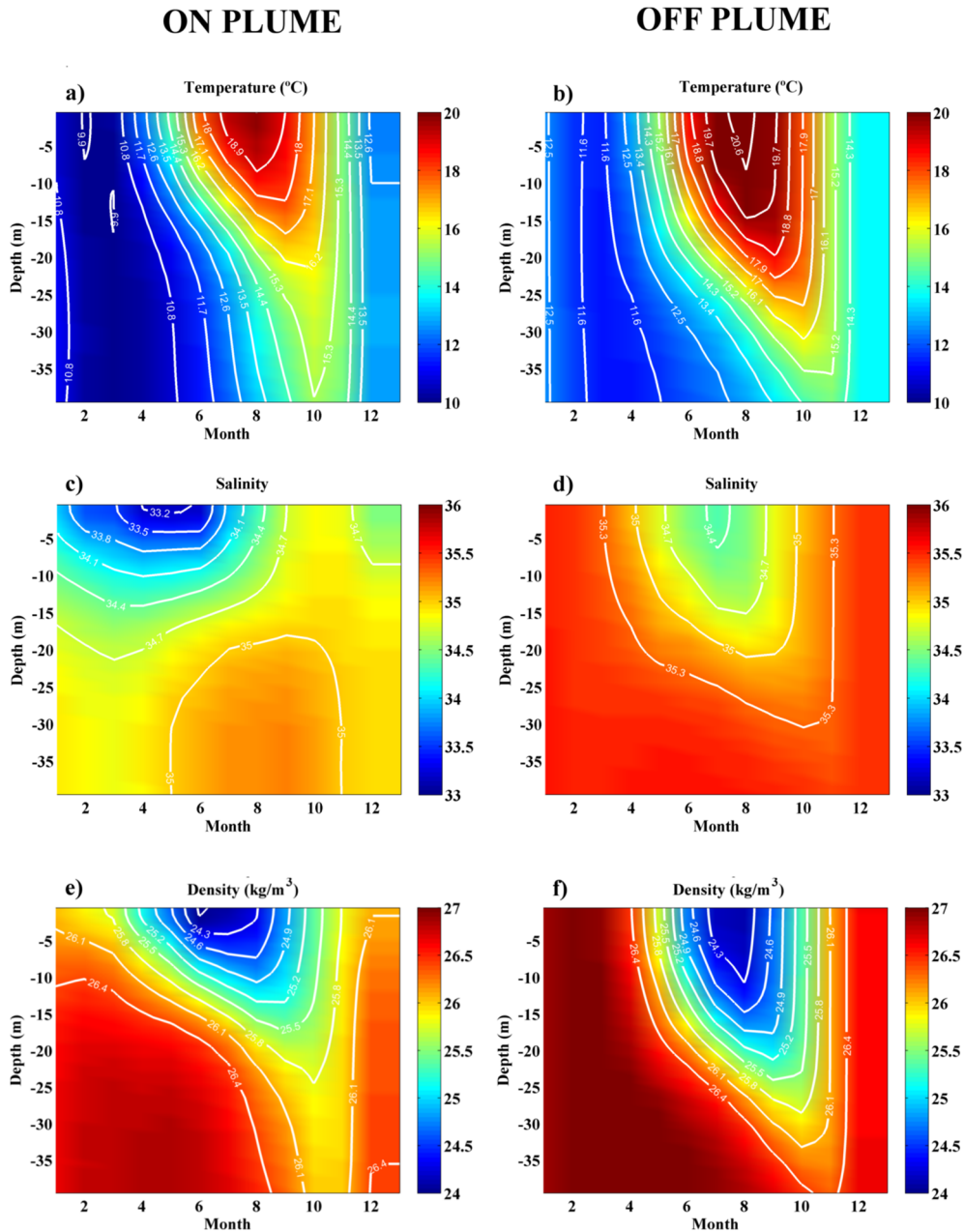
Figure 7.16. Monthly vertical profiles (40 m depth) of (a, b) temperature (ºC), (c, d) salinity, and (e, f) density (kg m⁻³) for coastal (left column) and oceanic (right column) locations (see Figure 7.1) over the period 2002-2014.

The density field showed some similarities inside and outside the plume (Figure 16e, f). Thus, the strongest stratification is observed in summer and is maintained by temperature. However, winter stratification maintained by freshwater (salinity) is only observed inside the plume (Figure 16e). This may be the mechanism that isolates surface water from deeper water, resulting in the different warming trends observed in winter inside and outside the area affected by the river as commented above.

The main differences between the thermohaline properties of coastal and adjacent ocean waters are summarized in Table 7.4.

	Inside	Outside
Winter thermal inversion	yes	no
Winter stratification	yes	no
Maximum of near surface salinity	Early autumn	Winter
Maximum of near bottom salinity	August	Almost constant
Minimum of near surface salinity	Winter-Early spring	Summer
Minimum of near bottom salinity	Winter	Almost constant

Table 7.4. Main differences in thermohaline characteristics between the area occupied by the turbid plume (inside plume) and the adjacent ocean (outside plume).

7.5. Conclusions

The behavior of the Loire and Gironde plumes under the effects of their main forcing (river discharge and wind) and atmospheric patterns (EA and NAO) was analyzed using composites created from MODIS satellite data over the period 2003-2015. In addition, the impact of freshwater inputs on thermohaline properties in the adjacent ocean was evaluated using data derived from IBI and $OISTT_{1/4}$ databases. From this analysis the following conclusions can be made:

- River discharge is the most important driver modulating the development of the Loire and Gironde plumes. The Loire plume immediately responds to discharge variations, as the maximum correlation (0.7) was obtained without lag. On the other hand, the Gironde plume reacts to river discharge variations with a delay of 2 days due to the size of the estuary formed before emptying into the ocean. Thus, the Loire plume is more sensitive to river discharge than the Gironde plume.

- Wind is the second main driver that affects the development and spreading of turbid plumes, either favoring or limiting the plume's mixing with the adjacent ocean water. Dilution of suspended material with ocean water is enhanced by upwelling and seaward winds and inhibited by downwelling and landward winds. The maximum extension of the turbid plume occurs under landward winds. These winds limit the transport and dilution of suspended material into the ocean, resulting in higher turbidity values in the near-field area due to the retention of

suspended material near the coast. Downwelling favorable winds cause a similar effect, although at a lesser extent.

- EA is the atmospheric pattern that has the greatest impact on the turbid plume during winter months, as indicated by correlation coefficients that were slightly higher than those for NAO. This is mainly due to the Bay of Biscay's location, which is between two regions with different responses (wind and precipitation) to NAO and closer to one of the centers of the EA dipole. The Loire-Gironde turbid plume occupies a larger area under positive EA and NAO indices. Both patterns exert their influence more in terms of conditioning landward winds than in terms of river discharge. No significant correlations were found between NAO and river discharge.

- The Loire and Gironde River discharges create important differences in thermohaline properties inside and outside the turbid plume. In particular, winter stratification is only observed inside the plume, thereby explaining the different warming ratios observed inside and outside the plume: Cooling is detected in the area occupied by the plume and warming at ocean locations during winter months.

General Conclusions

This thesis was conceived as an attempt to characterize and compare the most important plumes formed in the Iberian Peninsula coast, as well as their response to the main forcing (river discharge, wind and tide). For that, the mean plume states for the synoptic patterns considered were obtained using composites created from MODIS data. The developed methodology was used to also characterize the most important French Atlantic plumes, as well as, the impact of the main teleconnection indices on them. In addition, the influence of these plumes on the thermohaline seawater properties was also assessed. The main conclusions obtained during the period under study are the following:

➢ *Iberian plumes:*

- In general terms, extension and turbidity of plumes show to be dependent on the sediment load, which is characteristic of each river. Ebro River presented the maximum mean plume area, 1277 km^2, while Guadiana River had the minimum one, 89 km^2. The other Iberian Rivers under analysis presented intermediate plume extensions (ranging from 179 km^2 for Minho to 940 km^2 for Guadalquivir).

- River discharge is the main forcing affecting Iberian plumes. The dependence of plume extension on runoff is high for Minho, Douro, Guadiana and Guadalquivir, moderate for Tagus, and low for Ebro plume.

  o The area occupied by the turbid plumes increases with river discharge, whose increase generates more suspended matter drag to the mouth. In general, plume variability responded immediately to river discharge variations, except for rivers with large estuaries (Tagus and Guadalquivir), in which case plume development is lagged respect to river discharge due to the water residence time inside the estuaries.

  o All Iberian plumes are well developed under high discharges, however only Guadalquivir and Ebro plumes are able to form a radially and consistent plume pattern even under low discharges. On the other hand, Minho and Douro Rivers not form plume with low discharges. Tagus and Guadiana present an intermediate situation, with plume visible but not completely developed.

- Wind is a secondary forcing on Iberian plumes, especially noticeable under high river discharges. The dependence of plume extension on wind is high for Minho, Douro and Guadiana, moderate for Tagus, and low for Guadalquivir and Ebro.

  o All Atlantic plumes reached the maximum extension under landward cross-shore winds because accumulate the material near coast decreasing the cross-shore transport and limiting the loss of material by dilution in ocean water. On the other hand, the Atlantic plumes reached their minimum extension under

seaward cross-shore winds since produce the fast dilution of plume material in adjacent ocean water.

o Alongshore winds promote intermediate plume extensions. In general terms, upwelling favorable winds favor the dilution of plume material in ocean waters due to the offshore Ekman transport whereas downwelling favorable winds retain the material against the coast to the side toward wind blows due to the onshore Ekman transport generated.

o Ebro plume reached the maximum and minimum plume extension under opposite wind situations, seaward and landward cross-shore winds, respectively. This is supported by the influence of the Liguro-Provençal Current, which displaces Ebro plume southwestward. In fact, Ebro presents a low dependence on the other forcing. Basically, the plume is driven by the coastal current.

- The semidiurnal tidal cycle only affects the Atlantic plumes. The dependence of plume extension on semidiurnal tidal cycle is high for Guadiana, moderate for Minho and Tagus, and low for Douro and Guadalquivir.

o Atlantic plumes reached a greater extension during low tides due to the plume retraction provoked by high tides.

- The fortnightly tidal cycle only affects significantly to Tagus plume due to the shape and size of its estuary. The dependence of Tagus plume on fortnightly tidal cycle is moderate.

o Tagus plume was larger during spring tides due to the higher amount of material exported from the estuary.

➢ *French Atlantic plumes:*

- River discharge is the most important forcing on Loire and Gironde plumes development. Loire plume immediately responded to discharge fluctuations whereas Gironde presented a delay of 2 days associated to the water residence time inside the estuary. Loire plume showed to be more sensitive to discharge variability than Gironde plume. In addition, a great and continuous plume is formed between both estuaries when both discharges are high, which is supported by the synchronism of both rivers.

- Wind also affects the development of both plumes. Upwelling and seaward winds favor the mixing between plume material and ocean waters whereas downwelling and landward winds limit the mixing, isolating both water masses, and therefore, promoting greater differences between the thermohaline properties of the plume and ocean water. Maximum plume extension was reached under landward winds.

- The positive phase of EA and NAO teleconnection patters induces a larger plume, with EA exerting a greater influence.

- The plume formed by Loire and Gironde River discharges presented important differences in the thermohaline properties respect to the adjacent ocean water. As main important features the winter stratification was only observed inside the area occupied by the merged plume formed by both rivers. This also conditioned the different temperature patterns observed between both areas. The ocean area warms while the coastal area occupied by the plume cools, which is reinforced during periods when river discharge and southwesterly winds are over their mean values.

Acronym and Abbreviation List

- **AMO**: Atlantic Multidecadal Oscillation.

- **AS$^+$**: Alongshore winds which cause an Ekman transport offshore.

- **AS$^-$**: Alongshore winds which cause an Ekman transport onshore.

- **AVHRR**: Advanced Very High Resolution Radiometer.

- **CFSR**: Climate Forecast System Reanalysis.

- **COPERNICUS**: European Programme for the establishment of a European capacity for Earth Observation.

- **CS$^+$**: Seaward winds.

- **CS$^-$**: Landward winds.

- **E**: Irradiance.

- **<E>**: Mean plume extension.

- **EA**: East Atlantic pattern.

- **E$_d$**: Downward irradiance.

- **<E$_{max}$>**: Largest plume extension.

- **<E$_{min}$>**: Smallest plume extension.

- **ESA**: European Space Agency.

- **E$_u$**: Upward irradiance.

- **f**: Coriolis parameter.

- **F$_0$**: Extraterrestrial solar flux.

- **F$_m$**: Densimetric mouth Froude number.

- **g´**: Reduced gravity.

- **GSFC**: Goddard Space Flight Center.

- **h$_0$**: Inflow depth.

- **h$_p$**: Plume thickness.

- **IBI**: Atlantic-Iberian Biscay Irish-Ocean Physics Reanalysis.

- **IOCCG**: International Ocean-Color Coordinating Group.

- **K_b**: Bulk Kelvin number.

- **K_m**: Mouth Kelvin number.

- **L**: Inflow width.

- **LPC**: Liguro-Provençal Current.

- **L_w**: Water-leaving radiance.

- **MD**: Moderately developed plume state.

- **MERIS**: Medium Resolution Imaging Spectrometer.

- **MODIS**: Moderate Resolution Imaging Spectroradiometer.

- **MOHID**: Water Modelling System.

- **N**: Negligible plume state.

- **NAO**: North Atlantic Oscillation.

- **NASA**: National Aeronautics and Space Administration.

- **NASW**: North Atlantic Surface Water.

- **NCDC**: National Climatic Data Center.

- **NCEP**: National Centers for Environmental Prediction.

- **NEMO:** Nucleus for European Modelling of the Ocean.

- **NIR**: Near-Infrared.

- **nLw**: Normalized water-leaving radiance.

- **NOAA**: National Oceanic and Atmospheric Administration.

- **NOMADS**: National Operational Model Archive and Distribution System.

- **$OISST_{1/4}$**: NOAA ¼ ° daily Optimum Interpolation Sea Surface Temperature.

- **OSPAR**: Convention for the Protection of the Marine Environment of the North-East Atlantic.

- **Q_L**: Latent heat flux.

- **Q_{LW}**: Longwave flux.

- **Q_S**: Sensible heat flux.

- **Q_{SW}**: Shortwave flux.

- **Q_T**: Net heat flux.

- **R_D**: Rossby radius.

- **$R_{<E>}$**: Range of forcing influence.

- **R_m**: Mouth Rossby number.

- **ROFI**: Region Of Freshwater Influence.

- **ROMS**: Regional Ocean Modelling System.

- **Rrs**: Remote sensing reflectance.

- **SeaDAS**: SeaWIFS Data Analysis System.

- **SeaWIFS**: Sea-Viewing Wide Field-of-View Sensor.

- **SMOS**: Soil Moisture and Ocean Salinity.

- **SNIRH**: Sistema Nacional de Informações sobre Recurso Hídricos.

- **SNR**: Signal noise ratio.

- **SST**: Sea Surface Temperature.

- **SWIR**: Short Wave Infrared.

- **<T>**: Mean turbid value.

- **TRIM3D**: Three-dimensional hydrodynamic model.

- **TSS**: Total Suspended concentrations.

- **u**: velocity of the flow current at the estuary mouth.

- **UNESCO-MAB**: United Nations Educational, Scientific and Cultural Organization-Man and the Biosphere Programme.

- **v**: Inflow velocity.

- **W_b**: Plume extent.

- **WD**: Well developed plume state.

- **WIBP**: Western Iberian Buoyant Plume.

- **W_m**: Width of river mouth.

List of Figures

List of Tables

Bibliography

[Alvarez et al., 2006] Alvarez, I., deCastro, M., Gomez-Gesteira, M., Prego, R., 2006. Hydrographic behavior of the Galician Rias Baixas (NW Spain) under the spring intrusion of the Miño River. *Journal of Marine Systems, 60*, 144-152. http://dx.doi.org/10.1016/j.jmarsys.2005.12.005.

[Alvarez et al., 2008] Alvarez, I., Gomez-Gesteira, M., deCastro, M., Novoa, E.M., 2008. Ekman transport along the Galician Coast (NW, Spain) calculated from QuikSCAT winds. *Journal of Marine Systems, 72*(1), 101-105. http://dx.doi.org/10.1016/j.jmarsys.2007.01.013.

[Alvarez et al., 2011] Alvarez, I., Gomez-Gesteira, M., Lorenzo, M.N., Crespo, A.J.C., Dias, J.M., 2011. Comparative analysis of upwelling influence between the western and northern coast of the Iberian Peninsula. *Continental Shelf Research, 31*(5), 388-399. http://dx.doi.org/10.1016/j.csr.2010.07.009.

[Alvarez et al., 2014] Comparison of different wind products and buoy wind data with seasonality and interannual climate variability in the southern Bay of Biscay (2000-2009). *Deep Sea Research Part II: Topical Studies in Oceanography, 106*, 38-48. http://dx.doi.org/10.1016/j.dsr2.2013.09.028.

[Arnau et al., 2004] Arnau, P., Liquete, C., Canals, M., 2004. River mouth plume events and their dispersal in the Northwestern Mediterranean Sea. *Oceanography, 17*, 22-31.

[Aurin et al., 2013] Aurin, A., Mannino, A., Franz, B., 2013. Spatially resolving ocean color and sediment dispersion in river plumes, coastal systems, and continental shelf waters. *Remote Sensing of Environment, 137*, 212-225. http://dx.doi.org/10.1016/j.rse.2013.06.018.

[Aznar et al., 2016] Aznar, R., Sotillo, M.G., Cailleau, S., Lorente, P., Levier, B., Amo-Baladrón, A., Reffray, G., Álvarez-Fanjul, E., 2016. Strengths and weaknesses of the CMEMS forecasted and reanalyzed solutions for the Iberia-Biscay-Ireland (IBI) waters. *Journal of Marine Systems, 159*, 1-14. http://dx.doi.org/10.1016/j.jrasys.2016.02.007.

[Baith et al., 2001] Baith, K., Lindsay, R., Fu, G., McClain, C., 2001. SeaDAS: data analysis system developed for ocean color satellite sensors. Eos, Transactions *American Geophysical Union, 82*(18), 202-205. http://dx.doi.org/10.1029/01EO00109.

[Barnston and Livezey, 1987] Barnston, A.G., Livezey, R.E., 1987. Classification, seasonality and persistence of low frequency atmospheric circulation patterns.

Monthly Weather Review, 115(6), 1083-1126. http://dx.doi.org/10.1175/1520-0493(1987)115<1083:CSAPOL>2.0.CO;2.

[Belkin, 2009] Belkin, I.M., 2009. Rapid warming of Large Marine Ecosystems. *Progress in Oceanography, 81*, 207-213, http://dx.doi.org/10.1016/j.pocean.2009.04.011.

[Bellier et al., 2007] Bellier, E., Planque, B., Petitgas, P., 2007. Historical fluctuations in spawning location of anchovy (*Engraulis encrasicolus*) and sardine (*Sardina pilchardus*) in the Bay of Biscay during 1967-1973 and 2000-2004. *Fisheries Oceanography, 16*(1)*, 1-15. http://dx.doi.org/10.1111/j.1365-2419.2006.00410.x.

[Binding and Bowers, 2003] Binding, C.E., Bowers, D.G., 2003. Measuring the salinity of the Clyde Sea from remotely sensed ocean colour. *Estuarine Coastal and Shelf Science, 57*, 605-611. http://dx.doi.org/10.1016/S0272-7714(02)00399-2.

[Borja et al., 2008] Borja, A., Fontan, A., Sáenz, J.O.N., Valencia, V., 2008. Climate, oceanography, and recruitment: the case of the Bay of Biscay anchovy (*Engraulis encrasicolus*). *Fisheries Oceanography, 17*(6), 477-493. http://dx.doi.org/10.1111/j.1365-2419.2008.00494.x.

[Braunschweig et al., 2003] Braunschweig, F., Martins, F., Chambel, P., Neves, R., 2003. A methodology to estimate renewal time scales in estuaries: The Tagus Estuary case. *Ocean Dynamics, 53*(3), 137-145. http://dx.doi.org/10.1007/s10236-003-0040-0.

[Caballero et al., 2014] Caballero, I., Morris, E.P., Ruiz, J., Navarro, G., 2014. Assessment of suspended solids in the Guadalquivir estuary using new DEIMOS-1 medium spatial resolution imagery. *Remote Sensing of Environment, 146*, 148-158. http://dx.doi.org/10.1016/j.rse.2013.08.047.

[Carvalho et al., 2014] Carvalho, D., Rocha, A., Gómez-Gesteira, M., Silva Santos, C., 2014. Comparison of reanalyzed, analyzed, satellite-retrieved and NWP modelled winds with buoy data along the Iberian Peninsula Coast. *Remote Sensing of Environment, 152,* 480-492. http://dx.doi.org/10.1016/j.rse.2014.07.017.

[Casey et al., 2010] Casey, K.S., Brandon, T.B., Cornillon, P., Evans, R., 2010. The past, present, and future of the AVHRR Pathfinder SST program. In *Oceanography from space,* (pp. 273-287). Springer Netherlands.

[Cattiaux et al., 2011] Cattiaux, J., Vautard, R., Yiou, P., 2011. North-Atlantic SST amplified recent wintertime European land temperature extremes and trends. *Climate dynamics, 36*(11-12), 2113-2128. http://dx.doi.org/10.1007/s00382-010-0869-0.

[Chant et al., 2008] Chant, R.J., Wilkin, J., Zhang, W., Choi, B., Hunter, E., Castelao, R., Glenn, S., Jurisa, J., Schofield, O., Houghton, R., Kohut, J., Frazer, T., Moline, M., 2008. Dispersal of the Hudson River plume in the New York Bight: synthesis

of observational and numerical studies during LaTTE. *Oceanography, 21*(4), 148-161.

[Chao, 1998] Chao, S.Y., 1988. Wind-driven motion of estuarine plumes. *Journal of Physical Oceanography*, *18*(8), 1144-1166. http://dx.doi.org/10.1175/1250-0485(1988)018<1144:WDMOEP>2.0.CO;2.

[Chavula et al., 2009] Chavula, G., Brezonik, P., Thenkabail, P., Johnson, T., Bauer, M., 2009. Estimating the surface temperature of Lake Malawi using AVHRR and MODIS satellite imagery. *Physics and Chemistry of the Earth, Parts A/B/C, 34(13)*, 749-754. http://dx.doi.org/10.1016/j.pce.2009.08.001.

[Chen et al., 2007] Chen, Z., Hu, C., Muller-Karger, F., 2007. Monitoring turbidity in Tampa Bay using MODIS/Aqua 250-m imagery. *Remote Sensing of Environment, 109(2)*, 207-220. http://dx.doi.org/10.1016/j.rse.2006.12.019.

[Choi and Wilkin, 2007] Choi, B.J., Wilkin, J.L., 2007. The effect of wind on the dispersal of the Hudson River plume. *Journal of Physical Oceanography, 37*(7), 1878-1897. http://dx.doi.org/10.1175/JPO3081.1.

[Coelho and Veloso-Gomes, 2004] Coelho, C., Veloso-Gomes, F., 2004. Crosshore beach profile models–Application to Aveiro coast. *Journal of Coastal Research, SI39*, 345-350.

[Costoya et al., 2015] Costoya, X., deCastro, M., Gómez-Gesteira, M., Santos, F., 2015. Changes in sea Surface temperature seasonality in the Bay of Biscay over the last decades (1982-2014). *Journal of Marine Systems, 150*, 91–101, http://dx.doi.org/10.1016/j.jmarsys.2015.06.002.

[Cravo et al., 2006] Cravo, A., Madureire, M., Felícia, H., Rita, F., Bebianno, J., 2006. Impact of outflow from the Guadiana River on the distribution of suspended particulate matter and nutrients in the adjacent coastal zone. *Estuarine, Coastal and Shelf Science, 70*, 63-75. http://dx.doi.org/10.1016/j.ecss.2006.05.034.

[Dagg et al., 2004] Dagg, M., Benner, R., Lohrenz, S., Lawrence, D., 2004. Transformation of dissolved and particulate materials on continental shelves influenced by large rivers: plume processes. *Continental Shelf Research, 24*, 833-858. http://dx.doi.org/10.1006/j.csr.2004.02.003.

[Davies-Colley and Smith, 2001] Davies-Colley, R.J., Smith, D.G., 2001. Turbidity, suspended sediment, and water clarity: a review. *Journal of the American Water Resources Association, 37*(5), 1085-1101. http://dx.doi.org/10.1111/j.1752-1688.2001.tb03624.x.

[deCastro et al., 2006] deCastro, M., Alvarez, I., Varela, M., Prego, R., Gómez-Gesteira, M., 2006. Miño River dams discharge on neighbor Galician Rias Baixas (NW Iberian Peninsula): hydrological, chemical and biological changes in water

column. *Estuarine, Coastal and Shelf Science, 70*, 52-62. http://dx.doi.org/10.1016/S1385-1101(03)00061-3.

[deCastro et al., 2008] deCastro, M., Gómez-Gesteira, M., Lorenzo, M.N., Alvarez, I., Crespo, A.J.C., 2008. Influence of atmospheric modes on coastal upwelling along the western coast of the Iberian Peninsula, 1985 to 2005. *Climate Research, 36*(2), 169-179, http://dx.doi.org/10.3354/cr00742.

[deCastro et al., 2009] deCastro, M., Gómez-Gesteira, M., Alvarez, I., Gesteira, J.L.G., 2009. Present warming within the context of cooling-warming cycles observed since 1854 in the Bay of Biscay. *Continental Shelf Research, 29*(8), 1053-1059. http://dx.doi.org/10.1016/j.csr.2008.11.016.

[Dias, 1987] Dinâmica sedimentary e evolução recente da plataforma continental portuguesa setentrional. (Ph. D. thesis). Lisbon, Portugal: University of Lisbon, 150 pp.

[Dias, 1990] A evolução actual do litoral Português. *Geonovas 11*, 15-28.

[Dias et al., 2002] Dias, J.M.A., Jouanneau, J.M., Gonzalez, R., Araújo, M.F., Drago, T., Garcia, C., Oliveira, A., Rodrigues, A., Vitorino, J., Weber, O., 2002. Present day sedimentary processes on the northern Iberia shelf. *Progress in Oceanography, 52*, 249-259. http://dx.doi.org/ 10.1016/S0079-6611(02)00009-5.

[Diez-Minguito et al., 2012] Díez-Minguito, M., Baquerizo, A., Ortega-Sánchez, M., Navarro, G., Losada, M.A., 2012. Tide transformation in the Guadalquivir estuary (SW Spain) and process-based zonation. *Journal of Geophysical Research: Oceans, 117*, C03019. http://dx.doi.org/ 10.1029/2011JC007344.

[Durand et al., 2002] Durand, N., Fiandrino, A., Freunié, P., Ouillon, S., Forget, P., Naudin, J.J., 2002. Suspended matter dispersion in the Ebro ROFI: an integrated approach. *Continental Shelf Research, 22*, 267-284. http://dx.doi.org/ 10.1016/S0278-4343(01)00057-7.

[Dzwonkowski and Yan, 2005] Dzwonkowski, B., Yan, X.-H., 2005. Tracking of a Chesapeake Bay estuarine outflow plume with satelite-based ocean colour data. *Continental Shelf Research, 25*(16), 1942-1958. http://dx.doi.org/10.1016/j.csr.2005.06.011.

[Enfield et al., 2001] Enfield, D.B., Mestas-Nuñez, A.M., Trimble, P.J., 2001. The Atlantic multidecadal oscillation and its relation to rainfall and river flows in the continental U.S. *Geophysical Research Letters, 28*(10), 2077-2080. http://dx.doi.org/10.1029/2000GL012745.

[Fennel and Mutzke, 1997] Fennel, W., Murzke, A., 1997. The initial evolution of a buoyant plume. *Journal of Marine Systems, 12*, 53-68. http://dx.doi.org/10.1016/S0924-7963(96)00088-7.

[Ferrer et al., 2009] Ferrer, L., Fontán, A., Mader, J., Chust, G., González, M., Valencia, V., Uriarte, A., Colling, M.B., 2009. Low-salinity plumes in the oceanic region of the Basque Country. *Continental Shelf Research, 29,* 970-984. http://dx.doi.org/10.1016/j.csr.2008.12.014.

[Fong and Geyer, 2001] Fong, D.A., Geyer, W.R., 2001. Response of a river plume during an upwelling favorable wind event. *Journal of Geophysical Research, 106*, 1067-1084. http://dx.doi.org/10.1029/2000JC900134.

[Fong and Geyer, 2002] Fong, D.A., Geyer, W.R., 2002. The alongshore transport of freshwater in a surface-trapped river plume. *Journal of Physical Oceanography, 23,* 212. http://dx.doi.org/10.1175/1520-0485(2002)032<0957:TATOFI>2.0.CO;2.

[Fontan et al., 2008] Fontan, A., Valencia, V., Borja, A., Goikoetxea, N., 2008. Oceano-meteorological conditions and coupling in the southeastern Bay of Biscay, for the period 2001-2005: A comparison with the past two decades. *Journal of Marine Systems, 72,* 167-177. http://dx.doi.org/10.1016/j.jmarsys.2007.08.003.

[Font et al., 1990] Font, J., Salat, J., Julia, A., 1990. Marine circulation along the Ebro continental margin. *Marine Geology, 95*, 165-177. http://dx.doi.org/10.1016/0025-3227(90)90114-Y.

[Garcia Berdeal et al., 2002] Garcia Berdeal, I., Hickey, B.M., Kawase, M., 2002. Influence of wind stress and ambient flow on a high discharge river plume. *Journal of Geophysical Research: Oceans*, *107*(C9). http://dx.doi.org/10.1029/2001JC000932.

[Garcia-Soto and Pingree, 2012] Garcia-Soto, C., Pingree, R.D., 2012. Atlantic multidecadal oscillation (AMO) and sea surface temperature in the Bay of Biscay and adjacent regions. *Journal of the Marine Biological Association of the United Kingdom, 92*(2), 213-234. http://dx.doi.org/10.1017/S0025315410002134.

[Garvine, 1982] Garvine, R.W., 1982. A steady state model for buoyant surface plume hydrodynamics in coastal waters. *Tellus, 34(3)*, 293-306. http://dx.doi.org/10.3402/tellusa.v34i3.10813.

[Garvine, 1995] Garvine, R.W., 1995. A dynamical system for classifying buoyant coastal discharges. *Continental Shelf Research, 15*(13), 1585-1596. http://dx.doi.org/10.1016/0278-4343(94)00065-U.

[Garvine, 2001] Garvine, R.W., 2001. The impact of model configuration in studies of buoyant coastal discharge. *Journal of Marine Research, 59(2)*, 193-225. http://dx.doi.org/10.1357/002224001762882637.

[Geyer et al., 2000] Geyer, W., Hill, P., Milligan, T., Traykovski, P., 2000. The structure of the Eel River plume during floods. *Continental Shelf Research, 20*(16), 2067-2093. http://dx.doi.org/10.1016/S0278-4343(00)00063-7.

[Goikoetxea et al., 2009] Goikoetxea, N., Borja, A., Fontán, A., González, M., Valencia, V., 2009. Trends and anomalies of the sea Surface temperature during the last 60 years within the southeastern Bay of Biscay. *Continental Shelf Research, 29*, 1060-1060. http://dx.doi.org/101016/j.csr.2008.11.014.

[Gomez-Gesteira et al., 2006] Gomez-Gesteira, M., Moreira, C., Alvarez, I., deCastro, M., 2006. Ekman transport along the Galician coast (northwest Spain) calculated from forecasted winds. *Journal of Geophysical Research: Oceans, 111*, C1005. http://dx.doi.org/10.1029/2005JC003331.

[Gomez-Gesteira et al., 2008] Gómez-Gesteira, M., deCastro, M., Alvarez, I., Gómez-Gesteira, J.L.G., 2008. Coastal SST warming trend along the continental part of the Atlantic Arc (1985–2005). *Journal of Geophysical Research: Oceans, 113*, C04010. http://dx.doi.org/10.1029/2007JC004315.

[Gonçalves et al., 2012] Gonçalves, H., Teodoro, A.C., Almeida, H., 2012. Identification, characterization and analysis of the Douro river plume from MERIS data. *IEEE Journal of Selected Topics in Applied Earth Observations and Remote Sensing, 5*(5), 1553-1563. http://dx.doi.org/10.1109/JSTARS.2012.2199740.

[González-Nuevo and Nogueira, 2014] González-Nuevo, G., Nogueira, E., 2014. Temporal and spatial variability of river plumes in the NW and N Iberian shelf (1987-2007). *Continental Shelf Research, 91*, 95-108. http://dx.doi.org/10.1016/j.csr.2014.09.005.

[Gonzalez et al., 2001] Gonzalez, R., Alveirinho Dias, J., Ferreira, O., 2001. Recent Rapid Evolution of the Guadiana Estuary Mouth (Southwestern Iberian Peninsula). *Journal of Coastal Research, SI34*, 516-527.

[Gonzalez et al., 2007] Gonzalez, R., Araújo, M.F., Burdloff, D., Cachão, M., Cascalho, J., Corredeira, C., Dias, J.M.A., Fradique, C., Ferreira, J., Gomes, C., Machado, A., Mendes, I., Rocha, F., 2007. Sediment and pollutant transport in the Northern Gulf of Cadiz: A multi-proxy approach. *Journal of Marine Systems, 68*, 1-23. http://dx.doi.org/10.1016/j.jmarsys.2006.10.007.

[Grimes and Kingsford, 1996] Grimes, C.B., Kingsford, M.J., 1996. How do riverine plumes of different sizes influence fish larvae: do they enhance recruitment?. *Marine and Freshwater Research, 47*(2), 191-2008. http://dx.doi.org/10.1071/MF9960191.

[Güttler et al., 2013] Güttler, F.N., Niculescu, S., Gohin, F., 2013. Turbidity retrieval and monitoring of Danube Delta waters using multi-sensor optical remote sensing data: An integrated view from the delta plain lakes to the western-northwestern Black Sea coastal zone. *Remote Sensing of Environment, 132*, 86-101. http://dx.doi.org/10.1016/j.rse.2013.01.009.

[Hetland, 2005] Hetland, R.D., 2005. Relating river plume structure to vertical mixing. *Journal of Physical Oceanography, 35*(9), 1667-1688. http://dx.doi.org/10.1175/JPO2774.1.

[Hickey et al., 2010] Hickey, B.M., Kudela, R.M., Nash, J.D., Bruland, K.W., Peterson, W.T., MacCready, P., Lessard, E.J., Jay, D.A., Banas, N.S., Baptista, A.M., Dever, E.P., Kosro, P.M., Kilcher, L.K., Horner-Devine, A.R., Zaron, E.D., McCabe, R.M., Peterson, J.O., Orton, P.M., Pan, J., Lohan, M.C., 2010. River influences on shelf ecosystems: introduction and synthesis. *Journal of Geophysical Research: Oceans, 115(2),* 1-26. http://dx.doi.org/10.1029/2009JC005452.

[Hopkings et al., 2013] Hopkings, J., Lucas, M., Dufau, C., Sutton, M., Stum, J., Lauret, O., Channelliere, C., 2013. Detection and variability of the Congo River plume from satellite derived sea surface temperature, salinity, ocean colour and sea level. *Remote Sensing of Environment, 139*, 365-385, http://dx.doi.org/10.1016/j.rse.2013.08.015.

[Horner-Devine et al., 2009] Horner-Devine, A.R., Jay, D.A., Orton, P.M., Spahn, E.Y., 2009. A conceptual model of the strongly tidal Columbia River plume. *Journal of Marine Systems, 78(3),* 460-475. http://dx.doi.org/10.1016/j.jmarsys.2008.11.025.

[Horner-Devine et al., 2015] Horner-Devine, A.R., Hetland, R.D., MacDonald, D.G., 2015. Mixing and transport in coastal river plumes. *Annual Review of Fluid Mechanics, 47*, 569-594. http://dx.doi.org/10.1146/annurev-fluid-010313-141408.

[Howden and Murtugudde, 2001] Howden, S.D., Murtugudde, R., 2001. Effects of river inputs into the Bay of Bengal. *Journal of Geophysical Research, 106*(C9), 19825-19843. http://dx.doi.org/10.1029/2000JC000656.

[Huret et al., 2007] Huret, M., Gohin, F., Delmas, D., Lunven, M., Garçon, V., 2007. Use of SeaWiFS data for light availability and parameter estimation of a phytoplankton production model of the Bay of Biscay. *Journal of Marine Systems, 65*, 509-531. http://dx.doi.org/10.1016/j.jmarsys.2005.07.007.

[Hurrel, 1995] Hurrel, J.W., 1995. Decadal trends in the North Atlantic Oscillation: regional temperatures and precipitation. *Science, 269*(5224), 676-679.

[Hu et al., 2003] Hu, C., Muller-Karger, E., Biggs, D.C., Carder, K.L., Nababan, B., Nadeau, D., Vanderbloemen, J., 2003. Comparison of ship and satellite bio-optical measurements on the continental margin of the NE Gulf of Mexico. *International Journal of Remote Sensing, 24*, 2597-2612. http://dx.doi.org/10.1080/0143116031000067007.

[Ibáñez et al., 1996] Ibáñez, C., Prat, N., Canicio, A., 1996. Changes in the hydrology and sediment transport produced by large dams on the lower Ebro river and its estuary. *Regulated Rivers: Research and Management, 12*, 51-62.

[IOCCG, 2011] Bio-optical sensors on Argo floats. 11, Reports of the International Ocean-Colour Coordinating Group, Dartmouth, Canada, 89 pp.

[Jurisa and Chant, 2012] Jurisa, J.T., Chant, R., 2012. The coupled Hudson River estuarine-plume response to variable wind and river forcings. *Ocean Dynamics, 62*(5), 771-784. http://dx.doi.org/10.1007/s10236-012-0527-7.

[Kelly-Gerreyn et al., 2006] Kelly-Gerreyn, B.A., Hydes, D.J., Jégou, A.M., Lazure, P., Fernand, L.J., Puillat, I., Garcia-Soto, C., 2006. Low salinity intrusions in the western English Channel, *Continental Shelf Research, 26*, 1241–1257, http://dx.doi.org/10.1016/j.csr.2006.03.007.

[Kilham and Roverts, 2011] Kilham, N.E., Roberts, D., 2011. Amazon River time series of surface sediment concentration from MODIS. *International Journal of Remote Sensing, 32*(10), 2659-2679. http://dx.doi.org/10.1080/01431161003713044.

[Kirk, 1994] Kirk, J.T.O., 1994. Light and photosynthesis in aquatic ecosystems. *Cambridge University Press,* Cambridge, United Kingdom, 2 ed., 509 pp.

[Körtzinger, 2003] Körtzinger, A., 2003. A significant CO_2 sink in the tropical Atlantic Ocean associated with the Amazon River plume. *Geophysical Research Letters, 30*(24), 2287. http://dx.doi.org/10.1029/2003GL018841.

[Koutsikopoulos and LeCann, 1996] Koutsikopoulos, C., Le Cann, B., 1996. Physical processes and hydrological structures related to the Bay of Biscay anchovy. *Scientia Marina, 60*, 9-19.

[Lahet and Stramski, 2010] Lahet, F., Stramski, D., 2010. MODIS imagery of turbid plumes in San Diego coastal waters during rainstorm events. *Remote Sensing of Environment, 114*, 332-344. http://dx.doi.org/10.1016/j.rse.2009.09.017.

[Lazure and Jegou, 1998] Lazure, P., Jegou, A.M., 1998. 3D modelling of seasonal evolution of Loire and Gironde plumes on Biscay Bay continental shelf. *Oceanologica Acta, 21*(2), 165–177. http://dx.doi.org/10.1016/S0399-1784(98)80006-6.

[Lazure et al., 2009] Lazure, P., Garnier, V., Dumas, F., Herry, C., Chifflet, M., 2009. Development of a hydrodynamic model of the Bay of Biscay. Validation of hydrology. *Continental Shelf Research, 29*, 985–997. http://dx.doi.org/10.1016/j.csr.2008.12.017.

[Le Fèvre and Frontier, 1988] Le Fèvre, J., Frontier, S., 1988. Influence of temporal characteristics of physical phenomena on plankton dynamics, as shown by North-West European marine ecosystems, 1988. *Toward a theory on biological-physical*

interactions in the world ocean, 245-272, Springer Netherlands. http://dx.doi.org/10.1007/978-94-009-3023-0_14.

[Lentz and Fewings, 2012] Lentz, S.J., Fewings, M.R., 2012. The wind- and wave-driven inner-shelf circulation. *Annual Review of Marine Science, 4*, 317-343. http://dx.doi.org/10.1146/annurev-marine-120709-142745.

[Lentz and Largier, 2006] Lentz, S.J., Largier, J., 2006. The influence of wind forcing on the Chesapeake Bay buoyant coastal current. *Journal of Physical Oceanography, 36*(7), 1305-1316. http://dx.doi.org/10.1175/JPO2909.1.

[Le Pape et al., 2003] Le Pape, O., Chauvet, F., Désaunay, Y., Guérault, D., 2003. Relationship between interannual variations of the river plume and the extent of nursery grounds for the common sole (*Solea solea,* L.) in Vilaine Bay. Effects on recruitment variability. *Journal of Sea Research, 40*, 177-185. http://dx.doi.org/10.1016/j.ecss.2006.05.035.

[Levier et al., 2016] Levier, B., Sotillo, M.G., Reffray, G., Aznar, R., 2016. Quality Information Document for IBI reanalysis Product. Copernicus Marine Environment Monitoring Service. http://marine.copernicus.eu/documents/QUID/CMEMS-IBI-QUID-005-002.pdf.

[Levitus et al., 2012] Levitus, S., Antonov, J.I., Boyer, T.P., Baranova, O.K., Garcia, H.E., Locarnini, R.A., Mishonov, A.V., Reagan, J.R., Seidov, D., Yarosh, E.S., Zweng, M.M., 2012. World ocean heat content and thermosteric sea level change (0-2000m), 1995-2010. *Geophysical Research Letters, 39*, L01603. http://dx.doi.org/10.1029/2012GL051106.

[Llope et al., 2006] Llope, M., Anadón, R., Viesca, L., Quevedo, M., González-Quirós, R., Stenseth, N.C., 2006. Hydrography of the Southern Bay of Biscay shelf-break region: Interacting the multiscale physical variability over the period 1993-2003. *Journal of Geophysical Research: Oceans, 111,* C09021. http://dx.doi.org/10.1029/2005JC002963.

[Lobo et al., 2004] Lobo, F.J., Sánchez, R., González, R., Dias, J.M.A., Hernández-Molina, F.J., Fernández-Salas, L.M., Díaz del Río, V., Mendes, I., 2004. Contrasting styles of the Holocene highstand sedimentation and sediment dispersal systems in the northern shelf of the Gulf of Cadiz. *Continental Shelf Research, 24*, 461-482. http://dx.doi.org/10.1016/j.csr.2003.12.003.

[Loisel et al., 2013] Loisel, H., Vantrepotte, V., Jamet, C., Dat, D.N., 2013. Challenges and new advances in ocean color remote sensing of coastal waters. In *Topics in Oceanography.* Intech.

[Lorenzo and Taboada, 2005] Lorenzo, M.N., Taboada, J.J., 2005. Influences of atmospheric variability on freshwater input in Galician Rias in winter. *Journal of*

Atmospheric & Ocean Science, 10(4), 377-387. http://dx.doi.org/10.1080/17417530601127472.

[Lorenzo et al., 2008] Lorenzo, M.N., Taboada, J.J., Gimeno, L., 2008. Links between circulation weather types and teleconnection patterns and their influence on precipitation patterns in Galicia (NW Spain). *International Journal of Climatology, 28*(11), 1493-1505. http://dx.doi.org/10.1002/joc.1646.

[Marta-Almeida and Dubert, 2006] Marta-Almeida, M., Dubert, J., 2006. The structure of tides in the Westerns Iberian region. *Continental Shelf Research, 26*(3), 385-400. http://dx.doi.org/10.1016/j.csr.2005.11.011.

[Masó and Tintoré, 1991] Masó, M., Tintoré, J., 1991. Variability of the shelf water off the northeast Spanish coast. *Journal of Marine Systems, 1*, 441-450. http://dx.doi.org/10.1016/0924-7963(91)90008-I.

[Massei et al., 2010] Massei, N., Laignel, B., Deloffre, J., Mesquita, J., Motelay, A., Lafite, R., Durand, A., 2010. Long-term hydrological changes of the Seine River flow (France) and their relation to the North Atlantic Oscillation over the period 1950-2008. *International Journal of Climatology, 30*(14), 2146-2154. http://dx.doi.org/10.1002/joc.2022.

[Materia et al., 2012] Materia, S., Gualdi, S., Navarra, A., Terray, L., 2012. The effect of Congo River freshwater discharge on Eastern Equatorial Atlantic climate variability. *Climate dynamics, 39*, 2109-2015. http://dx.doi.org/10.1007/s00382-012-1514-x.

[May et al., 2003] May, C.L., Koseff, J.R., Lucas, L.V., Cloern, J.E., Schoellhamer, D.H., 2003. Effects of spatial and temporal variability of turbidity on phytoplankton blooms. *Marine Ecology Progress Series, 254*, 111-128.

[Mendes et al., 2016] Mendes, R., Sousa, M.C., deCastro, M., Gómez-Gesteira, M., Dias, J.M., 2016. New insights into the Western Iberian Buoyant Plume: Interaction between the Douro and Minho River plumes under winter conditions. *Progress in Oceanography, 141*, 30-43, http://dx.doi.org/10.1016/j.pocean.2015.11.006.

[Mestres et al., 2003] Mestres, M., Sierra, J.P., Sánchez-Arcilla, A., González del Río, J., Wolf, T., Rodríguez, A., Ouillon, S., 2003. Modelling of the Ebro River plume. Validation with field observations. *Scientia Marina, 67*(4), 379-391. http://dx.doi.org/10.3989/scimar.2003.67n4379.

[Miller and McKee, 2004] Miller R.L., McKee, B.A., 2004. Using MODIS Terra 250 m imagery to map concentrations of total suspended matter in coastal waters. *Remote Sensing of Environment, 93*, 259-266. http://dx.doi.org/10.1016/j.rse.2004.07.012.

[Moita et al., 2003] Moita, M.T., Oliveira, P.B., Mendes, J.C., Palma, A.S., 2003. Distribution of chlorophyll a and *Gymnodinium catenatum* associated with coastal

upwelling plumes off central Portugal. *Acta Oecologica, 24*(1), S125-S132. http://dx.doi.org/10.1016/S1146-609X(03)00011-0.

[Molleri et al., 2010] Molleri, G.S.F., Novoa, E.M.L., Kampel, M., 2010. Space-time variability of the Amazon River plume based on satellite ocean color. *Continental Shelf Research, 30*, 342-352. http://dx.doi.org/10.1016/j.csr.2009.11.015.

[Morales et al., 2006] Morales, J.A., Delgado, I., Gutierrez-Mas, J.M., 2006. Sedimentary characterization of bed types along the Guadiana estuary (SW Europe) before the construction of the Alqueva dam. *Estuarine, Coastal and Shelf Science, 70*(1-2), 117-131. http://dx.doi.org/10.1016/j.ecss.2006.05.049.

[Mourato, 2008] Mourato, P., 2008. Hidromar-Boletim do Instituto Hidrográfico (*Nº 103*).

[Navarro and Ruiz, 2006] Navarro, G., Ruiz, J., 2006. Spatial and temporal variability of phytoplankton in the Gulf of Cádiz through remote sensing images. *Deep Sea Research Part II: Topical Studies in Oceanography, 53*(11-13), 1241-1260. http://dx.doi.org/10.1016/j.dsr2.2006.04.014.

[Neves, 2010] Neves, F.J., 2010. Dynamics and Hydrology of the Tagus Estuary: Results from *In Situ* Observations. (Ph. D. thesis). Lisbon, Portugal: University of Lisbon, 210 pp.

[Nezlin et al., 2005] Nezlin, N.P., DiGiacomo, P.M., Stein, E.D., Ackerman, D., 2005. Stormwater runoff plumes observed by SeaWiFS radiometer in the Southern California bight. *Remote Sensing of Environment, 98*, 494-510. http://dx.doi.org/10.1016/j.rse.2005.08.008.

[Oliveira et al., 1982] Oliveira, I.M., Valle, A.J.S.F., Miranda, F.C.C., 1982. Littoral problems in the Portuguese west coast. *Coastal Engineering Proceedings, 1*(18).

[Oliveira et al., 2009] Oliveira, P.B., Nolasco, R., Dubert, J., Moita, T., Peliz, A., 2009. Surface temperature, chlorophyll and advection patterns during a summer upwelling event off central Portugal. *Continental Shelf Research, 29*, 759-774. http://dx.doi.org/10.1016/j.csr.2008.08.004.

[OSPAR Commission, 2000] OSPAR Commission, 2000. Quality Status Report 2000: Region IV – Bay of Biscay and Iberian Coast. OSPAR Commission.

[Otero and Siegel, 2004] Otero, M.P., Siegel, D.A., 2004. Spatial and temporal characteristics of sediment plumes and phytoplankton blooms in the Santa Barbara Channel. *Deep Sea Research Part II: Topical Studies in Oceanography, 51*(10), 1129-1149. http://dx.doi.org/10.1016/j.dsr2.2004.04.004.

[Otero et al., 2008] Otero, P., Ruiz-Villarreal, M., Peliz, A., 2008. Variability of river plumes off Northwest Iberia in response to wind events. *Journal of Marine Systems, 72*, 238-255. http://dx.doi.org/10.1016/j.jmarsys.2007.05.016.

[Otero et al., 2013] Otero, P., Ruiz-Villarreal, M., García-García, L., González-Nuevo, G., Cabanelas, J.M., 2013. Coastal dynamics off Northwest Iberia during a stormy winter period. *Ocean Dynamics, 63*(1), 115-129. http://dx.doi.org/10.1007/s10236-012-0585-x.

[Palacios et al., 2009] Palacios, S.L., Peterson, T.D., Kudela, R.M., 2009. Development of synthetic salinity from remote sensing for the Columbia River plume. *Journal of Geophysical Research: Oceans, 114*, C00B05. http://dx.doi.org/10.1029/2008JC004895.

[Park et al., 2011] Park, T., Jang, C.J., Jungclaus, J.H., Haak, H., Park, W., Oh, I.S., 2011. Effects of the Changjiang river discharge on sea surface warming in the Yellow and East China Seas in summer. *Continental Shelf Research, 31*, 15-22. http://dx.doi.org/10.1016/j.csr.2010.10.012.

[Patti et al., 2008] Patti, B., Guisande, C., Vergara, A.R., Riveiro, I., Maneiro, I., Barreiro, A., Bonanno, A., Buscaino, G., Cuttitta, A., Basilone, G., Mazzola, S., 2008. Factors responsible for the differences in satellite-based chlorophyll a concentration between the major global upwelling areas. *Estuarine, Coastal and Shelf Science, 76*(4), 775-786. http://dx.doi.org/10.1016/j.ecss.2007.08.005.

[Pawlowicz et al., 2002] Pawlowicz, R., Beardsley, B., Lentz, S., 2002. Classical tidal harmonic analysis including error estimates in MATLAB using T_TIDE. *Computers & Geosciences, 28*(8), 929-937. http://dx.doi.org/10.1016/S0098-3004(02)00013-4.

[Peliz et al., 2002] Peliz, A., Rosa, T.L., Santos, A.M.P., Pissarra, J.L., 2002. Fronts, jets, and counter-flows in the Western Iberian upwelling system. *Journal of Marine Systems, 35*(1), 61-77. http://dx.doi.org/10.1016/S0924-7963(02)00076-3.

[Pérez et al., 2000] Pérez, F.F., Pollard, R.T., Read, J.F., Valencia, V., Cabanas, J.M., Ríos, A.F., 2000. Climatological coupling of the thermohaline decadal changes in Central Water of the Eastern North Atlantic. *Scientia Marina, 64*, 347-353. http://dx.doi.org/10.3989/scimar.2000.64n3347.

[Petus et al., 2010] Petus, C., Chust, G., Gohin, F., Doxaran, F., Froidefond, J.M., Sagarminaga, Y., 2010. Estimating turbidity and total suspended matter in the Adour River plume (South Bay of Biscay) using MODIS 250-m imagery. *Continental Shelf Research, 30*, 79-392. http://dx.doi.org/10.1016/j.csr.2009.12.007.

[Petus et al., 2014] Petus, C., Marieu, V., Novoa, S., Chust, G., Bruneau, N., Froidefond, J.M., 2014. Monitoring spatio-temporal variability of the Adour River turbid plume (Bay of Biscay, France) with MODIS 250-m imagery. *Continental Shelf Research, 74*, 35-49, http://dx.doi.org/10.1016/j.csr.2013.11.011.

[Planque et al., 2003] Planque, B., Beillois, P., Jégou, A.M., Lazure, P., Petitgas, P., Puillat, I., 2003. Large-scale hydroclimatic variability in the Bay of Biscay: the 1990s in the context of interdecadal changes. *ICES Marine Science Symposia, 219*, 61-70.

[Planque et al., 2007] Planque, B., Bellier, E., Lazure, P., 2007. Modelling potential spawning habitat of sardine (Sardina pilchardus) and anchovy (Engraulis encrasicolus) in the Bay of Biscay. *Fisheries Oceanography, 16*(1), 16-30. http://dx.doi.org/10.1111/j.1365-2419.2006.00411.x.

[Pond and Pickard, 1998] Pond, S., Pickard, G.L., 1998. Introductory dynamical oceanography. *Butterworth-Heinemann, Oxford*, 329 pp.

[Prego et al., 2007] Prego, R., Guzmán-Zuñiga, D., Varela, M., deCastro, M., Gómez-Gesteira, M., 2007. Consequences of Winter upwelling events on biogeochemical and phytoplankton patterns in a western Galician ria (NW Iberian peninsula). *Estuarine, Coastal and Shelf Science, 73*(3-4), 409-422. http://dx.doi.org/10.1016/j.ecss.2007.02.004.

[Pritchard and Huntley, 2006] Pritchard, M., Huntley, D.A., 2006. A simplified energy and mixing budget for a small river plume discharge. *Journal of Geophysical Research: Oceans, 111*, C03019. http://dx.doi.org/10.1029/2005JC002984.

[Puillat et al., 2004] Puillat, I., Lazure, P., Jégou, A., Lampert, L., Miller, P., 2004. Hydrographical variability on the French continental shelf in the Bay of Biscay, during the 1990s. *Continental Shelf Research, 24*(10), 1143-1163. http://dx.doi.org/10.1016/j.csr.2004.02.008.

[Puillat et al., 2006] Puillat, I., Lazure, P., Jégou, A.M., Lampert, L., Miller, P., 2006. Mesoscale hydrological variability induced by northwesterly wind on the French continental shelf of the Bay of Biscay. *Scientia Marina 70*(1), 15–26.

[Reifel et al., 2009] Reifel, K.M., Johnson, S.C., DiGiacomo, P.M., Mengel, M.J., Nezlin, N.P., Warrick, J.A., Jones, B.H., 2009. Impacts of stormwater runoff in the Southern California Bight: Relationships among plume constituents. *Continental Shelf Research, 29*, 1821-1835. http://dx.doi.org/10.1016/j.csr.2009.06.011.

[Reinart and Reinhold, 2008] Reinart, A., Reinhold, M., 2008. Maping surface temperature in large lakes with MODIS data. *Remote Sensing of Environment, 112*(2), 603-611. http://dx.doi.org/10.1016/j.rse.2007.05.015.

[Relvas et al., 2009] Relvas, P., Luis, J., Santos, A.M.P., 2009. Importance of the mesoscale in the decadal changes observed in the northern Canary upwelling system. *Geophysical Research Letters, 36*, L22601. http://dx.doi.org/10.1029/2009GL040504.

[Reynolds et al., 2007] Reynolds, R.W., Smith, T.M., Liu, C., Chelton, D.B., Casey, K.S., Schlax, M.G., 2007. Daily high-resolution-blended analyses for sea surface

temperature. *Journal of Climate, 20*(22), 5473-5496. http://dx.doi.org/10.1175/2007JCL1824.1.

[Reynolds, 2009] Reynolds, R., 2009. What´s new in Version 2. OISST web page, NOAA/NCDC.

[Reynolds and Chelton, 2010] Reynolds, R.W., Chelton, D.W., 2010. Comparisons of daily sea surface temperature analysis for 2007-08. *Journal of Climate, 23,* 3545-3562. http://dx.doi.org/10.1175/2010JCLI3294.1.

[Ribeiro et al., 2005] Ribeiro, A.C., Peliz, A., Santos, A.M.P., 2005. A study of the response of chlorophyll-a biomass to a winter upwelling event off Western Iberia using SeaWiFS and in situ data. *Journal of Marine Systems, 53*(1), 87-107. http://dx.doi.org/10.1016/j.jmarsys.2004.05.031.

[Robinson, 2010] Robinson, I.S., 2010. Discovering the Ocean from Space: the unique applications of satellite oceanography. *Springer Berlin Heidelberg.* Berlin, Heidelberg, 630 pp.

[Rusu et al., 2011] Rusu, L., Bernardino, M., Guedes Soares, C., 2011. Modelling the influence of currents on wave propagation at the entrance of the Tagus estuary. *Ocean Engineering, 38*(10), 1174-1183. http://dx.doi.org/10.1016/j.oceaneng.2011.05.016.

[Rusu and Guedes Soares, 2013] Coastal impact induced by a Pelamis wave farm operating in the Portuguese nearshore. *Renewable Energy, 58*, 34-49. http://dx.doi.org/10.1016/j.renene.2013.03.001.

[Saha et al., 2010] Saha, S., Moorthi, S., Pan, H.L., Wu, X., Wang, J., Nadiga, S., Tripp, P., Kistler, R., Woollen, J., Behringer, D., Liu, H., Stokes, D., Grumbine, R., Gayno, G., Hou, Y.T., Chuang, H.Y., Juang, H.M.H., Sela, J., Iredell, M., Treadon, R., Kleist, D., van Delst, P., Keyser, D., Derber, J., Ek, M., Meng, J., Wei, H., Yang, R., Lord, S., van den Dool, H., Kumar, A., Wang, W., Long, C., Chelliah, M., Xue, Y., Huang, B., Schemm, J.K., Ebisuzaki, W., Lin, R., Xie, P., Chen, M., Zhou, S., Higgins, W., Zou, C.Z., Liu, Q., Chen, Y., Han, Y., Cucurull, L., Reynolds, R.W., Rutledge, G., Goldberg, M., 2010. The NCEP Climate Forecast System Reanalysis. *Bulletin of the American Meteorological Society, 91*(8), 1015-1057. http://dx.doi.org/10.1175/2010BAMS3001.1.

[Salat et al., 2002] Salat, J., Garcia, M.A., Cruzado, A., Palanques, A., Arín, L., Gomis, D., Guillén, J., de León, A., Puigdefàbregas, J., Sospedra, J., Velásquez, Z.R., 2002. Seasonal changes of water mass structure and shelf slope exchanges at the Ebro Shelf (NW Mediterranean). *Continental Shelf Research, 22*, 327-348. http://dx.doi.org/10.1016/S0278-4343(01)00031-0.

[Saldias et al., 2012] Saldías, G.S., Sobarzo, M., Largier, J., Moffat, C., Letelier, R., 2012. Seasonal variability of turbid river plumes off central Chile based on high-

resolution MODIS imagery. *Remote Sensing of Environment, 123*, 220-233. http://dx.doi.org/10.1016/j.rse.2012.03.010.

[Saldias et al., 2016a] Saldias, G.S., Largier, J.L., Mendes, R., Pérez-Santos, I., Vargas, C.A., Sorbazo, M., 2016a. Satellite-measured interanual variability of turbid river plumes off central-southern Chile: Spatial patterns and the influence of climate variability. *Progress in Oceanography, 146*, 212-222, http://dx.doi.org/10.1016/j.pocean.2016.07.007.

[Saldias et al., 2016b] Saldias, G.S., Shearman, R.K., Barth, J.A., Tufillaro, N., 2016b. Optics of the offshore Columbia River plume from glider observations and satellite imagery. *Journal of Geophysical Research: Oceans, 121*, 2367-2384, http://dx.doi.org/10.1012/2015JC011431.

[Sánchez-Garcia et al., 2013] Sánchez-García, L., de Andrés, J.R., Gélinas, Y., Schmidt, M.W.I., Louchouarn, P., 2013. Different pools of black carbon in sediments from the Gulf of Cádiz (SW Spain): Method comparison and spatial distribution. *Marine Chemistry, 151*, 13-22. http://dx.doi.org/10.1016/j.marchem.2013.02.006.

[Santos et al., 2004] Santos, A.M.P., Peliz, A., Dubert, J., Oliveira, P.B., Angélico, M.M., Ré, P., 2004. Impact of a winter upwelling event on the distribution and transport of sardine (Sardina pilchardus) eggs and larvae off western Iberia: a retention mechanism. *Continental Shelf Research, 24*(2), 149-165. http://dx.doi.org/10.1016/j.csr.2003.10.004.

[Santos et al., 2011] Santos, F., Gómez-Gesteira, M., deCastro, M., Alvarez, I., 2011. Upwelling along the western coast of the Iberian Peninsula: Dependence of trends on fitting strategy. *Climate Research, 48*, 213-218, http://dx.doi.org/10.3354/cr00972.

[Santos et al., 2012a] Santos, F., Gomez-Gesteira, M., deCastro, M., Alvarez, I., 2012. Variability of coastal and ocean water temperature in the upper 700 m along the Western Iberian Peninsula from 1975 to 2006. *PLoS One, 7*(12), 1-7, http://dx.doi.org/10.1371/journalpone.0050666.

[Santos et al., 2012b] Santos, F., Gómez-Gesteira, M., deCastro, M., Alvarez, I., 2012. Differences in coastal and oceanic SST trends due to the strengthening of coastal upwelling along the Benguela current system. *Continental Shelf Research, 34*, 79-86, http://dx.doi.org/10.1016/j.csr.2011.12.004.

[Santos et al., 2012c] Santos, F., deCastro, M., Gómez-Gesteira, M., Alvarez, I., 2012. Differences in coastal and oceanic SST warming rates along the Canary upwelling ecosystem from 1982 to 2010. *Continental Shelf Research, 47*, 1-6, http://dx.doi.org/10.1016/j.csr.2012.07.023.

[Schiller et al., 2011] Schiller, R.V., Kourafalou, V.H., Hogan, P., Walker, N.D., 2011. The dynamics of the Mississippi River plume: Impact of topography, wind and

offshore forcing on the fate of plume waters. *Journal of Geophysical Research: Oceans, 116*, C06029. http://dx.doi.org/10.1029/2010JC006883.

[Shi and Wang, 2009] Shi, W., Wang, M., 2009. Satellite observations of flood-driven Mississippi River plume in the spring of 2008. *Geophysical Research Letters, 36*, L07607. http://dx.doi.org/10.1029/2009GL037210.

[Sierra et al., 2002] Sierra, J.P., Sánchez-Arcilla, A., González del Río, J., Flos, J., Movellán, E., Mösso, C., Matínez, R., Rodilla, M., Falco, S., Romero, I., 2002. Spatial distribution of nutrients in the Ebro estuary and plume. *Continental Shelf Research, 22*, 361-378. http://dx.doi.org/10.1016/S0278-4343(01)00061-9.

[Simpson et al., 1993] Simpson, J.H., Bos, W.G., Schirmer, F., Souza, A.J., Rippeth, T.P., Jones, S.E., Hydes, D., 1993. Periodic stratification in the Rhine ROFI in the North Sea. *Oceanologica Acta, 16*(1), 23-32.

[Sousa et al., 2013] Sousa, M.C., Alvarez, I., Vaz, N., Gomez-Gesteira, M., Dias, J.M., 2013. Assessment of wind pattern accuracy from the QuikSCAT satellite and the WRF model along the Galician coast (Northwest Iberian Peninsula). *Monthly Weather Review, 141*(2), 742-753. http://dx.doi.org/10.1175/MWR-D-11-00361.1.

[Sousa et al., 2014a] Sousa, M.C., Vaz, N., Alvarez, I., Gomez-Gesteira, M., Dias, J.M., 2014. Modeling the Minho River plume intrusion into the Rias Baixas (NW Iberian Peninsula). *Continental Shelf Research, 85*, 30-41. http://dx.doi.org/10.1016/j.csr.2014.06.004.

[Sousa et al., 2014b] Sousa, M.C., Vaz, N., Alvarez, I., Gomez-Gesteira, M., Dias, J.M., 2014. Influence of the Minho River plume on the Rias Baixas (NW of the Iberian Peninsula). *Journal of Marine Systems, 139,* 248-260. http://dx.doi.org/10.1016/j.jmarsys.2014.06.012.

[Tenore et al., 1995] Tenore, K.R., Alonso-Noval, M., Alvarez-Ossorio, M., Atkinson, L.P., Cabanas, J.M., Cal, R.M., Campos, H.J., Castillejo, F., Chesney, E.J., Gonzalez, N., Hanson, R.B., McClain, C.R., Miranda, A., Roman, M.R., Sanchez, J., Santiago, G., Valdes, L., Varela, M., Yoder, J., 1995. Fisheries and oceanography off Galicia, NW Spain: Mesoscale spatial and temporal changes in physical processes and resultant patterns of biological productivity. *Journal of Geophysical Research: Oceans, 100*(C6), 10943-10966. http://dx.doi.org/10.1029/95JC00529.

[Teodoro et al., 2009] Teodoro, A.C., Gonçalves, H., Veloso-Gomes, F., Gonçalves, J.A., 2009. Modelling of the Douro River Plume size, obtained through image segmentation of MERIS data. *IEEE Geoscience and Remote Sensing Letters, 6*(1), 87-91. http://dx.doi.org/10.1109/LGRS.2008.2008446.

[Thomas and Weatherbee, 2006] Thomas, A.C., Weatherbee, R.A., 2006. Satellite-measured temporal variability of the Columbia River plume. *Remote Sensing of Environment, 100*(2), 167-178. http://dx.doi.org/10.1016/j.rse.2005.10.018.

[Thompson and Wallace, 1998] Thompson, D.W., Wallace, J.M., 1998. The Arctic Oscillation signature in the wintertime geopotential height and temperature fields. *Geophysical Research Letters, 25*(9), 1297-1300. http://dx.doi.org/10.1029/98GL00950.

[Trigo and DaCamara, 2000] Trigo, R.M., DaCamara, C.C., 2000. Circulation weather types and their influence on the precipitation regime in Portugal. *International Journal of Climatology, 20*(13), 1559-1581.

[Turner and Rabalais, 1994] Turner, R.E., Rabalais, N.N., 1994. Coastal eutrophication near the Mississippi river delta. *Nature, 368*, 619-621.

[Turner and Millward, 2002] Tuner, A., Millward, G.E., 2002. Suspended particles: their role in estuarine biogeochemical cycles. *Estuarine, Coastal and Shelf Science, 55,* 857-883. http://dx.doi.org/10.1006/ecss.2002.1033.

[Ulses et al., 2008] Ulses, C., Estournel, C., Puig, P., Durrieu de Madron, S., Marsaleix P., 2008. Dense shelf water cascading in the northwestern Mediterranean during the cold Winter 2005: Quantification of the export through the Gulf of Lion and the Catalan margin. *Geophysical Research Letters, 35*, L07610, http://dx.doi.org/10.1029/2008GL033257.

[Uncles et al., 1988] Uncles, R., Stephens, J., Woodrow, T., 1988. Seasonal cycling of estuarine sediment and contaminant transport. *Estuaries, 11*, 108-116. http://dx.doi.org/10.2307/1351998.

[Uncles, 2002] Uncles, R.J., 2002. Estuarine Physical Processes Research: Some Recent Studies and Progress. *Estuarine, Coastal and Shelf Science, 55*, 829-856. http://dx.doi.org/ 10.1006/ecss.2002.1032.

[Valencia et al., 2003] Valencia, V., Borja, A., Fontán, A., Pérez, F.F., Ríos, A.F., 2003. Temperature and salinity fluctuations in the Basque Coast (SW Bay of Biscay) from 1986 to 2000 related to the climatic factors. *ICES Marine Science Symposia, 219*, 340-342.

[Valencia et al., 2004] Valencia, V., Franco, J., Borja, A., Fontán, A., 2004. Hydrography of the southeastern Bay of Biscay. *Oceanography and Marine Environment of the Basque Country. Elsevier Oceanography Series, 70*, 159-194.

[Valente and da Silva, 2009] Valente, A.S., da Silva, J.C.B., 2009. On the observability of the fortnightly cycle of the Tagus estuary turbid plume using MODIS ocean colour images. *Journal of Marine Systems, 75*, 131-137. http://dx.doi.org/10.1016/j.jmarsys.2008.08.008.

[Vale and Sundby, 1987] Vale, C., Sundby, B., 1987. Suspended sediment fluctuations in the Tagus estuary on semi-diurnal and fortnightly time scales. *Estuarine, Coastal and Shelf Science, 25*, 495-508. http://dx.doi.org/10.1016//0272-7714(87)90110-7.

[Vaz et al., 2009] Vaz, N., Fernandes, L., Leitão, P.C., Dias, J.M., Neves, R., 2009. The Tagus estuarine plume induced by wind and river runoff: Winter 2007 case study. *Journal of Coastal Research, SI56*, 1090-1094.

[Vaz et al., 2011] Vaz, N., Mateus, M., Dias, J.M., 2011. Semidiurnal and spring-neap variations in the Tagus Estuary: Application of a process-oriented hydro-biogeochemical model. *Journal of Coastal Research, SI64*, 1619-1623.

[Vaz and Dias, 2014] Vaz, N., Dias, J.M., 2014. Residual currents and transport pathways in the Tagus estuary, Portugal: the role of freshwater discharge and wind. *Journal of Coastal Research, SI70*, 610-615.

[Vaz et al., 2015] Vaz, N., Mateus, M., Plecha, S., Sousa, M.C., Leitão, P.C., Neves, R., Dias, J.M., 2015. Modeling SST and chlorophyll patterns in a coupled estuary-coastal system of Portugal: The Tagus case study. *Journal of Marine Systems, 147*, 123-137. http://dx.doi.org/10.1016/j.jmarsys.2014.05.022.

[Veloso-Gomes et al., 2004] Veloso-Gomes, F., Taveira-Pinto, F., das Neves, L., Barbosa, J.P., Coelho, C., 2004. Erosion risk levels at the NW Portuguese coast: The Douro mouth-Cape Mondego stretch. *Journal of Coastal Conservation, 10*(1), 43-52. http://dx.doi.org/10.1652/1400-0350(2004)010[0043:ERLATN]2.0.CO;2.

[Vieira and Bordalo, 2000] Vieira, M.E., Bordalo, A.A., 2000. The Douro estuary (Portugal): A mesotidal salt wedge. *Oceanologica Acta, 23*(5), 585-594. http://dx.doi.org/10.1016/S0399-1784(00)01107-5.

[Vizy and Cook, 2010] Vizy, E.K., Cook, K.H., 2010. Influence of the Amazon/Orinoco Plume on the summertime Atlantic climate. *Journal of Geophysical Research: Atmospheres, 115*, D21112. http://dx.doi.org/10.1029/2010JD014049.

[Walker, 1996] Walker, N.D., 1996. Satellite assessment of Mississippi River plume variability: causes and predictability. *Remote Sensing of Environment, 58*(1), 21-35. http://dx.doi.org/10.1016/0034-4257(95)00259-6.

[Walker et al., 2005] Walker, N.D., Wiseman Jr, W.J., Rouse Jr, L.J., Babin, A., 2005. Effects of river discharge, wind stress, and slope eddies on circulation and the satellite-observed structure of the Mississippi River Plume. *Journal of Coastal Research, 21*(6), 1228-1244. http://dx.doi.org/10.2112/04-0347.1.

[Wang, 2006] Wang, B., 2006. Cultural eutrophication in the Changjiang (Yangtze River) plume: History and perspective. *Estuarine, Coastal and Shelf Science, 69*, 471-477. http://dx.doi.org/10.1016/j.ecss.2006.05.010.

[Wang et al., 2007] Wang, M., Tang, J., Shi, W., 2007. MODIS-derived ocean color products along the China east coastal region. *Geophysical Research Letters, 34*, L06611. http://dx.doi.org/10.1029/2006GL028599.

[Wang and Shi, 2009] The NIR-SWIR combined atmospheric correction approach for MODIS ocean color data processing. *Optics Express, 15*(24), 15722-15733. http://dx.doi.org/10.1364/OE.15.015722.

[Warrick and Milliman, 2003] Warrick, J.A., Milliman, J.D., 2003. Hyperpycnal sediment discharge from semiarid southern California rivers: Implications for coastal sediment budgets. *Geology, 31*(9), 781-784. http://dx.doi.org/10.1130/G19671.1.

[Warrick and Fong, 2004] Warrick, J.A., Fong, D.A., 2004. Dispersal scaling from the world´s rivers. *Geophysical Research Letters, 31*(4), L04301. http://dx.doi.org/10.1029/2003GL019114.

[Whitney and Garvine, 2005] Whitney, M.M., Garvine, R.W., 2005. Wind influence on a coastal buoyant outflow. *Journal of Geophysical Research: Oceans, 110*, C03014. http://dx.doi.org/10.1029/2003JC002261.

[Wilber and Clarke, 2001] Wilber, D.H., Clarke, D.G., 2001. Biological effects of suspended sediments: a review of suspended sediment impacts on fish and shellfish with relation to dredging activities in estuaries. *North American Journal of Fisheries Management, 21*(4), 855-875, http://dx.doi.org/10.1577/1548-8675(2001)021<0855:BEOSSA>2.0CO;2.

[Xing and Davies, 1999] Xing, J., Davies, A.M., 1999. The effect of wind direction and mixing upon the spreading of a buoyant plume in a non-tidal regime. *Continental Shelf Research, 19*, 1437-1483. http://dx.doi.org/10.1016/S0278-4343(99)00025-4.

[Xing and Davies, 2002] Xing, J., Davies, A.M., 2002. Influence of topographic features and along shelf flow upon the Ebro plume. *Continental Shelf Research, 22*, 199-227. http://dx.doi.org/10.1016/S0278-4343(99)00025-1.

[Xu et al., 2011] Xu, K., Harris, C.H., Hetland, R.D., Kaihatu, J.N., 2011. Dispersal of Mississippi and Atchafalaya sediment on the Texas-Louisiana shelf: Model estimates for the year 1993. *Continental Shelf Research, 31*, 1558-1575. http://dx.doi.org/10.1016/j.csr.2011.05.008.

[Yankovsky and Chapman, 1997] Yankovsky, A.E., Chapman, D.C., 1997. A simple theory for the fate of buoyant coastal discharges. *Journal of Physical Oceanography,* 27, 1386-1401. http://dx.doi.org/10.1175/1520-0485(1997)027<1386:ASTFTF>2.0.CO;2.

[Yankovsky, 2000] Yankovsky, A.E., 2010. The cyclonic turning and propagation of buoyant coastal discharge along the shelf. *Journal of Marine Research, 58*(4), 585-607. http://dx.doi.org/10.1357/002224000321511034.

[Zavialov et al., 2003] Zavialov, P.O., Kostianoy, A.G., 2003. SAFARI cruise: Mapping river discharge effects on Southern Brazilian shelf. *Geophysical Research Letters, 30*(21), 2126. http://dx.doi.org/10.1029/2003GL018265.

[Zheng et al., 2015] Zheng, G., DiGiacomo, P.M., Kaushal, S.S., Yuen-Murphy, M.A., Duan, S., 2015. Evolution of sediment plumes in the Chesapeake Bay and implications of climate variability. *Environmental Science and Technology, 49*, 6494-6503, http://dx.doi.org/10.1021/es506361p.

List of Publications

Articles

Mendes, R., Vaz, N., **Fernández-Nóvoa, D.**, da Silva, J.C.B., deCastro, M., Gómez-Gesteira, M., Dias, J.M., 2014. Observation of a turbid plume using MODIS imagery: The case of Douro estuary (Portugal). *Remote Sensing of Environment, 154*, 127-138. doi: 10.1016/j.rse.2014.08.003.

Fernández-Nóvoa, D., Mendes, R., deCastro, M., Dias, J.M., Sánchez-Arcilla, A., Gómez-Gesteira, M., 2015. Analysis of the influence of river discharge and wind on the Ebro turbid plume using MODIS-Aqua and MODIS-Terra data. *Journal of Marine Systems, 142*, 40-46. doi: 10.1016/j.jmarsys.2014.09.009.

Costoya, X., **Fernández-Nóvoa, D.**, deCastro, M., Santos, F., Lazure, P., Gómez-Gesteira, M., 2016. Modulation of sea surface temperature warming in the Bay of Biscay by Loire and Gironde Rivers. *Journal of Geophysical Research: Oceans, 121*, 966-979. doi: 10.1002/2015JC011157.

Costoya, X., **Fernández-Nóvoa, D.**, deCastro, M., Gómez-Gesteira, M., 2017. Loire and Gironde turbid plumes: Characterization and influence on thermohaline properties. *Journal of Sea Research*. doi: 10.1016/j.seares.2017.04.003.

Fernández-Nóvoa, D., deCastro, M., Des, M., Costoya, X., Mendes, R., Gómez-Gesteira, M., 2017. Characterization of Iberian turbid plumes by means of synoptic patterns obtained through MODIS imagery. *Journal of Sea Research, 126*, 12-25. doi: 10.1016/j.seares.2017.06.013.

Fernández-Nóvoa, D., Gómez-Gesteira, M., Mendes, R., deCastro, M., Vaz, N., Dias, J.M., 2017. Influence of main forcing affecting the Tagus turbid plume under high river discharges using MODIS imagery. *Plos ONE, 12(10)*: e0187036. doi: 10.1371/journal.pone.0187036.

Oral presentations at international conferences

Fernández-Nóvoa, D., Mendes, R., deCastro, M., Dias, J.M., Gómez-Gesteira, M., 2014. Main forcing drivers of the most important Iberian rivers plumes through satellite data. *ECSA 54. Coastal systems under change: tuning assessment and management tools.* 12-16 May. Sesimbra, Portugal.

Fernández-Nóvoa, D., Gómez-Gesteira, M., Mendes, R., deCastro, M., Vaz, N., Dias, J.M., 2015. Satellite imagery to evaluate the main drivers influencing the Tagus turbid plume development. *ECSA 55. Unbounded boundaries and shifting baselines: Estuaries and coastal seas in a rapidly changing world.* 6-9 September. London, UK.

Fernández-Nóvoa, D., Gómez-Gesteira, M., deCastro, M., Mendes, R., Des, M., Dias, J.M., 2015. Characterization, analysis and comparative of the most important Atlantic Iberian river plumes using MODIS imagery. *VIII Symposium on the Iberian Atlantic Margin.* 21-23 September. Málaga, Spain.

Fernández-Nóvoa, D., deCastro, M., Costoya, X., Gómez-Gesteira, M., 2016. Variability of the main river plumes of the Bay of Biscay under the influence of forcing drivers and teleconnection indices. *XV International Symposium on Oceanography of the Bay of Biscay.* 22-24 June. Bilbao, Spain.

Oral presentations at national conferences

Fernández-Nóvoa, D., Mendes, R., deCastro, M., Dias, J.M., Gómez-Gesteira, M., 2014. Analysis of the influence of river discharge and wind on the Ebro turbid plume using MODIS-Aqua imagery. *Encontro de Oceanografia: APOCEAN.* 21-22 March. Nazaré, Portugal.

Poster presentations at international conferences

Fernández-Nóvoa, D., Mendes, R., deCastro, M., Dias, J.M., Gómez-Gesteira, M., 2014. Analysis of the most important river plumes along the Atlantic Iberian coast by means of satellite data. *IMMR'14: International Meeting on Marine Research*. 10-11 July. Peniche, Portugal.

Fernández-Nóvoa, D., deCastro, M., Des, M., Costoya, X., Mendes, R., Gómez-Gesteira, M., 2017. Capability of MODIS radiance to analyze Iberian turbid plumes. *EGU: European Geosciences Union General Assembly 2017*. 23-28 April. Vienna, Austria.

Fernández-Nóvoa, D., deCastro, M., Des, M., Costoya, X., Mendes, R., Gómez-Gesteira, M., 2017. Testing the accuracy of MODIS radiance to detect river plumes by means of IBI salinity data. *International Ocean Colour Science Meeting 2017*. 15-18 May. Lisbon, Portugal.